

**Investigation of the Hsp90 C-terminal Binding Site, Novel Inhibitors and
Isoform-Dependent Client Proteins**

By

Laura B. Peterson

Submitted to the graduate degree program in Medicinal Chemistry and the Graduate Faculty of
the University of Kansas in partial fulfillment of the requirements for the degree of Doctor of
Philosophy.

Brian S. J. Blagg, Ph.D.
Chairperson

Thomas E. Prisinzano, Ph.D.

Michael F. Rafferty, Ph.D.

Jon A. Tunge, Ph.D.

Rick T. Dobrowsky, Ph.D.

Date Defended: May 30th, 2012

The Dissertation Committee for Laura B. Peterson
certifies that this is the approved version of the following dissertation:

**Investigation of the Hsp90 C-terminal Binding Site, Novel Inhibitors and
Isoform-Dependent Client Proteins**

Brian S. J. Blagg, Ph.D.
Chairperson

Date approved: June 1st, 2012

Abstract

The heat shock proteins represent an important class of pro-survival proteins that are intimately involved in cell survival, adaptation to cellular stress, and protein management. Heat shock protein 90 kDa (Hsp90) is a molecular chaperone responsible for the post-translational maturation of nascent polypeptides. Many of the Hsp90-dependent client proteins are involved in oncogenic processes, and accordingly, Hsp90 has emerged as a promising target for anti-cancer therapies.

Unfortunately, the clinical evaluation of Hsp90 inhibitors has been met with dosing, scheduling, and toxicity issues. The Hsp90 inhibitors that have reached clinical trials bind to the Hsp90 N-terminal ATP-binding site and demonstrate pan-Hsp90 inhibition, as they bind to and inhibit all four human Hsp90 isoforms. This characteristic may rationalize the undesired toxicities related to Hsp90 inhibition. Interestingly, the identification and characterization of isoform specific client proteins has not been extensively explored. In addition, N-terminal Hsp90 inhibition results in the induction of the heat shock response, whereby the expression of Hsp90 and other heat shock proteins is induced. This attribute of N-terminal inhibitors results in the clinically observed dosing and scheduling detriments as levels of Hsp90 increase with administration of the drug.

Described herein is the design, synthesis and biological evaluation of novel Hsp90 inhibitors that avoid the above mentioned therapeutic liabilities of currently known Hsp90 inhibitors. The identification and characterization of an Hsp90-isoform dependent client protein and an Hsp90-isoform selective inhibitor is also presented.

Acknowledgements

For me, graduate school provided a chance for personal growth and a platform to challenge myself. Without the many mentors, family members, and friends I have made and maintained while at the University of Kansas, this experience would not have been nearly as fulfilling. Those people deserve my recognition and gratitude.

First, thank you to my advisor, Dr. Brian S. J. Blagg. Brian was a constant source of knowledge, motivation, and inspiration and he helped me to grow as a scientist. I would also like to thank the other members of the Blagg Laboratory of all who greatly influenced my graduate career. Specifically, Adam Duerfeldt was an amazing colleague and friend who engaged in insightful discussions and generally made my time here more enjoyable. Outside of the Blagg Laboratory, thank you to Dr. Thomas Prisinzano and his lab members, all of whom greatly impacted my graduate school career. I would also like to thank Chrisostomos Prodromou for mentoring me during my research rotation at the Institute of Cancer Research.

Besides support from my KU network, I would never be where I am today without my family. To my Mom and Dad who had high expectations for me and never let me settle for mediocrity and to my brother who is a great role model, friend, and my ultimate competition – thank you! Lastly, to my future husband, Alexander Grenning - who is my best friend and always pushes me to be better, his support and friendship means a tremendous amount to me.

In addition to the amazing people I have had the opportunity to meet and work with over the last five years, I must thank the Department of Medicinal Chemistry, the Smissman Fellowship, the NIH Dynamic Aspects of Chemical Biology Training Grant, and the American Chemical Society Division of Medicinal Chemistry Pre-doctoral Fellowship for financial support.

Table of Contents:

Chapter I
Introduction to Hsp90 Structure, Function, and Inhibition

I. Introduction	1
II. Heat Shock Protein 90.....	1
A. Hsp90 Structure.....	2
B. Hsp90 Function	4
III. Heat Shock Protein 90 Inhibitors.....	9
A. Therapeutic Opportunities.....	10
A.1. Cancer	10
A.2. Neurodegenerative Diseases	12
B. N-Terminal Inhibitors	16
C. C-Terminal Inhibitors.....	18
D. Other Inhibitors	19
IV. Clinical Detriments and Liabilities of Hsp90 Inhibition	20
A. Heat Shock Induction.....	20
B. Toxicities.....	22
C. Other Considerations.....	23
V. Conclusions and Future Directions of Hsp90 Inhibition	24
VI. References.....	25

Chapter II
Exploration of the Hsp90 C-terminal Binding Site

I. Introduction	37
A. C-terminal Domain Structure.....	38
B. C-terminal Domain Function and Modulation.....	41

II. Development of a CoMFA for Hsp90 C-Terminal Inhibitors.....	45
III. Development of a C-terminal Binding Site Model	50
A. Identification of the Novobiocin Binding Site in Hsp90's C-terminal Domain	50
B. Modeling of Novobiocin's Conformation.....	52
C. Modeling of the Hsp90 Novobiocin Binding Site.....	53
D. Correlation to Observed Effects Resulting from C-Terminal Inhibition	57
IV. Synthesis and Evaluation of a Series of Triazole Containing Novobiocin Analogues.....	60
A. Rationale for the Development of Triazole Containing Novobiocin Analogues.....	60
B. Synthesis of Triazole Containing Novobiocin Analogues	61
C. Biological Evaluation of Triazole Containing Novobiocin Analogues	63
V. Conclusions and Future Work.....	66
A. Structure Based Drug Design of Novel C-terminal Inhibitors.....	67
B. Progress towards a C-terminal Inhibitor Co-Crystal Structure	68
VI. Materials and Methods	69
A. Development of a CoMFA for Hsp90 C-Terminal Inhibitors	69
B. Identification of the Novobiocin Binding Site in Hsp90's C-terminal Domain	75
C. Synthesis and Evaluation of a Series of Triazole Containing Novobiocin Analogues	76
VII. References	99

Chapter III

Biological Evaluation of Isoform Selective Hsp90 Inhibitors and Characterization of Isoform Dependent Client Proteins

I. Introduction	104
A. Hsp90 α/β	105
B. Grp94.....	106
C. Trap-1	108

II. The hERG Channel is Dependent upon the Hsp90 α Isoform for Maturation and Trafficking	109
A. hERG Interacts Solely with Hsp90 α	110
B. Hsp90 α and Hsp90 β Knockdown have Differential Effects on hERG Trafficking.....	113
C. Implications for Hsp90 Inhibitor Development	116
III. Development of Grp94 Selective Inhibitors and Assays to Evaluate Grp94-inhibitory Activity	117
A. Design of a Grp94 Inhibitor	119
B. Development of a Grp94 Inhibitor Assay	121
C. Subsequent Biological Evaluation of a Grp94 Inhibitor	126
D. Summary of and Implications for Grp94 Inhibition	131
IV. Conclusions and Future Work	132
V. Materials and Methods.....	134
A. The hERG Channel is Dependent upon the Hsp90 α Isoform for Maturation and Trafficking	134
B. Development of Grp94 Selective Inhibitors and Assays to Evaluate Grp94-inhibitory Activity	137
VI. References.....	140

Chapter IV
Exploration of Curcumin as a Novel Hsp90 Inhibitor

I. Introduction	147
II. Evaluation of Curcumin as an Hsp90 Inhibitor.....	151
A. Curcumin Binds Purified Recombinant Hsp90.....	151
B. Curcumin Inhibits Hsp90-dependent Refolding of Heat Denatured Luciferase	152

C. Curcumin Inhibits the Maturation of Hsp90-dependent Proteins in MCF-7 Breast Cancer Cells	153
D. Curcumin Inhibits Proliferation at a Concentration that Mirrors its Ability to Prevent Folding of Hsp90-dependent Substrates	154
III. Design, Synthesis and Evaluation of Electron Rich Curcumin Analogues	154
A. Synthesis of 1,3-Diketone Analogues	155
B. Synthesis of Pyrazole and Isoxazole Analogues	156
C. Electrophilicity of Curcumin and Analogues	157
D. Biological Evaluation of Curcumin and Analogues	160
IV. Conclusions and Future Work	163
V. Materials and Methods	163
VI. References	185

List of Figures:

Chapter I
Introduction to Hsp90 Structure, Function, and Inhibition

Figure 1. The structure of Hsp90	2
Figure 2. The Hsp90-mediated protein folding cycle	5
Figure 3. Hsp90 Conformations.....	7
Figure 4. Hsp90 α/β residues involved in post-translational modifications	9
Figure 5. Modulation of Hsp90 via small molecules.....	10
Figure 6. Representative natural product Hsp90 N-terminal inhibitors.....	16
Figure 7. Representative synthetic Hsp90 N-terminal inhibitors.....	17
Figure 8. C-terminal Hsp90 inhibitors	18
Figure 9. Natural product inhibitors of Hsp90 that disrupt the Hsp90-Cdc37 interaction	19
Figure 10. HSF1 mediated induction of the heat shock response.....	21

Chapter II
Exploration of the Hsp90 C-terminal Binding Site

Figure 11. C-terminal Hsp90 inhibitors	37
Figure 12. Structure of HtpG C-Terminal Domain.....	39
Figure 13. Overlay of Hsp90 CTD from various species	40
Figure 14. Alignment of select Novobiocin analogues used in CoMFA generation	46
Figure 15. Plot of predicted LogIC ₅₀ versus experimentally derived LogIC ₅₀ values.....	47
Figure 16. Contour maps generated from CoMFA analysis	48
Figure 17. Common structure activity relationships established through CoMFA and inhibitor design and synthesis	49
Figure 18. Novobiocin derivatives used in photoaffinity labeling studies	50
Figure 19. Crosslinking of 1a to Hsp90CT is specific.....	51

Figure 20. Conformation of NB as bound to DNA gyrase used in molecular modeling studies with Hsp90 CTD.....	53
Figure 21. Hsp90 closed clamped crystal structure	54
Figure 22. Modeled structure of the Novobiocin binding site in hHsp90 α	55
Figure 23. Amide- and Triazole-containing Novobiocin analogues.....	61
Figure 24. Western blot analysis for compound 16b from MCF-7 cell lysates.....	65
Figure 25. Structure-based drug design effort using the Hsp90 C-terminal binding site model ..	67
Figure 26. hHsp90 α constructs prepared in efforts to obtain an Hsp90 C-terminal inhibitor co-crystal structure.....	68

Chapter III

Biological Evaluation of Isoform Selective Hsp90 Inhibitors and Characterization of Isoform Dependent Client Proteins

Figure 27. Comparison of the hHsp90 isoforms	104
Figure 28. hERG co-immunoprecipitates with Hsp90 α and not Hsp90 β	111
Figure 29. Hsp90 α knockdown reduces hERG trafficking.....	113
Figure 30. Hsp90 α levels directly affect hERG trafficking efficiency	115
Figure 31. Clinically evaluated N-terminal Hsp90 inhibitors.....	117
Figure 32. Natural product Hsp90 inhibitors, GDA and RDC, along with their chimera, RDA	118
Figure 33. Structure-based design of Grp94-selective inhibitors	119
Figure 34. Proposed Grp94 inhibitors.....	121
Figure 35. Binding of compounds 22–26 to Grp94	121
Figure 36. Development of a Grp94 assay.....	122
Figure 37. Toll trafficking depends upon Grp94	123
Figure 38. Fluorescence microscopy images and data of Toll trafficking inhibition	124
Figure 39. Toll trafficking inhibition as determined by flow cytometry	125

Figure 40. Western blot analysis of 23 from HEK293 cell lysates	126
Figure 41. Induction of BiP Expression by treatment with 23	127
Figure 42. Inhibition of IFG-II secretion by 23	128
Figure 43. Compound 23 alters Grp94 conformation	129
Figure 44. Effect of compound 23 on Drosophila larval growth	130
Figure 45. The elucidation of Hsp90 isoform-dependent client proteins	133

Chapter IV
Exploration of Curcumin as a Novel Hsp90 Inhibitor

Figure 46. Structure of curcumin	147
Figure 47. Titration of purified recombinant Hsp90 with curcumin.....	151
Figure 48. Effect of curcumin on Hsp90-dependent refolding of luciferase in rabbit reticulocyte lysate	152
Figure 49. Western blot analyses of several Hsp90 client proteins from MCF-7 cell lysates after treatment with varying concentrations of curcumin	153
Figure 50. ¹ H NMR spectra for the addition of benzyl mercaptan to curcumin	158
Figure 51. ¹ H NMR spectra for the addition of benzyl mercaptan to compound 47 after the time indicated.....	159
Figure 52. Western blot analysis for compound 47 from MCF-7 cell lysates.....	162

List of Tables:

Chapter I
Introduction to Hsp90 Structure, Function, and Inhibition

Table 1. Hsp90-associated proteins that comprise the Hsp90 protein folding machinery4

Table 2. Hsp90-dependent proteins associated with the six hallmarks of cancer11

Table 3. Example neurodegenerative diseases and pathogenic proteins associated with aggregation.....13

Chapter II
Exploration of the Hsp90 C-terminal Binding Site

Table 4. Statistical Parameters for Final CoMFA Model.....47

Table 5. Anti-proliferative activities of triazole containing novobiocin analogues64

Table 6. Comparison of anti-proliferative activities: amide-containing versus triazole-containing novobiocin analogues.....65

Table 7. Novobiocin analogues used in the development of a C-terminal inhibitor CoMFA model.....70

Chapter III
Biological Evaluation of Isoform Selective Hsp90 Inhibitors and Characterization of Isoform Dependent Client Proteins

Table 8. hERG interacting proteins112

Chapter IV
Exploration of Curcumin as a Novel Hsp90 Inhibitor

Table 9. Client proteins of Hsp90 also affected by curcumin149

Table 10. Relative integration of protons resulting from 1,4-conjugate addition to curcumin...159

Table 11. Anti-proliferative activities of curcumin and analogues161

List of Schemes:

Chapter II
Exploration of the Hsp90 C-terminal Binding Site

Scheme 1. Synthesis of Azido-coumarin.....	62
Scheme 2. "Click" procedure with various alkynes used	62
Scheme 3. Noviosylation of triazole appended coumarins	63

Chapter IV
Exploration of Curcumin as a Novel Hsp90 Inhibitor

Scheme 4. Preparation of 1,3-diketone curcumin analogues	154
Scheme 5. Synthesis of pyrazole and isoxazole curcumin analogues	155

**INVESTIGATION OF THE HSP90 C-TERMINAL BINDING SITE, NOVEL
INHIBITORS AND ISOFORM-DEPENDENT CLIENT PROTEINS**

Chapter I

Introduction to Hsp90 Structure, Function, and Inhibition

I. Introduction

Proteins are synthesized in the ribosome as linear polypeptides. These unfolded, nascent polypeptides in the dense, crowded environment of the cell are highly susceptible to improper folding and aggregation. Specifically, the hydrophobic amino acids that are normally found in the core of a three-dimensional protein tend to aggregate in the polar environment of the cell. The molecular chaperone family of proteins has evolved to prevent protein aggregation, to aid in the maturation and proper folding of proteins and to generally maintain protein homeostasis (proteostasis).¹⁻⁵ Generally termed, molecular chaperones include any protein that interacts with a substrate or client protein to either stabilize or aid in its conformational maturation.

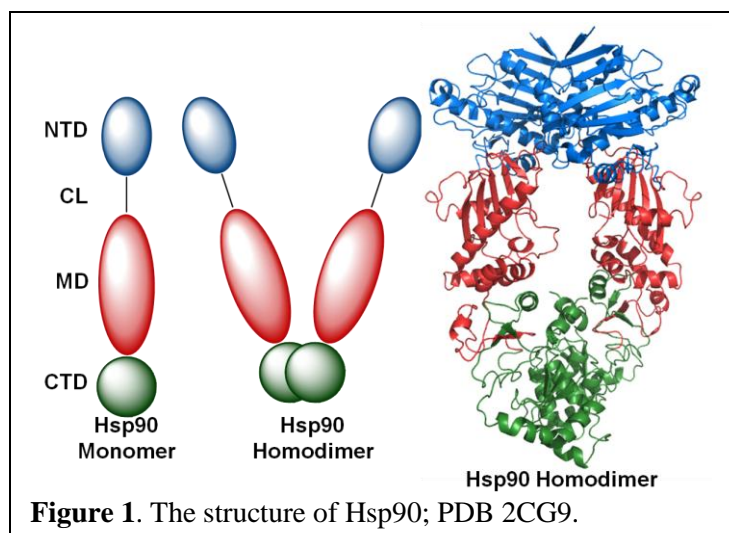
The heat shock proteins (Hsps), or stress proteins, are a family of molecular chaperones that are upregulated during cellular stress, a time at which protein denaturation and aggregation is prevalent. The Hsps are named by molecular weight and the various members of this family perform a vast array of cellular functions including protein folding, refolding of denatured proteins, protein trafficking, aggregate solubilization, and they also mediate protein degradation.³ Hsps represent important therapeutic targets for the treatment of protein folding and aggregating diseases, such as Alzheimer's disease, cystic fibrosis, or Parkinson's disease. In addition, cancer cells have been shown to depend upon Hsps due to increased protein synthesis. These therapeutic avenues highlight the necessity to understand the molecular chaperone system as well as the need to identify modulators that can impact human disease.

II. Heat Shock Protein 90

The 90 kDa heat shock proteins (Hsp90) are responsible for the post translational maturation of many proteins, as well as the solubilization of protein aggregates and the refolding of denatured proteins.⁶⁻¹⁰ Over 200 distinct proteins have been identified as Hsp90 client proteins that depend upon Hsp90 for their maturation.¹¹⁻¹² Hsp90 represents one of the most prevalent molecular chaperones in eukaryotic cells, comprising 1–2% of total cytosolic proteins in unstressed conditions and up to 4–6% during stress.^{7,13-14} Although there are 17 genes that encode for Hsp90 in the human genome, only 6 of these are responsible for encoding the four functional isoforms.¹⁵⁻¹⁸ The two predominant Hsp90 isoforms are Hsp90 α and Hsp90 β , which are found primarily in the cytosol. Hsp90 α is induced upon exposure to stress, whereas Hsp90 β is constitutively active and is considered a housekeeping chaperone. The genes for both α and β are located on chromosome 4, and are regulated through independent transcriptional events.¹⁵ The Hsp75/tumor necrosis factor receptor associated protein 1 (Trap1) resides in the mitochondrial matrix and plays a role in oxidative cell death and maintaining mitochondrial integrity.^{15,19} The endoplasmic reticulum resident Hsp90 isoform, 94kDa glucose-regulated protein (Grp94), chaperones both secreted and membrane proteins and participates in embryonic development, Ca²⁺ balance, immune response, and cell adhesion.^{15,20-21}

A. Hsp90 Structure

Hsp90 functions as a homodimer while each monomer of the Hsp90 dimer is comprised of four domains: a highly conserved N and C-terminal domain, a middle domain and



a charged linker that connects the N-terminal and middle domains (**Figure 1**).²²⁻²⁶ The 25kDa N-terminal domain (NTD) is responsible for binding ATP in a unique, bent conformation that is reminiscent of other members of the GHKL superfamily (gyrase, Hsp90, histidine kinase, and MutL).²⁷ Proteins in this family share a common Bergerat ATP-binding fold, named appropriately after Agnes Bergerat who first identified this motif in 1997.²⁸ This motif consists of four-interstranded β sheets and three α helices in a helix-sheet-helix orientation, wherein the ATP-binding site manifests interactions with residues in the loop region that connects the α helices and β sheets.²⁷ This Hsp90 ATP binding site has been under intense pharmaceutical investigation, as the majority of known Hsp90 inhibitors bind competitively versus ATP to this domain.

The 12 kDa C-terminal domain (CTD) is responsible for maintaining Hsp90s functional homodimeric state.^{24,29-30} The C-terminal domain is also responsible for coordinating interactions with several Hsp90 partner proteins and co-chaperones through its MEEVD sequence, which is recognized by proteins containing a tetratricopeptide repeat (TPR) motif.³¹⁻³⁴ The C-terminal domain also contains a putative nucleotide binding site, however, the C-terminal ATP binding site functions to facilitate nucleotide exchange at the N-terminus and does not manifest ATPase activity.³⁵⁻³⁶ The Hsp90 CTD also contains a small molecule binding site at which inhibitors bind and disrupt Hsp90 function.

The 40 kDa middle domain (MD) that is connected to the N-terminus via a highly charged linker is responsible for binding the γ -phosphate of ATP, when bound to the N-terminal binding pocket. This region is also important for the recognition and binding of client proteins and co-chaperones. It is largely amphipathic in nature and can mediate interactions with various proteins.^{6,37} The middle domain also appears to play a key role in mediating Hsp90's N-terminal

ATPase activity, as deletion of this region significantly retards Hsp90's inherent ATPase activity, suggesting coordination of ATP-hydrolysis by the entire protein, which may be conformationally driven.⁶

B. Hsp90 Function

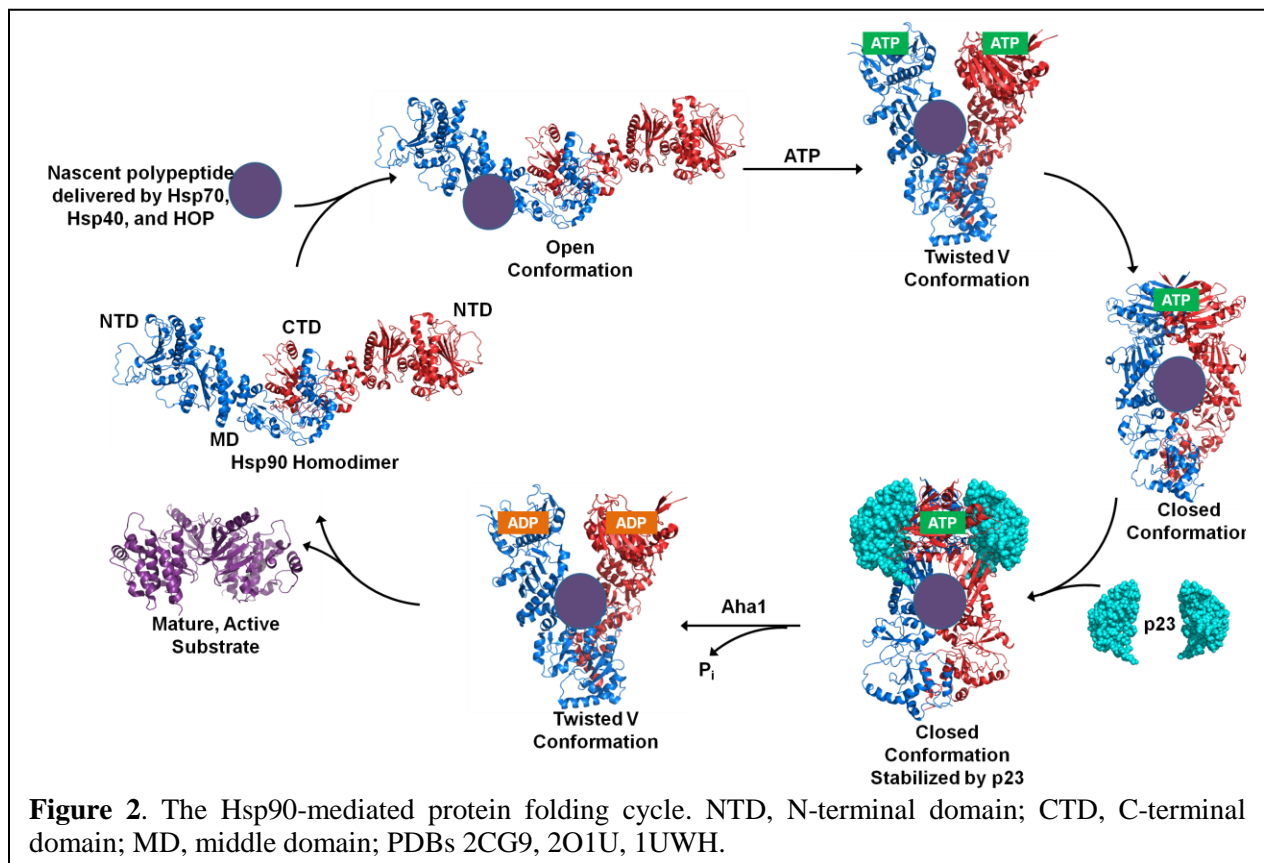
Hsp90 not only aids in the conformational maturation of nascent polypeptides and activation of receptors under normal cellular conditions, but under stressful conditions, such as elevated temperature, abnormal pH, or nutrient deprivation, Hsp90 can be overexpressed to aid in the rematuration of denatured proteins in conjunction with Hsp70.³⁸⁻⁴⁰ Evidence suggests that expression of Hsp90 and other heat shock proteins is mediated by the transcription factor, heat shock factor 1 (HSF1). Under normal conditions, Hsp90 binds HSF1, preventing HSF1 release and transcriptional activation of the heat shock response. However, it has been postulated that under cellular stress, the HSF1/Hsp90 complex is disassembled and HSF1 trimerizes and ultimately translocates to the nucleus, wherein it binds to the heat shock binding elements and initiates transcription of the heat shock genes that encode for Hsp27, Hsp40, Hsp70, and Hsp90.⁴¹⁻⁵⁴

Table 1. Hsp90-associated proteins that comprise the Hsp90 protein folding machinery; From Ref. 55.

Co-chaperone or Co-factor	Description	Reference
Ahal	Stimulates ATPase activity	56
Cdc37	Mediates activation of protein kinase substrates	57
CHIP	Involved in degradation of unfolded client proteins	58-59
CRN	Ubiquitin Ligase (E3) involved in client protein degradation	60
Cyclophilin-40	Peptidyl prolyl isomerase	61-62
FKBP51 and 52	Peptidyl prolyl isomerase	62-63
Hop	Mediates interaction between Hsp90 and Hsp70	64-65
Hsp40	Stabilizes and delivers client protein to Hsp90 folding machine	66-67
Hsp70	Stabilizes and delivers client protein to Hsp90 folding machine	68-70
NASP	Stimulates ATPase activity	71
p23	Stabilizes closed, clamped substrate bound conformation	22

PP5	Protein phosphatase 5	72-74
Sgt1	Client adaptor, involved in client recruitment	75
Tah1	Weak affect on ATPase activity	76
Tom70	Facilitates translocation of pre-proteins into mitochondrial matrix	77-78
Tpr2	Involved in ATP hydrolysis and substrate release	79
WISp39	Regulates p21 stability	80-81

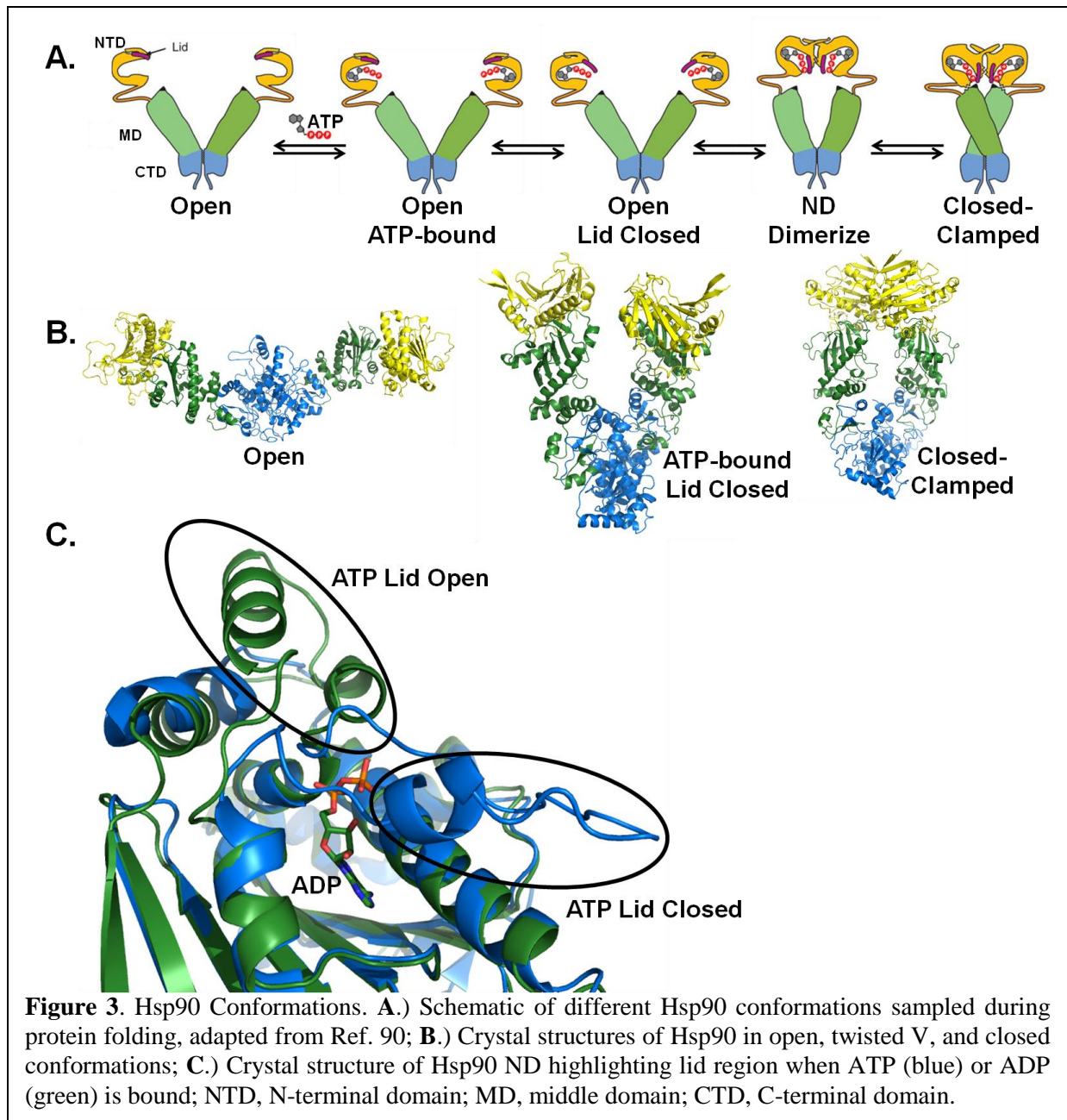
The mechanism by which Hsp90 mediates the maturation of nascent polypeptides remains unresolved. There are a number of proteins that combine to form a competent heteroprotein complex, regarded as the Hsp90 protein folding machine. Numerous co-chaperones, immunophilins and partner proteins bind the Hsp90 scaffold to form a competent protein folding machinery as denoted in **Table 1**.^{55,82}



A polypeptide substrate can obtain conformational maturity by proceeding through various complexes and conformations that are mediated by the Hsp90 scaffold (**Figure 2**).⁴ Succinctly, the nascent polypeptide exits the ribosome and is stabilized by an Hsp70-Hsp40-

ADP complex that prevents side chain interactions that can otherwise lead to aggregation.⁶⁹ This complex is often further stabilized by the Hsp70 interacting protein (Hip) or alternately, Bcl2-associated athanogene (BAG) homologues that facilitate exchange of ADP for ATP, resulting in concomitant release of the polypeptide substrate and dissociation of the complex.⁸³⁻⁸⁴ In the case of telomerase and steroid hormones receptors, Hsp organizing protein (Hop), which contains tetrapeptide repeats (TPRs) that are recognized by both Hsp70 and Hsp90, binds the Hsp70-protein complex and Hsp90, promoting transfer of the unfolded protein from Hsp70 to the Hsp90 homodimer, resulting in dissociation of Hsp70, Hip and Hop.^{32,34,64,85-87} After which, immunophilins and co-chaperones bind Hsp90 to form a heteroprotein complex that binds ATP at the N-terminus, and wraps around the bound client protein substrate.⁸⁸ N-terminal dimerization and conformational change occurs and p23 is recruited to the complex to stabilize the clamped, protein substrate-bound conformation, modulating ATP hydrolysis.⁷ Aha1 (activator of Hsp90 ATPase homologue 1) then stimulates Hsp90's inherent ATPase activity providing energy for conformational rearrangement of both Hsp90 and client protein.¹³ In an uncharacterized process, the client protein undergoes topological rearrangement to produce the bioactive conformation, which is subsequently released from the Hsp90 protein folding machinery.^{63,89}

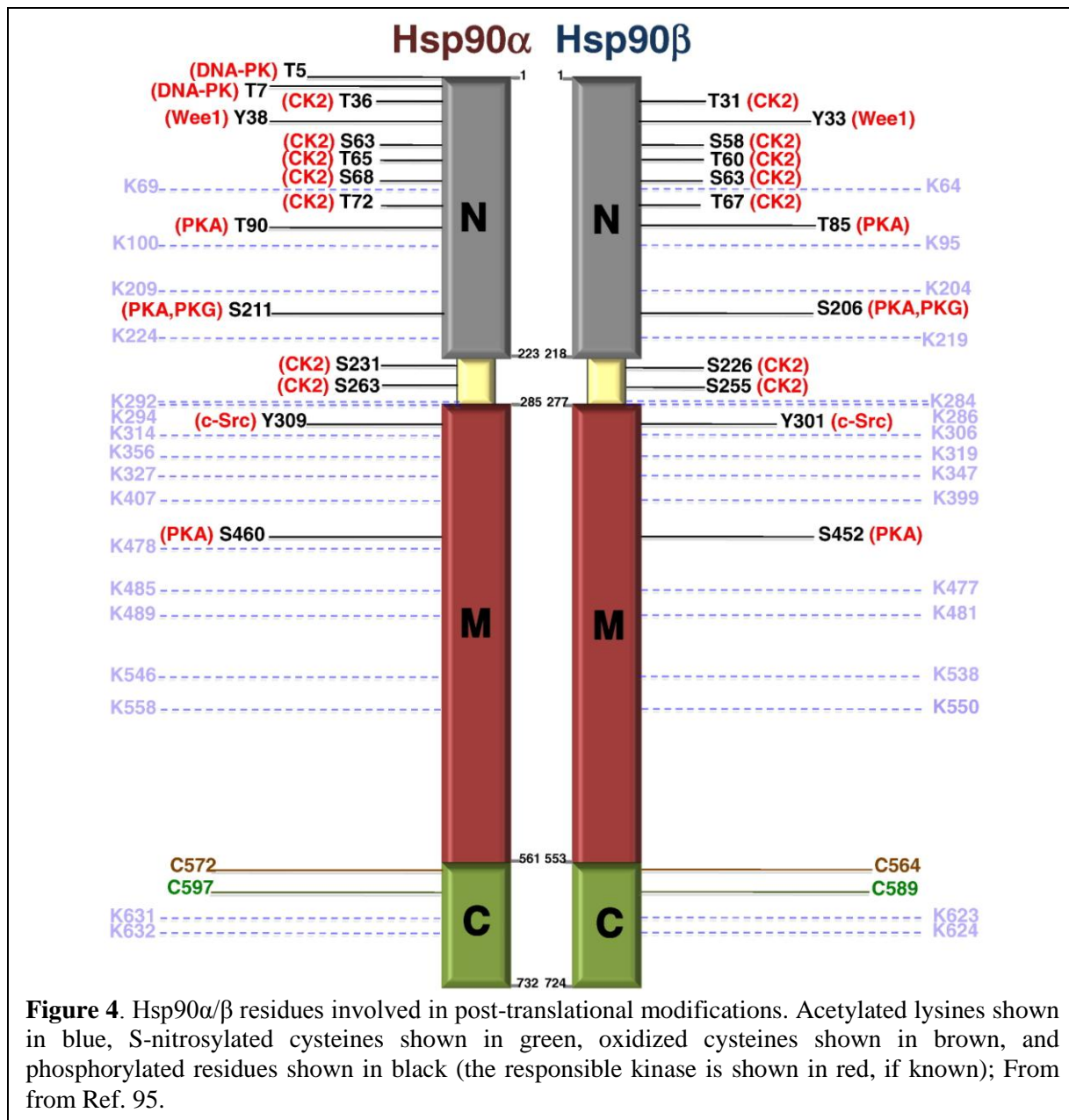
Structurally, Hsp90 must accommodate multiple conformations during the protein folding cycle, including protein loading, ATP binding and hydrolysis, co-chaperone binding, and client protein release (**Figure 3**).^{22,90-93} Hsp90 begins its conformational state in a CTD-dimerized, open state that is unable to bind ATP. In this conformation, Hsp90 reveals hydrophobic patches, ideal for client protein binding.⁹² Upon substrate binding, interactions between the NTD and MD are disrupted, opening the ATP binding cleft. Proximal to the ATP binding site exists a “lid”



region, and once ATP binds, the lid closes (**Figure 3A/3C**).⁹⁴ Hydrophobic residues on the lid are exposed and primed to promote N-terminal dimerization. This reorganization from NTD open to NTD dimerized conformations is proposed to assist client protein restructuring. Once the NTD dimerizes, the Hsp90 homodimer achieves a fully closed, clamped conformation wherein multiple hydrophobic and hydrogen bonding interactions are observed between the two monomers.²² Together, the NTD and MD promote the hydrolysis of ATP. Upon hydrolysis, the

homodimer further compacts causing expulsion of the client protein, as all hydrophobic interactions are maintained between the two monomers, and not the substrate. Once the client protein is released, Hsp90 relaxes into its semi open state and the lid opens to release ADP and returns Hsp90 to its open conformation for subsequent processing. In addition to the important role ATP/ADP and the Hsp90 co-chaperones play throughout the conformational cycle, post-translational modifications also impact Hsp90 conformation and function.⁹⁵⁻⁹⁶

Hsp90's activity is in part regulated by post-translational modifications, including phosphorylation, acetylation, S-nitrosylation, oxidation, and ubiquitination (**Figure 4**). Hsp90 contains multiple phosphorylation sites and phosphorylation appears to be a central mechanism used to control the activity of the chaperone machine.^{95,97} It has been shown that phosphorylation effects Hsp90s conformation,⁹³ residence within the cell,⁹⁸⁻⁹⁹ interactions with client proteins,¹⁰⁰⁻¹⁰¹ inhibitor sensitivity,¹⁰² ATPase activity,⁹³ and even Hsp90 degradation.⁹⁸ In general, phosphorylation of Hsp90 results in a reduced chaperone activity and association with client proteins, while a fully dephosphorylated Hsp90 exhibits maximal activity. Hsp90 acetylation also results in destabilization of the Hsp90-client protein complex and subsequent degradation of client proteins. The clients ErbB2, v-Src, mutant p53, androgen receptor, Raf-1, and HIF1 α as well as the co-chaperones CHIP, Hsp70 and p23 display weaker affinity for acetylated Hsp90.^{95,103-104} Cysteine oxidation of Hsp90 represents a response to oxidative stress and causes the proteasome-mediated degradation of several known Hsp90 client proteins, including Cdk4, cyclin D1, Raf-1, Akt and mutant p53.^{95,105} Cysteines located in the Hsp90 CTD also undergo S-nitrosylation. Nitric oxide synthase (eNOS) depends upon Hsp90 for maturation and is responsible for the production of nitric oxide (NO). Cysteine nitrosylation results from this NO

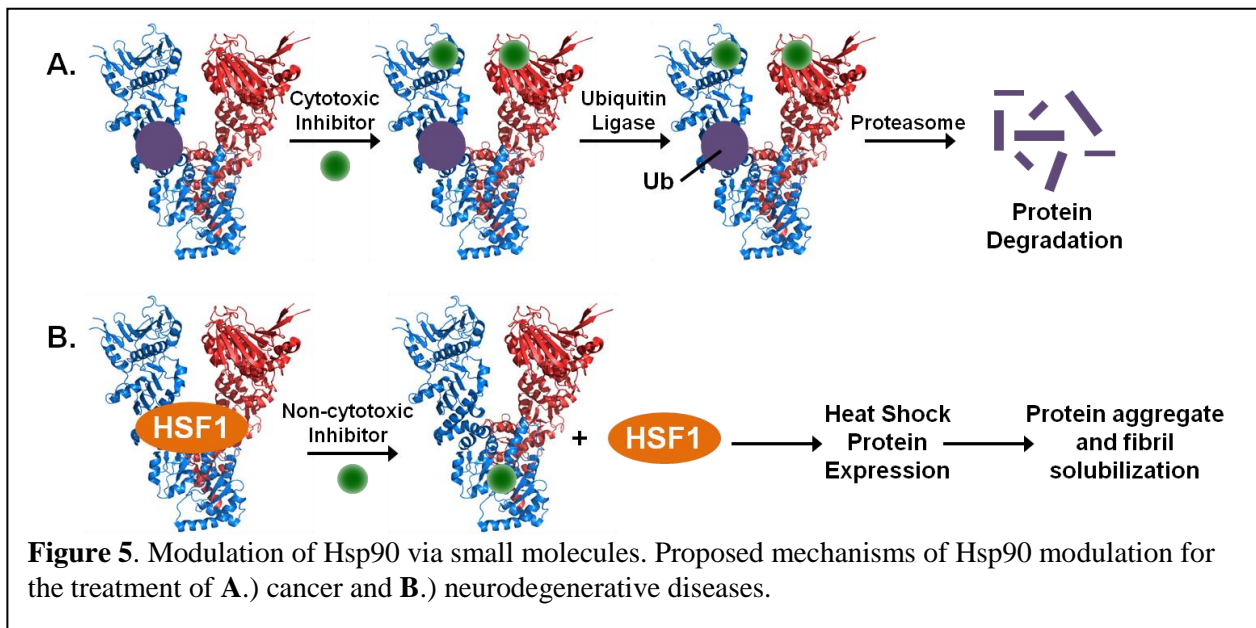


production, and ultimately serves as a negative feedback mechanism, as S-nitrosylation results in an inhibitory effect on Hsp90. This inhibitory action has been attributed to a conformational shift as well as a decrease in Hsp90 ATPase activity.¹⁰⁶⁻¹⁰⁸ Lastly, Hsp90 lysines can be ubiquitinated to signal Hsp90 degradation by the proteasome.^{95,98,109-110} These post-translational modifications provide another essential layer to control Hsp90 activity.

III. Heat Shock Protein 90 Inhibitors

A. Therapeutic Opportunities

Hsp90 is responsible for the conformational maturation of many nascent polypeptides. In addition, the Hsp90 protein folding machinery assists in the solubilization and refolding of aggregated and denatured proteins. As a result, small molecule modulators of Hsp90 can exert differing activities. Inhibition of Hsp90 by cytotoxic agents results in the degradation of Hsp90-



client proteins by preventing formation of the productive, closed clamped conformation between Hsp90 and substrate, thereby targeting the complex for ubiquitylation and proteasomal degradation.^{58,111-112} Compounds that manifest such activities possess excellent therapeutic potential for the treatment of cancer, as multiple signaling cascades can be simultaneously disrupted via Hsp90 inhibition (**Figure 5A**).¹¹³ In contrast, induction of Hsp90 expression by non-toxic molecules can lead to increased chaperone levels that minimize the accumulation of aggregated proteins.¹¹⁴⁻¹¹⁵ Small molecules that induce Hsp expression represent novel approaches for the treatment of neurodegenerative diseases such as Alzheimer's and Parkinson's disease, as well as Multiple Sclerosis (**Figure 5B**).

A.1. Cancer

Traditionally, therapeutic strategies for the treatment of cancer have focused on disruption of individual oncogenic enzymes and/or receptors. Newer paradigms for cancer chemotherapy have evolved to use combination therapies comprised of multiple drugs, each of which targets an individual protein. An alternative approach has been made available through Hsp90 inhibition, which allows for the simultaneous disruption of multiple signaling pathways, thus exerting a combinatorial attack on transformed cell machinery. Consequently, Hsp90 inhibition represents a new and powerful therapeutic approach towards the treatment of cancer.^{13,116} In 2000, Hanahan and Weinberg described the six hallmarks of cancer manifested by alteration of key regulatory proteins, enzymes and receptors that become hijacked by malignant cells.¹¹⁷⁻¹¹⁸ These hallmarks include 1) self-sufficiency in growth signals, 2) insensitivity to antigrowth signals, 3) evasion of apoptosis, 4) limitless replicative potential, 5) sustained angiogenesis, and 6) tissue invasion/metastasis. As shown in **Table 2**,⁵⁵ disruption of the Hsp90 protein folding machinery directly affects all six hallmarks of cancer by preventing maturation of proteins associated directly with each hallmark.^{14,112,119} No other cellular target has been ascribed to effect all hallmarks of cancer, beyond Hsp90, making it one of the most sought after cancer targets at this time.¹²⁰

Table 2. Hsp90-dependent proteins associated with the six hallmarks of cancer; From Ref. 55.

Hallmark	Client Protein(s)
1. Self-sufficiency in growth signals	Raf-1, AKT, Her2, MEK, Bcr-Abl
2. Insensitivity to anti-growth signals	Plk, Wee1, Myt1, CDK4, CDK6,
3. Evasion of apoptosis	RIP, AKT, mutant p53, c-MET, Apaf-1, Survivin
4. Limitless replicative potential	Telomerase (h-Tert)
5. Sustained angiogenesis	FAK, AKT, Hif-1 α , VEGFR, Flt-3
6. Tissue invasion/metastasis	c-MET

Due to the overwhelming need to fold overexpressed and mutated proteins, it is not surprising that Hsp90 and associated chaperones are elevated in human cancers.¹²¹⁻¹²² In addition, high Hsp90 expression in cancer has been correlated with decreased survival.¹²³ More interesting, it has been demonstrated that Hsp90 in cancer cells exhibits a higher affinity for inhibitors than Hsp90 from normal cells, providing an opportunity to develop drugs that manifest high differential selectivity.^{14,124-125} In tumor cells, Hsp90 resides in a heteroprotein complex bound to both client proteins and co-chaperones, whereas Hsp90 in non-transformed cells resides in the homodimeric state.¹²⁴⁻¹²⁵ This heteroprotein complex exhibits a higher affinity for ATP. Consequently, small molecules that bind competitively versus ATP, bind and inhibit the client protein maturation process with higher selectivity for the Hsp90 machinery present in malignant cells over normal cells. Inhibition of Hsp90 is an exciting therapeutic target for the treatment of cancer, and results from current clinical trials will significantly impact future cancer treatment strategies.

A.2. Neurodegenerative Diseases

Neurodegenerative diseases are diseases that arise from cell death that occurs in the central nervous system, including neurons associated with movement, sensory, memory and decision making.¹²⁶ Neuronal cell death in these diseases has a variety of origins, but one important commonality is the accumulation of misfolded proteins that result in cytotoxicity. Because molecular chaperones prevent protein aggregation, refold denatured proteins, and solubilize protein aggregates, it has been proposed that the heat shock proteins may be viable therapeutic targets for treatment of numerous neurodegenerative diseases, examples of which are provided in **Table 3**.^{55,127}

Table 3. Example neurodegenerative diseases and pathogenic proteins associated with aggregation; From Ref. 55.

Disease	Protein
Alzheimer's Disease	Amyloid β Tau
Parkinson's Disease	α -Synuclein
Huntington's Disease	Mutant Huntingtin
Spinal and Bulbar Muscular Atrophy	Mutant Androgen Receptor
Amyotrophic Lateral Dismutase	Mutant Superoxide-Dismutase-1

An example of this utility of a small molecule Hsp90 modulator is with Alzheimer's disease (AD). Alzheimer's disease is the most common neurodegenerative disorder, affecting more than 10% of the population 65 and older and nearly 30 million people worldwide.¹²⁸⁻¹²⁹ Pathologically, AD is caused by formation of β -amyloid ($A\beta$) plaques and neurofibrillary tangles (NFT's) in the extra (tau aggregates) and intracellular ($A\beta$ aggregates) space of neurons and synapses. There are several hypotheses to describe how these aggregates cause disease. One scenario is that these oligomers are toxic to neuronal cells. However, it has also been postulated that $A\beta$ plaques can initiate immune response by the recruitment of microglia and subsequent astrocytosis.¹²⁹⁻¹³² Recently, Hsp90 emerged as a novel target for the treatment of AD. The rationale behind such an approach is based on the premise that small molecule inhibitors of Hsp90 induce expression of the heat shock proteins, which ultimately leads to solubilization of protein aggregates, refolding of misfolded proteins, and directing misfolded proteins and protein aggregates to the ubiquitin-proteasome pathway for degradation. Alternative hypothesis suggest that Hsp90 can prevent fibril formation by binding and stabilizing the susceptible polypeptides.¹³³

In 2003, Dou and coworkers demonstrated that upregulation of the heat shock response that occurs upon administration of the N-terminal Hsp90 inhibitor, geldanamycin (GDA), resulted in decreased formation of NFT's, decreased levels of aggregated tau, and an increase in

soluble tau in both the hippocampus of transgenic mice containing mutant tau and in tissue samples from the brain of AD patients.¹³⁴ Under non-pathogenic conditions, tau enhances microtubule stability.¹³⁵ However, in AD the hyperphosphorylation of tau is observed and causes dissociation of microtubules, allowing incorporation into NFT's.^{115,134} These researchers demonstrated that the level of microtubule associated tau increased after treatment with GDA. A reduction in microtubule associated tau was observed alongside a concomitant increase in cytosolic aggregated tau in cells treated with Hsp90- and Hsp70-targeted siRNA.¹³⁴

Human H4 neuroglioma cells were treated with synthetic Hsp90 inhibitors to investigate the effects of Hsp90 inhibition on both tau levels and heat shock response.¹³⁶ It was observed that several inhibitors induced heat shock response, as evidenced by elevated levels of Hsp70, Hsp40 and Hsp27. Cells treated with these same compounds also exhibited decreased levels of tau, indicating a reciprocal relationship between tau and heat shock levels. No toxicity was observed in these studies, which has been one of the limiting factors in the development of Hsp90 inhibitors such as GDA,¹³⁷ because GDA induces client protein degradation at the same concentration it induces heat shock response. Additionally, an Hsp90 inhibitor of the purine scaffold, EC102, caused reduction of aberrant tau in the brain of a mouse transgenic for tauopathy after i.p. injection. This result is promising as the inhibitor was capable of crossing the BBB and reduced tau levels without toxicity to the mice.¹³⁶

An alternative treatment for AD may involve regulation of A β formation and aggregation. During in vitro studies, it was observed that recombinant Hsp70/Hsp40 and Hsp90 were able to suppress A β aggregate formation. Hsp90 and the Hsp70/Hsp40 complex inhibited A β formation and slowed the rate of aggregation in a chaperone concentration-dependent manner.¹³⁸ Additionally, Hsp40/Hsp70 and Hsp90's ATPase activity was necessary for

inhibition of protein aggregation, as experiments performed using ATP γ S, an ATP analogue that is hydrolyzed at a much slower rate, inhibited the anti-aggregation properties of the chaperone machine, especially in the case of Hsp70/Hsp40, as Hsp90's effect on aggregation was not significantly affected by ATP γ S. Two mechanisms by which the heat shock proteins inhibit A β assembly have been proposed. In one model, the chaperone binds misfolded amyloid in an ATP-independent manner, preventing it from aggregation. This model is inconsistent with the observed dependency on Hsp90 ATPase activity. Alternately, the chaperone may bind A β in an ATP-dependent manner changing A β 's conformation to one that is less susceptible to aggregation.¹³⁸

Although geldanamycin is a potent inhibitor of Hsp90 and is a standard control used in Hsp90 inhibitory assays, its therapeutic window is very narrow as it manifests cytotoxicity. Therefore, efforts have been made to identify more suitable small-molecule inhibitors; specifically, those with the potential to cross the BBB, which is required for the treatment of neurological diseases. In the Blagg Laboratory, a novobiocin analogue, **A4** was developed that demonstrated exceptional promise as a neuroprotective agent with no signs of toxicity at 100 μ M.¹³⁹ In freshly prepared neuronal cells treated with A β alone, significant toxicity was observed, however, embryonic primary neurons treated with A β in the presence of **A4** showed significantly decreased toxicity in a dose-dependent manner.

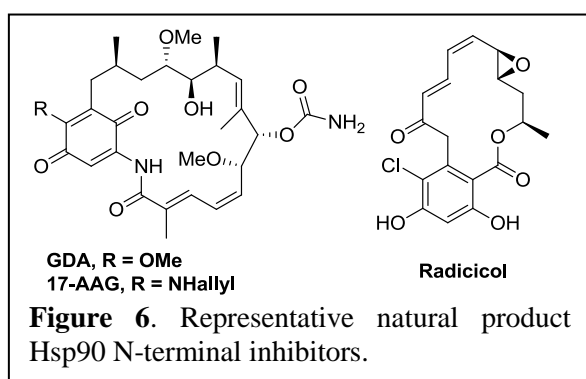
Hsp90 has also been shown to play a role in other neurodegenerative diseases, such as Parkinson's disease, amyotrophic lateral sclerosis, multiple sclerosis, and the polyglutamine (PolyQ) diseases spinal and bulbar muscular atrophy and Huntington's disease.⁵⁵ Hsp90 modulators have been evaluated in cell culture and animal models of these diseases and have shown some promising activity. Subsequent identification of additional non-toxic Hsp90

inhibitors that cause HSF-1 mediated induction of the heat shock response will be necessary for the development of this class of Hsp90 inhibitors.

In summary, Hsp90 is a molecular chaperone responsible for the conformational maturation of nascent polypeptides and it may cooperate with Hsp70 to bring about the refolding of misfolded or denatured proteins. Inhibition of Hsp90 exhibits the potential to treat unrelated disease states ranging from cancer to neurodegeneration. Inhibition of Hsp90 by cytotoxic agents offers exciting promise for the treatment of cancer, which results in degradation of Hsp90-dependent client proteins directly associated with all six hallmarks of cancer. As a therapeutic target, Hsp90 inhibitors possess the ability to simultaneously attack cancer through multiple signaling nodes simultaneously, resulting in a combinatorial attack that may be equivalent to the administration of multiple drugs. In contrast, modulation of Hsp90 by non-cytotoxic small molecules results in disassembly of the HSF-1/Hsp90 complex, and overexpression of the heat shock proteins. The resulting Hsps include Hsp90, Hsp70, Hsp40 and Hsp27, and together solubilize aggregated proteins that are often the causes or contributors to many neurodegenerative diseases. Consequently, Hsp90 represents a unique and exciting therapeutic target for the development of Hsp90 modulators that offer the potential to treat several disease states via a single protein target.⁵⁵

B. N-Terminal Inhibitors

Hsp90 contains several small molecule binding sites. The N-terminal ATP binding site has been the most widely studied while less is known about the binding site contained within the C-terminal and middle domains. The first



known inhibitors of Hsp90 bind competitively to the N-terminal nucleotide binding site (**Figure 6**). In 1970, the benzoquinone-containing ansamycin, namely geldanamycin (GDA), was isolated from *Streptomyces hygroscopicus* and was later reported to manifest anti-tumor activity through Hsp90 inhibition.¹⁴⁰⁻¹⁴¹ Radicicol (RDC), another natural product Hsp90 inhibitor, was also shown to manifest anti-tumor activity through competitive inhibition of the Hsp90 N-terminal ATP binding site.¹⁴²⁻¹⁴³ Unfortunately, neither GDA nor RDC are suitable for drug development. GDA administration manifests toxicity, likely due to the formation of superoxide radicals resulting from the redox-active nature of the quinone central to its core.¹⁴⁴⁻¹⁴⁵ RDC suffers from poor *in vivo* activity caused by the inherent reactivity of the $\alpha,\beta,\gamma,\delta$ -unsaturated ketone and allylic epoxide which react with a variety of biological nucleophiles. These reaction products are unable to bind Hsp90 with significant affinity. However, both RDC and GDA have been co-crystallized with Hsp90 and have been instrumental to the design of other classes of Hsp90 NTD inhibitors.

Inhibitors of the NTD have been the subject of many clinical trials for the treatment of cancer, and currently, the geldanamycin derivative, 17-allylamino-17-demethoxygeldanamycin (17-AAG), is in Phase III clinical trials.¹⁴⁶⁻¹⁵² Toxicity of the benzoquinone containing compound, 17-AAG, is of concern, however new formulations and structural analogues have improved tolerability.¹⁵³⁻¹⁵⁴ Synthetic Hsp90 inhibitors have also been described that circumvent the toxic liabilities of 17-AAG (**Figure 7**).^{150,152,155} The first synthetic class of

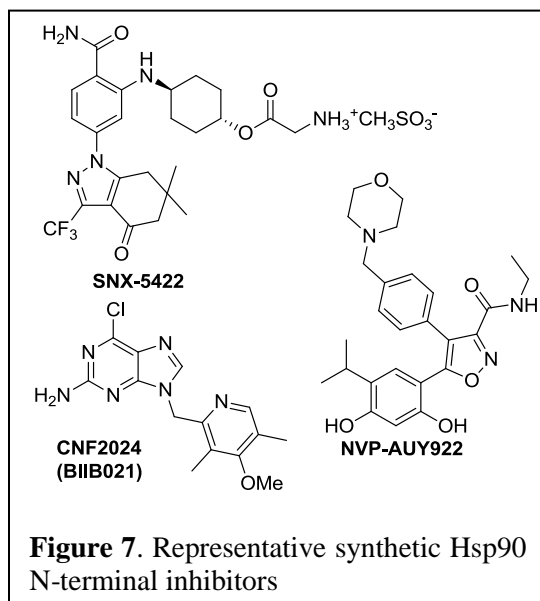
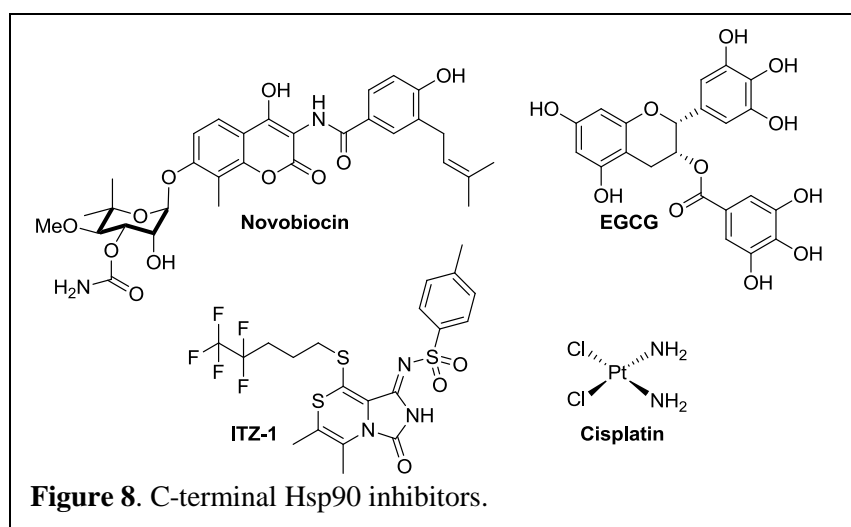


Figure 7. Representative synthetic Hsp90 N-terminal inhibitors

Hsp90 inhibitors to be clinically evaluated was the purine-scaffold inhibitors, such as CNF2024, based on the natural ligand, ATP. SNX-5422 is a benzamide-containing inhibitor that manifested improved preliminary biological properties, but appears to produce cardiotoxicity.¹⁵⁰ Another synthetic class of Hsp90 N-terminal inhibitors contain a resorcinol moiety, such as the Novartis compound, NVP-AUY922, which is currently in Phase I/II clinical trials.¹⁵² In addition to the binding site contained within the N-terminus, Hsp90 contains a putative nucleotide binding site at the C-terminus for small molecule inhibitors.

C. C-Terminal Inhibitors

The natural product antibiotic, Novobiocin (NB), was identified as a putative Hsp90 inhibitor (**Figure 8**). First discovered as a DNA gyrase inhibitor, it was originally thought that NB targeted the Hsp90 N-terminus due to its unique bent conformation observed when bound to DNA gyrase. Immobilized NB was able to pull down Hsp90 constructs containing N- but not C-terminal truncations, with the binding site being localized to C-terminal fragments containing amino acids 538-728.¹⁵⁶⁻¹⁵⁷ Additionally, NB was shown to induce the degradation of Hsp90 client proteins in a breast cancer cell line (SKBr-3).¹⁵⁶⁻¹⁵⁷ Mechanistically, the binding of NB to



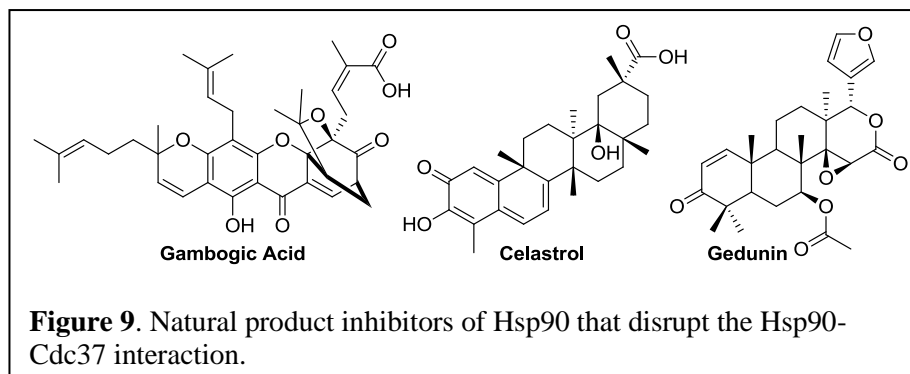
Hsp90 induces a conformation that is distinct from geldanamycin- or molybdate-bound Hsp90.^{35-36,158-159} For example, in the presence of NB, two major sites hypersensitive to proteolysis by trypsin (R400

and K615/R620 of human Hsp90 α) and a minor site in Hsp90's charged linker region become resistant to cleavage.¹⁵⁹⁻¹⁶⁰ In addition, NB binding protects recombinant Hsp90 C-terminal domain constructs from trypsin-mediated proteolysis and disrupts binding of TPR-containing co-chaperones to the C-terminal MEEVD motif.^{159,161} Analogues of NB have been synthesized to overcome the low biological activity manifested by NB.¹⁶²⁻¹⁷³

Other inhibitors of the Hsp90 C-terminal domain include (**Figure 8**): Epigallocatechin gallate (EGCG), a polyphenol found in green tea extracts;¹⁷⁴ cisplatin, the platinum-containing chemotherapeutic agent;¹⁷⁵⁻¹⁷⁶ and ITZ-1, which was identified in 2010 as a C-terminal inhibitor by Kimura and co-workers.¹⁷⁷ These inhibitors of the C-terminus, along with NB, provide a mechanistic advantage over N-terminal inhibitors and therefore may be more suitable for drug development, as discussed below and in Chapter 2.

D. Other Inhibitors

A third class of Hsp90 inhibitors exist that bind Hsp90 and disrupt the protein-protein interactions between Hsp90 and



either the co-chaperone Cdc37 or Hop.¹⁵⁵ Cdc37 assists Hsp90 in the maturation of protein kinase client proteins. Cdc37 prevents Hsp90 conformational rearrangement after ATP binding, facilitating the interaction between Hsp90 and its kinase client.¹⁷⁸⁻¹⁷⁹ Furthermore, genetic knockdown of Cdc37 results in the destabilization and subsequent degradation of Hsp90 kinase client proteins, Her2 (ErbB2), Raf-1 (cRAF), CDK4, CDK6, and Akt.¹⁸⁰ Three natural products,

celastrol,¹⁸¹⁻¹⁸³ gedunin,¹⁵⁵ and gambogic acid,¹⁸⁴ prevent the association of Cdc37 with Hsp90 and cause a dose-dependent degradation of Hsp90 kinase client proteins (**Figure 9**).¹⁵⁵ Inhibitors of this class provide a mechanism to limit off-target effects, as they disrupt only one subset of Hsp90 client proteins.

In 2008, Yi and coworkers performed a high-throughput screen to identify molecules capable of disrupting interactions between Hsp90 and the co-chaperone, Hop.¹⁸⁵⁻¹⁸⁶ Hop, the Hsp organizing protein, mediates the interaction between Hsp70, Hsp90 and their shared client proteins and facilitates the delivery of the immature protein from Hsp70 to Hsp90.⁶⁴⁻⁶⁵ Molecules that disrupt the Hsp90–Hop interaction provide an alternative route to destabilize and degrade Hsp90 client proteins. These molecules may prove useful in combination therapy with conventional Hsp90 inhibitors as two subsequent steps in the Hsp90 protein folding pathway can be blocked.

IV. Clinical Detriments and Liabilities of Hsp90 Inhibition

Although there has been great interest and effort towards the development of Hsp90 inhibitors for the treatment of cancer and other diseases, significant clinical challenges have emerged during clinical evaluation. Cardio-, hepato- and ocular toxicities, as well as significant dosing and scheduling issues, have been observed throughout phase I and II clinical trials.

A. Heat Shock Induction

One important consideration in the pursuit of clinically relevant Hsp90 inhibitors is the fact that Hsp90 N-terminal inhibitors induce the pro-survival, heat shock response (**Figure 10**).¹⁸⁷⁻¹⁸⁸ The heat shock response results in an increased expression of the heat shock proteins, mediated by the transcription factor heat shock factor 1 (HSF1). In unstressed cells, HSF1 is found in an inactive, Hsp90-bound state.^{49,53} Upon heat shock, or administration of an N-terminal

Hsp90 inhibitor, HSF1 is released from the heteroprotein complex.¹⁸⁹ As a monomer, it lacks DNA binding capabilities, but once dissociated from Hsp90, HSF1 trimerizes, is

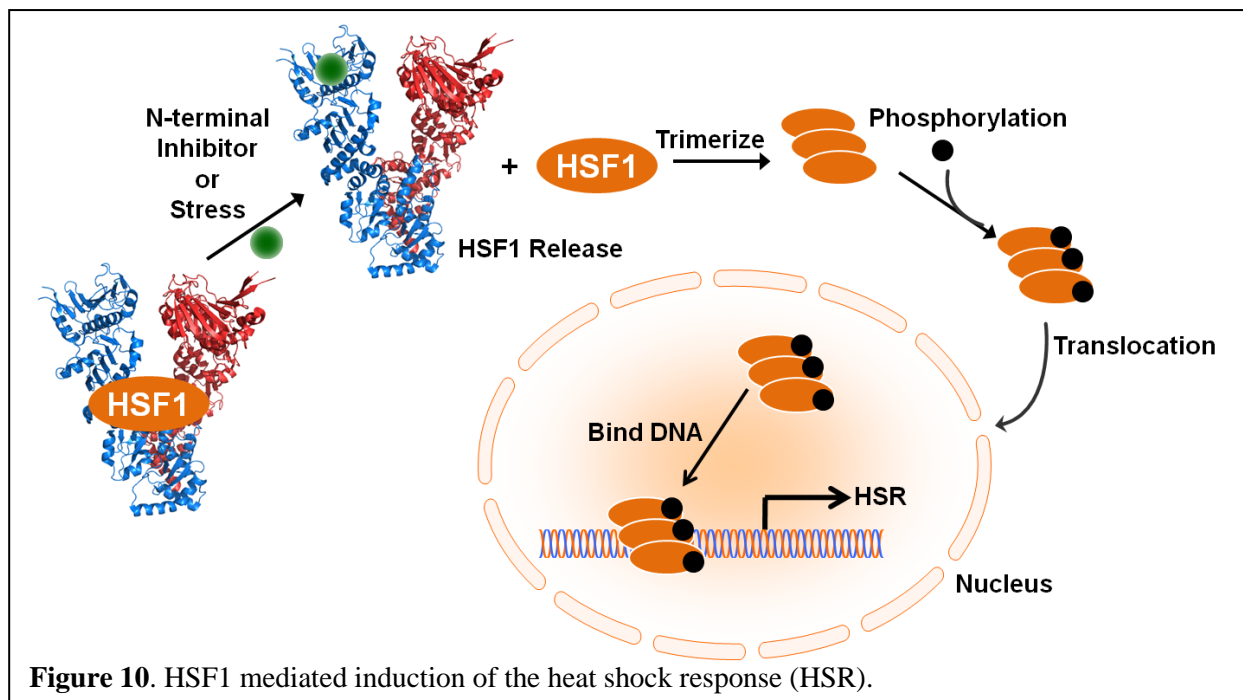


Figure 10. HSF1 mediated induction of the heat shock response (HSR).
hyperphosphorylated and translocates from the cytoplasm to the nucleus.¹⁹⁰ As an activated trimer, HSF1 is able to bind the heat shock element sequence and initiates transcription, inducing the expression of Hsp90 and other heat shock proteins.¹⁹¹ N-terminal Hsp90 inhibitors also cause the dissociation of HSF1 from Hsp90 and initiate the heat shock response. Induction of this pro-survival response upon N-terminal inhibition is concerning because it results in increased expression of Hsp90, Hsp70 and the other heat shock proteins that protect the cell and potentially negate the cytotoxic effects caused by Hsp90 inhibition. In addition, Hsp90 levels are significantly increased upon treatment with an inhibitor causes dosing and scheduling issues.^{150,192} Fortunately, C-terminal cytotoxic Hsp90 inhibitors manifest an opposing effect on the heat shock response. C-terminal inhibitors appear to lock HSF1 into an Hsp90-bound state and promote its ubiquitinylation and degradation via the proteasome.¹⁸⁷ This facet of C-terminal

inhibition has garnered interest, as inhibitors of this class may overcome the liabilities associated with N-terminal inhibition.

B. Toxicities

In addition to induction of the heat shock response, other problems have arisen during the clinical evaluation of Hsp90 inhibitors. Several toxicities have been observed, including cardio-, hepato-, and ocular toxicity. It is not completely clear if these toxicities are mechanism-based or are the consequence of specific chemical scaffolds. Throughout the clinical evaluation of 17-AAG, hepatotoxicity was observed and was dose-limiting.^{150,192} This toxicity is likely scaffold-dependent due to the quinone ring.¹⁹³⁻¹⁹⁴ Quinones are subject to oxidation by cytochromes P450 producing intermediates capable of oxidative damage, such as DNA lesions.¹⁹⁵ In addition, quinones are capable of reacting with a variety of biological molecules, specifically those that contain a thiol to produce toxic byproducts.¹⁹⁶ Combined with only modest efficacy, the enthusiasm for 17-AAG as a monotherapy has been dampened. In addition, this quinone-mediated hepatotoxicity highlights the potential difficulties inherent to the design of Hsp90 inhibitors based on the geldanamycin scaffold.

Cardiotoxicity represents a second toxicity observed throughout the clinical evaluation of structurally distinct Hsp90 inhibitors.¹⁵⁰ Cardiotoxicity often results from disruption of the potassium rectifier channel expressed in heart tissue. The α -subunit of the voltage gated potassium channel, the human *ether-a-gogo*-related gene product, hERG, constitutes a major component of the ion channel responsible for repolarization of cardiac action potential.¹⁹⁷⁻¹⁹⁸ Off-target pharmacological inhibition of the hERG channel results in elongation of the QT interval, torsades de pointes, and even sudden cardiac death.¹⁹⁸⁻¹⁹⁹ Compounds can bind directly to and inhibit the hERG channel, prevent the functional trafficking of hERG to the cell

membrane, or can both bind hERG and prevent trafficking.²⁰⁰⁻²⁰¹ Of specific consideration for Hsp90 inhibitors, hERG has previously been identified as an Hsp90-dependent client protein and depends upon Hsp90 for its functional trafficking.²⁰²⁻²⁰³ In the presence of Hsp90 inhibitors, such as GDA, hERG is retained in the ER as its immature, core-glycosylated form, resulting in decreased hERG-associated current amplitudes.²⁰² Clinically, it is not clear whether the hERG-related therapeutic liability is severe enough to preclude further clinical evaluation.

Another major toxicity observed in the clinical evaluation of several different Hsp90 inhibitors is ocular toxicity.²⁰⁴⁻²⁰⁶ Cytostaticity and cytotoxicity in cultured human retinal pigment epithelial cells, critical components involved in photoreception, were observed upon exposure to 17-AAG. One hypothesis to explain this observation is the decrease in Akt and Erk1/2 signaling as these two kinases are required for both the survival and proliferation of retinal pigment epithelial cells.²⁰⁶ Drug tissue distribution and scheduling regimen greatly affect this toxicity and provide potential strategies to mitigate this detriment.

C. Other Considerations

In addition to target-related toxicities, several other factors must be considered in the pursuit of a clinically relevant Hsp90 inhibitor. One important consideration is the development of both intrinsic and acquired resistance. Potential mechanisms of resistance include: altered drug metabolism, changes in drug influx/efflux, and mutation of the target itself. Target mutation was not originally a concern for Hsp90 inhibitors as it was believed that any mutation that causes a decreased affinity for an inhibitor would also cause decreased affinity for the natural ligand, ATP,²⁰⁷ which would ultimately reduce chaperone activity and compromise normal processes. Recently, studies performed in *Humicola fuscoatra* showed that a single point mutation in Hsp90 could reduce its affinity for RDC but not ATP or GDA, challenging this hypothesis.²⁰⁸⁻²⁰⁹

Another mechanism of resistance includes altered cellular efflux/influx. 17-AAG has been shown to be substrate for the P-glycoprotein (PGP) efflux pump, causing a decrease in efficacy in PGP-expressing cells. In addition to target mutation and drug efflux, metabolism can greatly affect biological activity. One illustrative example is the bio-reduction of 17-AAG and other quinone-containing ansamycins. It has been established that the reduced, hydroquinone-containing ansamycin analogues manifest higher affinities for Hsp90 as compared to their oxidized, quinone-containing counterparts.²¹⁰ DT-diaphorase (DTD), the enzyme encoded by the NQO1 gene, is an NAD(P)H-dependent reductase and is responsible for reduction of the 17-AAG quinone.²¹¹⁻²¹² A small percentage of the population (5-20%) has a mutation in the NQO1 gene, a mutation resulting in expression of DTD with reduced activity.²¹³ In addition, NQO1 expression is variable across tumor types.²¹⁴⁻²¹⁶ This example highlights the necessity to understand the metabolic liability of each Hsp90 inhibitor and demonstrates that the metabolic fate may result in a variable clinical response based on the genetic makeup of the patients.

It will be essential to the Hsp90 community to delineate and elucidate the mechanisms of toxicity, resistance, metabolism and other downstream biological effects. The results from these studies will aid in the design of clinical trials and the determination of certain tumor types and patient populations that will benefit from Hsp90 inhibition without significant toxicities.

V. Conclusions and Future Directions of Hsp90 Inhibition

Interest in Hsp90 inhibitors for the treatment of cancer and neurodegenerative diseases has grown exponentially since identification of geldanamycin as the first Hsp90 inhibitor in 1994.¹⁴¹ Over the last 25 years, several classes of Hsp90 inhibitors have been identified, each with unique mechanisms of inhibition and each displaying somewhat differing biological effects. Several of these inhibitors have been clinically evaluated for a variety of different cancers,

unfortunately, the results of these trials has somewhat been disappointing. The results from these trials emphasize the need to thoroughly understand the biology of the target, to better understand how different classes of inhibitors affect the molecular chaperone, and to determine how cellular environments affect drug efficacy.

Several strategies exist that may help circumvent the known pitfalls resulting from Hsp90 inhibition. First, inhibitors of the C-terminal domain do not cause induction of the heat shock response, but maintain anti-proliferative activity. Compounds in this class should not suffer from dosing and scheduling issues observed with N-terminal inhibitors. Second, the development of isoform-selective inhibitors may result in fewer negative effects upon Hsp90 inhibition. All known Hsp90 inhibitors exhibit *pan*-inhibition, i.e. they target all four human isoforms simultaneously. An isoform-selective inhibitor will not only help delineate the roll of each isoform, but may prove to be clinically more viable. Lastly, inhibitors that work by alternate mechanisms, such as co-chaperone disruptors, provide a mechanism to disrupt only a subset of Hsp90 client proteins, and may also result in less undesired effects. In summary, Hsp90 is still an attractive therapeutic target, but new strategies for inhibition are necessary to overcome the clinical liabilities observed for prototypical N-terminal inhibitors.

VI. References

1. Ellis, R. J.; Minton, A. P. Protein aggregation in crowded environments. *Biol. Chem.* **2006**, *387*, 485-497.
2. Hartl, F. U. Molecular chaperones in cellular protein folding. *Nature* **1996**, *381*, 571-580.
3. Hartl, F. U.; Bracher, A.; Hayer-Hartl, M. Molecular chaperones in protein folding and proteostasis. *Nature* **2011**, *475*, 324-332.
4. Walter, S.; Buchner, J. Molecular chaperones-cellular machines for protein folding. *Angew. Chem. Int. Ed.* **2002**, *41*, 1098-1113.
5. Saibil, H. R. Chaperone machines in action. *Curr. Opin. Struc. Biol.* **2008**, *18*, 35-42.
6. Meyer, P.; Prodromou, C.; Hu, B.; Vaughan, C.; Roe, S. M.; Panaretou, B.; Piper, P. W.; Pearl, L. H. Structural and functional analysis of the middle segment of Hsp90: implications for ATP hydrolysis and client protein and cochaperone interactions. *Mol. Cell* **2003**, *11*, 647-658.
7. Pratt, W. B.; Toft, D. O. Regulation of Signaling Protein Function and Trafficking by the Hsp90/Hsp70-based Chaperone Machinery. *Exp. Biol. Med.* **2003**, *228*, 111-133.

8. Soti, C.; Nagy, E.; Giricz, Z.; Vigh, L.; Csermely, P.; Ferdinandy, P. Heat shock proteins as emerging therapeutic targets. *Brit. J. Pharmacol.* **2005**, *146*, 769-780.
9. Sreedhar, A. S.; Csermely, P. Novel roles of Hsp90 inhibitors and Hsp90 in: redox regulation and cytoarchitecture. *Rec. Res. Devel. Life Sci.* **2003**, *1*, 153-171.
10. Chiosis, G.; Vilenchik, M.; Kim, J.; Solit, D. Hsp90: the vulnerable chaperone. *Drug Discov. Today* **2004**, *9*, 881-888.
11. Picard, D. <http://www.picard.ch/downloads/Hsp90interactors.pdf>.
12. Picard, D. <http://www.picard.ch/downloads/Hsp90facts.pdf>.
13. Whitesell, L.; Lindquist, S. L. Hsp90 and the chaperoning of cancer. *Nat. Rev. Cancer* **2005**, *5*, 761-772.
14. Zhang, H.; Burrows, F. Targeting multiple signal transduction pathways through inhibition of Hsp90. *J. Mol. Med.* **2004**, *82*, 488-499.
15. Chen, B.; Piel, W. H.; Gui, L.; Bruford, E.; Monteiro, A. The HSP90 family of genes in the human genome: Insights into their divergence and evolution. *Genomics* **2005**, *86*, 627-637.
16. Csermely, P.; Schnaider, T.; Soti, C.; Prohaszka, Z.; Nardai, G. The 90-kDa molecular chaperone family structure, function, and clinical applications. a comprehensive review. *Pharmacol. Ther.* **1998**, *79*, 129-168.
17. Sreedhar, A. S.; Kalmar, E.; Csermely, P. Hsp90 isoforms: functions, expression and clinical importance. *FEBS Lett.* **2004**, *562*, 11-15.
18. Johnson, J. L. Evolution and function of diverse Hsp90 homologs and cochaperone proteins. *BBA - Mol. Cell Res.* **2012**, *1823*, 607-613.
19. Altieri, D. C.; Stein, G. S.; Lian, J. B.; Languino, L. R. TRAP-1, the mitochondrial Hsp90. *BBA - Mol. Cell Res.* **2012**, *1823*, 767-773.
20. Marzec, M.; Eletto, D.; Argon, Y. GRP94: An HSP90-like protein specialized for protein folding and quality control in the endoplasmic reticulum. *BBA - Mol. Cell Res.* **2012**, *1823*, 774-787.
21. McLaughlin, M.; Vandebroek, K. The endoplasmic reticulum protein folding factory and its chaperones: new targets for drug discovery? *Brit. J. Pharmacol.* **2011**, *162*, 328-345.
22. Ali, M. M.; Roe, S. M.; Vaughan, C. K.; Meyer, P.; Panaretou, B.; Piper, P. W.; Prodromou, C.; Pearl, L. H. Crystal structure of an Hsp90-nucleotide-p23/Sba1 closed chaperone complex. *Nature* **2006**, *440*, 1013-1017.
23. Krishna, P.; Gloor, G. The Hsp90 family of proteins in *Arabidopsis thaliana*. *Cell Stress Chaperon.* **2001**, *6*, 238-246.
24. Nemoto, T.; Sato, N.; Iwanari, H.; Yamashita, H.; Takegi, T. Domain structures and immunogenic regions of the 90-kDa heat-shock protein (Hsp90). *J. Biol. Chem.* **1997**, *272*, 26179-26187.
25. Prodromou, C.; Pearl, L. H. Structure and functional relationships of Hsp90. *Curr. Cancer Drug Tar.* **2003**, *3*, 301-323.
26. Young, J. C.; Schneider, C.; Hartl, F. U. In vitro evidence that Hsp90 contains two independent chaperone sites. *FEBS Lett.* **1997**, *418*, 139-143.
27. Dutta, R.; Inouye, M. GHKL, An emergent ATPase/kinase superfamily. *Trends Biochem. Sci.* **2000**, *25*, 24-28.
28. Bergerat, A.; Massy, B. d.; Gadelle, D.; Varoutas, P.-C.; Nicolas, A.; Forterre, P. An atypical topoisomerase II from archaea with implications for meiotic recombination. *Nature* **1997**, *386*, 414-417.
29. Nemoto, T.; Ohara-Nemoto, Y.; Ota, M.; Takagi, T.; Yokoyama, K. Mechanism of dimer formation of the 90-kDa heat-shock protein. *Eur. J. Biochem.* **1995**, *233*, 1-8.
30. Wayne, N.; Bolon, D. B. Dimerization of Hsp90 is required for *in vivo* function: Design and analysis of monomers and dimers. *J. Biol. Chem.* **2007**, *282*, 35386-35395.
31. Blatch, G. L.; Lässle, M. The tetratricopeptide repeat: a structural motif mediating protein-protein interactions. *BioEssays* **1999**, *21*, 932-939.

32. Carrello, A.; Ingley, E.; Minchin, R. F.; Tsai, A.; Ratajczak, T. The Common Tetratricopeptide Repeat Acceptor Site for Steroid Receptor-associated Immunophilins and HOP Is Located in the Dimerization Domain of Hsp90. *J. Biol. Chem.* **1999**, *274*, 2682-2689.
33. D'Andrea, L. D.; Regan, L. TPR proteins: the versatile helix. *Trends Biochem. Sci.* **2003**, *28*, 655-662.
34. Das, A. K.; Cohen, P. T. W.; Barford, D. The structure of the tetratricopeptide repeats of protein phosphatase 5: implications for TRP-mediated protein-protein interactions. *EMBO J.* **1998**, *17*, 1192-1199.
35. Soti, C.; Racz, A.; Csermely, P. A nucleotide-dependent molecular switch controls ATP binding at the C-terminal domain of Hsp90. *J. Biol. Chem.* **2002**, *277*, 7066-7075.
36. Soti, C.; Vermes, A.; Haystead, T. A. J.; Csermely, P. Comparative analysis of the ATP-binding sites of Hsp90 by nucleotide affinity cleavage: a distinct nucleotide specificity of the C-terminal ATP-binding site. *Eur. J. Biochem.* **2003**, *270*, 2421-2428.
37. Huai, Q.; Wang, H.; Liu, Y.; Kim, H.-Y.; Toft, D.; Ke, H. Structures of the N-terminal and middle domains of *E. coli* Hsp90 and conformational changes upon ADP binding. *Structure* **2005**, *13*, 579-590.
38. Ferrarini, M.; Heltai, S.; Zocchi, M. R.; Rugarli, C. Unusual expression and localization of heat-shock proteins in human tumor cells. *Int. J. Cancer* **1992**, *51*, 613-619.
39. Nathan, D. F.; Vos, M. H.; Lindquist, S. *In vivo* functions of the *Saccharomyces Cerevisiae* Hsp90 chaperone. *P. Natl. Acad. Sci.* **1997**, *94*, 12949-12956.
40. Schneider, C.; Sepp-Lorenzino, L.; Nimmesgern, E.; Ouerfelli, O.; Danishefsky, S.; Rosen, N.; Hartl, F. U. Pharmacologic shifting of a balance between protein refolding and degradation mediated by Hsp90. *P. Natl. Acad. Sci.* **1996**, *93*, 14536-14541.
41. Ali, A.; Bharadwaj, S.; O'Carroll, R.; Ovsenek, N. Hsp90 interacts with and regulates the activity of heat shock factor 1 in *Xenopus* oocytes. *Mol. Cell Biol.* **1998**, *18*, 4949-4960.
42. Bharadwaj, S.; Ali, A.; Ovsenek, N. Multiple components of the Hsp90 chaperone complex function in regulation of heat shock factor 1 *in vivo*. *Mol. Cell Biol.* **1999**, *19*, 8033-8041.
43. Guo, Y.; Guettouche, T.; Fenna, M.; Boellmann, F.; Pratt, W. B.; Toft, D. O.; Smith, D. F.; Voellmy, R. Evidence for a mechanism of repression of heat shock factor 1 transcriptional activity by a multichaperone complex. *J. Biol. Chem.* **2001**, *276*, 45791-45799.
44. Kim, H. R.; Kang, H. S.; Kim, H. D. Geldanamycin induces heat shock protein expression through activation of HSF1 in K562 erythroleukemic cells. *IUBMB Life* **1999**, *48*, 429-433.
45. Marchler, G.; Wu, C. Modulation of *Drosophila* heat shock transcription factor activity by the molecular chaperone DroJ1. *EMBO J.* **2001**, *20*, 499-509.
46. Morimoto, R. I. Cells in Stress: Transcriptional Activation of Heat Shock Genes. *Science* **1993**, *259*, 1409-1410.
47. Rabindran, S. K.; Wisniewski, J.; Li, L.; Li, G. C.; Wu, C. Interaction between heat shock factor and Hsp70 is insufficient to suppress induction of DNA-binding activity *in vivo*. *Mol. Cell Biol.* **1994**, *14*, 6552-6560.
48. Shamovsky, I.; Ivannikov, M.; Kandel, E. S.; Gershon, D.; Nudler, E. RNA-mediated response to heat shock in mammalian cells. *Nature* **2006**, *440*, 556-560.
49. Shi, Y.; Mosser, D. D.; Morimoto, R. I. Molecular chaperones as HSF1-specific transcriptional repressors. *Genes Dev.* **1998**, *12*, 654-666.
50. Trinklein, N. D.; Murray, J. I.; Hartman, S. J.; Botstein, D.; Myers, R. M. The role of heat shock transcription factor 1 in the genome-wide regulation of the mammalian heat shock response. *Mol. Biol. Cell* **2004**, *15*, 1254-1261.
51. Whitesell, L.; Bagatell, R.; Falsey, R. The stress response: implications for the clinical development of Hsp90 inhibitors. *Curr. Cancer Drug Tar.* **2003**, *3*, 349-358.
52. Zhao, C.; Hashiguchi, K.; Kondoh, W.; Du, W.; Hata, J.; Yamada, T. Exogenous expression of heat shock protein 90 kDa retards the cell cycle and impairs the heat shock response. *Exp. Cell Res.* **2002**, *275*, 200-214.

53. Zou, J.; Guo, Y.; Guettouche, T.; Smith, D. F.; Voellmy, R. Repression of heat shock transcription factor HSF1 activation by Hsp90 (Hsp90 complex) that forms a stress-sensitive complex with HSF1. *Cell* **1998**, *94*, 471-480.
54. Zou, J.; Rungger, D.; Voellmy, R. Multiple layers of regulation of human heat shock transcription factor 1. *Mol. Cell Biol.* **1995**, *15*, 4319-4330.
55. Peterson, L. B.; Blagg, B. S. J. To fold or not to fold: modulation and consequences of Hsp90 inhibition. *Future Med. Chem.* **2009**, *1*.
56. Lotz, G. P.; Lin, H.; Harst, A.; Obermann, W. M. Aha1 binds to the middle domain of Hsp90, contributes to client protein activation, and stimulates the ATPase activity of the molecular chaperone. *J. Biol. Chem.* **2003**, *278*, 17228-17235.
57. Vaughan, C. K.; Mollapour, M.; Smith, J. R.; Truman, A.; Hu, B.; Good, V. M.; Panaretou, B.; Neckers, L.; Clarke, P. A.; Workman, P.; Piper, P. W.; Prodromou, C.; Pearl, L. H. Hsp90-dependent activation of protein kinases is regulated by chaperone-targeted dephosphorylation of Cdc37. *Mol. Cell* **2008**, *31*, 886-895.
58. Connell, P.; Ballinger, C. A.; Jiang, J., Wu, Y.; Thompson, L. J.; Hohfeld, J.; Patterson, C. The co-chaperone CHIP regulates protein triage decisions mediated by heat-shock proteins. *Nat. Cell Biol.* **2001**, *3*, 93-96.
59. Murata, S.; Minami, Y.; Minami, M.; Chiba, T.; Tanaka, K. CHIP is a chaperone-dependent E3 ligase that ubiquitylates unfolded protein. *EMBO Rep.* **2001**, *2*, 1133-1138.
60. Hatakeyama, S.; Matsumoto, M.; Yada, M.; Nakayama, K. I. Interaction of U-box-type ubiquitin-protein ligases (E3s) with molecular chaperones. *Genes Cells* **2004**, *9*, 533-548.
61. Hoffmann, K.; Handschumacher, R. E. Cyclophilin-40: evidence for a dimeric complex with hsp90. *Biochem. J.* **1995**, *307*, 5-8.
62. Pirkl, F.; Buchner, J. Functional analysis of the Hsp90-associated human peptidyl prolyl cis/trans isomerases FKBP51, FKBP52 and Cyp40. *J. Mol. Biol.* **2001**, *308*, 795-806.
63. Chen, S.; Sullivan, W. P.; Toft, D. O.; Smith, D. F. Differential interactions of p23 and the TRP-containing proteins Hop, Cyp40, FKBP52 and FKBP51 with Hsp90 mutants. *Cell Stress Chaperon.* **1998**, *3*, 118-129.
64. Chen, S.; Smith, D. F. Hop as an adaptor in the heat shock protein 70 (Hsp70) and hsp90 chaperone machinery. *J. Biol. Chem.* **1998**, *273*, 35194-35200.
65. Johnson, B. D.; Schumacher, R. J.; Ross, E. D.; Toft, D. O. Hop modulates hsp70/hsp90 interactions in protein folding. *J. Biol. Chem.* **1998**, *273*, 3679-3686.
66. Hernández, M. P.; Chadli, A.; Toft, D. O. Hsp40 binding is the first step in the Hsp90 chaperoning pathway for the progesterone receptor. *J. Biol. Chem.* **2002**, *277*, 11873-11881.
67. Minami, Y.; Minami, M. Hsc70/Hsp40 chaperone system mediates the Hsp90-dependent refolding of firefly luciferase. *Genes Cells* **1999**, *4*, 721-729.
68. Freeman, B. C.; Morimoto, R. I. The human cytosolic molecular chaperones hsp90, hsp70 (hsc70) and hdj-1 have distinct roles in recognition of a non-native protein and protein refolding. *EMBO J.* **1996**, *15*, 2969-2979.
69. Frydman, J. Folding of newly translated proteins *in vivo*: the role of molecular chaperones. *Ann. Rev. Biochem.* **2001**, *70*, 603-647.
70. Hutchison, K. A.; Dittmar, K. D.; Czar, M. J.; Pratt, W. B. Proof that hsp70 is required for assembly of the glucocorticoid receptor into a heterocomplex with hsp90. *J. Biol. Chem.* **1994**, *269*, 5043-5049.
71. Alekseev, O. M.; Widgren, E. E.; Richardson, R. T.; O'Rand, M. G. Association of NASP with HSP90 in mouse spermatogenic cells: stimulation of ATPase activity and transport of linker histones into nuclei. *J. Biol. Chem.* **2005**, *280*, 2904-2911.
72. Chen, M.-S.; Silverstein, A. M.; Pratt, W. B.; Chinkers, M. The tetratricopeptide repeat domain of protein phosphatase 5 mediates binding to glucocorticoid receptor heterocomplexes and acts as a dominant negative mutant. *J. Biol. Chem.* **1996**, *271*, 32315-32320.

73. Conde, R.; Xavier, J.; McLoughlin, C.; Chinkers, M.; Ovsenek, N. Protein phosphatase 5 is a negative modulator of heat shock factor 1. *J. Biol. Chem.* **2005**, *280*, 28989-28996.
74. Silverstein, A. M.; Galigniana, M. D.; Chen, M. S.; Owens Grillo, J. K.; Chinkers, M.; Pratt, W. B. Protein phosphatase 5 is a major component of glucocorticoid receptor.hsp90 complexes with properties of an FK506-binding immunophilin. *J. Biol. Chem.* **1997**, *272*, 16224-16230.
75. Catlett, M. G.; Kaplan, K. B. Sgt1p is a unique co-chaperone that acts as a client adaptor to link Hsp90 to Skp1p. *J. Biol. Chem.* **2006**, *281*, 33739-33748.
76. Millson, S. H.; Vaughan, C. K.; Zhai, C.; Ali, M. M. U.; Panaretou, B.; Piper, P. W.; Pearl, L. H.; Prodromou, C. Chaperone ligand-discrimination by the TPR-domain protein Tah1. *Biochem. J.* **2008**, *413*, 261-268.
77. Fan, A. C.; Bhangoo, M. K.; Young, J. C. Hsp90 functions in the targeting and outer membrane translocation steps of Tom70-mediated mitochondrial import. *J. Biol. Chem.* **2006**, *281*, 33313-33324.
78. Young, J. C.; Hoogenraad, N. J.; Hartl, F. U. Molecular chaperones Hsp90 and Hsp70 deliver preproteins to the mitochondrial import receptor Tom70. *Cell* **2003**, *112*, 41-50.
79. Brychzy, A.; Rein, T.; Winklhofer, K. F.; Hartl, F. U.; Young, J. C.; Obermann, W. M. Cofactor Tpr2 combines two TPR domains and a J domain to regulate the Hsp70/Hsp90 chaperone system. *EMBO J.* **2003**, *22*, 3613-3623.
80. Jascur, T.; Brickner, H.; Salles-Passador, I.; Barbier, V.; El Khissiin, A.; Smith, B.; Fotedar, R.; Fotedar, A. Regulation of p21(WAF1/CIP1) stability by WISp39, a Hsp90 binding TPR protein. *Mol. Cell* **2005**, *17*, 237-249.
81. Moffatt, N. S.; Bruinsma, E.; Uhl, C.; Obermann, W. M.; Toft, D. O. Role of the cochaperone Tpr2 in Hsp90 chaperoning. *Biochemistry* **2008**, *47*, 8203-8213.
82. Caplan, A. J. What is a co-chaperone? *Cell Stress Chaperon.* **2003**, *8*, 105-107.
83. Hohfeld, J.; Jentsch, S. GrpE-like regulation of the Hsc70 chaperone by the anti-apoptotic protein BAG-1. *EMBO J.* **1997**, *16*, 6209-6216.
84. Sondermann, H.; Scheufler, C.; Schneider, C.; Hohfeld, J.; Hartl, F. U.; Moarefi, I. Structure of a Bag/Hsc70 complex: convergent functional evolution of Hsp70 nucleotide exchange factors. *Science* **2001**, *291*, 1553-1557.
85. Forsythe, H. L.; Jarvis, J. L.; Turner, J. W.; Elmore, L. W.; Holt, S. E. Stable association of Hsp90 and p23, but not Hsp70, with active human telomerase. *J. Biol. Chem.* **2001**, *19*, 15571-15574.
86. Kosano, H.; Stensgard, B.; Charlesworth, M. C.; McMahon, N.; Toft, D. The assembly of progesterone receptor-hsp90 complexes using purified proteins. *J. Biol. Chem.* **1998**, *273*, 32973-32979.
87. Murphy, P. J. M.; Kanelakis, K. C.; Galigniana, M. D.; Morishima, Y.; Pratt, W. B. Stoichiometry, abundance, and functional significance of the Hsp90/Hsp70-based multiprotein chaperone machinery in reticulocyte lysate. *J. Biol. Chem.* **2001**, *276*, 30092-30098.
88. Prodromou, C.; Panaretou, B.; Chohan, S.; Siligardi, G.; O'Brien, R.; Ladbury, J. E.; Roe, S. M.; Piper, P. W.; Pearl, L. H. The ATPase cycle of Hsp90 drives a molecular 'clamp' via transient dimerization of the N-terminal domains. *EMBO J.* **2000**, *19*, 4383-4392.
89. Ratajczak, T.; Carrello, A. Cyclophilin 40 (CyP-40), mapping of its Hsp90 binding domain and evidence that FKBP52 competes with CyP-40 for Hsp90 binding. *J. Biol. Chem.* **1996**, *271*, 2961-2965.
90. Hessling, M.; Richter, K.; Buchner, J. Dissection of the ATP-induced conformational cycle of the molecular chaperone Hsp90. *Nat. Struct. Mol. Biol.* **2009**, *16*, 287-293.
91. Krukenberg, K. A.; Forster, F.; Rice, L. M.; Sali, A.; Agard, D. A. Multiple conformations of E. coli Hsp90 in solution: insights into the conformational dynamics of Hsp90. *Structure* **2008**, *16*, 755-765.
92. Shiau, A. K.; Harris, S. F.; Southworth, D. R.; Agard, D. A. Structural Analysis of E. coli hsp90 reveals dramatic nucleotide-dependent conformational rearrangements. *Cell* **2006**, *127*, 329-340.

93. Soroka, J.; Wandinger, Sebastian K.; Mäusbacher, N.; Schreiber, T.; Richter, K.; Daub, H.; Buchner, J. Conformational switching of the molecular chaperone Hsp90 via regulated phosphorylation. *Mol. Cell* **2012**, *45*, 517-528.
94. Colombo, G.; Morra, G.; Meli, M.; Verkhivker, G. Understanding ligand-based modulation of the Hsp90 molecular chaperone dynamics at atomic resolution. *P. Natl. Acad. Sci.* **2008**, *105*, 7976-7981.
95. Mollapour, M.; Neckers, L. Post-translational modifications of Hsp90 and their contributions to chaperone regulation. *BBA - Mol. Cell Res.* **2012**, *1823*, 648-655.
96. Scroggins, B. T.; Neckers, L. Post-translational modification of heat-shock protein 90: impact on chaperone function. *Expert. Opin. Drug Discov.* **2007**, *2*, 1403-1414.
97. Zhao, Y.-G.; Gilmore, R.; Leone, G.; Coffey, M. C.; Weber, B.; Lee, P. W. K. Hsp90 Phosphorylation Is Linked to Its Chaperoning Function. *J. Biol. Chem.* **2001**, *276*, 32822-32827.
98. Mollapour, M.; Tsutsumi, S.; Donnelly, A. C.; Beebe, K.; Tokita, M. J.; Lee, M.-J.; Lee, S.; Morra, G.; Bourboulia, D.; Scroggins, B. T.; Colombo, G.; Blagg, B. S.; Panaretou, B.; Stetler-Stevenson, W. G.; Trepel, J. B.; Piper, P. W.; Prodromou, C.; Pearl, L. H.; Neckers, L. Swe1^{Weel}-dependent tyrosine phosphorylation of Hsp90 regulates distinct facets of chaperone function. *Mol. Cell* **2010**, *37*, 333-343.
99. Lei, H.; Venkatakrishnan, A.; Yu, S.; Kazlauskas, A. Protein Kinase A-dependent Translocation of Hsp90 α Impairs Endothelial Nitric-oxide Synthase Activity in High Glucose and Diabetes. *J. Biol. Chem.* **2007**, *282*, 9364-9371.
100. Duval, M.; Le Bœuf, F.; Huot, J.; Gratton, J.-P. Src-mediated phosphorylation of Hsp90 in response to vascular endothelial growth factor (VEGF) is required for VEGF receptor-2 signaling to endothelial NO synthase. *Mol. Biol. Cell* **2007**, *18*, 4659-4668.
101. Ogiso, H.; Kagi, N.; Matsumoto, E.; Nishimoto, M.; Arai, R.; Shirouzu, M.; Mimura, J.; Fujii-Kuriyama, Y.; Yokoyama, S. Phosphorylation Analysis of 90 kDa Heat Shock Protein within the Cytosolic Arylhydrocarbon Receptor Complex†. *Biochemistry* **2004**, *43*, 15510-15519.
102. Mollapour, M.; S. Tsutsumi; Kim, Y. S.; Trepel, J.; Neckers, L. Casein kinase 2 phosphorylation of Hsp90 threonine 22 modulates chaperone function and drug sensitivity. *Oncotarget* **2011**, *2*, 407-417.
103. Scroggins, B. T.; Robzyk, K.; Wang, D.; Marcu, M. G.; Tsutsumi, S.; Beebe, K.; Cotter, R. J.; Felts, S.; Toft, D.; Karnitz, L.; Rosen, N.; Neckers, L. An Acetylation Site in the Middle Domain of Hsp90 Regulates Chaperone Function. *Mol. Cell* **2007**, *25*, 151-159.
104. Yang, Y.; Rao, R.; Shen, J.; Tang, Y.; Fiskus, W.; Nechtman, J.; Atadja, P.; Bhalla, K. Role of Acetylation and Extracellular Location of Heat Shock Protein 90 α in Tumor Cell Invasion. *Cancer Res.* **2008**, *68*, 4833-4842.
105. Chen, W.-Y.; Chang, F.-R.; Huang, Z.-Y.; Chen, J.-H.; Wu, Y.-C.; Wu, C.-C. Tubocapsenolide A, a Novel Withanolide, Inhibits Proliferation and Induces Apoptosis in MDA-MB-231 Cells by Thiol Oxidation of Heat Shock Proteins. *J. Biol. Chem.* **2008**, *283*, 17184-17193.
106. Martínez-Ruiz, A.; Villanueva, L.; de Orduña, C. G.; López-Ferrer, D.; Higuera, M. Á.; Tarín, C.; Rodríguez-Crespo, I.; Vázquez, J.; Lamas, S. S-nitrosylation of Hsp90 promotes the inhibition of its ATPase and endothelial nitric oxide synthase regulatory activities. *P. Natl. Acad. Sci.* **2005**, *102*, 8525-8530.
107. Morra, G.; Verkhivker, G.; Colombo, G. Modeling Signal Propagation Mechanisms and Ligand-Based Conformational Dynamics of the Hsp90 Molecular Chaperone Full-Length Dimer. *PLoS Comput. Biol.* **2009**, *5*, e1000323.
108. Retzlaff, M.; Stahl, M.; Eberl, H. C.; Lagleder, S.; Beck, J.; Kessler, H.; Buchner, J. Hsp90 is regulated by a switch point in the C-terminal domain. *EMBO Rep.* **2009**, *10*, 1147-1153.
109. Blank, M.; Mandel, M.; Keisari, Y.; Meruelo, D.; Lavie, G. Enhanced ubiquitinylation of heat shock protein 90 as a potential mechanism for mitotic cell death in cancer cells induced with hypericin. *Cancer Res.* **2003**, *63*, 8241-8247.

110. Kundrat, L.; Regan, L. Identification of residues on Hsp70 and Hsp90 ubiquitinated by the cochaperone CHIP. *J. Mol. Biol.* **2010**, *395*, 587-594.
111. Ballinger, C. A.; Connell, P.; Y., W.; Hu, Z.; Thompson, L. J.; Yin, L. Y.; Patterson, C. Identification of CHIP, a novel tetratricopeptide repeat-containing protein that interacts with heat shock proteins and negatively regulates chaperone functions. *mol. Cell Biol.* **1999**, *19*, 4535–4545.
112. Workman, P. Combinatorial attack on multistep oncogenesis by inhibiting the Hsp90 molecular chaperone. *Cancer Lett.* **2004**, *206*, 149-157.
113. Taldone, T.; Gozman, A.; Maharaj, R.; Chiosis, G. Targeting Hsp90: small-molecule inhibitors and their clinical development. *Curr. Opin. Pharmacol.* **2008**, *8*, 370-374.
114. Muchowski, P. J. Protein misfolding, amyloid formation, and neurodegeneration: a critical role for molecular chaperones? *Neuron* **2002**, *35*, 9-12.
115. Muchowski, P. J.; Wacker, J. L. Modulation of neurodegeneration by molecular chaperones. *Nat. Rev. Neurosci.* **2005**, *6*, 11-22.
116. Bishop, S. C.; Burlison, J. A.; Blagg, B. S. J. Hsp90: a novel target for the disruption of multiple signaling cascades. *Curr. Cancer Drug Tar.* **2007**, *7*, 369-388.
117. Hanahan, D.; Weinberg, R. A. The hallmarks of cancer. *Cell* **2000**, *100*, 57-70.
118. Hanahan, D.; Weinberg, Robert A. Hallmarks of cancer: The next generation. *Cell* **2011**, *144*, 646-674.
119. Workman, P.; Burrows, F.; Neckers, L.; Rosen, N. Drugging the cancer chaperone Hsp90: Combinatorial therapeutic exploitation of oncogene addiction and tumor stress. *Ann. NY Acad. Sci.* **2007**, *1113*, 202-216.
120. Neckers, L. Chaperoning oncogenes: Hsp90 as a target of geldanamycin. *Handb. Exp. Pharmacol.* **2006**, *172*, 259-277.
121. Jameel, A.; Skilton, R. A.; Campbell, T. A.; Chander, S. K.; Coombes, R. C.; Luqmani, Y. A. Clinical and biological significance of Hsp89 α in human breast cancer. *Int. J. Cancer* **1992**, *50*, 409-415.
122. Yufu, Y.; Nishimura, J.; Nawata, H. High constitutive expression of heat shock protein 90 α in human acute leukemia cells. *Leuk. Res.* **1992**, *16*, 597-605.
123. Pick, E.; Kluger, Y.; Giltmane, J. M.; Moeder, C.; Camp, R. L.; Rimm, D. L.; Kluger, H. M. High HSP90 expression is associated with decreased survival in breast cancer. *Cancer Res.* **2007**, *67*, 2932-2937.
124. Chiosis, G.; Huezo, H.; Rosen, N.; Mimnaugh, E.; Whitesell, L.; Neckers, L. 17AAG: low target binding affinity and potent cell activity - finding an explanation. *Mol. Cancer Ther.* **2003**, *2*, 123-129.
125. Kamal, A.; Thao, L.; Sensintaffar, J.; Zhang, L.; Boehm, M. F.; Fritz, L. C.; Burrows, F. J. A high-affinity conformation of Hsp90 confers tumour selectivity on Hsp90 inhibitors. *Nature* **2003**, *425*, 407-410.
126. Ross, C. A.; Poirier, M. A. Protein aggregation and neurodegenerative disease. *Nat. Med.* **2004**, S10-S17.
127. Chaudhury, S.; Welch, T. R.; Blagg, B. S. J. Hsp90 as a target for drug development. *ChemMedChem* **2006**, *1*, 1331-1340.
128. Mattson, M. P. Pathways towards and away from Alzheimer's disease. *Nature* **2004**, *430*, 631-639.
129. Selkoe, D. J. Alzheimer disease: mechanistic understanding predicts novel therapies. *Ann. Intern. Med.* **2004**, *140*, 627-638.
130. Akiyama, H.; Barger, S.; Barnum, S.; Bradt, B.; Bauer, J.; al., G. M. C. e. Inflammation and Alzheimer's disease. *Neurobiol. Aging* **2000**, *21*, 383-421.
131. Lambert, M. P.; Barlow, A. K.; Chromy, B. A.; Edwards, C.; Freed, R.; Liosatos, M.; Morgan, T. E.; Rozovsky, I.; Trommer, B.; Viola, K. L.; Wals, P.; Zhang, C.; Finch, C. E.; Krafft, G. A.;

- Klein, W. L. Diffusible, nonfibrillar ligands derived from A β 1-42 are potent central nervous system neurotoxins. *P. Natl. Acad. Sci.* **1998**, *95*, 6448-6453.
132. Walsh, D. M.; Klyubin, I.; Fadeeva, J. V.; Cullen, W. K.; Anwyl, R.; Wolfe, M. S.; Rowan, M. J.; Selkoe, D. J. Naturally secreted oligomers of amyloid β protein potently inhibit hippocampal long-term potentiation *in vivo*. *Nature* **2002**, *416*, 535-539.
133. Yan, Y.; Wang, C. Protection mechanisms against A β 42 aggregation *Curr. Alzheimer Res.* **2008**, *5*, 548-554.
134. Dou, F.; Netzer, W. J.; Tanemura, K.; Li, F.; Hartl, U.; Takashima, A.; Gouras, G. K.; Greengard, P.; Xu, H. Chaperones increase association of Tau protein with microtubules. *P. Natl. Acad. Sci.* **2003**, *100*, 721-726.
135. Richter-Landsberg, C. The cytoskeleton in oligodendrocytes: microtubule dynamics in health and disease. *J. Mol. Neurosci.* **2008**, *35*, 55-63.
136. Dickey, C. A.; Kamal, A.; Lundgren, K.; Klosak, N.; Bailey, R. M.; Dunmore, J.; Ash, P.; Shoraka, S.; Zlatkovic, J.; Eckman, C. B.; Patterson, C.; Dennis, W. D.; Nahman Jr, N. S.; Hutton, M.; Burrows, F.; Petrucelli, L. The high-affinity Hsp90-CHIP complex recognizes and selectively degrades phosphorylated tau client proteins. *J. Clin. Invest.* **2007**, *117*, 648-658.
137. Dickey, C. A.; Eriksen, J.; Kamal, A.; Burrows, F.; Kasibhatla, S.; Eckman, C. B.; Hutton, M.; Petrucelli, L. Development of a high throughput drug screening assay for the detection of changes in tau levels - proof of concept with Hsp90 inhibitors. *Curr. Alzheimer Res.* **2005**, *2*, 231-238.
138. Evans, C. G.; Wisen, S.; Gestwicki, J. E. Heat shock proteins 70 and 90 inhibit early stages of amyloid β -(1-42) aggregation *in vitro*. *J. Biol. Chem.* **2006**, *281*, 33182-33191.
139. Ansar, S.; Burlison, J. A.; Hadden, M. K.; Yu, X. M.; Desino, K. E.; Bean, J.; Neckers, L.; Audus, K. L.; Michaelis, M. L.; Blagg, B. S. J. A non-toxic Hsp90 inhibitor protects neurons from A β -induced toxicity *Bioorg. Med. Chem. Lett.* **2007**, *17*, 1984-1990.
140. DeBoer, C.; Meulman, R. J.; Wnuk, R. J.; Peterson, D. H. Geldanamycin, a new antibiotic. *J. Antibiotics* **1970**, *23*, 442-447.
141. Whitesell, L.; Mimnaugh, E. G.; De Costa, B.; Myers, C. E.; Neckers, L. M. Inhibition of heat shock protein HSP90-pp60v-src heteroprotein complex formation by benzoquinone ansamycins: essential role for stress proteins in oncogenic transformation. *P. Natl. Acad. Sci.* **1994**, *91*, 8324-8328.
142. Schulte, T. W.; Akinaga, S.; Soga, S.; Sullivan, W.; Stensgard, B.; Toft, D.; Neckers, L. M. Antibiotic Radicicol Binds to the N-Terminal Domain of Hsp90 and Shares Important Biological Activities with Geldanamycin. Cell Stress Chaperones. *Cell Stress Chaperon.* **1998**, *3*, 100-108.
143. Sharma, S. V.; Agatsuma, T.; Nakano, H. Targeting of the protein chaperone, HSP90, by the transformation suppressing agent, radicicol. *Oncogene* **1998**, *16*, 2639-2645.
144. Benchekroun, N. M.; Myers, C. E.; Sinha, B. K. Free radical formation by ansamycin benzoquinone in human breast tumor cells: implications for cytotoxicity and resistance. *Free Radic. Biol. Med.* **1994**, *17*, 191-200.
145. Samuni, Y.; Ishii, H.; Hyodo, F.; Samuni, U.; Krishna, M. C.; Goldstein, S.; Mitchell, J. B. Reactive oxygen species mediate hepatotoxicity induced by the Hsp90 inhibitor geldanamycin and its analogues. *Free Radic. Biol. Med.* **2010**, *48*, 1559-1563.
146. Banerji, U.; O'Donnell, A.; Scurr, M.; Pacey, S.; Stapleton, S.; Asad, Y.; Simmons, L.; Maloney, A.; Raynaud, F.; Campbell, M.; Walton, M.; Lakhani, S.; Kaye, S.; Workman, P.; Judson, I. Phase I pharmacokinetic and pharmacodynamic study of 17-allylamino, 17-demethoxygeldanamycin in patients with advanced malignancies. *J. Clin. Oncol.* **2005**, *23*, 4152-4161.
147. Modi, S.; Stopeck, A. T.; Gordon, M. S.; Mendelson, D.; Solit, D. B.; Bagatell, R.; Weining, M.; Wheler, J.; Rosen, N.; Norton, L.; Cropp, G. F.; Johnson, R. G.; Hannah, A. L.; Hudis, C. A. Combination of Trastuzumab and Tanespimycin (17-AAG, KOS-953) is safe and active in Trastuzumab-refractory Her2 overexpressing breast cancer: A Phase I dose-escalation study. *J. Clin. Oncol.* **2007**, *25*, 5410-5417.

148. Schnur, R. C.; Corman, M. L.; Gallaschun, R. J.; Cooper, B. A.; Dee, M. F.; Doty, J. L.; Muzzi, M. L.; DiOrio, C. I.; Barbacci, E. G.; Miller, P. E.; Pollack, V. A.; Savage, D. M.; Sloan, D. E.; Pustilnik, L. R.; Moyer, J. D.; Moyer, M. P. erbB-2 Oncogene inhibition by geldanamycin derivatives: synthesis, mechanism of action, and structure-activity relationships. *J. Med. Chem.* **1995**, *38*, 3813-3820.
149. Schnur, R. C.; Corman, M. L.; Gallaschun, R. J.; Cooper, B. A.; Dee, M. F.; Doty, J. L.; Muzzi, M. L.; Moyer, J. D.; DiOrio, C. I.; Barbacci, E. G.; Miller, P. E.; O'Brien, A. T.; Foster, M. J.; Pollack, B. A.; Savage, D. M.; Sloan, D. E.; Pustilnik, L. R.; Moyer, M. P. Inhibition of the oncogene product p185erbB-2 *in vitro* and *in vivo* by geldanamycin and dihydrogeldanamycin derivatives. *J. Med. Chem.* **1995**, *1995*, 3806-3812.
150. Biamonte, M. A.; Van de Water, R.; Arndt, J. W.; Scannevin, R. H.; Perret, D.; Lee, W. Heat shock protein 90: inhibitors in clinical trials. *J. Med. Chem.* **2010**, *53*, 3-17.
151. Gao, Z.; Garcia-Echeverria, C.; Jensen, M. R. Hsp90 inhibitors: Clinical development and future opportunities in oncology therapy. *Curr. Opin. Drug Discov. Devel.* **2010**, *13*, 193-202.
152. Kim, Y. S.; Alarcon, S. V.; Lee, S.; Lee, M. J.; Giaccone, G.; Neckers, L.; Trepel, J. B. Update on Hsp90 inhibitors in clinical trial. *Curr. Top. Med. Chem.* **2009**, *9*, 1479-1492.
153. Banerji, U. Preclinical and Clinical Activity of the Molecular Chaperone Inhibitor 17-Allylamino, 17-Demethoxygeldanamycin in Malignant Melanoma. *Proc. Am. Assoc. Cancer Res.* **2003**, *44*, 677.
154. Sausville, E. A. Clinical Development of 17-Allylamino, 17-demethoxygeldanamycin. *Curr. Cancer Drug Tar.* **2003**, *3*, 377-383.
155. Brandt, G. E.; Blagg, B. S. J. Alternate strategies of Hsp90 modulation for the treatment of cancer and other diseases. *Curr. Top. Med. Chem.* **2009**, *9*, 1447-1461.
156. Marcu, M. G.; Chadli, A.; Bouhouche, I.; Catelli, M. G.; Neckers, L. The heat shock protein 90 antagonist novobiocin interacts with a previously unrecognized ATP-binding domain in the carboxyl terminus of the chaperone. *J. Biol. Chem.* **2000**, *2000*, 37181-37186.
157. Marcu, M. G.; Schulte, T. W.; Neckers, L. Novobiocin and related coumarins and depletion of heat shock protein 90-dependent signalling proteins. *J. Natl. Cancer Inst.* **2000**, *92*, 242-248.
158. Garnier, C.; Lafitte, D.; Tsvetkov, P. O.; Barbier, P.; Leclerc-Devin, J.; Millot, J. M.; Briand, C.; Makarov, A. A.; Catelli, M. G.; Peyrot, V. Binding of ATP to heat shock protein 90: evidence for an ATP-binding site in the C-terminal domain. *J. Biol. Chem.* **2002**, *277*, 12208-12214.
159. Yun, B.-G.; Huang, W.; Leach, N.; Hartson, S. D.; Matts, R. L. Novobiocin induces a distinct conformation of Hsp90 and alters Hsp90-cochaperone-client interactions. *Biochemistry* **2004**, *43*, 8217-8229.
160. Matts, R. L.; Manjarrez, J. R. Assays for identification of Hsp90 inhibitors and biochemical methods for discriminating their mechanism of action. *Curr. Top. Med. Chem.* **2009**, *9*, 1462-1478.
161. Allan, R. K.; Mok, D.; Ward, B. K.; Ratajczak, T. Modulation of chaperone function and cochaperone interaction by novobiocin in the C-terminal domain of Hsp90: evidence that coumarin antibiotics disrupt Hsp90 dimerization. *J. Biol. Chem.* **2006**, *281*, 7161-7171.
162. Burlison, J. A.; Avila, C.; Vielhauer, G.; Lubbers, D. J.; Holzbeierlein, J.; Blagg, B. S. J. Development of novobiocin analogues that manifest anti-proliferative activity against several cancer cell lines. *J. Org. Chem.* **2008**, *73*, 2130-2137.
163. Burlison, J. A.; Blagg, B. S. J. Synthesis and Evaluation of Coumermycin A1 Analogues that Inhibit the Hsp90 Protein Folding Machinery. *Org. Lett.* **2006**, *8*, 4855-4858.
164. Burlison, J. A.; Neckers, L.; Smith, A. B.; Maxwell, A.; Blagg, B. S. J. Novobiocin: Redesigning a DNA Gyrase Inhibitor for Selective Inhibition of Hsp90. *J. Am. Chem. Soc.* **2006**, *128*, 15529-15536.
165. Donnelly, A.; Blagg, B. S. J. Novobiocin and additional inhibitors of the Hsp90 C-terminal nucleotide binding pocket. *Curr. Med. Chem.* **2008**, *15*, 2702-2717.

166. Donnelly, A.; Mays, J. R.; Burlison, J. A.; Nelson, J. T.; Vielhauer, G.; Holzbeierlein, J.; Blagg, B. S. J. The design, synthesis, and evaluation of coumarin ring derivatives of the novobiocin scaffold that exhibit antiproliferative activity. *J. Org. Chem.* **2008**, *73*, 8901-8920.
167. Donnelly, A. C.; Zhao, H.; Reddy, K. B.; Blagg, B. S. J. Cytotoxic sugar analogues of an optimized novobiocin scaffold. *Med. Chem. Comm.* **2010**, *1*, 165-170.
168. Shelton, S. N.; Shawgo, M. E.; Matthews, S. B.; Lu, Y.; Donnelly, A. C.; Szabla, K.; Tanol, M.; Vielhauer, G. A.; Rajewski, R. A.; Matts, R. L.; Blagg, B. S.; Robertson, J. D. KU135, a novel novobiocin-derived C-terminal inhibitor of the 90-kDa heat shock protein, exerts potent antiproliferative effects in human leukemic cells. *Mol. Pharmacol.* **2009**, *76*, 1314-1322.
169. Zhao, H.; B., R. K.; Blagg, B. S. J. Synthesis and Evaluation of Noviose Replacements on Novobiocin That Manifest Antiproliferative Activity. *ACS Med. Chem. Lett* **2010**, *1*, 311-315.
170. Yu, X. M.; Shen, G.; Neckers, L.; Blake, H.; Holzbeierlein, J.; Cronk, B.; Blagg, B. S. Hsp90 inhibitors identified from a library of novobiocin analogues. *J. Am. Chem. Soc.* **2005**, *127*, 12778-12779.
171. Kusuma, B. R.; Peterson, L. B.; Zhao, H.; Vielhauer, G.; Holzbeierlein, J.; Blagg, B. S. J. Targeting the heat shock protein 90 dimer with dimeric inhibitors. *J. Med. Chem.* **2011**, *54*, 6234-6253.
172. Zhao, H.; Donnelly, A. C.; Kusuma, B. R.; Brandt, G. E. L.; Brown, D.; Rajewski, R. A.; Vielhauer, G.; Holzbeierlein, J.; Cohen, M. S.; Blagg, B. S. J. Engineering an Antibiotic to Fight Cancer: Optimization of the Novobiocin Scaffold to Produce Anti-proliferative Agents. *J. Med. Chem.* **2011**, *54*, 3839-3853.
173. Peterson, L. B.; Blagg, B. S. J. Click chemistry to probe Hsp90: Synthesis and evaluation of a series of triazole-containing novobiocin analogues. *Bioorg. Med. Chem. Lett.* **2010**, *20*, 3957-3960.
174. Palermo, C. M.; Westlake, C. A.; Gasiewicz, T. A. Epigallocatechin gallate inhibits aryl hydrocarbon receptor gene transcription through an indirect mechanism involving binding to a 90 kDa heat shock protein. *Biochemistry* **2005**, *44*, 5041-5052.
175. Sreedhar, A. S.; Soti, C.; Csermely, P. Inhibition of Hsp90: a new strategy for inhibiting protein kinases. *Biochim. Biophys. Acta.* **2004**, *1697*, 233-242.
176. Itoh, H.; Ogura, M.; Komatsuda, A.; Wakui, H.; Miura, A. B.; Tashima, Y. A novel chaperone-activity-reducing mechanism of the 90-kDa molecular chaperone Hsp90. *Biochem. J.* **1999**, *343*, 697-703.
177. Kimura, H.; Yukitake, H.; Tajima, Y.; Suzuki, H.; Chikatsu, T.; Morimoto, S.; Funabashi, Y.; Omae, H.; Ito, T.; Yoneda, Y.; Takizawa, M. ITZ-1, a Client-selective Hsp90 inhibitor, efficiently induces heat shock factor 1 activation. *Chem. Biol.* **2010**, *17*, 18-27.
178. Roe, S. M.; Ali, M. M.; Meyer, P.; Vaughan, C. K.; Panaretou, B.; Piper, P. W.; Prodromou, C.; Pearl, L. H. The Mechanism of Hsp90 regulation by the protein kinase-specific cochaperone p50(cdc37). *Cell* **2004**, *116*, 87-98.
179. Siligardi, G.; Panaretou, B.; Meyer, P.; Singh, S.; Woolfson, D. N.; Piper, P. W.; Pearl, L. H.; Prodromou, C. Regulation of Hsp90 ATPase activity by the co-chaperone Cdc37p/p50^{cdc37}. *J. Biol. Chem.* **2002**, *277*, 20151-20159.
180. Smith, J. R.; Clarke, P. A.; de Billy, E.; Workman, P. Silencing the cochaperone CDC37 destabilizes kinase clients and sensitizes cancer cells to HSP90 inhibitors. *Oncogene* **2008**, *28*, 157-169.
181. Sreeramulu, S.; Gande, S. L.; Göbel, M.; Schwalbe, H. Molecular mechanism of inhibition of the human protein complex Hsp90–Cdc37, a kinome chaperone–cochaperone, by triterpene Celastrol. *Angew. Chem. Int. Ed.* **2009**, *48*, 5853-5855.
182. Trott, A.; West, J. D.; Klaić, L.; Westerheide, S. D.; Silverman, R. B.; Morimoto, R. I.; Morano, K. A. Activation of heat shock and antioxidant responses by the natural product Celastrol: Transcriptional signatures of a thiol-targeted molecule. *Mol. Biol. Cell* **2008**, *19*, 1104-1112.

183. Westerheide, S. D.; Bosman, J. D.; Mbadugha, B. N. A.; Kawahara, T. L. A.; Matsumoto, G.; Kim, S.; Gu, W.; Devlin, J. P.; Silverman, R. B.; Morimoto, R. I. Celastrols as inducers of the heat shock response and cytoprotection. *J. Biol. Chem.* **2004**, *279*, 56053-56060.
184. Davenport, J.; Manjarrez, J. R.; Peterson, L.; Krumm, B.; Blagg, B. S. J.; Matts, R. L. Gambogic Acid, a natural product inhibitor of Hsp90. *J. Nat. Prod.* **2011**, *74*, 1085-1092.
185. Yi, F.; Regan, L. A Novel class of small molecule inhibitors of Hsp90. *ACS Chem. Biol.* **2008**, *3*, 645-654.
186. Yi, F.; Zhu, P.; Southall, N.; Inglese, J.; Austin, C. P.; Zheng, W.; Regan, L. An AlphaScreenTM-based high-throughput screen to identify inhibitors of Hsp90-cochaperone interaction. *J. Biomol. Screen.* **2009**, *14*, 273-281.
187. Conde, R.; Belak, Z. R.; Nair, M.; O'Carroll, R. F.; Ovsenek, N. Modulation of Hsf1 activity by novobiocin and geldanamycin. *Biochem. Cell Biol.* **2009**, *87*, 845-851.
188. McCollum, A. K.; TenEyck, C. J.; Stensgard, B.; Morlan, B. W.; Ballman, K. V.; Jenkins, R. B.; Toft, D. O.; Erlichman, C. P-Glycoprotein-mediated resistance to Hsp90-directed therapy is eclipsed by the heat shock response. *Cancer Res.* **2008**, *68*, 7419-7427.
189. Bagatell, R.; Paine-Murrieta, G. D.; Taylor, C. W.; Pulcini, E. J.; Akinaga, S.; Benjamin, I. J.; Whitesell, L. Induction of a heat shock factor 1-dependent stress response alters the cytotoxic activity of Hsp90-binding agents. *Clin. Cancer Res.* **2000**, *6*, 3312-3318.
190. Zuo, J.; Rungger, D.; Voellmy, R. Multiple layers of regulation of human heat shock transcription factor 1. *Mol. Cell Biol.* **1995**, *15*, 4319-4330.
191. Xia, W.; Voellmy, R. Hyperphosphorylation of heat shock transcription factor 1 is correlated with transcriptional competence and slow dissociation of active factor trimers. *J. Biol. Chem.* **1997**, *272*, 4094-4102.
192. Holzbeierlein, J.; Windsperger, A.; Vielhauer, G. Hsp90: A Drug Target? *Curr. Oncol. Rep.* **2010**, *12*, 95-101.
193. Ishihara, Y.; Ishii, S.; Sakai, Y.; Yamamura, N.; Onishi, Y.; Shimamoto, N. Crucial role of cytochrome P450 in hepatotoxicity induced by 2,3-dimethoxy-1,4-naphthoquinone in rats. *J. App. Tox.* **2011**, *31*, 173-178.
194. Ishihara, Y.; Shimamoto, N. A Role of Cytochrome P450 in Quinone-Induced Hepatotoxicity. *Hepatotoxicity*; John Wiley & Sons, Ltd, 2008, 287-297.
195. Berlin, V.; Haseltine, W. A. Reduction of adriamycin to a semiquinone-free radical by NADPH cytochrome P-450 reductase produces DNA cleavage in a reaction mediated by molecular oxygen. *J. Biol. Chem.* **1981**, *256*, 4747-4756.
196. Brunmark, A.; Cadenas, E. Redox and addition chemistry of quinoid compounds and its biological implications. *Free Radic. Biol. Med.* **1989**, *7*, 435-437.
197. Perrin, M. J.; Subbiah, R. N.; Vandenberg, J. I.; Hill, A. P. Human ether-a-go-go related gene (hERG) K⁺ channels: Function and dysfunction. *Prog. Biophys. Mol. Bio.* **2008**, *98*, 137-148.
198. Vandenberg, J. I.; Walker, B. D.; Campbell, T. J. HERG K⁺ channels: friend and foe. *Trends Pharmacol. Sci.* **2001**, *22*, 240-246.
199. Fermini, B.; Fossa, A. A. The impact of drug-induced QT interval prolongation on drug discovery and development. *Nat. Rev. Drug Discov.* **2003**, *2*, 439-447.
200. Brown, A. M. hERG Assay, QT Liability, and Sudden Cardiac Death. *Cardiac Safety of Noncardiac Drugs*; Humana Press, 2005, 67-81.
201. Wible, B. A.; Hawryluk, P.; Ficker, E.; Kuryshv, Y. A.; Kirsch, G.; Brown, A. M. HERG-Lite: A novel comprehensive high-throughput screen for drug-induced hERG risk. *J. Pharmacol. Toxicol.* **2005**, *52*, 136-145.
202. Ficker, E.; Dennis, A. T.; Wang, L.; Brown, A. M. Role of the cytosolic chaperones Hsp70 and Hsp90 in maturation of the cardiac potassium channel hERG. *Circ. Res.* **2003**, *92*, e87-e100.
203. Nanduri, J.; Bergson, P.; Wang, N.; Ficker, E.; Prabhakar, N. R. Hypoxia inhibits maturation and trafficking of hERG K⁺ channel protein: Role of Hsp90 and ROS. *Biochem. Biophys. Res. Commun.* **2009**, *388*, 212-216.

204. Elfiky, A.; Saif, M. W.; Beeram, M.; Brien, S. O.; Lammanna, N.; Castro, J. E.; Woodworth, J.; Perea, R.; Storgard, C.; Hoff, D. D. V. *J. Clin. Oncol.* **26**: 2008 (May 20 suppl; abstr 2503).
205. Rajan, A.; Kelly, R. J.; Trepel, J. B.; Kim, Y. S.; Alarcon, S. V.; Kummar, S.; Gutierrez, M.; Crandon, S.; Zein, W. M.; Jain, L.; Mannargudi, B.; Figg, W. D.; Houk, B. E.; Shnaidman, M.; Brega, N.; Giaccone, G. A Phase I Study of PF-04929113 (SNX-5422), an Orally Bioavailable Heat Shock Protein 90 Inhibitor, in Patients with Refractory Solid Tumor Malignancies and Lymphomas. *Clin. Cancer Res.* **2011**, *17*, 6831-6839.
206. Wu, W.-C.; Wu, M.-H.; Chang, Y.-C.; Hsieh, M.-C.; Wu, H.-J.; Cheng, K.-C.; Lai, Y.-H.; Kao, Y.-H. Geldanamycin and its analog induce cytotoxicity in cultured human retinal pigment epithelial cells. *Exp. Eye Res.* **2010**, *91*, 211-219.
207. Solit, D. B.; Chiosis, G. Development and application of Hsp90 inhibitors. *Drug Discov. Today* **2008**, *13*, 38-43.
208. Duerfeldt, A. S.; Blagg, B. S. J. Hydrating for Resistance to Radicicol. *ACS Chem. Biol.* **2009**, *4*, 245-247.
209. Prodromou, C.; Nuttall, J. M.; Millson, S. H.; Roe, S. M.; Sim, T.-S.; Tan, D.; Workman, P.; Pearl, L. H.; Piper, P. W. Structural basis of the radicicol resistance displayed by a fungal Hsp90. *ACS Chem. Biol.* **2009**, *4*, 289-297.
210. Kelland, L. R.; Sharp, S. Y.; Rogers, P. M.; Myers, T. G.; Workman, P. DT-Diaphorase expression and tumor cell sensitivity to 17-allylamino,17-demethoxygeldanamycin, an inhibitor of heat shock protein 90. *J. Natl. Cancer Inst.* **1999**, *91*, 1940-1949.
211. Guo, W.; Reigan, P.; Siegel, D.; Zirrolli, J.; Gustafson, D.; Ross, D. Formation of 17-Allylamino-demethoxygeldanamycin (17-AAG) hydroquinone by NAD(P)H:Quinone Oxidoreductase 1: Role of 17-AAG hydroquinone in heat shock protein 90 inhibition. *Cancer Res.* **2005**, *65*, 10006-10015.
212. Guo, W.; Reigan, P.; Siegel, D.; Zirrolli, J.; Gustafson, D.; Ross, D. The bioreduction of a series of benzoquinone ansamycins by NAD(P)H:Quinone oxidoreductase 1 to more potent heat shock protein 90 inhibitors, the hydroquinone ansamycins. *Mol. Pharmacol.* **2006**, *70*, 1194-1203.
213. Kelsey, K. T.; Ross, D.; Traver, R. D.; Christiani, D. C.; Zuo, Z. F.; Spitz, M. R.; Wang, M.; Xu, X.; Lee, B. K.; Schwartz, B. S.; Wiencke, J. K. Ethnic variation in the prevalence of a common NAD(P)H quinone oxidoreductase polymorphism and its implications for anti-cancer chemotherapy. *Brit. J. Cancer* **1997**, *76*, 852-854.
214. Belinsky, M.; Jaiswal, A. K. NAD(P)H:quinone oxidoreductase1 (DT-diaphorase) expression in normal and tumor tissues. *Cancer Metastasis Rev.* **1993**, *12*, 103-117.
215. Fitzsimmons, S. A.; Workman, P.; Grever, M.; Paull, K.; Camalier, R.; Lewis, A. D. Reductase enzyme expression across the national cancer institute tumor cell line panel: correlation with sensitivity to Mitomycin C and EO9. *J. Natl. Cancer Inst.* **1996**, *88*, 259-269.
216. Robertson, N.; Stratford, I. J.; Houlbrook, S.; Carmichael, J.; Adams, G. E. The sensitivity of human tumour cells to quinone bioreductive drugs: What role for DT-diaphorase? *Biochem. Pharmacol.* **1992**, *44*, 409-412.

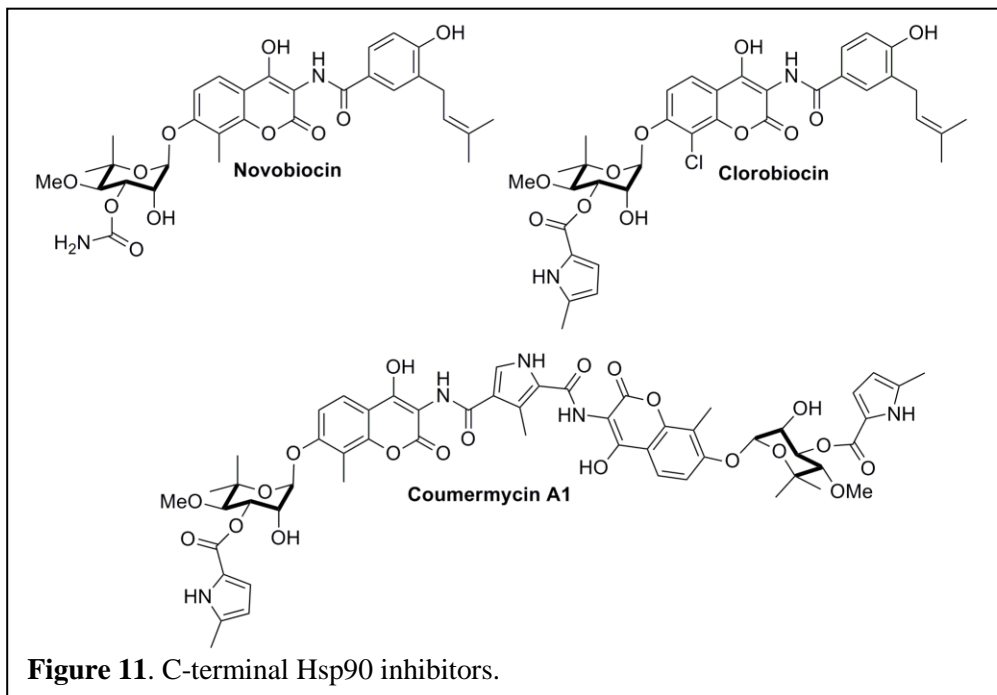
Chapter II

Exploration of the Hsp90 C-terminal Binding Site

I. Introduction

Hsp90 is the core component of a chaperone machine that modulates the folding, activation, and stability of more than 200 substrates. Hsp90 functions by undergoing a series of conformational changes that are driven by the binding and hydrolysis of ATP, which are modulated through Hsp90's interactions with a variety of co-chaperones and partner proteins.¹⁻² Because Hsp90-dependent clients are directly associated with all six hallmarks of cancer,³⁻⁴ Hsp90 is under intense investigation as a pharmacological target for the treatment of cancer.⁵⁻⁶

Hsp90 contains druggable sites at both its N- and C-terminal domains. High affinity Hsp90 inhibitors that bind the Hsp90 N-terminal nucleotide binding site are well characterized, as they have been co-crystallized with this domain (i.e., geldanamycin and radicicol).⁷⁻⁸ In fact, several N-terminal inhibitors are currently in clinical trials for the treatment of cancer.⁹⁻¹⁰ In



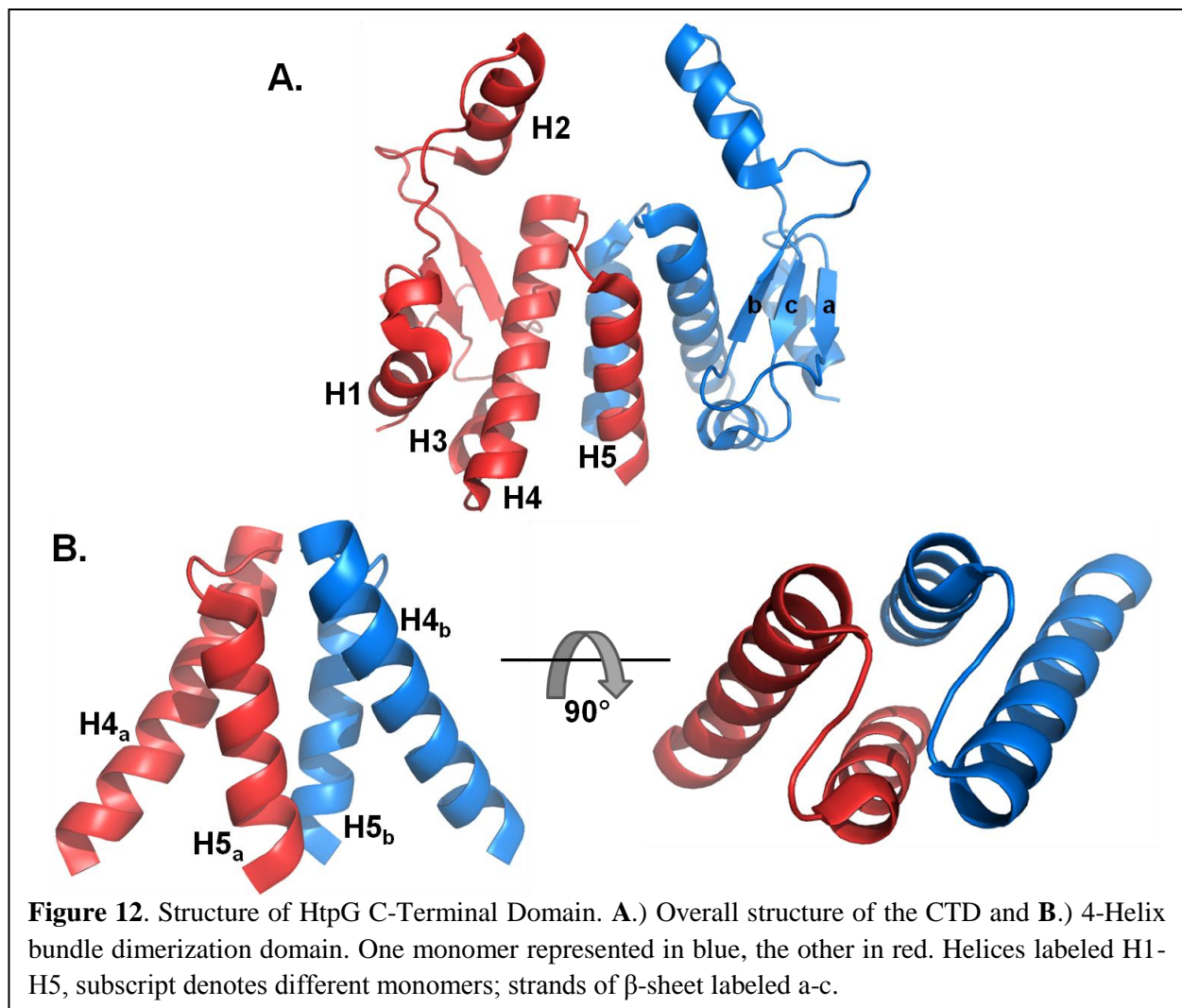
2000, Neckers and co-workers identified the first C-terminal inhibitor of Hsp90 by demonstrating the ability of the Hsp90 C-terminus to bind novobiocin (NB) and proposed this domain to represent a nucleotide-binding site that allosterically regulates nucleotide binding at the N-terminus.¹¹⁻¹²

Not only does NB inhibit Hsp90 function by binding to the C-terminus of Hsp90, but related family members chlorobiocin (CB) and coumermycin A1 also display Hsp90 inhibitory profiles that are different from those manifested by N-terminal inhibitors (**Figure 11**). In addition, C-terminal inhibitors exhibit unique effects on Hsp90's conformation, activity, and interactions with co-chaperones and clients,¹¹⁻¹⁴ highlighting this site as a potential target for Hsp90 modulation. Unfortunately, the mechanism of action for Hsp90 "C-terminal inhibitors" has not been adequately pursued in large part due to their poor pharmacological potency (100-700 μ M) and the lack of concrete structural data regarding the C-terminal binding site.^{11-12,14-15}

A. C-terminal Domain Structure

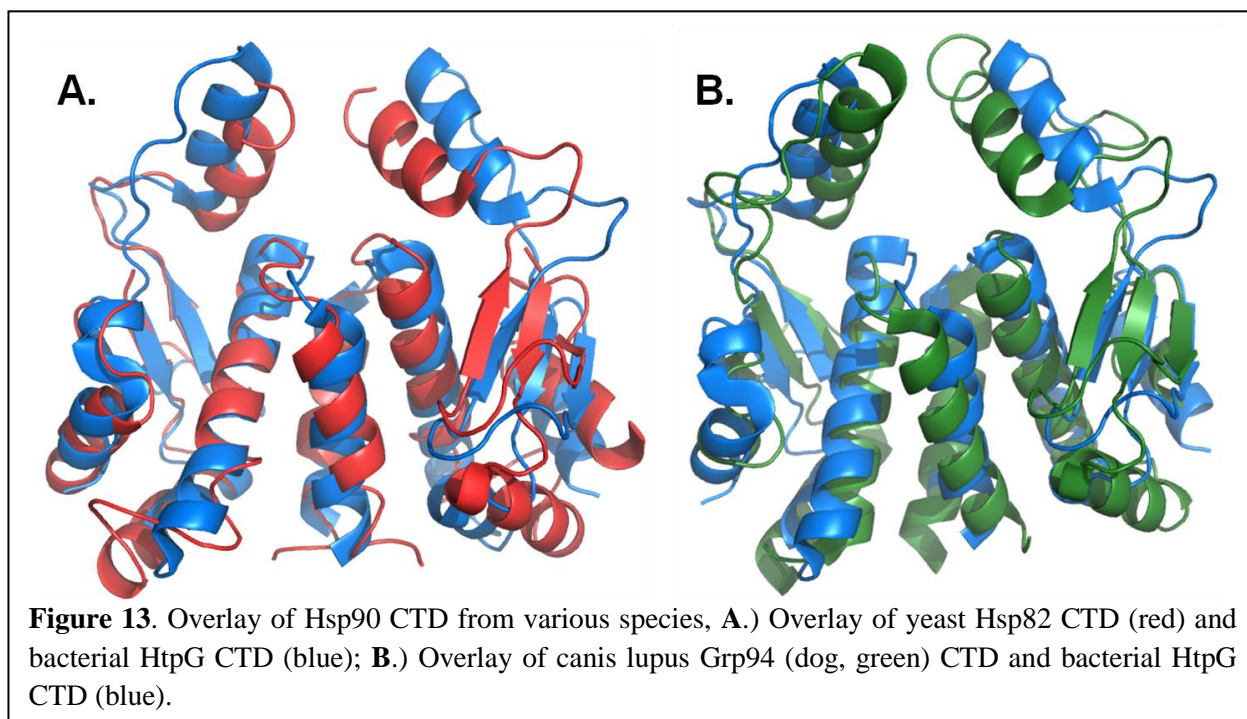
The C-terminal domain (CTD) of Hsp90 mediates dimerization of the chaperone. Prior to crystal structure determination, several groups used Native polyacrylamide gel electrophoresis (PAGE), sedimentation, circular dichroism, and other spectroscopic techniques to determine the oligomeric state and overall topology of Hsp90. It was evident from these studies that Hsp90 was predominantly homodimeric in nature. In 1995, Nemoto and co-workers used mutational analysis to determine the domain of Hsp90 that was responsible for dimerization. They found that residues 533-732 (hHsp90 α) in the CTD were sufficient to form dimers, and furthermore postulated that duplicate interactions existed between the two monomers, i.e. the same residues on each monomer were responsible for dimerization and that the dimerization domain was symmetrical.¹⁶ The first crystal structure of the Hsp90 CTD was solved in 2004 and confirmed

prior work by Nemoto *et al.* Harris and co-workers solved the structure of high temperature protein-G (HtpG), the bacterial homologue of Hsp90 to 2.6 Å (**Figure 12A**).¹⁷ This crystal structure provided insights into how this domain modulates the function of Hsp90. The Hsp90 CTD is comprised of 5 α -helices (H1 – H5) and a 3-stranded anti-parallel β -sheet. Helix 1 (H1) connects the middle domain (MD) to the β -sheet. H1 leads directly to strands a and b, while H2 is located in the loop between strands b and c. Strand c is followed by the three helices H3, H4, and H5, while the CTD terminates at the MEEVD sequence recognized by tetratricopeptide repeat containing proteins. HtpG and other prokaryotic Hsp90s do not contain the MEEVD motif



so this moiety was not observed in the HtpG crystal structure.

A four-helix bundle was evident as the major contributor to CTD dimerization. Helix 4 and Helix 5 from each monomer are arranged with C2 symmetry and maintain hydrophobic interactions with each other (**Figure 12B**). In addition, the dissociation constant, K_D , for dimerization of this domain was determined to be 24 nM, which correlates well with the yeast Hsp90 CTD dimerization K_D of 60 nM.¹⁷⁻¹⁸ Another important feature displayed in the CTD structure is the largely amphiphathic helix (H2) that projects towards the N-terminus in a region that is solvent exposed. This helix is believed to play a role in the binding of client proteins and mediating protein-protein interactions. Since 2004, subsequent structures of the CTD have been solved including the full length yeast Hsp90 (hsp82) and the full length human ER isoform (Grp94).¹⁹⁻²¹ Overlays of these structures highlight conservation of the 4-helix bundle, while slight reorientation of the other helices and the beta sheet is observed amongst the different structures (**Figure 13**).



SAXS and cryo-electron microscopy studies have clearly demonstrated the Hsp90 C-terminus adopts distinct conformations.²²⁻²⁴ In addition, as first suggested by Agard and co-workers, Hugel *et al.* have recently confirmed that the Hsp90 C-terminus undergoes significant conformational changes including opening of the dimerization domain. This equilibrium shifts from 43% CTD open (no nucleotide) to either 58% or 77% CTD open when ATP or ADP is bound, respectively.²⁵ Opening of the CTD can be inhibited by the Hsp90 co-chaperone Hop (yeast = Sti1). The opening of the CTD provides a potential mechanism for client protein release, much like the mechanism of the related GHKL family member, DNA gyrase, which passes double stranded DNA through the protein. In addition, Retzlaff *et al.* identified a conserved cysteine residue in the Hsp90 CTD that upon nitrosylation effects Hsp90 conformation, ATPase activity, and chaperone function.²⁶ This cysteine residue has been named the “switch point,” highlighting its importance in regulating chaperone activity. The structural information that has been collected over the last 15 years has been essential in understanding and interpreting the function of Hsp90, specifically the function of its CTD.

B. C-terminal Domain Function and Modulation

The Hsp90 CTD plays several integral roles in maintaining chaperone function. The CTD mediates dimerization, contains a binding site for co-chaperones that influence the ATPase activity, contains a substrate binding site, and potentially houses a second nucleotide binding site. In fact, yeast engineered to express a CTD-deficient Hsp90 (yHsp82) resulted in an organism with compromised viability.²⁷ The first role elucidated for the Hsp90 CTD was its ability and necessity to mediate dimerization. Nemoto *et al.* identified the last 200 residues in the CTD to be necessary for dimerization while deletion of the N-terminal domain (NTD) had no effect on dimerization.¹⁶ They also noted that the last 129 residues are not sufficient to form

dimers, which indicates that the 4-helix bundle is not sufficient for dimerization, as it resides within the last 100 residues. Moreover, deletion of residues 665-681 (hHsp90 α) resulted in Hsp90 monomers that were unable to hydrolyze ATP.²⁸⁻²⁹ Residues 665-681 are contained within the 4-helix bundle (residues hHsp90 α 661-696). Using the yeast homologue of Hsp90, Hsp82, which contains no cysteine residues, Wegele and co-workers engineered several Hsp82 mutants that express C-terminal cysteines that could be chemically ligated to form disulphide-containing dimers.³⁰ These mutants actually manifested similar ATPase activities as the wild type protein, suggesting that dimerization is the main function of the CTD. Mutants lacking both the CTD and MD manifested significantly diminished ATPase activity (2% of wt) indicating that the MD and CTD must also be present to provide additional interactions with the NTD to promote ATP hydrolysis.³⁰

The role of the CTD in chaperoning client proteins was first realized in 1997 when Yang and co-workers identified two separate regions of Hsp90 that were capable of preventing the aggregation of denatured polypeptides.³¹ These sites were identified in both the NTD and CTD, indicating that both Hsp90 termini play a role in stabilizing and chaperoning client proteins. It was later realized that the CTD chaperone site binds partially folded proteins independent of ATP binding but dependent upon the binding of partner proteins and co-chaperones.³² Many Hsp90 co-chaperones and partner proteins contain tetratricopeptide repeat (TPR) domains. This motif recognizes the MVEED sequence contained within the last five residues of the cytosolic Hsp90s (hHsp90 α/β). Mutation of the Hsp90 MVEED domain to MAAVD prevented the interaction of Hsp90 with the co-chaperones Hop, Cyp40, FKBP51, and FKBP52.²⁹ Surprisingly, in the same study by Chen *et al.*, deletion of residues 665-681 (hHsp90 α) also resulted in

diminished interactions with the above co-chaperones and p23, indicating that dimerization may also be critical for co-chaperone recognition and binding.²⁹

In addition to mediating dimerization, facilitating co-chaperone binding, and housing client protein binding sites, the Hsp90 CTD also contains a putative nucleotide binding site. First described in 2000, Marcu and co-workers demonstrated that truncated proteins that contain only the Hsp90 CTD were able to bind immobilized ATP-sepharose.¹¹ It was later demonstrated that this nucleotide binding site becomes accessible only upon occupation of the N-terminal ATP binding site.³³⁻³⁴ Using sequence alignment and topology prediction tools, this nucleotide binding site was proposed to represent a Rossman fold.³⁴ However, this was later contested as the CTD nucleotide binding site did not bind nicotinamide adenine dinucleotide (NAD⁺), which is the nucleotide of choice for Rossman folds.³⁵ The CTD binds both pyrimidine and purine-containing nucleotides when the NTD binding site is occupied. Both GTP and UTP are able to bind the CTD, unlike the NTD nucleotide binding site, which is specific for adenine-containing nucleotides.³⁵ The CTD does not display ATPase activity, but instead has been hypothesized to regulate the various Hsp90 conformations.

Simultaneous with discovery of the CTD nucleotide binding site, the natural product Novobiocin (NB) was shown to bind within the CTD. NB is a natural product antibiotic previously known to bind DNA gyrase and originally was hypothesized to bind Hsp90's NTD due to similarities in the ATP conformation when bound to both proteins.³⁶ Hsp90 was shown to bind immobilized NB-sepharose, and was only competitively removed by the addition of other soluble coumarins or ATP, but not with N-terminal inhibitors, GDA or RDC.¹² Subsequent studies with NB showed that NB prevented nucleotide binding to both the NTD and CTD nucleotide binding sites.³³ The NB binding site was localized to residues 384-732 (hHsp90 α)

through truncation studies. Surprisingly, NB competed for Hsp90 binding to immobilized GDA or RDC. In addition, NB was able to cause the proteasome-mediated degradation of ErbB2, v-src, and Raf-1, three Hsp90-dependent client proteins. In subsequent studies by the same group, the NB binding site was further localized to residues 542-732 (hHsp90 α), while the peptide corresponding to residues 666-680 (hHsp90 α) was able to block NB binding.¹¹ In addition, the deletion mutant, Δ 661-681, failed to bind immobilized NB, which indicated the NB binding site and the CTD dimerization domain were overlapping. In the same study, NB was found to prevent interactions between Hsp90 and both Hsc70 and p23.¹¹ Hsc70 is known to bind near the C-terminus, while p23 binds to the NTD, demonstrating cross-talk between the N- and C-termini, as NB causes structural reorganization in the NTD that prevents p23 binding. Prior to these studies, Hartson and co-workers demonstrated that molybdate prevents GDA from binding, inhibited firefly luciferase refolding while protected the CTD from proteolysis, and enhanced interactions with p23.³⁷ At the time of this study, the CTD binding site had not been discovered, but in hindsight it can be rationalized that molybdate binds to the CTD to affect chaperone function and conformation.

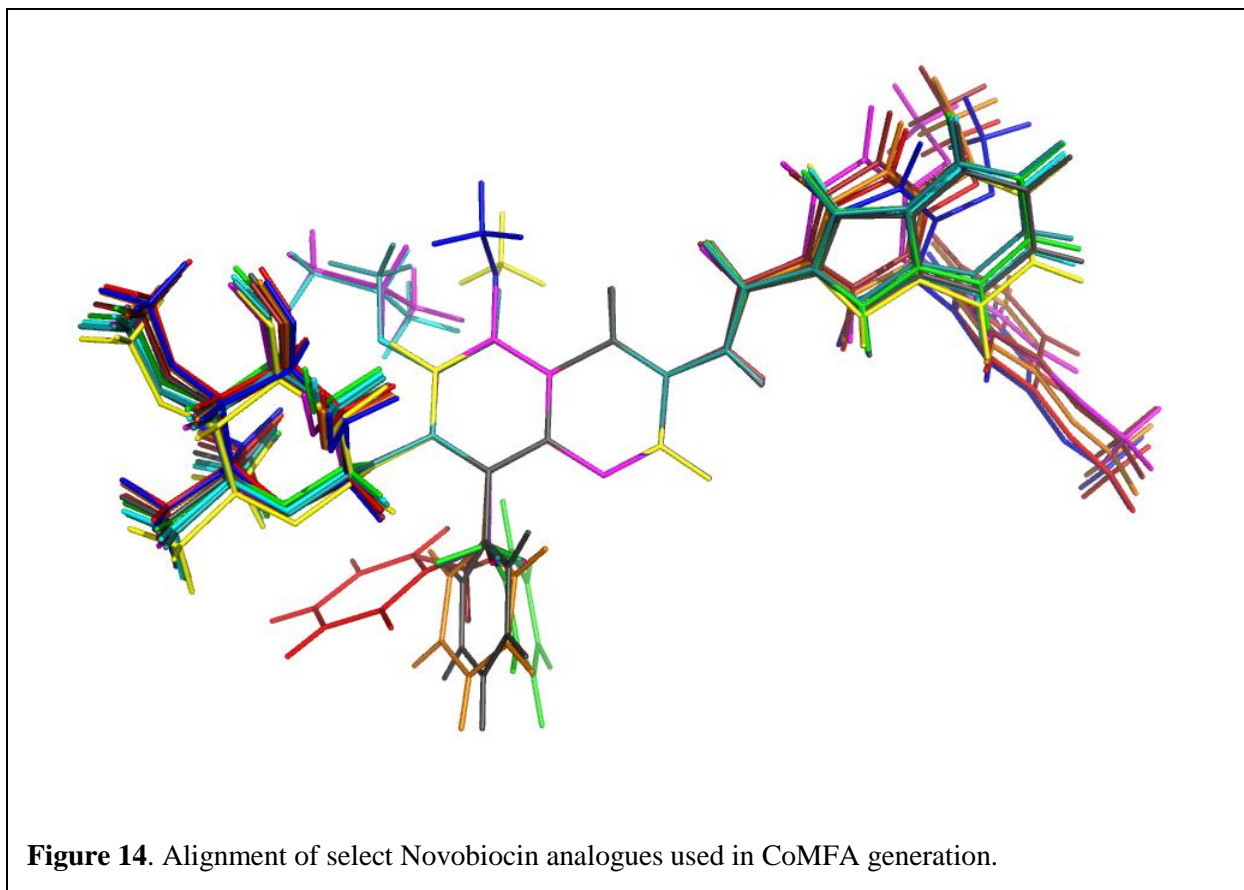
Yun and co-workers determined the effect of NB on Hsp90 in rabbit reticulolysate.¹⁴ NB was able to inhibit the maturation of heme-regulated eIF2 α kinase (HRI) and cause disassociation of Hsp70, p23, and FKBP52 from the chaperone complex, but did not cause disruption of the Hsp90-Hop or Hsp90-Cdc37 interactions. In the same study, NB and other C-terminal inhibitors were shown to protect the Hsp90 CTD from proteolysis, presumably by altering its conformation and shielding specific residues from the protease. A related dimeric coumarin-containing antibiotic, coumermycin A1, prevented dimerization of the Hsp90 CTD.¹³

C-terminal inhibitors exhibit unique effects on Hsp90's conformation, activity, and interactions with co-chaperones and clients, highlighting this site as a target for Hsp90 modulation. One of the most unique and important features of C-terminal inhibition is lack of induction of the heat shock response. The heat shock response represents one of the biggest detriments associated with N-terminal inhibition. Therefore, C-terminal inhibitors have garnered significant attention. Unfortunately, the mechanism of Hsp90 "C-terminal inhibitors" has not been adequately pursued in large part due to the poor pharmacological potency of first generation analogues (100-700 μM). Subsequent analogues of NB have been explored that manifest improved Hsp90-inhibitory and anti-cancer activity, however the inability to obtain co-crystal structures with these molecules bound to the chaperone has hampered further development. This chapter describes the pursuit of uncovering the Hsp90 C-terminal inhibitor binding site through molecular modeling, inhibitor design, and biochemical techniques.

II. Development of a CoMFA for Hsp90 C-Terminal Inhibitors

Although, initial development of C-terminal Hsp90 inhibitors based on the novobiocin scaffold has generated interesting lead compounds, further drug design has been hindered by the lack of concrete structural and biochemical data regarding the exact location of the binding pocket.³⁸⁻⁵⁰ At first, analogue design had been carried out without information regarding the nature of the binding pocket as no binding models existed for the C-terminal binding site. Consequently, we sought to develop a 3-dimensional quantitative structure-activity relationship (3D QSAR) model to describe the C-terminal binding site. A comparative molecular field analysis (CoMFA) was performed to correlate structural features with biological activity in a quantitative manner. Novobiocin analogues previously synthesized in the Blagg laboratory were used to generate the CoMFA (IC_{50} anti-proliferation = 500 nM to >100 μM ; See Materials and

Methods).^{40,42} The compounds were first aligned using the coumarin ring as the core moiety after energy minimization and partial charge assignment (**Figure 14**). A CoMFA was then generated in SYBYL v8.0, using partial least squares regression analysis, which correlates the biological



activity (IC_{50} values experimentally determined) with the CoMFA parameters of sterics and electronics. The overall value of the CoMFA was analyzed using a 3-D cross-validated correlation score (Q^2) using the leave-one-out technique. Compounds that caused the Q^2 value to fall below 0.5 were considered outliers and eliminated from the data set, while a CoMFA with a cross-validated correlation score above 0.6 exhibits predictive value. Several iterations of compound removal were necessary, resulting in a final CoMFA model that utilized 72 compounds and generated a Q^2 value of 0.617. The statistical parameters of the CoMFA generated are shown in **Table 4**.

Table 4. Statistical parameters for final CoMFA model.

Statistical Parameter	Value
Q^2	0.617
Number of Components	6
R^2	0.919
Predictive R^2	0.880
Standard Error of Prediction	0.184
F_{ratio}	90.4
<i>Field Contributions</i>	
Steric	0.413
Electrostatic	0.587

The CoMFA parameters demonstrate the utility and reliability of this model, while the predicted IC_{50} values generated using the CoMFA model compare well with the actual IC_{50} values (**Figure 15**, $R^2 = 0.88$). The CoMFA model can be graphically displayed in contour maps that provide insights into the structural (both steric and electrostatic) properties that influence biological

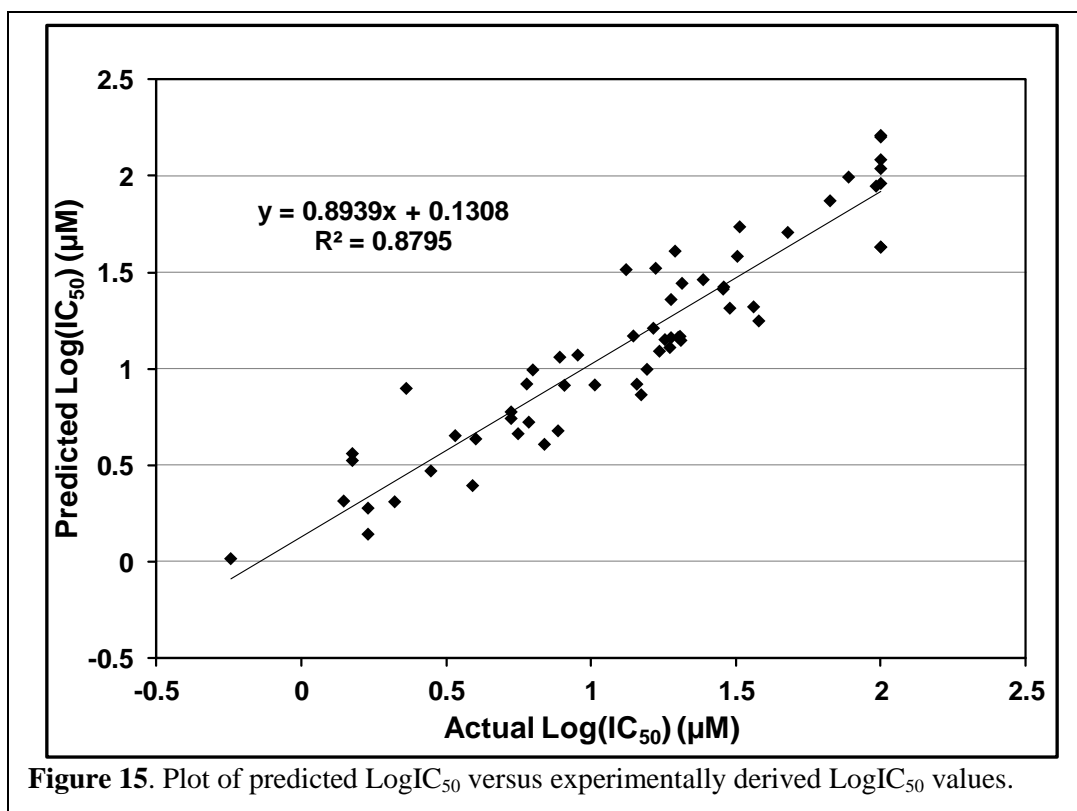
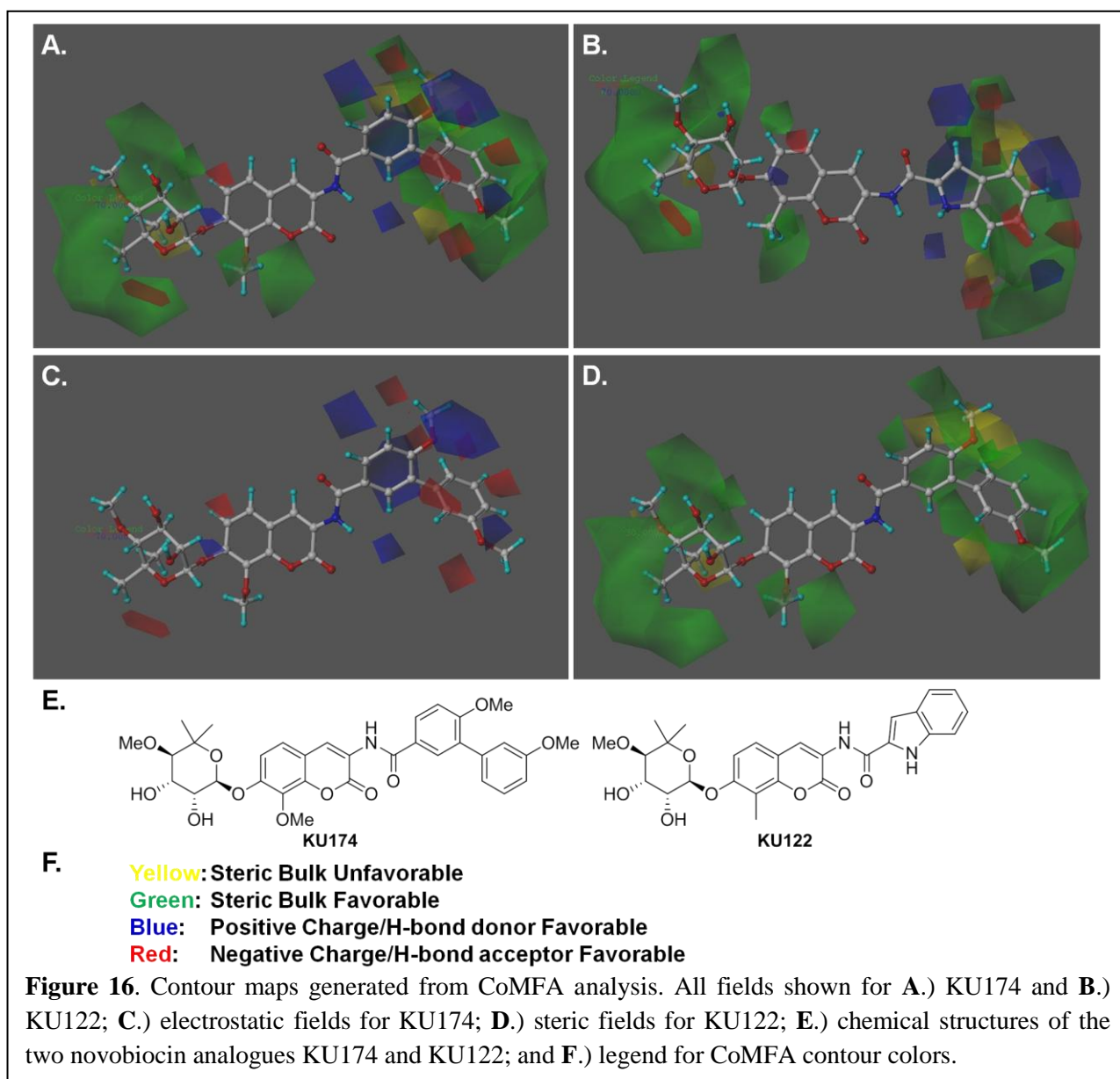


Figure 15. Plot of predicted $LogIC_{50}$ versus experimentally derived $LogIC_{50}$ values.

activity.

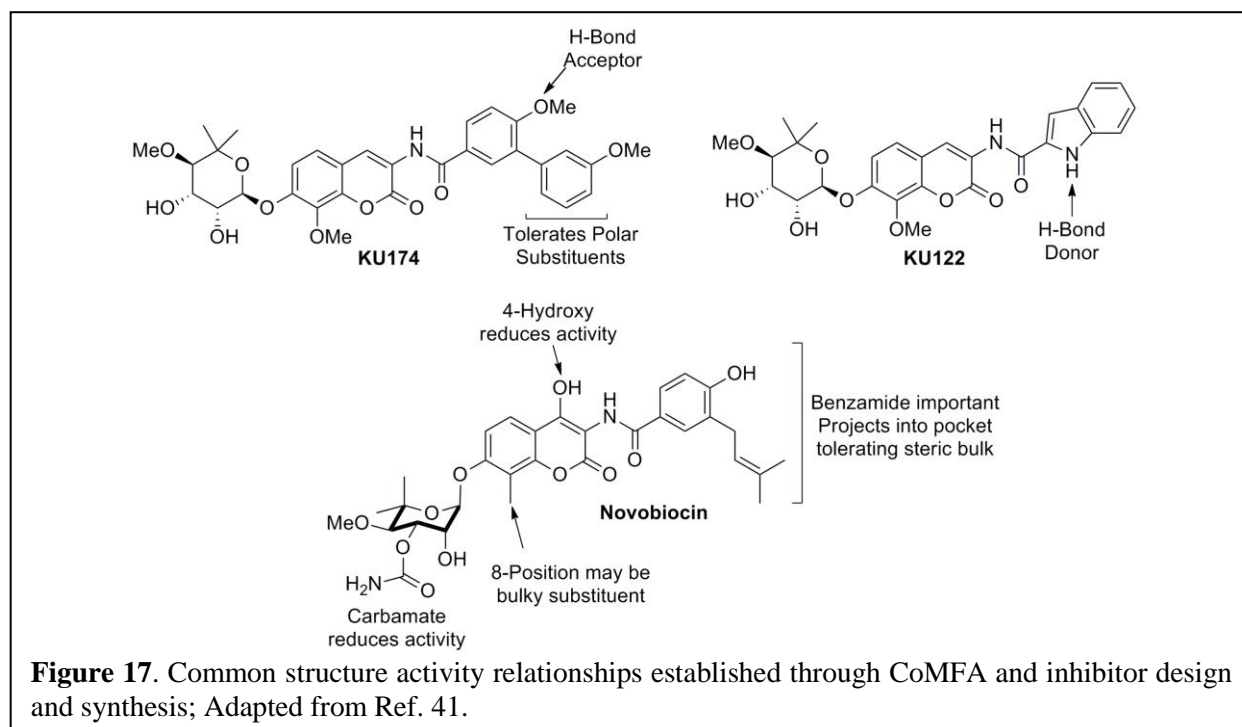
The contour maps generated from this CoMFA using **KU174** (IC_{50} 10 μ M) and **KU122** (IC_{50} 570 nM) as reference molecules are shown in **Figure 16**. Regions that tolerate steric bulk (green) are evident in **Figure 16**. Specifically the areas surrounding both the noviose sugar and



the amide side chain (biaryl or indole) seem to accommodate steric bulk. In addition the coumarin 8-methyl seems to project towards a pocket that allows somewhat bulky substituents.

The 4-substituent of the biaryl ring does not seem to allow steric bulk, indicated by the yellow area.

Red and blue contours describe the electrostatic contributions generated in the CoMFA. The indole contained within **KU122** appears to provide an important hydrogen bond via its N–H bond (**Figure 16B**). Several other areas surrounding the amide side chain play an important electrostatic role in binding.



This CoMFA provided insight into the nature of the C-terminal Hsp90 binding site and correlated well with observed structure-activity relationships (SAR) delineated through small molecule design and synthesis (**Figure 17**). Another group from Lanzhou University in China has also reported the development of a CoMFA and CoMSIA (comparative molecular similarity indices analysis) using 53 compounds synthesized in the Blagg laboratory.⁵¹ Their CoMFA analysis provided similar features to the one described above, but also suggested that an H-bond acceptor near the amide bond would increase activity. Although the CoMFA helped describe the

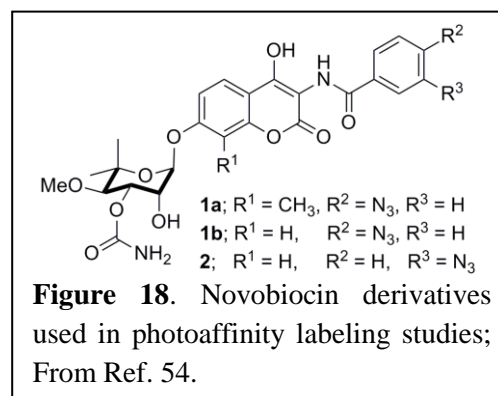
nature of the Hsp90 C-terminal binding site, this method was plagued by several disadvantages. First, the CoMFA model only has predictive value for novel compounds within the IC₅₀ range of the compounds that were used to design the CoMFA, 500 nM to >100 μM. Second, the alignment strategy assumes one moiety of the input molecules is rigid and only binds in one orientation, in this case, the coumarin core. More realistically, the coumarin may bind in a manner that can accommodate other functionalities present in the molecule. For these reasons, we sought to pursue a more biochemical approach to interrogate the C-terminal binding site.

III. Development of a C-terminal Binding Site Model

To circumvent limitations imposed upon the rational development of NB analogues through a structure-based approach, the NB binding site located in the Hsp90 C-terminus was sought after via photolabile NB derivatives, which upon covalent attachment to Hsp90 could aid in elucidation of the Hsp90 C-terminal binding site. As revealed by co-crystal structures of NB bound to closely related enzymes (e.g., DNA gyrase/topoisomerase⁵²⁻⁵³), the active conformation of NB could then be docked, and subjected to a ligand-supported refinement followed by a systematic molecular dynamics (MD) based methodology to identify the binding site for NB and its analogues.

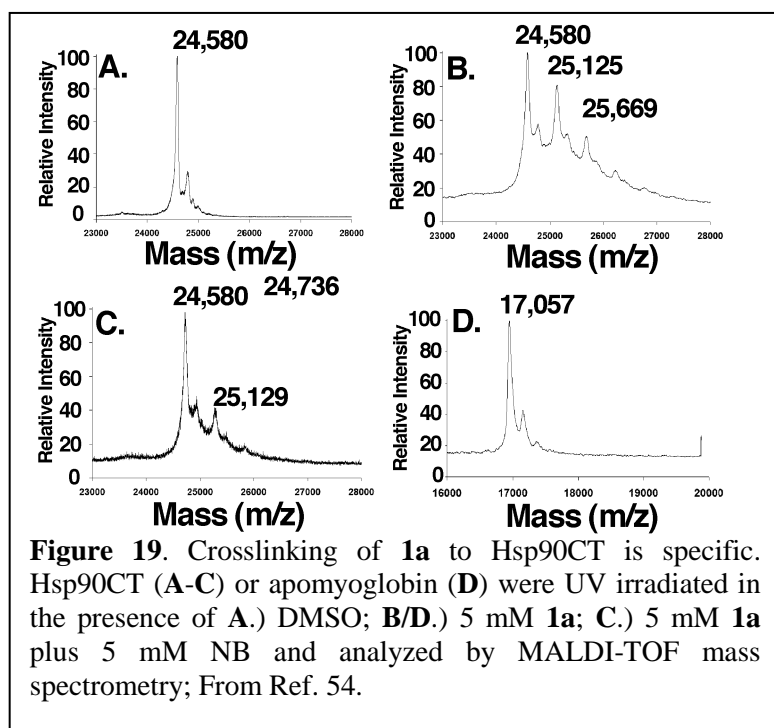
A. Identification of the Novobiocin Binding Site in Hsp90's C-terminal Domain

In collaboration with the Matts Laboratory at Oklahoma State University, residues in the Hsp90 CTD, proximal to the inhibitor binding site, were identified using a NB-based photoaffinity label.⁵⁴ Photolabile derivatives of NB were previously synthesized for the purpose of identifying the Hsp90 C-



terminal binding site (**Figure 18**).⁵⁵ As noted earlier, the Hsp90 C-terminus is resistant to proteolysis by trypsin in the presence of chlorobiocin. Similarly, compound **1a** also protected the Hsp90 C-terminus from tryptic digest indicating that the photoaffinity probe bound Hsp90 in a manner similar to novobiocin and chlorobiocin.¹⁴

Novobiocin analogues containing a photo-reactive azide moiety placed in the *para*- (**1a/1b**) or *meta*-position (**2**) were used in lieu of the phenol and prenyl side chain present in NB, respectively. A recombinant His-tagged Hsp90 C-terminal construct was incubated in the presence or absence of **1a** followed by UV-irradiation. No change in the *m/z* of Hsp90CT was detected upon MALDI-TOF analysis of the Hsp90 C-terminus upon UV-irradiation in the absence of **1a** (**Figure 19A**), however, in the presence of **1a** a new polypeptide peak (*m/z*= 25,125) with a mass approximately 545 Da greater than the parental peak (*m/z*= 24,580) was detected (**Figure 19B**). This mass corresponds to the molecular weight of compound **1a** minus



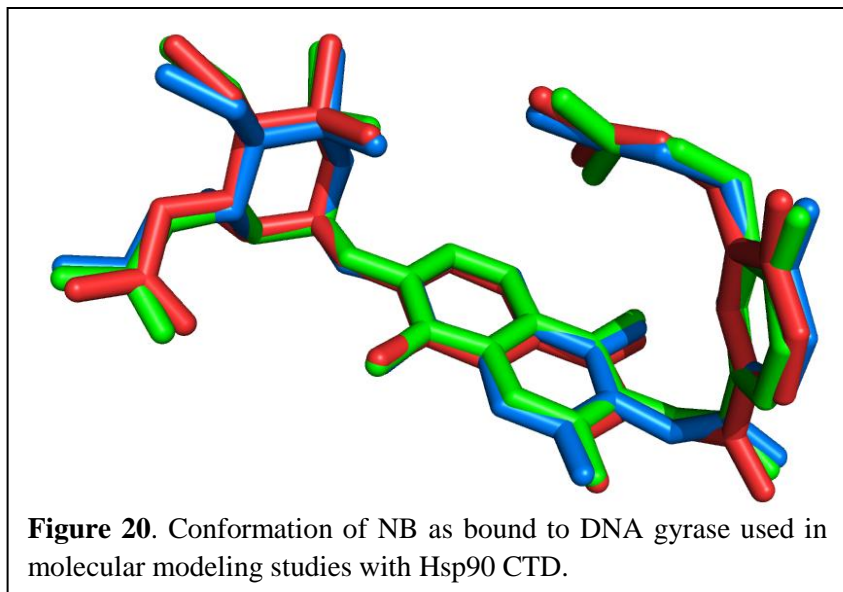
one molecule of N₂. To confirm that both the azide-containing molecule and the non-labeled novobiocin bind to the same location, crosslinking studies were carried out in the presence of an equimolar concentration of NB and **1a**, resulting in a >80% decrease in the intensity of the 25,125 peak (**Figure 19C**), indicating the inhibitors bind

competitively. A small portion of the Hsp90CT was found to be modified by two molecules of **1a**, therefore an experiment was performed with 10-fold lower concentrations of the photolabile inhibitor. A significant reduction in the amount of doubly modified Hsp90CT was observed, indicating that the first binding event is most specific. To demonstrate crosslinking specificity, apomyoglobin was irradiated in the presence of **1a**, and no crosslinking was observed, confirming selectivity of these compounds for Hsp90 (**Figure 19D**). Identical crosslinking peaks were detected when **2** was irradiated in the presence of Hsp90, confirming that azide placement on the benzamide side chain did not affect the reaction.

To determine the peptide sequence to which the photoactivatable derivative was crosslinked, control and **1b**-crosslinked and **2**-crosslinked Hsp90 were digested with trypsin, and the masses of the tryptic peptides were analyzed by ultra-high mass accuracy Fourier transform ion cyclotron resonance (FTICR) mass spectroscopy (mass accuracy of 10 ppm). Crosslinking of **2** is calculated to increase the theoretical mass of a crosslinked peptide by 527.1613 Da. Analysis of the data identified a peptide corresponding to a mass of ~527 amu greater than that predicted for an unlabeled peptide sequence, namely: 559-KKQEEK-564 or 560-KQEEKK-565 (1316.6093/~MH1+ 789.4465+527.1540). Through analysis of the fragmentation pattern and the MS2 and MS3 spectra, the photolabile novobiocin derivatives were determined to bind alongside the peptide 559-KKQEEK-564, and attach directly to K560. This segment is located in the Hsp90 C-terminus, within the region of the C-terminal fragment that is protected from proteolysis upon binding to chlorobiocin and novobiocin.

B. Modeling of Novobiocin's Conformation

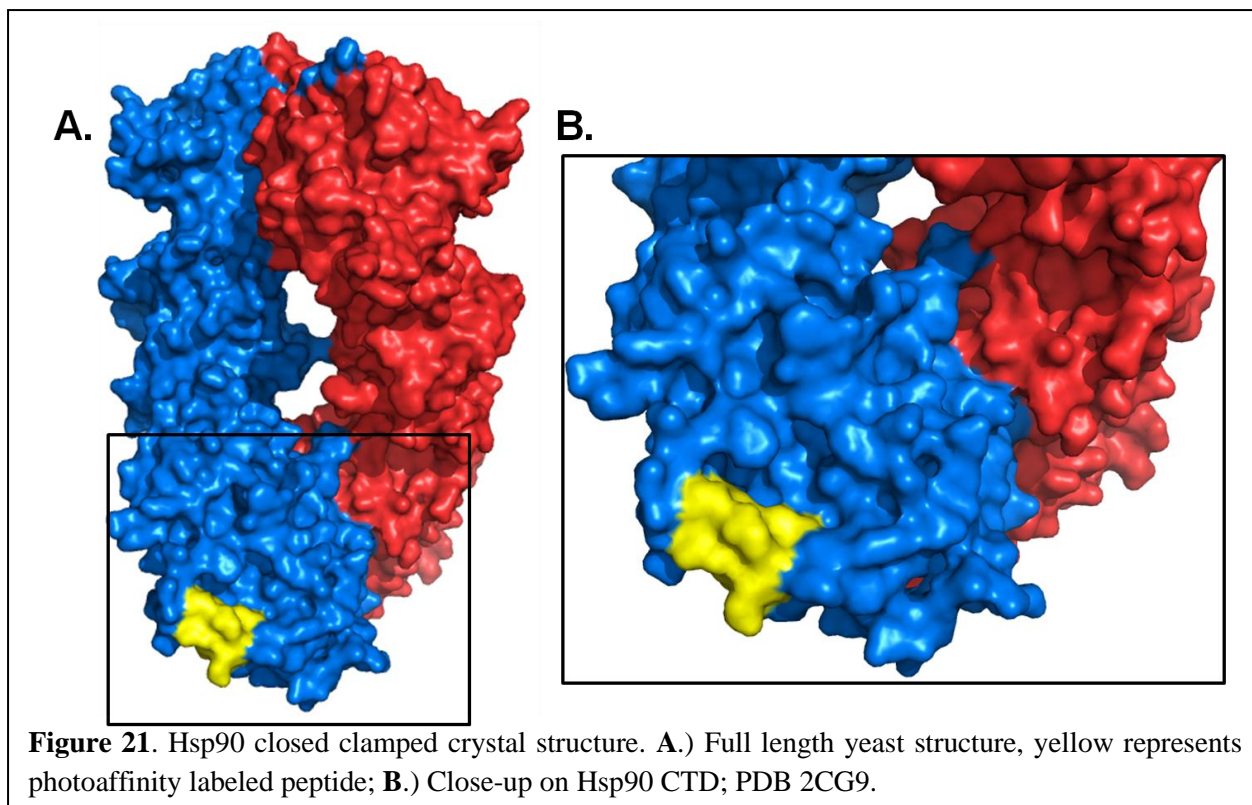
To further refine the NB binding site in Hsp90, conformations of NB co-crystallized with DNA gyrase/topoisomerase (PDB IDs: 1S14, 1AJ6, 1KIJ) were analyzed. NB was found to adopt a partially folded conformation in each of



these structures (**Figure 20**). This conformation of NB was extracted and used to dock into the site of Hsp90 identified via photoaffinity labeling.

C. Modeling of the Hsp90 Novobiocin Binding Site

The data generated from the photoaffinity labeling studies with NB provides information regarding the putative binding site of NB. After careful analysis of the homologous peptide in the full length, closed crystal structure of yeast Hsp90 (538-AEREKE-543), it was not clear whether a pocket large enough to accommodate NB was present in the regions flanking this peptide (**Figure 21**). Initial attempts to dock novobiocin into this crystal structure were unsuccessful. However in 2008, the solution structure of the bacterial Hsp90 homologue, HtpG, was determined by Agard and co-workers.²³ As the full length yeast crystal structure depicts Hsp90 in its closed, clamped conformation, it was postulated that the extended form, as found in solution, would unveil the C-terminal binding site. Generation of this open model allowed for identification of the C-terminal inhibitor binding site using the information garnered from the photoaffinity and proteolytic studies.



In an effort to correlate the binding site identified by photoaffinity studies with the open structure of Hsp90 α , a homology model of hHsp90 α was generated using the SAXS structure of HtpG as the template in collaboration with the Gennady Verkhivker Laboratory at the University of Kansas. The homology model of hHsp90 α was constructed using software “Modeller”.⁵⁶ The solution structure of HtpG (dimer) was used as a template for building of the model. The modeled structure was subsequently subjected to a molecular dynamics protocol for further refinement.

Docking of NB into the hHsp90 α homology model was guided by the following constraints: 1) Binding of NB to the C-terminal domain protects residues in the N-terminal region of the construct from proteolysis; 2) proteolytic fingerprinting identified the peptide KKQEEK in human Hsp90 α as the site of crosslinking for a photo-reactive NB derivative; and 3) the bioactive conformation of NB as shown in **Figure 20**. NB was docked rigidly in the hHsp90 α C-terminus by maintaining a distance constraint of 3.5Å between the hydroxyl of the noviose

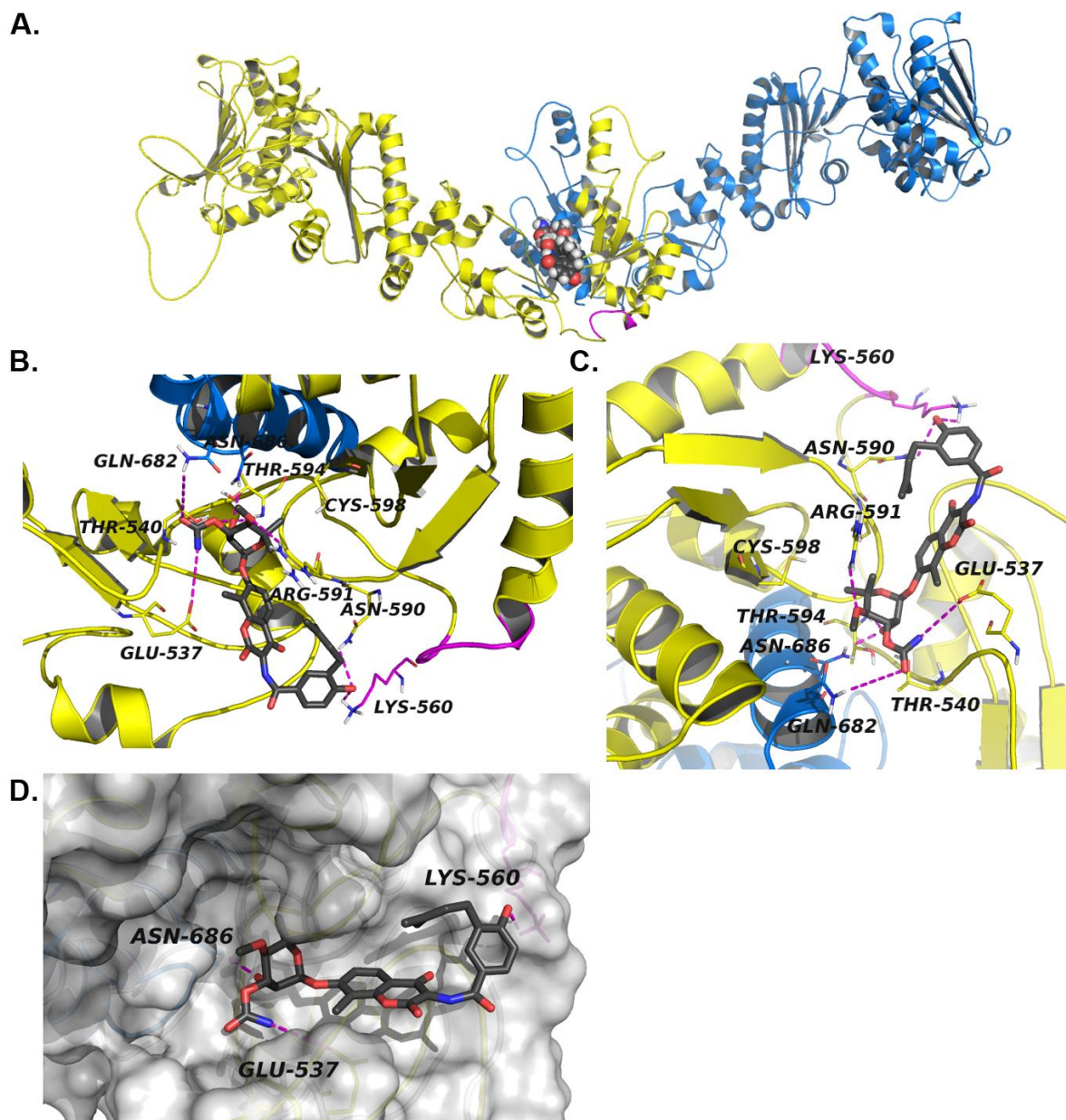


Figure 22. Modeled structure of the Novobiocin binding site in hHsp90 α . **A.**) The Hsp90 α homology model homodimer and the C-terminal binding site with NB (spheres) docked at the interface of two monomers (blue and yellow) **B.**) close-up of NB (grey sticks) docked in Hsp90 α homology model, the crosslinked fragment (lines) and predicted hydrogen bonds (dashes) are depicted in magenta and **C.**) close-up of NB noviose (grey sticks) docked in Hsp90 α homology model, predicted hydrogen bonds (dashes) are represented in magenta, **D.**) surface representation of Hsp90 α homology model CT binding site with NB (grey sticks) docked. Only one molecule of NB is shown to be bound to Hsp90 homodimer, an equivalent binding site contained on the other monomer has not been shown for clarity; From Ref. 54.

and the amide nitrogen of Asn686. A multiple sequence alignment of related proteins from different organisms indicated three conserved residues adjacent to the photoaffinity-labeled peptide fragment, Lys538, Lys558 and Glu562 in hHsp90 α . Minimization of protein side chains with a distance constraint of 3.5 Å between NB and residues Asn686, Lys538, and Glu562 was carried out while keeping NB and the protein backbone rigid to allow relaxation of the side chains and minimization of negative interactions. The binding site was subsequently defined as residues that reside within 8Å of NB and were subjected to minimization while keeping the rest of the protein and NB fixed to remove unfavorable steric and hydrophobic contacts and to allow side chains to relax and to facilitate NB alignment in the cavity. The resulting complex was further refined by a short MD simulation (100ps). This Hsp90 α -NB complex was found to be stable after simulation (RMSD<2Å). The interactions manifested between NB and Hsp90 α are depicted in **Figure 22**.

The NB binding site is located proximal to the 4-helix bundle, the CTD beta sheet and Helix 1 (**Figure 22**). It is evident from **Figure 22B/C** that NB maintains several interactions with multiples residues present in the binding site. These interactions can be summarized as follows:

- 1) A hydrogen bond (HB) interaction between the noviose sugar hydroxyl of novobiocin and Asn686 (H5) and Thr540 of hHsp90 α ;
- 2) HB interactions between the oxygen of the prenylated hydroxylphenyl ring of novobiocin and both Asn590 and Lys560 (H1) of hHsp90 α , a residue identified via photoaffinity labeling studies;
- 3) the CO and -NH of the noviose carbamate of novobiocin maintain HB interactions with Glu537 and Gln682 (H5);
- 4) Thr594 provides HB interactions with the oxygen of the glycosidic bond linking the noviose and coumarin ring; and
- 5) a HB interaction between the noviose methoxy group and Arg591.

Biochemically-guided modeling based on the open structure from bacterial Hsp90, HtpG, produced a human Hsp90 model that upon further refinement, unveiled the binding mode for Hsp90 C-terminal inhibitors. This mode of binding explains many of the previously observed biological and biochemical consequences that result upon Hsp90 C-terminal inhibition.

D. Correlation to Observed Effects Resulting from C-Terminal Inhibition

Although there have been previous attempts to model the NB binding site, the results were not consistent with available biochemical data. Prior models developed for the Hsp90 C-terminal inhibitor binding site were generated using homology modeling, MD simulations, and pocket-finder algorithms.⁵⁷⁻⁵⁸ However, using biochemical analyses, affinity labeling, and homology modeling, we have identified a binding site for C-terminal Hsp90 inhibitors that supports prior biochemical studies.

For example, Neckers and co-workers originally proposed the existence of a binding site in the Hsp90 C-terminus and determined that NB binding was localized to residues 542-732 (hHsp90 α).¹¹⁻¹² Additionally, it was demonstrated that addition of the C-terminal peptide 667-680 (hHsp90 α) reduced Hsp90's ability to bind immobilized NB, and Hsp90 binding to immobilized NB could be competed with this peptide.¹¹ In the model proposed, this peptide sequence is located in the α -helix proximal to the sugar binding pocket of NB, and is important for interactions with the noviose moiety on NB. Consistent with this pocket being adjacent to the NB binding site, Hartson and coworkers have shown that NB blocks the AC88 antibody (a monoclonal antibody that recognizes an epitope within the amino acids 668-684 in hHsp90 α) from binding Hsp90, thus providing two key pieces of previously reported biochemical data that supports the location of this binding site.^{14,37}

Furthermore, ATP binding plays an important role in the conformational reorganization of Hsp90, in a manner complementary to the dimerization of two Hsp90 monomers at the C-terminus, which is essential for Hsp90 activity. Once dimerization occurs at the C-terminus, Hsp90 undergoes a complex conformational cycle that facilitates reorganization and folding of client proteins.^{19,59} The C-terminal inhibitor, Coumermycin A1, was shown to disrupt C-terminal dimerization, and halt the conformational cycle.¹³ In addition, the protein folding process involves a multitude of co-chaperones and partner proteins. Novobiocin and related antibiotics have been shown to disrupt interactions with partner proteins that bind Hsp90 to both the C- and N-terminus, i.e. Cdc37, p23, Hsc70, FKBP52 and PP5.^{11,13-14} Additionally, prior proteolysis experiments with NB and related family members demonstrate that C-terminal occupation protects Hsp90 from proteolysis by altering its conformational state. Specifically, NB shields Lys615 and Arg620 from cleavage. This result can be explained by the examination of Hsp90 in its various conformational states. Lys615 and Arg620 are solvent exposed on the surface of an alpha helix in the semi-closed and closed states. However, in the extended form, Lys615 and Arg620 are shielded by surrounding residues, and hence, are not accessible to proteases. Interestingly, the pivot point of Hsp90's movement between the middle and C-terminal domains of Hsp90 (hHsp90 α residue 550) is located within close proximity to this binding site.^{21,23-24} Taken together, these data indicate that conformational changes within the C-terminus occur upon inhibitor binding and cause global conformational changes within the entire homodimer.

Additionally, Retzlaff and co-workers have demonstrated through mutational analyses that Hsp90 is regulated by a switch point in its C-terminal domain.²⁶ Mutation of the residue equivalent to Cys598 in hHsp90 α (Ile538 in HtpG) altered Hsp90's ATPase and chaperone activity, modified N-terminal and C-terminal domain associations, and shifted the

conformational equilibrium of Hsp90 within its ATPase cycle.²⁶ In our model, Cys598 forms part of the NB binding pocket (**Figure 22 B/C**). Thus, the model suggests that C-terminal inhibitors have the ability to interact with and stabilize the region around this pivot point, and potentially lock the Hsp90 homodimer in a single conformation. Consequently, upon C-terminal occupation, the Hsp90 machinery is stalled in the open conformation, which results in protection of Lys615 and Arg620 from proteolysis, hinders N-terminal ATP hydrolysis, and prevents the binding of N-terminal inhibitors. Once again, occupation of this putative binding pocket in the Hsp90 C-terminus can finally explain previously observed biochemical observations.

In addition, Hugel and coworkers recently determined the dynamics and kinetics of C-terminal dimerization, whereby the C-terminus is capable of opening in the presence of N-terminal ligands (i.e. ATP and ATP analogues). It was observed that N- and C-terminal dimerization is intimately related, and that C-terminal dimerization is not required for N-terminal dimerization. These findings suggest that the C-terminus is in constant flux, whereby a multitude of conformations exist.²⁵ In the model presented herein, novobiocin predominantly interacts with one monomer of the Hsp90 homodimer. Together with the data presented by Hugel, it can be reasoned that small molecule binding of the Hsp90 C-terminus may occur while this domain is open, preventing dimerization and continuation through the catalytic cycle. Alternatively, C-terminal inhibitors may bind after dimerization, preventing occupation of the N-terminal binding pocket by ATP, which is supported by prior studies by Marcu *et al.* whom demonstrated that novobiocin binding to the C-terminus prevented N-terminal occupation.¹²

Hsp90 C-terminal inhibitors have garnered significant attention during the past decade, specifically due to problems associated with N-terminal inhibition as observed in the clinic.⁶⁰ Structural information regarding the C-terminus, especially the NB binding site, has been scarce,

and attempts at co-crystallization have been unsuccessful. Accordingly, effective analogue design and data analysis have been hindered. Therefore, we have utilized photoaffinity labeling and proteolytic studies to identify residues that form the NB binding site. Through elucidation of the cross-linked peptide and molecular modeling alongside the reported solution structure of Hsp90, potential binding sites were carefully evaluated. As a result of these studies and those before us, we are finally able to provide a binding site for NB and other C-terminal inhibitors that accounts for the biological activities manifested by NB. This model provides a new standard for the development of future Hsp90 inhibitors that target the C-terminal binding pocket. In addition to the biochemical approach used to elucidate the Hsp90 C-terminal binding site, interest in C-terminal inhibitor design and synthesis has been a central focus in the Blagg Laboratory to establish structure–activity relationships for this class of inhibitors.

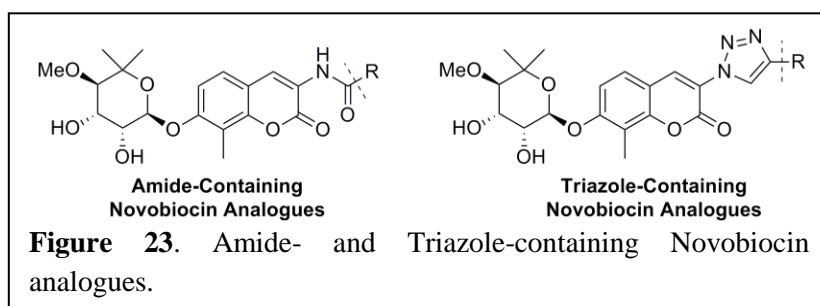
IV. Synthesis and Evaluation of a Series of Triazole Containing Novobiocin Analogues

A series of triazole-containing novobiocin analogues has been designed, synthesized and their inhibitory activity determined.⁶¹ These compounds contain a triazole ring in lieu of the amide moiety present in the natural product. The anti-proliferative effects of these compounds were evaluated against two breast cancer cell lines (SKBr-3 and MCF-7) and manifested activities similar to their amide-containing counterparts. In addition, Hsp90-dependent client protein degradation was observed via western blot analyses, further supporting a common mode of Hsp90 inhibition for both structural classes.

A. Rationale for the Development of Triazole Containing Novobiocin Analogues

Since the discovery of the Hsp90 C-terminal binding site, analogues of novobiocin have been synthesized and evaluated, with many of the compounds manifesting micromolar anti-proliferative activities.^{38-44,48-50} Modifications to both the coumarin core and benzamide side

chain have been pursued, resulting in the production of preliminary structure–activity relationships (**Figure 16**). The hydrogen bonding capabilities and the geometry of the amide bond appear to be important for novobiocin binding, however modifications to this moiety have not been evaluated for SAR. It was proposed that inclusion of 1,2,3-triazoles as a bioisosteric

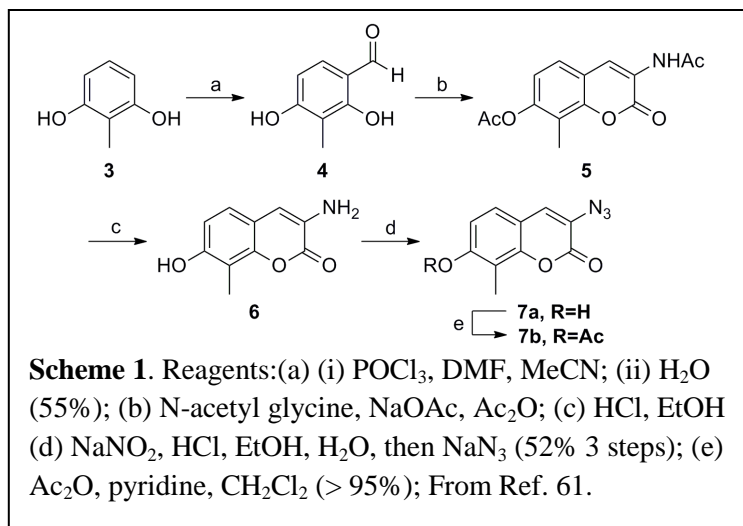


replacement for the amide moiety could facilitate SAR analysis for the aryl side chain by utilizing “click” chemistry while simultaneously

examining the necessity of the amide. The triazole serves as an amide bond replacement due to similarities in spatial characteristics. In addition, it is metabolically stable to hydrolysis and easily incorporated into small molecules.⁶²⁻⁶³ Although similar, triazoles do exhibit different hydrogen bonding capabilities and an altered geometry as compared to their amide counterparts, which aids in further elucidation of SAR (**Figure 23**). For these reasons, a series of 1,2,3-triazole containing novobiocin analogues was prepared.

B. Synthesis of Triazole Containing Novobiocin Analogues

Synthesis of the 8-methyl coumarin core, as found in novobiocin, commenced with commercially available 2-methyl resorcinol, **3** (**Scheme 1**). Compound **3** was formylated under Vilsmeier-Haack conditions enlisting POCl₃ and DMF, followed by hydrolysis to afford formyl-resorcinol **4**. Similar to the procedure of Sivakumar and co-workers, condensation of **4** with N-acetyl glycine in the presence of acetic anhydride, produced the bis-acylated coumarin, **5**.⁶⁴ Deacetylation of both the phenol and amine was accomplished upon heating with HCl and EtOH to afford 3-amino-7-hydroxy-8-methyl-coumarin, **6**. Conversion of amino-coumarin **6** to the

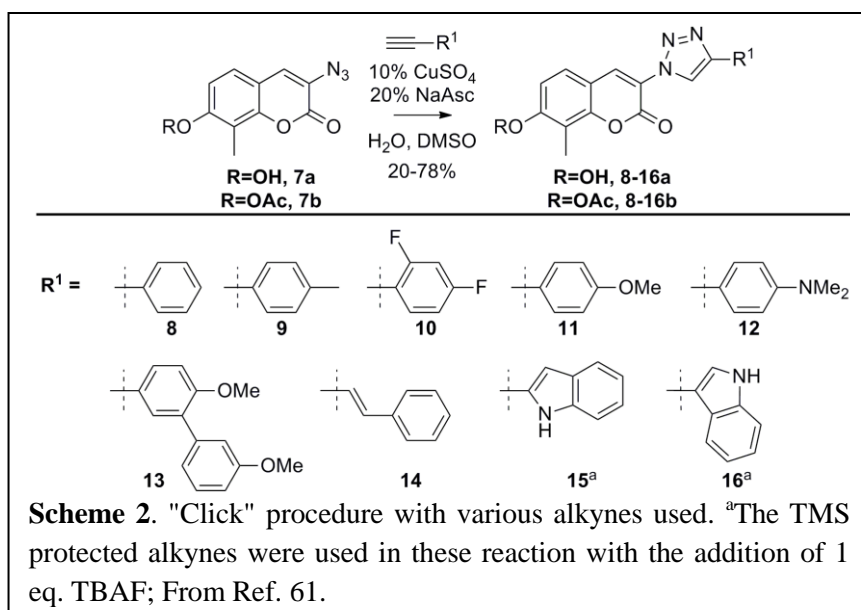


azide, which was required for the copper-catalyzed Huisgen 1,3-dipolar cycloaddition, was accomplished by in-situ generation of the 3-diazonium salt upon treatment with sodium nitrite in aqueous acid, followed by the addition of sodium azide to afford 3-

azido-coumarin, **7a**.⁶⁴ Acetylation of coumarin **7a** was accomplished with acetic anhydride in pyridine to afford **7b**.

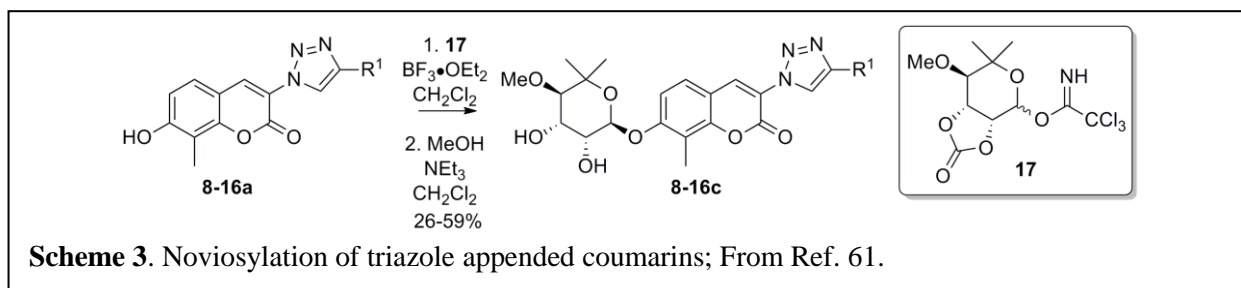
Upon the generation of compounds **7a** and **7b**, the copper-catalyzed Huisgen 1,3-dipolar cycloaddition with the corresponding alkynes was set to generate compounds **8–16a** and **8–16b** (**Scheme 2**). Standard conditions were used to effect this transformation, and a combination of DMSO and H₂O were found most suitable for optimal product formation and isolation. Alkynes

8–12 were chosen to investigate the electronic nature of the aryl side chain, including neutral (Me), electron withdrawing (F) and electron donating (OMe, NMe₂) properties as originally identified during classical novobiocin SAR



studies.³⁸ Alkynes **13–16** were chosen based on prior observations that the analogous amide derivatives manifested good anti-proliferative activities against multiple cell lines, and thus provide direct comparison between amide and triazole analogues.³⁸

Completion of the triazole-containing novobiocin analogues was achieved by incorporation of the noviose sugar into **8–16a** (Scheme 3). The phenols of compounds **8–16a** were noviosylated with the trichloroacetimidate of noviose carbonate (**15**) in the presence of boron trifluoride etherate.⁵⁵ The activated noviose, **17**, is synthesized from L-arabinose in 11 steps (9% yield overall, See Materials and Methods). Solvolysis of the cyclic carbonate with methanolic triethylamine afforded novobiocin analogues **8–16c**.



C. Biological Evaluation of Triazole Containing Novobiocin Analogues

Upon preparation of compounds **8–16 a, b** and **c**, their growth inhibitory activities against MCF-7(ER+) and SKBr-3(ER-, Her2 over-expressing) breast cancer cell lines were determined (Table 5). These results provide evidence that compounds **16a, 16b, 16c**, and **13c** are the most potent analogues prepared in this series. The structure–activity relationships suggest that analogues bearing sterically demanding side chains exhibit greater potency, as compounds with biaryl, indole, or homologated aryl groups (**13–16**) were more efficacious than substituted aryl compounds (**8–12**). In addition, comparison of compounds **8–12** suggests that *para*-substitution of the aryl ring with Me, OMe, NMe₂ or F is not well tolerated, as these compounds displayed

minimal anti-proliferative activity. These results suggest that the C-terminal binding pocket has a large hydrophobic pocket that can easily accommodate substituents as in compounds **13–16**.

Table 5. Anti-proliferative activities of triazole containing novobiocin analogues^a; From Ref. 61.

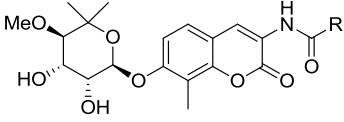
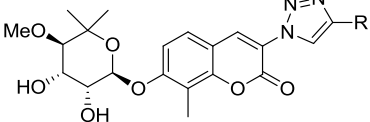
Compound	MCF-7			SKBr-3		
	(IC ₅₀ , μM) ^b			(IC ₅₀ , μM) ^b		
	a	b	c	a	b	c
NB		481.3 ± 1.5			474.7 ± 13.9	
8	25.2 ± 4.5	40.8 ± 8.4	64.4 ± 5.8	39.0 ± 3.1	76.34 ± 2.3	>100
9	23.2 ± 0.8	>100	>100	>100	90.8 ± 9.2	>100
10	33.5 ± 1.6	>100	>100	34.2 ± 4.1	>100	>100
11	>100	>100	>100	>100	>100	>100
12	>100	>100	>100	>100	>100	>100
13	28.0 ± 0.6	42.4 ± 4.9	13.2 ± 3.9	44.9 ± 3.4	50.8 ± 0.7	21.2 ± 6.0
14	33.7 ± 3.2	28.5 ± 2.2	14.6 ± 0.4	33.9 ± 6.7	65.1 ± 12.7	51.9 ± 3.0
15	38.3 ± 6.0	76.1 ± 8.4	NT	42.5 ± 0.9	50.4 ± 1.8	NT
16	8.2 ± 0.02	7.5 ± 0.7	18.3 ± 4.7	13.3 ± 2.9	6.5 ± 0.8	8.2 ± 0.1

^aValues represent mean ± standard error for at least two separate experiments performed in triplicate
^bIC₅₀ is defined as the concentration of compound necessary to inhibit cellular growth by 50%
 NT = Not Tested

Additionally, comparison between the amide containing analogues and triazole containing analogues provides further SAR (**Table 6**). As evident from the data presented in **Table 6**, the triazole moiety has little effect on anti-proliferative activity. Comparing the triazole and amide analogues containing the biaryl and 3-indole side chains indicate the activities for both sets of compounds are comparable against the two cell lines tested. One discrepancy observed between the amide and triazole analogues is that in which simple aryl side chains (**8–12**) manifest IC₅₀ values in the 10-20 μM range for the amide-containing molecules while the triazole compounds **8** and **11** display IC₅₀ values above 50 μM.³⁸ These results suggest that the triazole moiety affects biological activity in two ways: the availability of a hydrogen bond donor in the amide linkage and the steric bulk of the side chain. This hydrogen bond donor is lost upon

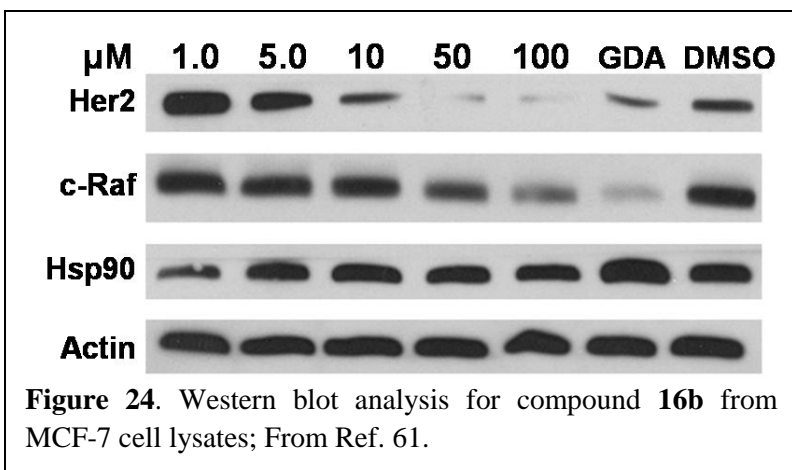
introduction of the triazole moiety, but interactions can be increased by the introduction of steric bulk in the side chain. This phenomenon correlates well with the CoMFA model described above, as a large area of steric bulk was a predictor for increased activity. In addition, the CoMFA model prepared by Huang and co-workers incorporated the triazole containing analogues.⁵¹ Their CoMFA predicts that the amide bond hydrogen-bond donor is necessary for biological activity. A preference for steric bulk has been observed in several series of novobiocin analogues, and appears to be a contributing factor to biological activity.

Table 6. Comparison of anti-proliferative activities: amide-containing versus triazole-containing novobiocin analogues; From Ref. 61.

		
	R=Biaryl	R=Biaryl (13c)
IC ₅₀ (MCF-7)	18.7 ± 1.8 ^{at}	13.2 ± 3.9
IC ₅₀ (SKBr-3)	7.5 ± 1.0 ^{at}	21.2 ± 6.0
	R=3-Indole	R=3-Indole (16c)
IC ₅₀ (MCF-7)	5.3 ± 0.3 ^{at}	18.3 ± 4.7
IC ₅₀ (SKBr-3)	12.2 ± 1.5 ^{at}	8.2 ± 0.1

^aBiological data taken from Ref. 16

After analysis of the triazole containing analogues anti-proliferative activity, Western blot analysis was performed for the most active compound, **16b**, to confirm that anti-proliferative activity results from Hsp90 inhibition (**Figure 24**). Western blot analysis of MCF-7 cells treated with increasing concentrations of **16b**, show the compound to induce Hsp90-dependent client protein



degradation in a dose-dependent manner, with an apparent IC_{50} value that correlates directly to the anti-proliferative IC_{50} value. Her2 and c-Raf are client proteins of Hsp90, and pharmacological inhibition of Hsp90 leads to their degradation via ubiquitinylation and proteome-mediated hydrolysis. Additionally, compound **16b** appears to have little effect on the heat shock response, as unaltered levels of Hsp90 were observed, consistent with inhibition of the Hsp90 C-terminus. Western blot analysis indicates that these compounds are interfering with the Hsp90-mediated protein folding process, and that the anti-proliferative activities for these compounds are directly related to Hsp90 inhibition.

A series of triazole containing novobiocin analogues was prepared and evaluated against two breast cancer cell lines. Western blot analysis affirmed Hsp90 inhibition by this class of compounds. The compounds described herein exhibit comparable activities to the corresponding amide-containing analogues. These results indicate that the amide moiety can be replaced by the triazole functionality, however, in some cases the loss of the hydrogen bond donor appears detrimental, but can be overcome by the inclusion of steric bulk in the triazole substituent.

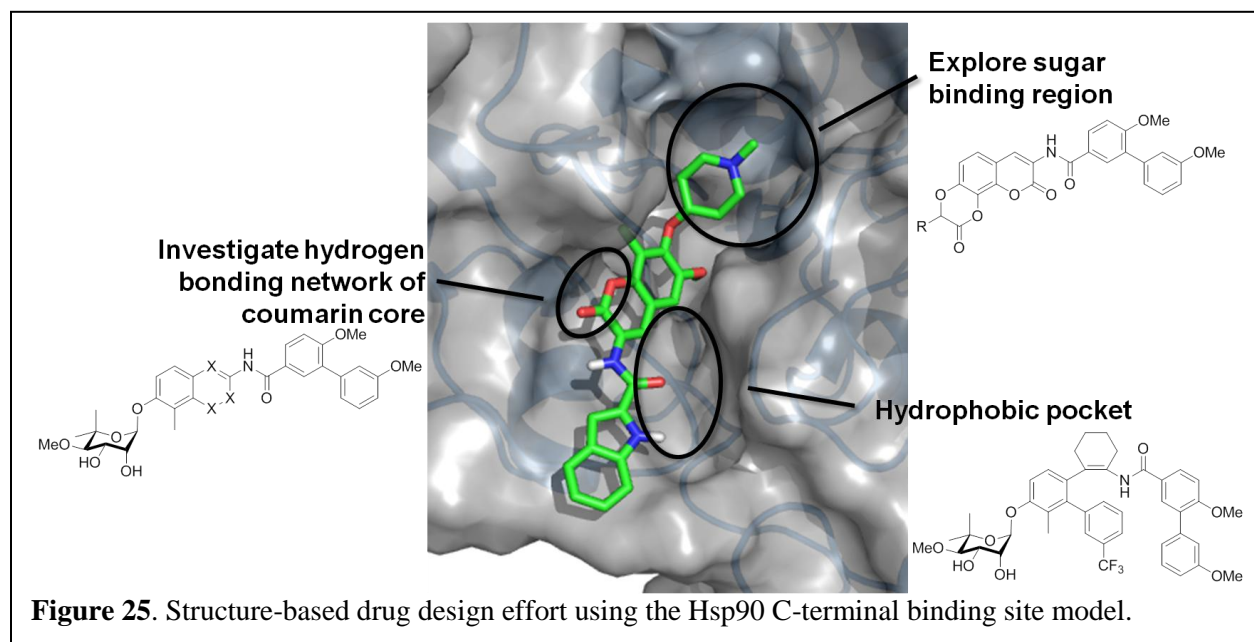
V. Conclusions and Future Work

Throughout the work described above, we have been able to define the binding pocket for C-terminal Hsp90 inhibitors for the first time. The CoMFA model provided valuable insights into the nature of the binding pocket and correlated well with observed SAR trends derived from prior studies. Subsequent biochemical elucidation of the C-terminal binding site using a NB-based photoaffinity label coupled with mass spectrometry was accomplished.⁵⁴ This model provides a means to design novel compounds in aims to generate a rational approach towards Hsp90 inhibitor development. Lastly, using a bioisosteric replacement method, we investigated the role of the amide bond contained within Novobiocin. Triazole-containing novobiocin

analogues were synthesized and evaluated, and demonstrated that the amide bond is not critical to biological activity, as amide-containing and triazole-containing analogues manifested similar activities.⁶¹ This work has led to an extensive structure-based design approach to Hsp90 C-terminal inhibitors; in addition, the pursuit of an Hsp90-C-terminal inhibitor crystal structure is underway.

A. Structure Based Drug Design of Novel C-terminal Inhibitors

Using the model of the C-terminal binding site, the Blagg laboratory has been able to pursue novel NB analogues using a structure-based approach (**Figure 25**). As evidenced from the

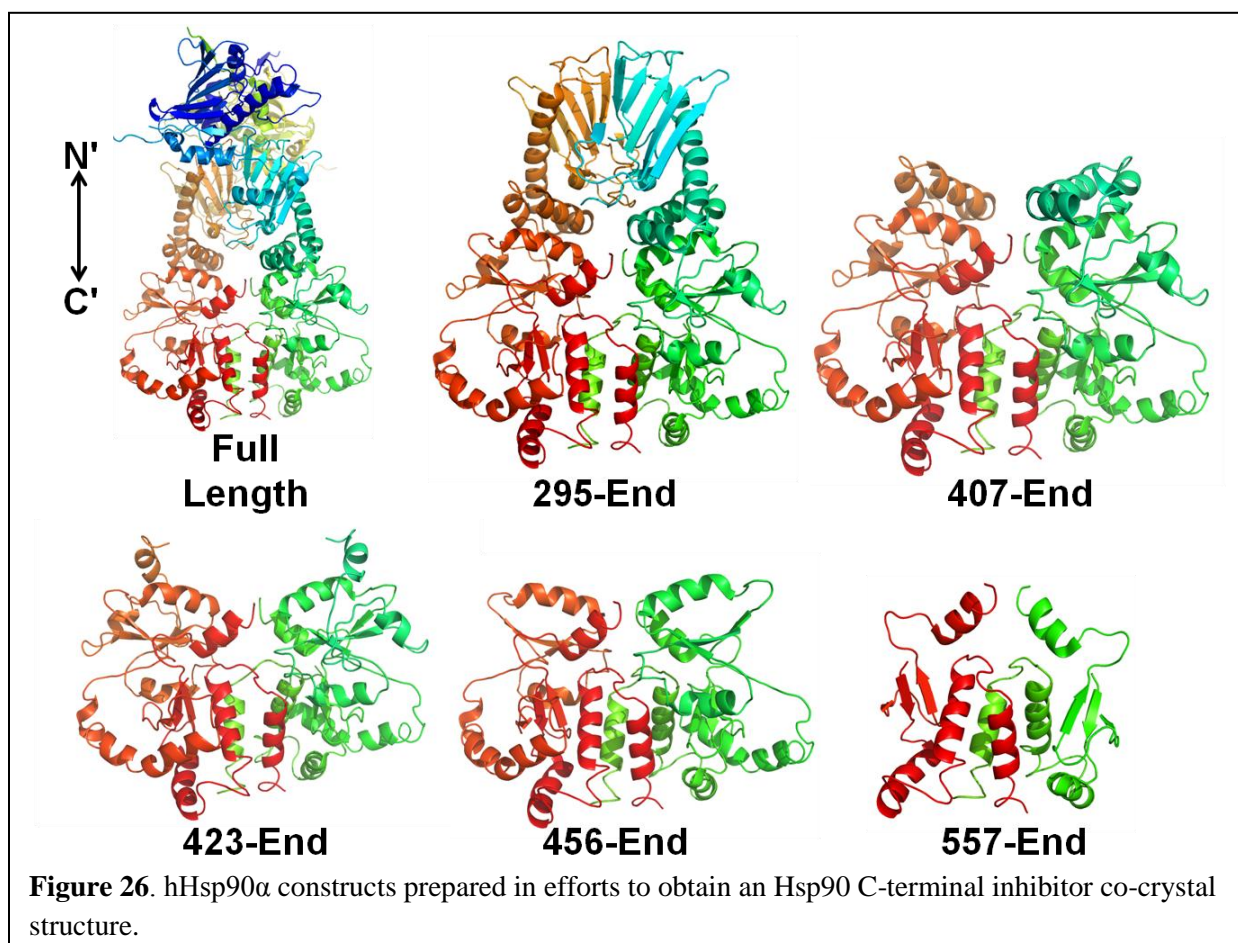


C-terminal model, there were several regions on the NB scaffold that could be modified to produce more additional interactions with the binding site. Several polar residues exist proximal to the lactone moiety and synthesis of coumarin-scaffold mimics will aid in the evaluation of these interactions. Second, there appears to be a large hydrophobic space adjacent to the amide bond. Using Diels–Alder chemistry, compounds can be synthesized that have cyclohexyl-derived moieties capable of occupying this region. In addition, a deep pocket resides near the sugar

binding region. Various mimics of the sugar moiety may fit in this pocket and provide additional interactions. Several colleagues in the Blagg Laboratory have utilized this model to design these and other C-terminal inhibitory compounds and to help explain previously observed SAR trends.

B. Progress towards a C-terminal Inhibitor Co-Crystal Structure

Although the C-terminal binding site model derived from photoaffinity studies has been very useful, we and others are still interested in the attainment of a C-terminal inhibitor bound co-crystal structure. During a research rotation in the Laurence Pearl – Chrisostomos Prodromou laboratory at the Institute of Cancer Research (now at The University of Sussex), I was involved in this effort. Previous attempts to obtain a co-crystal structure utilized yeast CTD constructs.



These protein constructs were able to form crystals but produced very poor diffraction data. We sought to utilize the human proteins, Hsp90 α and Hsp90 β , of varying lengths to optimize the

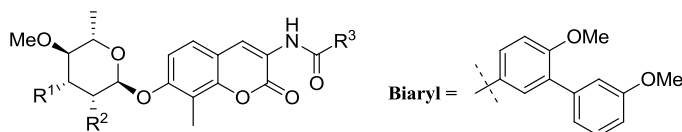
crystals for diffraction. A depiction of the varying constructs, ten total for each isoform (five terminate at residue 689, five terminate at residue 732 (C-terminal end)), are shown in **Figure 26**. The rationale behind these different constructs was that we aimed to simultaneously improve crystallization and stability properties while maintaining the CTD binding site. Constructs that were too short would not contain the inhibitor binding site, while the longer constructs may suffer from crystallization and diffraction issues as observed with the yeast constructs. In pursuit of this co-crystal structure, cloning of the hHsp90 α and hHsp90 β DNA was performed. The clones were ligated into the pET vector suitable for protein expression. Plasmids were transformed into a suitable competent *e. coli* and colonies were selected based on ampicillin resistance. Colonies were grown in liquid media followed by plasmid DNA isolation, purification, and sequencing. Following correct sequencing, protein expression and purification was carried out and preliminary crystallography screens were performed in a 96-well format. Upon the completion of my research rotation, Chrisostomos Prodromou continued this work by preparing the remaining constructs and expressing/purifying the proteins. Further crystallography screens were performed, producing several crystals capable of diffraction. To date, the resolution of these structures has not been adequate, and further refinement of the crystallization set up is underway.

VI. Materials and Methods

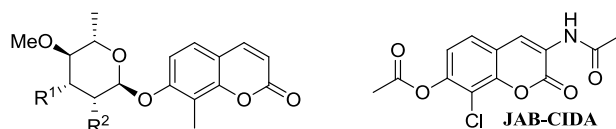
A. Development of a CoMFA for Hsp90 C-Terminal Inhibitors

Data Set. The structures of all compounds used to generate the CoMFA model, their anti-proliferative IC₅₀ values (MCF-7), and pIC₅₀ (LogIC₅₀) values are shown in **Table 7**.

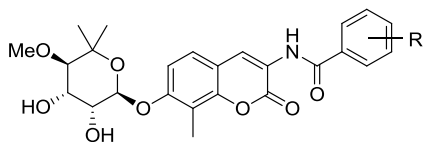
Table 7. Novobiocin analogues used in the development of a C-terminal inhibitor CoMFA model.



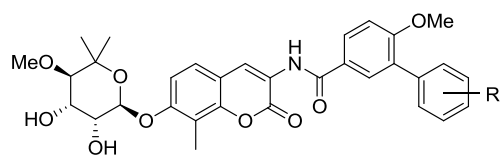
Compound	R ¹	R ²	R ³	IC ₅₀ (μM, MCF-7)	pIC ₅₀
DNBA1	OH	OH	Me	>100	2.00
DNBA2	OC(O)NH ₂	OH	Me	>100	2.00
DNBA3	H	H	Me	>100	2.00
DNBA4	OH	OH	Biaryl	7.7	0.89
DNBA5	OC(O)NH ₂	OH	Biaryl	1.7	0.23
DNBA6	H	H	Biaryl	1.7	0.23



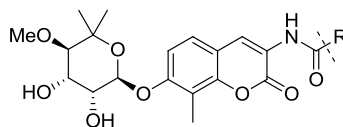
Compound	R ¹	R ²	R ³	IC ₅₀ (μM, MCF-7)	pIC ₅₀
DNBA7	OH	OH	Me	>100	2.00
DNBA8	OC(O)NH ₂	OH	Me	>100	2.00
DNBA9	H	H	Me	32.6	1.51
JAB-CIDA	--	--	--	>100	2.00



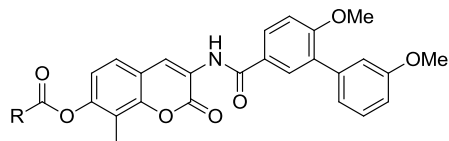
Compound	R	IC ₅₀ (μM, MCF-7)	pIC ₅₀
KU36	H	21.0	1.32
KU91	2-OMe	5.3	0.72
KU92	3-OMe	5.6	0.75
KU93	4-OMe	10.3	1.01
KU94	2-Ph	19.0	1.28
KU95	3-Ph	18.0	1.26
KU96	4-Ph	8.1	0.91
KU97	2-NO ₂	28.7	1.46
KU98	3-NO ₂	>100	2.00
KU99	4-NO ₂	>100	2.00
KU100	2-NH ₂	17.2	1.24
KU101	3-NH ₂	30.1	1.48
KU102	4-NH ₂	14.0	1.15
KU105	3-I, 4-OMe	6.3	0.80
KU106	3-Ph, 4-OMe	19.5	1.29



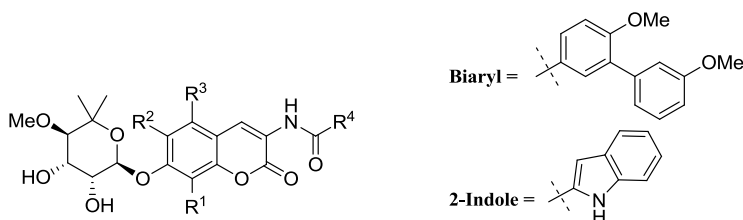
Compound	R	IC ₅₀ (μM, MCF-7)	pIC ₅₀
KU107	2-Me	18.9	1.28
KU108	3-Me	20.4	1.31
KU109	4-Me	16.7	1.22
KU110	2-OMe	15.6	1.19
KU111	3-OMe	18.7	1.27
KU112	4-OMe	37.9	1.58
KU113	2-OH	1.5	0.18
KU114	3-OH	5.3	0.72
KU115	4-OH	2.3	0.36



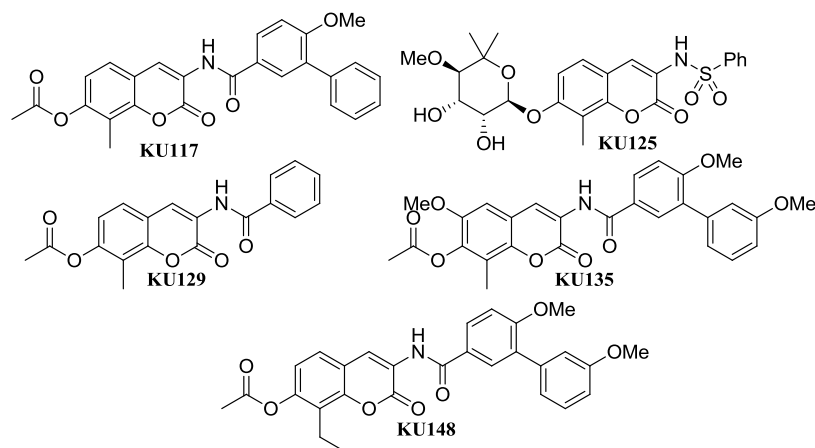
Compound	R	IC ₅₀ (μM, MCF-7)	pIC ₅₀
KU103		16.4	1.21
KU104		6.9	0.84
KU118		>100	2.00
KU119	2-Pyridyl	20.3	1.31
KU120	3-Pyridyl	47.8	1.68
KU121	4-Pyridyl	>100	2.00
KU122	2-Indole	0.57	-0.24
KU123	3-Indole	5.3	0.72
KU124		4	0.60
KU126		>100	2.00
KU130		1.7	0.23
KU136		>100	2.00
KU137		28.6	1.46
KU138		96.3	1.98



Compound	R	IC ₅₀ (μM, MCF-7)	pIC ₅₀
KU111OAc	Me	1.4	0.15
KU131	Et	2.9	0.46
KU132	Cyclohexyl	4.2	0.62
KU133	Cyclopropyl	3.4	0.53
KU134	2-OMe-phenyl	>100	2.00
KU139	n-Pentyl	2.9	0.46
KU140	Phenyl	29.5	1.47
KU141	4-Et-phenyl	>100	2.00
KU142	2-Naphthyl	77.5	1.89



Compound	R ¹	R ²	R ³	R ⁴	IC ₅₀ (μM, MCF-7)	pIC ₅₀
KU144	Me	OMe	H	Biaryl	>100	2.00
KU146	Et	H	H	Biaryl	14.4	1.16
KU147	Et	H	H	2-Indole	4.3	0.63
KU149	Me	OPr	H	Biaryl	>100	2.00
KU150	Me	OPr	H	2-Indole	2.1	0.32
KU153	CH ₂ Ph	H	H	Biaryl	>100	2.00
KU154	CH ₂ Ph	H	H	2-Indole	38.0	1.58
KU157	Me	H	OMe	Biaryl	82.8	1.92
KU158	Me	H	OMe	2-Indole	9.0	0.95
KU161	Me	<i>O</i> ⁱ Pr	H	Biaryl	66.9	1.83
KU162	Me	<i>O</i> ⁱ Pr	H	2-Indole	20.7	1.32
KU165	Ph	H	H	Biaryl	>100	2.00
KU166	Ph	H	H	2-Indole	38.8	1.59
KU169	Me	OMe	H	2-Indole	24.4	1.39
KU174	OMe	H	H	Biaryl	9.0	0.95
KU175	OMe	H	H	2-Indole	9.7	0.99



Compound	IC ₅₀ (μM, MCF-7)	pIC ₅₀
KU117	6.0	0.78
KU125	>100	2.00
KU129	36.4	1.56
KU135	1.5	0.18
KU148	14.9	1.17

Molecular Database Alignment. All molecular structures in the data set were built in Sybyl v8.0 and were minimized in the Tripos force field utilizing a distance dependent dielectric function, leaving all other parameters set to default. Gasteiger-Marsili partial charges were then calculated and assigned for each molecule. All compounds in the molecular database were then aligned using the coumarin ring as the core structure. The aligned database was then subjected to CoMFA analysis.

CoMFA. Steric energy (Lennard-Jones potential) and electrostatic (Coulomb potential) energy were measured for each molecule using a probe atom (sp³-hybridized carbon; +1 charge; 1.52Å van der Waals radius) in Sybyl using default settings with the Tripos force field. A partial least-squares (PLS) analysis was then performed. LogIC₅₀ (pIC₅₀; MCF-7 anti-proliferation) values were used as the dependent variable while the calculated steric and electrostatic CoMFA parameters served as the independent variable. The generated models were evaluated using the leave-one-out cross-validation strategy (q²). The optimum number of components (ONC) was the

value that gave the highest q^2 value (6). The ONC was then used in the generation of the final, non-cross validated PLS regression model which can be used to predict the activities of compounds not in the data set. For evaluation purposes, this model was used to predict the activities of the compounds in the training set ($R^2 = 0.88$).

B. Identification of the NB binding site in Hsp90's C-terminal Domain

Photoaffinity Labeling and Mass Spectrometry. Recombinant His-tagged Hsp90CT (amino acids 531-732 human Hsp90 α) was exposed to four flashes of 184 μ J of UV radiation in the presence of 0.5 mM of either **1**, **2** or DMSO (vehicle control), followed by digestion of the samples with trypsin. The tryptic peptides were subjected to capillary LC-MS/MS experiments using tandem LTQ-FT Mass Spectrometer (ThermoFinnigan) under conditions described previously,⁶⁵ followed by data analysis.

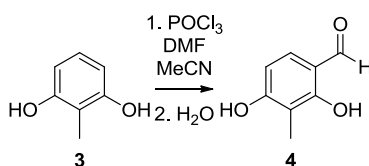
Docking of NB into HtpG Structure. Docking of NB into the open Hsp90 structure (HtpG solution structure) was performed in Sybyl v8.0 using Surflex-Dock docking software. The peptide identified in photoaffinity labeling studies (HtpG 500-SEKEAE-505) was used as a guide to build the binding site (protomol). The top 10 binding modes were analyzed and subjected to a molecular dynamics protocol. The binding model giving the best binding score after the MD protocol was used in generation of the binding model and homology model of hHsp90 α .

Hsp90 α Homology Model. The sequence of hHsp90 α was used to search similar sequences using NCBI blast.⁶⁶ A multiple sequence alignment was performed using ClustalW with default parameters to align these sequences and to identify structurally conserved regions and important residues, specifically between hHsp90 α and HtpG.⁶⁷ Homology modeling was performed with the program Modeller using the structure of HtpG as template.⁵⁶ The sequence alignment was

done as discussed previously and ten models were built followed by refinement using molecular dynamics as implied in Modeller (refine_fast). The model corresponding to the lowest value of the probability density function (pdf) and fewest restraints violations out of the generated models was used for further analysis. The minimization of the side chains was performed using Sybyl molecular modeling software.⁶⁸ Initially, the protein was held fixed except for the binding site residues (residues falling within 8Å of novobiocin molecule). Thereafter, all side chains and the binding site were kept free and minimization was done. All the minimization was done until the RMS gradient of 0.05 Kcal/MolÅ was obtained using AMBER9 force field.

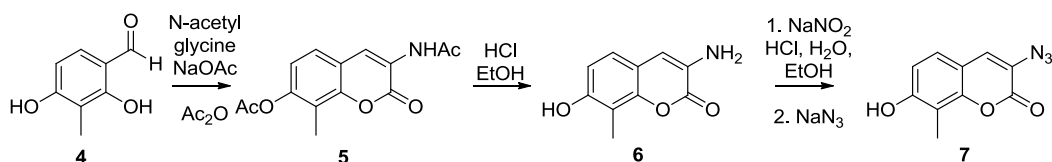
C. Synthesis and Evaluation of a Series of Triazole Containing Novobiocin Analogues

Experimental Procedures:

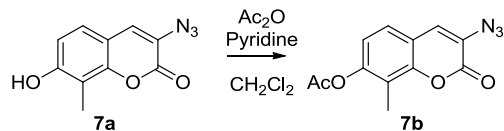


2,4-dihydroxy-3-methylbenzaldehyde (4). 2-Methyl-resorcinol (10.00 g, 80.58 mmol) in anhydrous CH₃CN (100 mL) was cooled to 0 °C, then *N,N*-dimethylformamide (7.45 mL, 96.22 mmol) and freshly distilled phosphorus oxychloride (8.98 mL, 96.34 mmol) were added in sequence, and the resulting solution was warmed to rt over 18 h. The white precipitate was collected by filtration, resuspended in H₂O (100 mL), and heated to reflux for 1 h. The suspension was cooled to 0 °C and the precipitate was collected by filtration to give **4** as a colorless solid (6.67 g, 54%): ¹H NMR (CDCl₃, 500 MHz) δ 11.68 (s, 1H), 9.69 (s, 1H), 7.29 (d, *J* = 8.5 Hz, 1H), 6.48 (d, *J* = 8.5 Hz, 1H), 2.14 (s, 3H); ¹³C NMR (CDCl₃, 125 MHz) δ 194.9, 162.4, 161.5, 133.2, 115.2, 111.3, 108.2, 7.3; IR (film) ν_{max} 3281, 1618, 1595, 1493, 1439, 1379,

1304, 1250, 1217, 1095, 793, 710 cm^{-1} ; HRMS (ESI⁺) m/z : $[\text{M} + \text{H}]^+$ calcd for $\text{C}_8\text{H}_8\text{O}_3$, 153.0552; found, 153.0559.



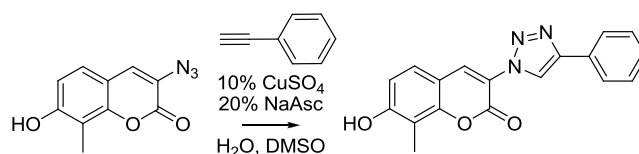
3-azido-7-hydroxy-8-methyl-2H-chromen-2-one (7a). Aldehyde **4** (3.50 g, 23.0 mmol), N-acetylglycine (2.69 g, 23 mmol) and sodium acetate (5.66 g, 69 mmol) in acetic anhydride (100 mL) was stirred at reflux for 4 h.⁶⁴ Cooling to rt then to 0°C provided a yellow precipitate which was filtered and rinsed with DI H₂O (**5**). Without purification, **5** was dissolved in concentrated HCl and EtOH (2:1, 30 mL) and refluxed for 1 hour. Water (40 mL) was added and the solution cooled to 0°C. NaNO₂ (3.178 g, 46 mmol) was added and stirred for 15 minutes. NaN₃ (4.50 g, 69 mmol) was then added in portions at 0°C and stirred for 1 h. at 0°C before filtering the resulting brown solid. The solid was then washed with cold water affording a brown solid (2.5 g, 52%): ¹H NMR (500 MHz, DMSO) δ 10.49 (s, 1H), 7.60 (d, $J = 1.6$, 1H), 7.36 (d, $J = 8.5$, 1H), 6.91 (d, $J = 8.5$, 1H), 2.20 (s, 3H); ¹³C NMR (126 MHz, DMSO) δ 158.1, 157.4, 150.8, 128.2, 125.8, 120.6, 112.6, 111.3, 110.6, 7.9; IR (film) ν_{max} 3402 (br), 2922, 2359, 2341, 2212, 2113, 1734, 1686, 1601, 1578, 1340, 1288, 1261, 1232, 1150, 1072, 980, 912 cm^{-1} .



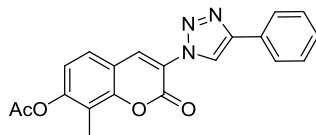
3-azido-8-methyl-2-oxo-2H-chromen-7-yl acetate (7b). To compound **7a** (500 mg, 2.30 mmol) in anhydrous CH₂Cl₂ (35 mL), acetic anhydride (325 μL , 3.45 mmol) then pyridine (100 μL , 1.20 mmol) were added and stirred for 16 h. at rt. The reaction was diluted with EtOAc, washed with water (100 mL), brine, and dried (Na₂SO₄). The solvent was removed in vacuo affording a

yellow solid that was used without further purification (860 mg, 98%): ^1H NMR (500 MHz, DMSO) δ 7.68 (s, 1H), 7.54 (d, $J = 8.4$, 1H), 7.15 (d, $J = 8.5$, 1H), 2.35 (s, 3H), 2.17 (s, 3H); ^{13}C NMR (126 MHz, DMSO) δ 168.8, 156.8, 150.1, 149.7, 126.5, 125.5, 124.8, 119.3, 118.0, 117.0, 20.5, 8.7; IR (film) ν_{max} 2934, 2359, 2343, 2137, 1753, 1722, 1624, 1605; 1447, 1431, 1371, 1339, 1223, 1144, 1090, 1018, 912 cm^{-1} .

General Procedure A: Cu-Mediated Triazole Formation

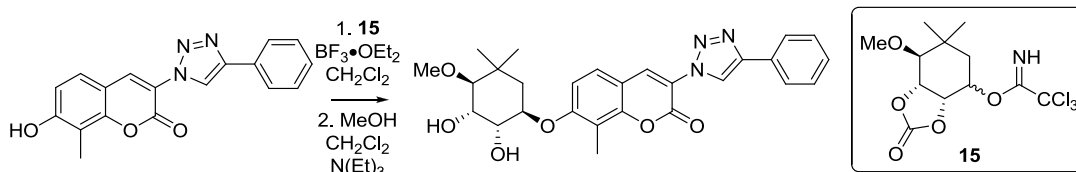


7-hydroxy-8-methyl-3-(4-phenyl-1H-1,2,3-triazol-1-yl)-2H-chromen-2-one (8a). Using a procedure similar to Sivakumar et al.⁶⁴, azide **7a** (203.3 mg, 0.93 mmol) was dissolved in 1:1 H₂O:DMSO (10 mL). Phenylacetylene (101 μL , 0.93 mmol), CuSO₄ (7.5% in DI H₂O, 310 μL , 0.09 mmol), and NaAsc (1 M in H₂O, 180 μL , 0.18 mmol) were added in that order and stirred for 16 h. at rt in the dark. H₂O was then added to, and the resulting precipitate was filtered and rinsed with H₂O. The triazole product was then purified by flash column chromatography. (SiO₂, 1:2 EtOAc:Hexanes) to afford **8a** as a yellow amorphous solid (128.4 mg, 43%): ^1H NMR (500 MHz, Acetone) δ 8.93 (s, 1H), 8.58 (s, 1H), 8.05 – 7.97 (m, 2H), 7.66 (d, $J = 8.5$ Hz, 1H), 7.49 (t, $J = 7.7$ Hz, 2H), 7.38 (t, $J = 7.4$ Hz, 1H), 7.06 (d, $J = 8.5$ Hz, 1H), 2.34 (s, 3H); ^{13}C NMR (126 MHz, DMSO) δ 160.4, 156.5, 152.7, 146.4, 137.2, 130.1, 129.0(2C), 128.2, 127.8, 125.4(2C), 122.1, 118.8, 113.2, 110.9, 110.3, 7.9; IR (film) ν_{max} 3416 (br), 2955, 2922, 2852, 1745, 1730, 1697, 1643, 1609, 1587, 1454, 1265, 1244, 1213, 1177, 1092, 1078 cm^{-1} ; HRMS (ES⁺) m/z : [M + H] calcd for C₁₈H₁₄N₃O₃ 320.1035; found 320.1022.



8-methyl-2-oxo-3-(4-phenyl-1H-1,2,3-triazol-1-yl)-2H-chromen-7-yl acetate (8b). Compound **8b** was prepared following General Procedure A with azide **7b** (15 mg, 0.06 mmol) and phenylacetylene (6.5 μ L, 0.06mmol) and was purified by column chromatography (SiO₂, 1:1 EtOAc:Hexanes) to afford a yellow amorphous solid (16.3 mg, 78%): ¹H NMR (400 MHz, DMSO) δ 9.08 (s, 1H), 8.80 (s, 1H), 7.99 (d, J = 7.1, 2H), 7.86 (d, J = 8.5, 1H), 7.49-7.53 (m, 2H), 7.40 (t, J = 7.25, 1H), 7.30 (d, J = 8.4, 1H), 2.40 (s, 3H), 2.26 (s, 3H); ¹³C NMR (126 MHz, Acetone) δ 168.9, 156.2, 153.3, 152.4, 151.4, 147.8, 134.5, 131.2, 129.5, 128.9, 127.7, 126.8, 126.2, 126.0, 121.7, 120.4, 120.0, 116.8, 20.2, 8.7; IR (film) ν_{max} 3063, 2955, 2926, 2127, 1763, 1726, 1607, 1447, 1418, 1369, 1236, 1196, 1165, 1134, 1084, 1013, 924, 903 cm^{-1} ; HRMS (ES⁺) m/z : [M + H] calcd for C₂₀H₁₆N₃O₄ 362.1141; found 362.1133.

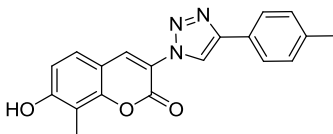
General Procedure B: Noviosylation and Carbonate Hydrolysis



7-((2S,3R,4S,5R)-3,4-dihydroxy-5-methoxy-6,6-dimethyltetrahydro-2H-pyran-2-yloxy)-8-methyl-3-(4-phenyl-1H-1,2,3-triazol-1-yl)-2H-chromen-2-one (8c). Boron trifluoride etherate (65 μ L, 0.53 mmol) was added to compound **8a** (85 mg, 0.27 mmol) and (3aR,4S,7R,7aR)-7-methoxy-6,6-dimethyl-2-oxo-tetrahydro-3aH-[1.3]dioxolo[4,5-c]pyran-4-yl 2,2,2-trichloroacetimidate (**17**) (0.532 mmol) in anhydrous CH₂Cl₂ (3 mL).⁵⁵ After stirring at rt for 18 h, triethylamine (100 μ L, 0.72 mmol) was added and the solvent was concentrated. The residue

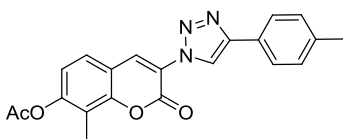
was partially purified via column chromatography (SiO₂, 3:1:1 Hexanes:CH₂Cl₂:EtOAc) and the coupled carbonate was used without further purification.

The isolated carbonate was dissolved in MeOH (40 mL), CH₂Cl₂ (2 mL), and triethylamine (4 mL) and stirred for 18 h at rt. The solvent was concentrated and the residue purified via column chromatography (SiO₂, 24:1 CH₂Cl₂:MeOH) to afford a white amorphous solid (44 mg, 34% over two steps): ¹H NMR (400 MHz, DMSO) δ 9.03 (s, 1H), 8.70 (s, 1H), 7.97 (d, *J* = 8.0, 2H), 7.79 (d, *J* = 8.7, 1H), 7.50 (m, 2H), 7.39 (t, *J* = 7.3, 1H), 7.27 (d, *J* = 8.8, 1H), 5.60 (s, 1H), 5.37 (d, *J* = 4.6, 1H), 5.06 (d, *J* = 6.1, 1H), 4.03 (dd, *J* = 12.1, 6.1 1H), 3.93 (s, 1H), 3.50 (s, 3H), 3.29 (d, *J* = 9.2, 1H), 2.26 (s, 3H), 1.26 (s, 3H), 1.02 (s, 3H); ¹³C NMR (126 MHz, DMSO) δ 158.1, 156.1, 151.7, 146.5, 136.5, 130.0, 129.0, 128.2 (2C), 127.9, 125.4 (2C), 122.1, 120.2, 113.0, 112.0, 111.1, 98.3, 83.2, 77.9, 70.7, 67.5, 61.1, 28.5, 22.8, 8.2; IR (film) ν_{max} 3496 (br), 1742, 1720, 1609, 1504, 1472, 1302, 1286, 1246, 1219, 1182, 1126, 1086, 1043, 1014, 984, 945 cm⁻¹; HRMS (ES⁺) *m/z*: [M + H] calcd for C₂₆H₂₈N₃O₇ 494.1927; found 494.1907.

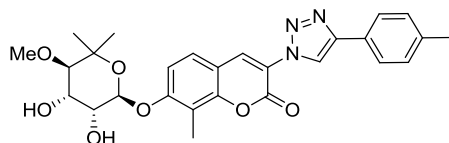


7-hydroxy-8-methyl-3-(4-p-tolyl-1H-1,2,3-triazol-1-yl)-2H-chromen-2-one (9a). Compound **9a** was prepared following General Procedure A with azide **7a** (150 mg, 0.69 mmol) and 1-ethynyl-4-methylbenzene (92 μL, 0.73 mmol) and was purified by column chromatography (SiO₂, 3:1:1 Hexanes:EtOAc:CH₂Cl₂) to afford a yellow amorphous solid (98.9 mg, 42%): ¹H NMR (500 MHz, DMSO) δ 10.86 (s, 2H), 8.94 (s, 2H), 8.63 (s, 1H), 7.84 (d, *J* = 8.1, 2H), 7.62 (d, *J* = 8.5, 1H), 7.30 (d, *J* = 7.9, 2H), 6.98 (d, *J* = 8.5, 1H), 2.35 (s, 3H), 2.23 (s, 3H); ¹³C NMR (126 MHz, DMSO) 160.3, 156.4, 152.6, 146.4, 137.6, 137.1, 129.5(2C), 127.8, 127.2, 125.3(2C), 121.7, 118.8, 113.1, 110.9, 110.3, 20.8, 7.9; IR (film) ν_{max} 3339 (br), 3300, 1757,

1713, 1682, 1537, 1375, 1319, 1288, 1211, 1112, 1061, 1014, 962, 933, 914 cm^{-1} ; HRMS (ES^+) m/z : $[\text{M} + \text{H}]$ calcd for $\text{C}_{19}\text{H}_{16}\text{N}_3\text{O}_3$ 334.1192; found 334.1175.

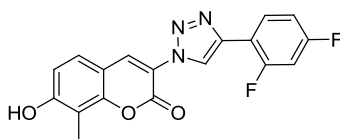


8-methyl-2-oxo-3-(4-p-tolyl-1H-1,2,3-triazol-1-yl)-2H-chromen-7-yl acetate (9b). Compound **9b** was prepared following General Procedure A with azide **7b** (150 mg, 0.58 mmol) and 1-ethynyl-4-methylbenzene (88 μL , 0.69 mmol) and was purified by column chromatography (SiO_2 , 3:1:1 Hexanes:EtOAc: CH_2Cl_2) to afford a white amorphous solid (117 mg, 54%): ^1H NMR (500 MHz, DMSO) δ 9.01 (s, 1H), 8.78 (s, 1H), 7.84-7.88 (m, 3H), 7.28-7.32 (m, 3H), 2.39 (s, 3H), 2.36 (s, 3H), 2.25 (s, 3H); ^{13}C NMR (126 MHz, DMSO) δ 168.7, 155.7, 152.1, 151.5, 146.7, 137.8, 135.0, 129.7(2C), 127.4, 127.0, 125.5(2C), 122.4, 121.4, 119.8, 118.4, 116.0, 20.8, 20.5, 8.8; IR (film) ν_{max} 3175, 3069, 2916, 1767, 1724, 1628, 1605, 1497, 1450, 1406, 1387, 1369, 1269, 1238, 1196, 1165, 1132, 1086, 1013, 926 cm^{-1} ; HRMS (ES^+) m/z : $[\text{M} + \text{H}]$ calcd for $\text{C}_{21}\text{H}_{18}\text{N}_3\text{O}_4$ 376.1297; found 376.1281.



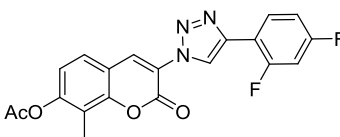
7-((2S,3R,4S,5R)-3,4-dihydroxy-5-methoxy-6,6-dimethyltetrahydro-2H-pyran-2-yloxy)-8-methyl-3-(4-p-tolyl-1H-1,2,3-triazol-1-yl)-2H-chromen-2-one (9c). Compound **9c** was prepared following General Procedure B with coumarin **9a** (70 mg, 0.21 mmol) and was purified by column chromatography (SiO_2 , 99:1 to 32:1 CH_2Cl_2 :MeOH) to afford an off-white amorphous solid (34.2 mg, 32% over two steps): ^1H NMR (500 MHz, DMSO) δ 8.96 (s, 1H), 8.68 (s, 1H), 7.85 (d, $J = 8.1$, 2H), 7.77 (d, $J = 8.7$, 1H), 7.30 (d, $J = 7.9$, 2H), 7.26 (d, $J = 8.9$, 1H), 5.59 (d, $J = 2.5$, 1H), 5.37 (d, $J = 4.7$, 1H), 5.06 (d, $J = 6.2$, 1H), 4.02 (ddd, $J = 3.3, 6.3, 9.4$,

1H), 3.95 – 3.89 (m, 1H), 3.50 (s, 3H), 3.29 (d, $J = 9.2$, 1H), 2.35 (s, 3H), 2.25 (s, 3H), 1.26 (s, 3H), 1.01 (s, 3H) ^{13}C NMR (126 MHz, DMSO) δ 158.1, 156.2, 151.7, 146.5, 137.6, 136.3, 129.5(2C), 127.9, 127.2, 125.3(2C), 121.6, 120.2, 113.0, 112.0, 111.2, 98.3, 83.2, 78.0, 70.7, 67.5, 61.1, 28.5, 22.8, 20.8, 8.2; IR (film) ν_{max} 3433 (br), 2386, 1724, 1715, 1607, 1165, 1128, 1107, 1086, 1070, 1049, 987, 962, 926 cm^{-1} ; HRMS (ES^+) m/z : $[\text{M} + \text{H}]$ calcd for $\text{C}_{27}\text{H}_{30}\text{N}_3\text{O}_7$ 508.2084; found 508.2067.

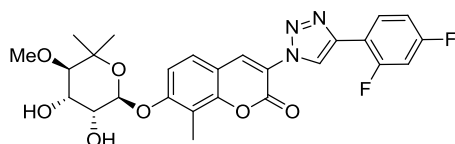


3-(4-(2,4-difluorophenyl)-1H-1,2,3-triazol-1-yl)-7-hydroxy-8-methyl-2H-chromen-2-one

(10a). Compound **10a** was prepared following General Procedure A with azide **7a** (150mg, 0.69 mmol) and 1-ethynyl-2,4-difluorobenzene (105 mg, 0.76 mmol) and was purified by column chromatography (SiO_2 , 2:1:1 Hexanes:EtOAc: CH_2Cl_2) to afford a yellow amorphous solid (50 mg, 20%): ^1H NMR (500 MHz, DMSO) δ 10.88 (s, 1H), 8.82 (d, $J = 3.5$, 1H), 8.65 (s, 1H), 8.22 (td, $J = 6.6, 8.7$, 1H), 7.62 (d, $J = 8.5$, 1H), 7.47 (ddd, $J = 2.6, 9.3, 11.5$, 1H), 7.28 (ddd, $J = 1.3, 2.7, 8.3$, 1H), 6.98 (d, $J = 8.5$, 1H), 2.22 (s, 3H); ^{13}C NMR (126 MHz, DMSO) δ 161.0 (d, $J_{\text{CF}} = 10.6$), 160.5, 159.6 (d, $J_{\text{CF}} = 13.2$), 157.6 (d, $J_{\text{CF}} = 12.8$), 156.6, 152.7, 139.2 (d, $J_{\text{CF}} = 3.6$), 137.2, 128.7 (d, $J_{\text{CF}} = 4.8$), 127.8, 124.2 (d, $J_{\text{CF}} = 11.7$), 118.7, 114.6 (d, $J_{\text{CF}} = 4.1$), 113.2, 112.6 (d, $J_{\text{CF}} = 3.6$), 110.6 (d, $J_{\text{CF}} = 83.2$), 104.7 (t, $J_{\text{CF}} = 27.0$), 7.9; IR (film) ν_{max} 3421 (br), 2849, 2772, 1732, 1715, 1626, 1593, 1560, 1493, 1441, 1321, 1267, 1090 cm^{-1} ; HRMS (ES^+) m/z : $[\text{M} + \text{H}]$ calcd for $\text{C}_{18}\text{H}_{12}\text{F}_2\text{N}_3\text{O}_3$ 356.0847; found 356.0844.

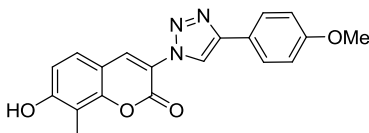


3-(4-(2,4-difluorophenyl)-1H-1,2,3-triazol-1-yl)-8-methyl-2-oxo-2H-chromen-7-yl acetate (10b). Compound **10b** was prepared following General Procedure A with azide **7b** (150 mg, 0.58 mmol) and 1-ethynyl-2,4-difluorobenzene (96 mg, 0.69 mmol) and was purified by column chromatography (SiO₂, 3:1:1 Hexanes:EtOAc:CH₂Cl₂) to afford a white amorphous solid (62 mg, 27%): ¹H NMR (500 MHz, DMSO) δ 8.88 (d, *J* = 3.5, 1H), 8.81 (s, 1H), 8.24 (td, *J* = 6.6, 8.7, 1H), 7.85 (d, *J* = 8.4, 1H), 7.49 (ddd, *J* = 2.6, 9.3, 11.5, 1H), 7.27-7.31 (m, 2H), 2.39 (s, 3H), 2.25 (s, 3H); ¹³C NMR (126 MHz, DMSO) δ 168.7, 163.0 (d, *J*_{CF} = 11.9), 161.0 (d, *J*_{CF} = 12.0), 155.8, 152.1, 151.5, 139.4 (d, *J*_{CF} = 3.0), 135.5, 128.9 (d, *J*_{CF} = 4.8), 128.8 (d, *J*_{CF} = 4.4), 127.4, 123.9 (d, *J*_{CF} = 11.9), 122.3, 119.8, 118.5, 115.9, 112.5 (d, *J*_{CF} = 20.8), 104.8 (t, *J*_{CF} = 26.4), 20.2, 9.1; IR (film) ν_{max} 3061, 2932, 2513, 1761, 1728, 1609, 1562, 1493, 1460, 1412, 1373, 1271, 1244, 1219, 1205, 1134, 1086, 1070, 1032, 926, 910 cm⁻¹; HRMS (ES⁺) *m/z*: [M + H] calcd for C₂₀H₁₄F₂N₃O₄ 398.0952; found 398.0965.



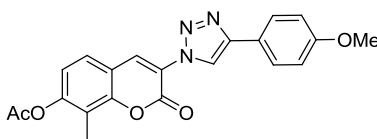
3-(4-(2,4-difluorophenyl)-1H-1,2,3-triazol-1-yl)-7-((2S,3R,4S,5R)-3,4-dihydroxy-5-methoxy-6,6-dimethyltetrahydro-2H-pyran-2-yloxy)-8-methyl-2H-chromen-2-one (10c). Compound **10c** was prepared following General Procedure B with coumarin **10a** and was purified by column chromatography (SiO₂, 99:1 to 32:1 CH₂Cl₂:MeOH) to afford a white amorphous solid (35.1 mg, 59% over two steps): ¹H NMR (500 MHz, DMSO) δ 8.84 (d, *J* = 3.5, 1H), 8.71 (s, 1H), 8.23 (td, *J* = 6.6, 8.7, 1H), 7.78 (d, *J* = 8.7, 1H), 7.48 (ddd, *J* = 2.6, 9.3, 11.6, 1H), 7.28 (ddd, *J* = 2.8, 8.8, 11.4, 1H), 7.27 (d, *J* = 8.6, 1H), 5.59 (d, *J* = 2.5, 1H), 5.37 (d, *J* = 4.7, 1H), 5.06 (d, *J* = 6.2, 1H), 4.02 (ddd, *J* = 3.3, 6.2, 9.4, 1H), 3.94 – 3.90 (m, 1H), 3.50 (s, 3H), 3.29 (d, *J* = 9.2, 1H), 2.25 (s, 3H), 1.26 (s, 3H), 1.01 (s, 3H); ¹³C NMR (126 MHz, DMSO) δ 161.0 (d, *J*_{CF} = 16.7), 159.6 (d,

$J_{\text{CF}} = 12.8$), 158.1, 157.5 (d, $J_{\text{CF}} = 16.8$), 156.3, 154.4 (d, $J_{\text{CF}} = 29.6$) 151.7, 139.2 (d, $J_{\text{CF}} = 2.3$) 136.5, 128.8, (d, $J_{\text{CF}} = 9.9$) 128.0, 124.0 (d, $J_{\text{CF}} = 12.6$), 120.2, 113.0, 112.5 (d, $J_{\text{CF}} = 22.3$), 111.4 (d, $J_{\text{CF}} = 93.5$), 104.8 (t, $J_{\text{CF}} = 26.0$), 98.3, 83.3, 77.9, 70.7, 67.4, 61.1, 28.5, 22.8, 8.1; IR (film) ν_{max} 3389 (br), 1726, 1717, 1609, 1250, 1236, 1198, 1132, 1086, 1070, 997, 966, 947 cm^{-1} ; HRMS (ES⁺) m/z : [M + H] calcd for C₂₆H₂₆F₂N₃O₇ 530.1739; found 530.1727.



7-hydroxy-3-(4-(4-methoxyphenyl)-1H-1,2,3-triazol-1-yl)-8-methyl-2H-chromen-2-one

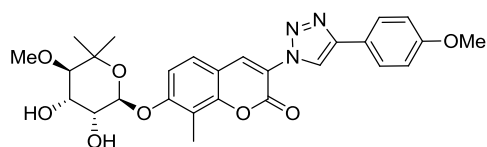
(11a). Compound **11a** was prepared following General Procedure A with azide **7a** (150 mg, 0.69 mmol) and 1-ethynyl-4-methoxybenzene (94 μL , 0.72 mmol) and was purified by column chromatography (SiO₂, 2:1:1 Hexanes:EtOAc:CH₂Cl₂) to afford a yellow amorphous solid (91.3 mg, 38%): ¹H NMR (500 MHz, d₆-Acetone) δ 8.69 (s, 1H), 8.43 (s, 1H), 7.81 (d, $J = 9.3$, 2H), 7.52 (d, $J = 8.9$, 1H), 6.93 (d, $J = 9.1$, 1H), 6.92 (d, $J = 9.3$, 2H), 3.73 (s, 1H), 2.20 (s, 3H); ¹³C NMR (126 MHz, d₆-Acetone) δ 160.8, 160.8, 157.2, 153.9, 147.9, 136.4, 128.6, 127.8(2C), 124.2, 121.1, 120.7, 115.1(2C), 114.0, 112.5, 112.0, 55.5, 8.1; IR (film) ν_{max} 3433 (br), 2956, 2920, 2849, 1726, 1713, 1606, 1591, 1556, 1502, 1454, 1418, 1385, 1308, 1261, 1175, 1128, 1086, 1028, 959 cm^{-1} ; HRMS (ES⁺) m/z : [M + H] calcd for C₁₉H₁₆N₃O₄ 350.1141; found 350.1149.



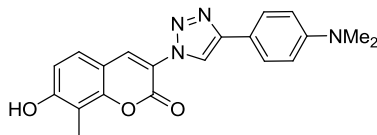
3-(4-(4-methoxyphenyl)-1H-1,2,3-triazol-1-yl)-8-methyl-2-oxo-2H-chromen-7-yl acetate

(11b). Compound **11b** was prepared following General Procedure A with azide **11b** (150 mg, 0.58 mmol) and 1-ethynyl-4-methoxybenzene (90 μL , 0.70 mmol) and was purified by column

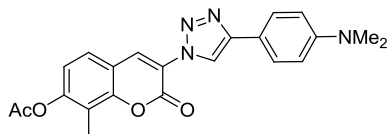
chromatography (SiO₂, 2:1:1 Hexanes:EtOAc:CH₂Cl₂) to afford a pale yellow amorphous solid (78.9 mg, 35%): ¹H NMR (500 MHz, DMSO) δ 8.96 (s, 1H), 8.77 (s, 1H), 7.91 (d, *J* = 8.7, 2H), 7.85 (d, *J* = 8.6, 1H), 7.28 (d, *J* = 8.5, 1H), 7.06 (d, *J* = 8.8, 2H), 3.81 (s, 3H), 2.39 (s, 3H), 2.25 (s, 3H); ¹³C NMR (126 MHz, DMSO) δ 168.7, 159.3, 155.6, 152.1, 151.4, 146.6, 135.0, 135.0, 127.3, 126.8(2C), 122.3, 121.1, 119.7, 118.3, 116.0, 114.4(2C), 55.1, 20.5, 8.7; IR (film) ν_{max} 3421, 3171, 3076, 2935, 1763, 1720, 1609, 1562, 1499, 1454, 1410, 1369, 1350, 1304, 1252, 1205, 1163, 1132, 1084, 1020, 927 cm⁻¹; HRMS (ES⁺) *m/z*: [M + H] calcd for C₂₁H₁₈N₃O₅ 392.1246; found 392.1232.



7-((2S,3R,4S,5R)-3,4-dihydroxy-5-methoxy-6,6-dimethyltetrahydro-2H-pyran-2-yloxy)-3-(4-(4-methoxyphenyl)-1H-1,2,3-triazol-1-yl)-8-methyl-2H-chromen-2-one (11c). Compound **11c** was prepared following General Procedure B with coumarin **11a** (70 mg, 0.20 mmol) and was purified by column chromatography (SiO₂, 49:1 CH₂Cl₂:MeOH) to afford a white amorphous solid (35.5 mg, 34% over two steps): ¹H NMR (500 MHz, DMSO) δ 8.91 (s, 1H), 8.67 (s, 1H), 7.89 (d, *J* = 8.8, 2H), 7.77 (d, *J* = 8.7, 1H), 7.26 (d, *J* = 8.9, 1H), 7.05 (d, *J* = 8.9, 2H), 5.59 (d, *J* = 2.5, 1H), 5.37 (d, *J* = 4.7, 1H), 5.06 (d, *J* = 6.2, 1H), 4.02 (ddd, *J* = 3.3, 6.3, 9.4, 1H), 3.94 – 3.90 (m, 1H), 3.81 (s, 3H), 3.50 (s, 3H), 3.29 (d, *J* = 9.2, 1H), 2.25 (s, 3H), 1.25 (s, 3H), 1.01 (s, 3H); ¹³C NMR (126 MHz, DMSO) δ 157.9, 156.7, 154.8, 150.4, 145.2, 134.9, 126.7, 125.4, 121.2, 119.7, 119.0, 113.1, 111.7, 110.7, 109.8, 97.0, 81.9, 76.6, 69.4, 66.2, 59.8, 53.8, 27.1, 21.6, 6.9; IR (film) ν_{max} 3402 (br), 2359, 2341, 1714, 1647, 1609, 1252, 1132, 1086, 1074, 991, 960 cm⁻¹; HRMS (ES⁺) *m/z*: [M + H] calcd for C₂₇H₃₀N₃O₈ 524.2033; found 524.2038.

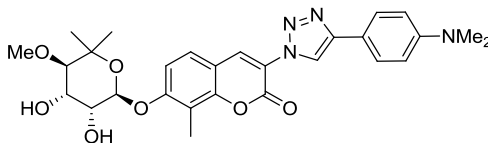


3-(4-(4-(dimethylamino)phenyl)-1H-1,2,3-triazol-1-yl)-7-hydroxy-8-methyl-2H-chromen-2-one (12a). Compound **12a** was prepared following General Procedure A with azide **7a** (150 mg, 0.69 mmol) and 4-ethynyl-N,N-dimethylaniline (105 mg, 0.72 mmol) and was purified by column chromatography (SiO₂, 90:9:1 CH₂Cl₂:EtOAc:Acetone) to afford a yellow amorphous solid (99 mg, 40%): ¹H NMR (500 MHz, d₆-Acetone) δ 9.42 (s, 1H), 8.59 (s, 1H), 8.41 (s, 1H), 7.69 (d, *J* = 8.9, 2H), 7.51 (d, *J* = 8.5, 1H), 6.92 (d, *J* = 8.5, 1H), 6.71 (d, *J* = 8.8, 2H), 2.87 (s, 6H), 2.20 (s, 3H); ¹³C NMR (126 MHz, d₆-Acetone) δ 160.7, 157.2, 153.8, 151.5, 148.6, 135.8, 128.4, 127.4(2C), 120.8, 120.0, 119.5, 114.0, 113.3(2C), 112.5, 112.1, 40.5(2C), 8.2; IR (film) ν_{max} 3350 (br), 2922, 2440, 2388, 1703, 1682, 1612, 1603, 1583, 1362, 1315, 1294, 1261, 1236, 1196, 1167, 1086, 1065, 935 cm⁻¹; HRMS (ES⁺) *m/z*: [M + H] calcd for C₂₀H₁₉N₄O₃ 363.1457; found 363.1441.



3-(4-(4-(dimethylamino)phenyl)-1H-1,2,3-triazol-1-yl)-8-methyl-2-oxo-2H-chromen-7-yl acetate (12b). Compound **12b** was prepared following General Procedure A with azide **7b** (150 mg, 0.58 mmol) and 4-ethynyl-N,N-dimethylaniline (101 mg, 0.70 mmol) and was purified by column chromatography (SiO₂, 19:1 CH₂Cl₂:EtOAc) to afford a yellow amorphous solid (95 mg, 42%): ¹H NMR (500 MHz, DMSO) δ 8.84 (s, 1H), 8.75 (s, 1H), 7.85 (d, *J* = 8.3, 1H), 7.78 (d, *J* = 8.9, 2H), 7.28 (d, *J* = 8.5, 1H), 6.82 (d, *J* = 9.0, 2H), 2.96 (s, 6H), 2.39 (s, 3H), 2.25 (s, 3H); ¹³C NMR (126 MHz, DMSO) δ 168.5, 155.7, 151.9, 151.4, 150.2, 147.2, 134.7, 127.3, 126.3(2C), 122.5, 119.9, 119.7, 118.3, 117.5, 116.1, 112.1(2C), 40.0(2C), 20.5, 8.8; IR (film)

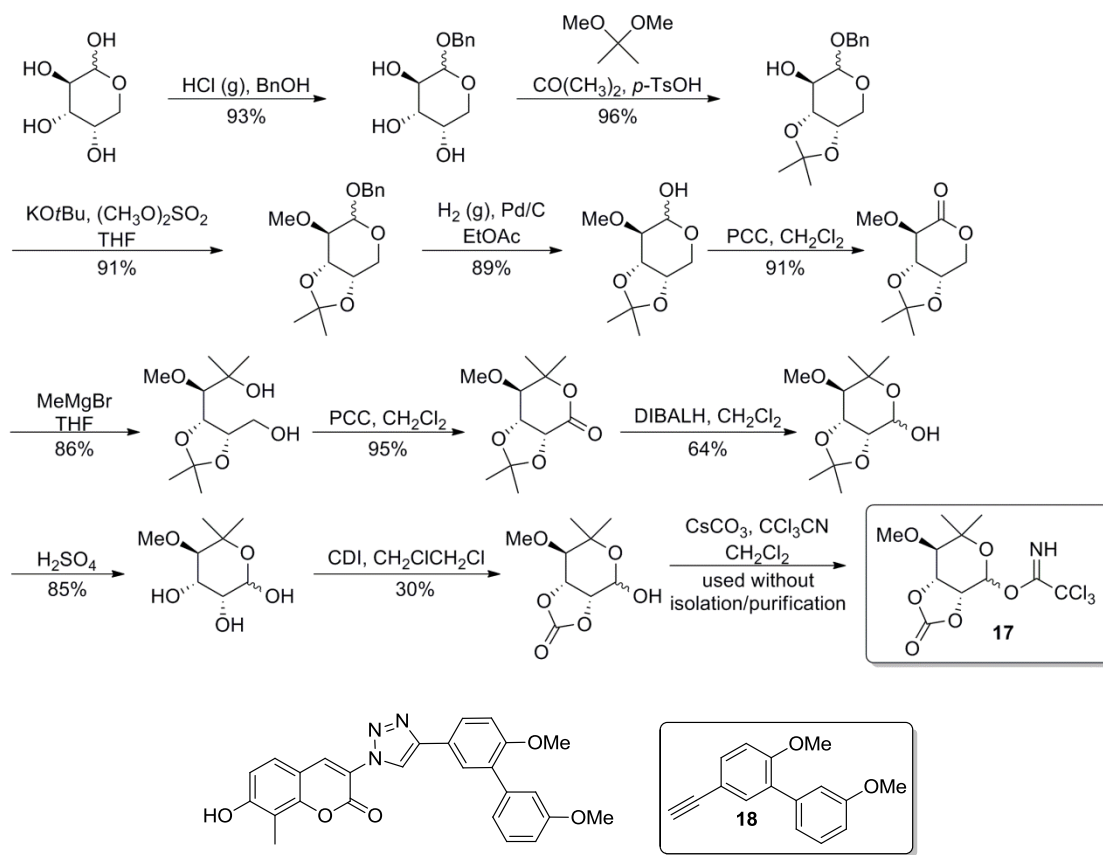
ν_{\max} 3028, 2922, 2897, 2359, 2341, 1761, 1720, 1618, 1605, 1506, 1450, 1427, 1360, 1344, 1213, 1194, 1171, 1167, 1136, 1084, 1061, 1026, 943, 908 cm^{-1} ; HRMS (ES^+) m/z : $[\text{M} + \text{H}]$ calcd for $\text{C}_{22}\text{H}_{21}\text{N}_4\text{O}_4$ 405.1563; found 405.1564.



7-((2S,3R,4S,5R)-3,4-dihydroxy-5-methoxy-6,6-dimethyltetrahydro-2H-pyran-2-yloxy)-3-(4-(4-(dimethylamino)phenyl)-1H-1,2,3-triazol-1-yl)-8-methyl-2H-chromen-2-one (12c).

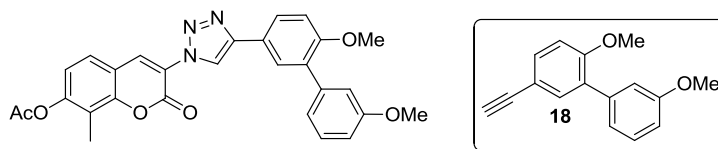
Compound **12c** was prepared following General Procedure B with coumarin **12a** (75 mg, 0.21 mmol) and was purified by column chromatography (SiO_2 , 49:1 CH_2Cl_2 :MeOH) to afford a yellow amorphous solid (39 mg, 35% over two steps): ^1H NMR (500 MHz, DMSO) δ 8.78 (s, 1H), 8.65 (s, 1H), 7.77 (d, $J = 8.5$ 1H), 7.76 (d, $J = 8.9$, 2H), 7.26 (d, $J = 8.9$, 1H), 6.81 (d, $J = 9.0$, 2H), 5.59 (d, $J = 2.5$, 1H), 5.36 (d, $J = 4.7$, 1H), 5.05 (d, $J = 6.2$, 1H), 4.02 (ddd, $J = 3.3$, 6.3, 9.4, 1H), 3.94 – 3.90 (m, 1H), 3.50 (s, 3H), 3.29 (d, $J = 9.2$, 1H), 2.95 (s, 6H), 2.25 (s, 3H), 1.25 (s, 3H), 1.01 (s, 3H); ^{13}C NMR (126 MHz, DMSO) δ 157.9, 156.1, 151.7, 150.2, 147.1, 136.0, 127.8, 126.3(2C), 120.4, 120.1, 117.6, 113.0, 112.3, 112.0(2C), 111.1, 98.3, 83.3, 78.0, 70.7, 67.5, 61.1, 40.0(2C), 28.5, 22.8, 8.2; IR (film) ν_{\max} 3421 (br), 2341, 2332, 1717, 1699, 1609, 1558, 1506, 1456, 1420, 1362, 1261, 1088, 987, 966 cm^{-1} ; HRMS (ES^+) m/z : $[\text{M} + \text{H}]$ calcd for $\text{C}_{28}\text{H}_{33}\text{N}_4\text{O}_7$ 537.2349; found 537.2361.

(3aR,7R,7aR)-7-methoxy-6,6-dimethyl-2-oxotetrahydro-3aH-[1,3]dioxolo[4,5-c]pyran-4-yl 2,2,2-trichloroacetimidate (17). As previously described in reference 69.

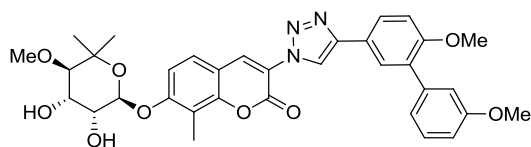


3-(4-(3',6-dimethoxybiphenyl-3-yl)-1H-1,2,3-triazol-1-yl)-7-hydroxy-8-methyl-2H-chromen-2-one (13a). Compound **13a** was prepared following General Procedure A with azide **7a** (150 mg, 69 mmol) and alkyne **18** (173 mg, 0.76 mmol) and was purified by column chromatography (SiO_2 , 2:2:1 Hexanes: CH_2Cl_2 :EtOAc) to afford a yellow amorphous solid (101 mg, 32%): ^1H NMR (500 MHz, DMSO) δ 10.86 (s, 1H), 8.99 (d, $J = 1.0$, 1H), 8.63 (d, $J = 1.3$, 1H), 7.94 (d, $J = 8.5$, 1H), 7.86 (d, $J = 2.3$, 1H), 7.62 (d, $J = 8.6$, 1H), 7.36 (t, $J = 7.9$, 1H), 7.24 (d, $J = 8.7$, 1H), 7.13 – 7.10 (m, 1H), 7.10 – 7.08 (m, 1H), 6.98 (d, $J = 8.5$, 1H), 6.94 (dd, $J = 2.3$, 8.0, 1H), 3.83 (s, 3H), 3.80 (s, 3H), 2.23 (s, 3H); ^{13}C NMR (126 MHz, DMSO) δ 160.5, 158.9, 156.4, 156.1, 152.6, 146.2, 139.1, 137.1, 130.1, 129.0, 127.8, 127.5, 125.9, 122.7, 121.7, 121.4, 118.7, 115.1,

113.1, 112.5, 112.2, 110.9, 110.3, 55.6, 55.0, 7.9; IR (film) ν_{\max} 3379 (br), 2937, 2833, 2588, 2357, 1717, 1701, 1605, 1583, 1477, 1456, 1425, 1387, 1315, 1298, 1273, 1258, 1238, 1167, 1142, 1090, 1047, 1018 cm^{-1} ; HRMS (ES^+) m/z : $[\text{M} + \text{H}]$ calcd for $\text{C}_{26}\text{H}_{22}\text{N}_3\text{O}_5$ 456.1559; found 456.1555.

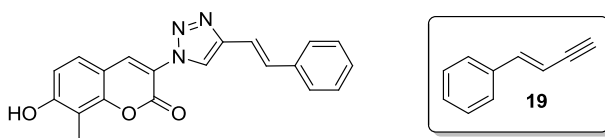


3-(4-(3',6-dimethoxybiphenyl-3-yl)-1H-1,2,3-triazol-1-yl)-8-methyl-2-oxo-2H-chromen-7-yl acetate (13b) Compound **13b** was prepared following General Procedure A with azide **7b** (135 mg, 0.52 mmol) and alkyne **18** (130 mg, 0.55 mmol) and was purified by column chromatography (SiO_2 , 2:1:1 Hexanes: CH_2Cl_2 :EtOAc) to afford a white amorphous solid (72 mg, 28%): ^1H NMR (500 MHz, DMSO) δ 9.08 (s, 1H), 8.78 (s, 1H), 7.98 (dd, $J = 2.3, 8.5$, 1H), 7.89 (d, $J = 2.3$, 1H), 7.85 (d, $J = 8.3$, 1H), 7.39 – 7.33 (m, 1H), 7.29 (d, $J = 8.5$, 1H), 7.24 (d, $J = 8.7$, 1H), 7.12 (dd, $J = 1.0, 7.6$, 1H), 7.11 – 7.08 (m, 1H), 6.94 (dd, $J = 1.7, 8.3$, 1H), 3.83 (s, 3H), 3.80 (s, 3H), 2.39 (s, 3H), 2.25 (s, 3H); ^{13}C NMR (126 MHz, DMSO) δ 168.7, 158.9, 156.2, 155.6, 152.0, 151.4, 146.4, 139.0, 135.1, 130.2, 129.0, 127.6, 127.3, 126.1, 122.6, 122.4, 121.7, 121.3, 119.8, 118.4, 116.0, 115.1, 112.5, 112.3, 55.7, 55.0, 20.6, 8.8; IR (film) ν_{\max} 3439, 2964, 2837, 2357, 2253, 2127, 1771, 1720, 1645, 1605, 1497, 1454, 1439, 1421, 1385, 1369, 1302, 1269, 1244, 1198, 1167, 1134, 1049, 1007, 932, 906 cm^{-1} ; HRMS (ES^+) m/z : $[\text{M} + \text{H}]$ calcd for $\text{C}_{28}\text{H}_{24}\text{N}_3\text{O}_6$ 498.1665; found 498.1653.



7-((2S,3R,4S,5R)-3,4-dihydroxy-5-methoxy-6,6-dimethyltetrahydro-2H-pyran-2-yloxy)-3-(4-(3',6-dimethoxybiphenyl-3-yl)-1H-1,2,3-triazol-1-yl)-8-methyl-2H-chromen-2-one (13c).

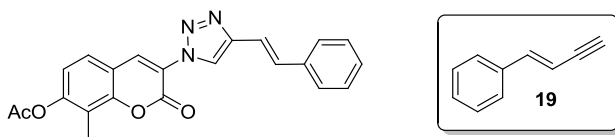
Compound **13c** was prepared following General Procedure B with coumarin **13a** (70 mg, 0.154 mmol) and was purified by column chromatography (SiO₂, 49:1 CH₂Cl₂:MeOH) to afford a pale yellow amorphous solid (29.2 mg, 30% over two steps): ¹H NMR (500 MHz, DMSO) δ 9.02 (s, 1H), 8.69 (s, 1H), 7.96 (dd, *J* = 2.3, 8.5, 1H), 7.88 (d, *J* = 2.3, 1H), 7.79 (d, *J* = 8.8, 1H), 7.37 (t, *J* = 7.9, 1H), 7.27 (d, *J* = 9.0, 1H), 7.25 (d, *J* = 8.7, 1H), 7.12 (d, *J* = 7.9, 1H), 7.11 – 7.09 (m, 1H), 6.97 – 6.93 (m, 1H), 5.60 (d, *J* = 2.5, 1H), 5.35 (d, *J* = 4.7, 1H), 5.04 (d, *J* = 6.2, 1H), 4.03 (ddd, *J* = 3.2, 6.3, 9.3, 1H), 3.95 – 3.91 (m, 1H), 3.84 (s, 3H), 3.81 (s, 3H), 3.51 (s, 3H), 3.30 (d, *J* = 9.2, 1H), 2.27 (s, 3H), 1.27 (s, 3H), 1.03 (s, 3H); ¹³C NMR (126 MHz, DMSO) δ 158.9, 158.0, 156.1, 151.8, 146.3, 139.1, 136.3, 130.1, 129.0, 127.9, 127.6, 126.0, 122.7, 121.7, 121.4, 120.2, 115.1, 113.1, 112.4, 112.3, 112.0, 111.2, 103.2, 98.3, 83.2, 78.0, 70.8, 67.5, 61.1, 55.6, 55.0, 28.4, 22.8, 8.3; IR (film) ν_{max} 3431 (br), 3173, 3065, 2976, 2935, 2835, 2359, 1801, 1724, 1609, 1580, 1501, 1479, 1458, 1441, 1425, 1387, 1321, 1259, 1173, 1142, 1113, 1090, 1022, 987, 966 cm⁻¹; HRMS (ES⁺) *m/z*: [M + H] calcd for C₃₄H₃₆N₃O₉ 630.2449; found 630.2418.



(E)-7-hydroxy-8-methyl-3-(4-styryl-1H-1,2,3-triazol-1-yl)-2H-chromen-2-one (14a).

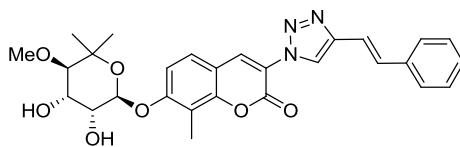
Compound **14a** was prepared following General Procedure A with azide **7a** (120 mg, 0.55 mmol) and alkyne **19**⁷⁰⁻⁷¹ (71 mg, 0.55 mmol) and was purified by column chromatography (SiO₂, 1:1 Hexanes:EtOAc) to afford an orange amorphous solid (87.1 mg, 46%): ¹H NMR (400 MHz, DMSO) δ 10.85 (s, 1H), 8.73 (s, 1H), 8.64 (s, 1H), 7.66 – 7.61 (m, *J* = 3.3, 7.9, 3H), 7.44 – 7.37 (m, 3H), 7.36 – 7.28 (m, 2H), 6.98 (d, *J* = 8.5, 1H), 2.23 (s, 3H); ¹³C NMR (126 MHz, DMSO) δ

160.3, 156.4, 152.6, 145.2, 136.5, 136.5, 130.0, 128.8(2C), 127.9, 127.8, 126.5(2C), 122.8, 118.8, 116.8, 113.2, 110.9, 110.3, 7.9; IR (film) ν_{\max} 3414 (br), 2922, 2850, 2359, 2332, 1717, 1701, 1610, 1589, 1420, 1313, 1261, 1236, 1088, 1055, 955 cm^{-1} ; HRMS (ES⁺) m/z : [M + H] calcd for C₂₀H₁₆N₃O₃ 346.1192; found 346.1183.



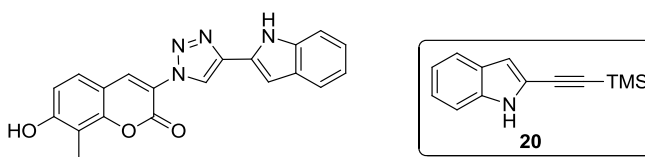
(E)-8-methyl-2-oxo-3-(4-styryl-1H-1,2,3-triazol-1-yl)-2H-chromen-7-yl acetate (14b).

Compound **14b** was prepared following General Procedure A with azide **7b** (100 mg, 0.39 mmol) and alkyne **19**⁷⁰⁻⁷¹ (49.5 mg, 0.39 mmol) and was purified by column chromatography (SiO₂, 1:1 EtOAc:Hexanes) to afford a yellow amorphous solid (91 mg, 61%): ¹H NMR (500 MHz, DMSO) δ 8.80 (s, 1H), 8.79 (s, 1H), 7.85 (d, J = 8.3, 1H), 7.64 (d, J = 7.3, 2H), 7.30-7.49 (m, 5H), 7.28 (d, J = 8.5, 1H), 2.39 (s, 3H), 2.25 (s, 3H); ¹³C NMR (126 MHz, DMSO) δ 168.7, 155.6, 152.0, 151.2, 145.4, 136.5, 134.4, 130.2, 128.8(2C), 128.0, 127.2, 126.5(2C), 122.7, 122.4, 119.8, 118.3, 116.6, 116.1, 20.5, 8.8; IR (film) ν_{\max} 3061, 2926, 2359, 2341, 2127, 1763, 1738, 1718, 1630, 1605, 1520, 1454, 1420, 1369, 1236, 1200, 1161, 1117, 1082, 1040, 1009, 989, 962, 924, 905 cm^{-1} ; HRMS (ES⁺) m/z : [M + H] calcd for C₂₂H₁₈N₃O₄ 388.1297; found 388.1288.



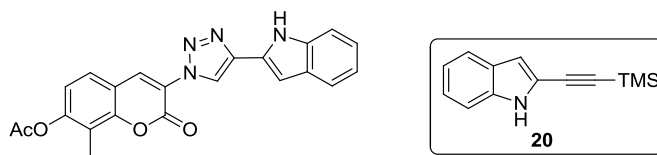
7-((2S,3R,4S,5R)-3,4-dihydroxy-5-methoxy-6,6-dimethyltetrahydro-2H-pyran-2-yloxy)-8-methyl-3-(4-styryl-1H-1,2,3-triazol-1-yl)-2H-chromen-2-one (14c). Compound **14c** was prepared following General Procedure B with coumarin **14a** (90 mg, 0.250 mmol) and was purified by column chromatography (SiO₂, 49:1 CH₂Cl₂:MeOH) to afford a pale yellow solid

(34.5 mg, 26% over two steps): ^1H NMR (500 MHz, DMSO) δ 8.76 (s, 1H), 8.70 (s, 1H), 7.78 (d, $J = 8.7$, 1H), 7.64 (d, $J = 7.6$, 2H), 7.49 – 7.24 (m, 6H), 5.60 (d, $J = 2.2$, 1H), 5.40 (d, $J = 4.7$, 1H), 5.09 (d, $J = 6.3$, 1H), 4.02 (ddd, $J = 3.2$, 6.3, 9.4, 1H), 3.92 (dt, $J = 3.8$, 7.5, 1H), 3.50 (s, 3H), 3.29 (d, $J = 9.2$, 1H), 2.25 (s, 3H), 1.25 (s, 3H), 1.01 (s, 3H); ^{13}C NMR (126 MHz, DMSO) δ 158.1, 156.1, 151.6, 145.2, 136.5, 135.6, 130.1, 128.8(2C), 128.0, 127.9, 126.5(2C), 122.7, 120.2, 116.7, 113.0, 112.1, 111.2, 98.3, 83.2, 78.0, 70.8, 67.5, 61.1, 28.5, 22.9, 8.1; IR (film) ν_{max} 3422 (br), 3171, 3057, 2980, 2935, 2359, 2341, 1799, 1717, 1609, 1497, 1450, 1423, 1385, 1366, 1256, 1167, 1113, 1086, 1041, 987, 966 cm^{-1} ; HRMS (ES $^+$) m/z : [M + H] calcd for $\text{C}_{28}\text{H}_{30}\text{N}_3\text{O}_7$ 520.2084; found 520.2070.



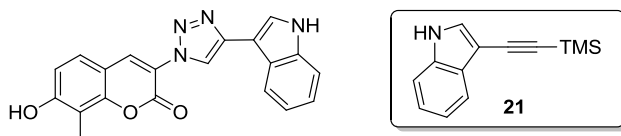
3-(4-(1H-indol-2-yl)-1H-1,2,3-triazol-1-yl)-7-hydroxy-8-methyl-2H-chromen-2-one (15a).

Compound **15a** was prepared following General Procedure A with azide **7a** (120 mg, 0.55 mmol) and alkyne **20**⁷² (118 mg, 0.55 mmol) with the addition of TBAF (1M, 553 μL , 0.55 mmol). **15a** was purified by column chromatography (SiO_2 , 3:1:1 Hexanes: CH_2Cl_2 :EtOAc) to afford a yellow amorphous solid (73 mg, 37%): ^1H NMR (500 MHz, DMSO) δ 11.80 (s, 1H), 10.87 (s, 1H), 9.02 (s, 1H), 8.70 (s, 1H), 7.65 (d, $J = 8.5$, 1H), 7.57 (d, $J = 8.0$, 1H), 7.43 (dd, $J = 0.8$, 8.1, 1H), 7.14 – 7.10 (m, 1H), 7.04 – 7.00 (m, 1H), 6.99 (d, $J = 8.5$, 1H), 6.94 (d, $J = 1.3$, 1H), 2.24 (s, 3H); ^{13}C NMR (126 MHz, DMSO) δ 160.4, 156.3, 152.6, 140.8, 136.6, 136.4, 128.5, 128.1, 127.8, 121.7, 121.5, 120.2, 119.5, 118.7, 113.2, 111.5, 110.9, 110.4, 99.0, 8.03; IR (film) ν_{max} 3258 (br), 2922, 2851, 2357, 2320, 1706, 1645, 1626, 1601, 1582, 1556, 1373, 1333, 1298, 1281, 1229, 1204, 1163, 1124, 1108, 1081, 999, 960, 916 cm^{-1} ; HRMS (ES $^+$) m/z : [M + H] calcd for $\text{C}_{20}\text{H}_{15}\text{N}_4\text{O}_3$ 359.1144; found 359.1131.



3-(4-(1H-indol-2-yl)-1H-1,2,3-triazol-1-yl)-8-methyl-2-oxo-2H-chromen-7-yl acetate (15b).

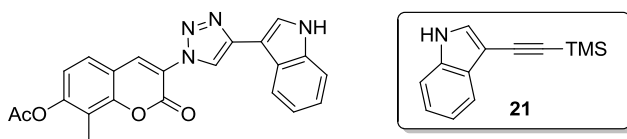
Compound **15b** was prepared following General Procedure A with azide **7b** (56 mg, 0.20 mmol) and alkyne **20**⁷² (45 mg, 0.2 mmol) with the addition of TBAF (1M, 211 μ L, 0.20 mmol). **15b** was purified by column chromatography (SiO₂, 3:1:1 Hexanes:CH₂Cl₂:EtOAc) to afford a yellow/green amorphous solid (28.3 mg, 35%): ¹H NMR (500 MHz, DMSO) δ 11.82 (s, 1H), 9.10 (s, 1H), 8.84 (s, 1H), 7.87 (d, *J* = 8.4, 1H), 7.56 (d, *J* = 7.7, 1H), 7.42 (dd, *J* = 0.8, 8.1, 1H), 7.28 (d, *J* = 8.5, 1H), 7.12 (ddd, *J* = 1.2, 7.1, 8.2, 1H), 7.04 – 7.00 (m, 1H), 6.97 (d, *J* = 1.3, 1H), 2.39 (s, 3H), 2.25 (s, 3H); ¹³C NMR (126 MHz, DMSO) δ 168.7, 155.7, 152.0, 151.4, 141.0, 136.6, 134.4, 128.3, 128.1, 127.3, 122.3, 121.7, 121.4, 120.1, 119.8, 119.4, 118.3, 116.0, 111.3, 99.2, 20.6, 8.8; IR (film) ν_{max} 3362, 3165, 3049, 2962, 2359, 2341, 1763, 1724, 1605, 1456, 1412, 1369, 1337, 1311, 1231, 1198, 1169, 1130, 1084, 1032, 1013, 968, 926 cm⁻¹; HRMS (ES⁺) *m/z*: [M + H] calcd for C₂₂H₁₇N₄O₄ 401.1250; found 401.1260.



3-(4-(1H-indol-3-yl)-1H-1,2,3-triazol-1-yl)-7-hydroxy-8-methyl-2H-chromen-2-one (16a).

Compound **16a** was prepared following General Procedure A with azide **7a** (165 mg, 0.76 mmol) and alkyne **21** (162 mg, 0.76 mmol) with the addition of TBAF (1M, 800 μ L, 0.76 mmol). **16a** was purified by column chromatography (SiO₂, 3:1 to 1:1 Hexanes:EtOAc) to afford a yellow amorphous solid (38 mg, 14%): ¹H NMR (500 MHz, DMSO) δ 11.44 (s, 1H), 10.87 (s, 1H), 8.82 (s, 1H), 8.63 (s, 1H), 8.08 (d, *J* = 7.8, 1H), 7.93 (d, *J* = 2.6, 1H), 7.62 (d, *J* = 8.5, 1H), 7.46 (d, *J* = 7.9, 1H), 7.21 – 7.16 (m, 1H), 7.14 (ddd, *J* = 1.2, 7.1, 8.0, 1H), 6.97 (d, *J* = 8.5, 1H), 2.23 (s,

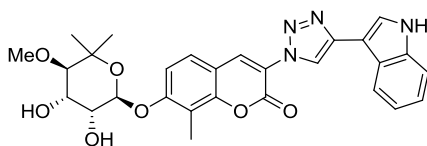
3H); ^{13}C NMR (126 MHz, DMSO) δ 160.3, 156.6, 152.6, 142.8, 136.8, 136.4, 127.7, 124.7, 123.6, 121.7, 120.0, 119.9, 119.6, 119.0, 113.1, 111.8, 110.9, 110.4, 105.4, 7.9; IR (film) ν_{max} 3342 (br), 2307, 1703, 1600, 1583, 1416, 1317, 1286, 1261, 1236, 1215, 1091, 1059 cm^{-1} ; HRMS (ES^+) m/z : [M + H] calcd for $\text{C}_{20}\text{H}_{15}\text{N}_4\text{O}_3$ 359.1141; found 359.1127.



3-(4-(1H-indol-3-yl)-1H-1,2,3-triazol-1-yl)-8-methyl-2-oxo-2H-chromen-7-yl acetate (16b).

Compound **16b** was prepared following General Procedure A with azide **7b** (100 mg, 0.39 mmol) and alkyne **21** (82 mg, 0.39 mmol) with the addition of TBAF (1M, 385 μL , 0.39 mmol).

16b was purified by column chromatography (SiO_2 , 3:1:1 Hexanes: CH_2Cl_2 :EtOAc) to afford a red/brown amorphous solid (80.1 mg, 35%): ^1H NMR (500 MHz, DMSO) δ 11.46 (s, 1H), 8.88 (s, 1H), 8.78 (s, 1H), 8.08 (d, $J = 7.7$, 1H), 7.96 (d, $J = 2.6$, 1H), 7.85 (d, $J = 8.5$, 1H), 7.46 (d, $J = 7.9$, 1H), 7.28 (d, $J = 8.5$, 1H), 7.20 – 7.16 (m, 1H), 7.16 – 7.11 (m, 1H), 2.39 (s, 3H), 2.25 (s, 3H); ^{13}C NMR (126 MHz, DMSO) δ 13C NMR (126 MHz, DMSO) δ 168.7, 155.7, 151.9, 151.4, 143.1, 136.3, 134.6, 127.3, 124.7, 123.8, 122.6, 121.8, 119.8, 119.8, 119.7, 119.7, 118.4, 116.0, 111.8, 105.2, 20.4, 8.9; IR (film) ν_{max} 3400, 3344, 2962, 2930, 2876, 1755, 1715, 1693, 1643, 1605, 1520, 1454, 1371, 1261, 1200, 1155, 1078, 1009, 908 cm^{-1} ; HRMS (ES^+) m/z : [M + H] calcd for $\text{C}_{22}\text{H}_{17}\text{N}_4\text{O}_4$ 401.1250; found 401.1240.

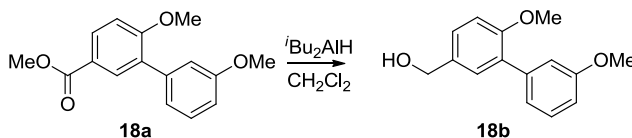


3-(4-(1H-indol-3-yl)-1H-1,2,3-triazol-1-yl)-7-((2S,3R,4S,5R)-3,4-dihydroxy-5-methoxy-6,6-dimethyltetrahydro-2H-pyran-2-yloxy)-8-methyl-2H-chromen-2-one (16c).

Compound **16c** was prepared following General Procedure B with coumarin **16a** (100mg, 0.28 mmol) and was

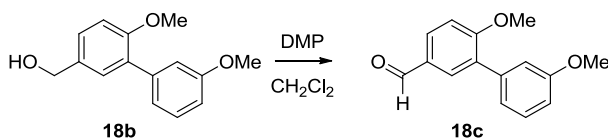
purified by column chromatography (SiO₂, 49:1 CH₂Cl₂:MeOH) to afford a yellow/green amorphous solid (47.1 mg, 32%): ¹H NMR (500 MHz, DMSO) δ 11.45 (s, 1H), 8.84 (s, 1H), 8.70 (s, 1H), 8.08 (d, *J* = 7.8, 1H), 7.95 (d, *J* = 2.6, 1H), 7.79 (d, *J* = 8.7, 1H), 7.48 – 7.45 (m, 1H), 7.27 (d, *J* = 8.9, 1H), 7.21 – 7.16 (m, 1H), 7.16 – 7.12 (m, 1H), 5.59 (d, *J* = 2.5, 1H), 5.37 (d, *J* = 4.7, 1H), 5.06 (d, *J* = 6.2, 1H), 4.02 (ddd, *J* = 3.3, 6.2, 9.4, 1H), 3.95 – 3.90 (m, 1H), 3.50 (s, 3H), 3.29 (d, *J* = 9.2, 1H), 2.27 (s, 3H), 1.26 (s, 3H), 1.02 (s, 3H); ¹³C NMR (126 MHz, DMSO) δ 158.0, 156.3, 151.6, 142.9, 136.4, 135.9, 127.8, 124.7, 123.7, 121.8, 120.5, 119.9, 119.7, 113.0, 112.1, 111.8, 111.2, 111.1, 105.4, 98.2, 83.1, 77.8, 70.6, 67.4, 60.9, 28.4, 22.7, 8.4; IR (film) ν_{max} 3423 (br), 2982, 2935, 1715, 1628, 1609, 1522, 1456, 1375, 1258, 1109, 1084, 966 cm⁻¹; HRMS (ES⁺) *m/z*: [M + H] calcd for C₂₈H₂₉N₄O₇ 533.2036; found 533.2014.

Preparation of Alkynes:

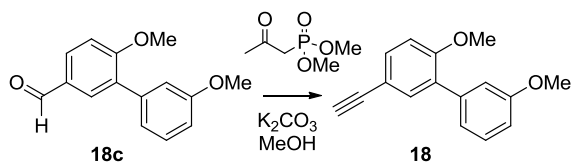


(3',6-dimethoxybiphenyl-3-yl)methanol (18b). To **18a**⁷³ (500 mg, 1.80 mmol) in CH₂Cl₂ (8 mL), di-isobutyl aluminum hydride (1.0 M in CH₂Cl₂, 4.20 mL, 4.20 mmol) was added at -78°C, was warmed to rt and stirred for 4 h. An equal volume of saturated, aqueous potassium sodium tartrate was added and stirred for 2 h at rt. The reaction contents were partitioned between water and CH₂Cl₂ and were extracted with CH₂Cl₂ (2 x 25 mL). The combined organic layers were washed with saturated aqueous NaCl, dried (Na₂SO₄), filtered, and concentrated. The residue was purified by column chromatography (SiO₂, 3:1 Hexanes:EtOAc) to give **18b** as a yellow viscous liquid (405 mg, 91%): ¹H NMR (500 MHz, CDCl₃) δ 7.36 – 7.31 (m, 3H), 7.13 – 7.10 (m, 1H), 7.09 (dd, *J* = 1.9, 2.5, 1H), 6.98 (d, *J* = 9.0, 1H), 6.89 (ddd, *J* = 0.9, 2.6, 8.3, 1H), 4.67 (d, *J* = 4.8, 2H), 3.84 (s, 3H), 3.82 (s, 3H); ¹³C NMR (126 MHz, CDCl₃) δ 159.2, 156.1, 139.6,

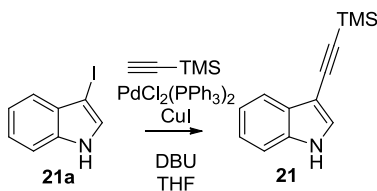
133.2, 130.6, 130.1, 129.0, 127.7, 122.0, 115.2, 112.6, 111.3, 65.1, 55.7, 55.3; IR (film) ν_{\max} 3348 (br), 2999, 2935, 2908, 2874, 2833, 1607, 1576, 1504, 1481, 1462, 1454, 1435, 1412, 1312, 1275, 1265, 1242, 1225, 1167, 1144, 1040, 1028 cm^{-1} ; HRMS (ES^+) m/z : $[\text{M} + \text{H}]$ calcd for $\text{C}_{15}\text{H}_{17}\text{O}_3$ 245.1178; found 245.1168.



3',6-dimethoxybiphenyl-3-carbaldehyde (18c). To **18b** (400 mg, 1.66 mmol) in CH_2Cl_2 (10 mL), Dess-Martin periodinane (843 mg, 2.0 mmol) was added at 0°C . The solution was then stirred upon warming to rt for 4 h. A 1:1 solution of aqueous saturated NaHCO_3 : $\text{Na}_2\text{S}_2\text{O}_3$ (20 mL) was then added and stirred until two layers were present. The partitioned layers were extracted with CH_2Cl_2 (2 x 25 mL), the combined organic layers were then washed with saturated NaHCO_3 , followed by saturated NaCl , dried (Na_2SO_4), and concentrated. The residue was purified by column chromatography (SiO_2 , 3:1 Hexanes:EtOAc) to give **18c** as a yellow viscous liquid (400 mg, 99%): ^1H NMR (500 MHz, CDCl_3) δ 9.95 (s, 1H), 7.87 – 7.90 (m, 2H), 7.36 (t, $J = 7.9$, 1H), 7.13 – 7.09 (m, 2H), 7.08 (dd, $J = 1.6, 2.4$, 1H), 6.93 (ddd, $J = 0.9, 2.6, 8.3$, 1H), 3.92 (s, 3H), 3.86 (s, 3H); ^{13}C NMR (126 MHz, CDCl_3) δ 190.9, 161.5, 159.3, 138.4, 132.4, 131.4, 131.2, 129.9, 129.2, 121.9, 115.3, 113.1, 111.1, 56.0, 55.3; IR (film) ν_{\max} 3366, 3072, 3003, 2939, 2910, 2837, 2727, 2359, 2035, 1680, 1597, 1582, 1501, 1481, 1456, 1439, 1418, 1371, 1310, 1290, 1267, 1254, 1219, 1169, 1142, 1130, 1051, 1036, 1020, 945, 918 cm^{-1} ; HRMS (ES^+) m/z : $[\text{M} + \text{H}]$ calcd for $\text{C}_{15}\text{H}_{15}\text{O}_3$ 243.1017; found 243.1005.



5-ethynyl-2,3'-dimethoxybiphenyl (18). Following the procedure by Mueller et al.,⁷⁴ to aldehyde **18c** (800 mg, 3.30 mmol) in MeOH (30 mL), K₂CO₃ (0.91 g, 6.6 mmol) was added followed by the addition of dimethyl-1-diazo-2-oxopropylphosphonate (595 μL, 4.0 mmol). After stirring for 12 h at rt, the reaction was diluted with Et₂O (100 mL) and organics washed with saturated NaHCO₃ and dried (MgSO₄). The residue was purified by column chromatography (SiO₂, 9:1 Hexanes:EtOAc) to give **18** as a yellow viscous liquid (152 mg, 77%): ¹H NMR (500 MHz, CDCl₃) δ 7.51 – 7.47 (m, 2H), 7.35 (t, *J* = 7.9, 1H), 7.10 (dd, *J* = 0.8, 7.6, 1H), 7.09 – 7.06 (m, 1H), 6.95 – 6.90 (m, 2H), 3.85 (d, *J* = 8.6, 6H), 3.04 (s, 1H); ¹³C NMR (126 MHz, CDCl₃) δ 159.3, 156.9, 138.8, 134.6, 132.7, 130.7, 129.0, 122.0, 115.2, 114.3, 112.9, 111.1, 83.5, 76.0, 55.7, 55.3; IR (film) ν_{max} 3285, 3051, 3001, 2959, 2939, 2906, 2835, 2529, 2359, 2104, 1601, 1580, 1501, 1479, 1462, 1439, 1394, 1317, 1248, 1217, 1165, 1051, 1038, 1024, 903 cm⁻¹; HRMS (ES⁺) *m/z*: [M + H] calcd for C₁₆H₁₅O₂ 239.1072; found 239.1067.



3-((trimethylsilyl)ethynyl)-1H-indole (21). Compound **21a**⁷⁵ (100 mg, 0.41 mmol) was dissolved in degassed THF (3 mL). PdCl₂(PPh₃)₂ (14.4 mg, 0.02 mmol), CuI (3.9 mg, 0.02 mmol), DBU (246 μL, 1.6 mmol) then ethynyltrimethylsilane (69.7 μL, 0.49 mmol) were added in that order. The reaction was stirred at 55°C under argon for 12 h. The reaction mixture was then diluted with EtOAc (10 mL) and filtered through celite. The organic layer was then washed with DI H₂O (2 x 10 mL) and saturated NaCl and dried (Na₂SO₄). The solvents were removed in vacuo and the residue was purified by column chromatography (SiO₂, 10:1 Hexanes:EtOAc) to afford a brown solid (45.4 mg, 52%): ¹H NMR (500 MHz, CDCl₃) δ 8.15 (s, 1H), 7.77 – 7.73

(m, 1H), 7.43 (d, $J = 2.6$, 1H), 7.38 – 7.35 (m, 1H), 7.25 – 7.19 (m, 2H), 0.29 (s, 9H); ^{13}C NMR (126 MHz, CDCl_3) δ 134.7, 128.3, 128.1, 122.8, 120.5, 119.8, 111.0, 98.6, 98.3, 95.5, 0.0(3C); IR (film) ν_{max} 3408, 3061, 2957, 2897, 2359, 2341, 2332, 2150, 1531, 1456, 1416, 1340, 1325, 1248, 1238, 1128, 1097, 1070, 1009 cm^{-1} ; HRMS (ES^+) m/z : [M + H] calcd for $\text{C}_{13}\text{H}_{15}\text{NSi}$ 214.1052; found 214.1045.

Anti-proliferation Assay. MCF-7 and SKBr-3 cells were maintained in a 1:1 mixture of Advanced DMEM/F12 (Gibco) supplemented with non-essential amino acids, L-glutamine (2 mM), streptomycin (500 $\mu\text{g}/\text{mL}$), penicillin (100 units/mL), and 10% FBS. Cells were grown to confluence in a humidified atmosphere (37 °C, 5% CO_2), seeded (2000/well, 100 μL) in 96-well plates, and allowed to attach overnight. Compound or geldanamycin at varying concentrations in DMSO (1% DMSO final concentration) was added, and cells were returned to the incubator for 72 h. At 72 h, the number of viable cells was determined using an MTS/PMS cell proliferation kit (Promega) per the manufacturer's instructions. Cells incubated in 1% DMSO were used as 100% proliferation, and values were adjusted accordingly. IC_{50} values were calculated from separate experiments performed in triplicate using GraphPad Prism.

Western Blot Analysis. MCF-7 cells were grown to confluence as described above, seeded in 10 cm culture dishes (1×10^6 cells/dish) and allowed to attach overnight. Compound was added at varying concentrations in DMSO (1% DMSO final concentration) and the cells were incubated with drug for 24 h. Cells were harvested in cold PBS and lysed in mammalian protein extraction reagent (MPER, Pierce) lysis buffer containing protease inhibitors (Roche) on ice for 1 h. Lysates were clarified at 14,000g for 10 min at 4° C. Protein concentrations were determined using the Pierce BCA protein assay kit per the manufacturer's instructions. Equal amounts of protein (2.5-10 μg) were electrophoresed under reducing conditions (10% acrylamide gel),

transferred to a polyvinylidene fluoride membrane (PVDF), and immunoblotted with the corresponding specific antibodies. Membranes were incubated with an appropriate horseradish peroxidase-labeled secondary antibody, developed with a chemiluminescent substrate, and visualized.

Antibodies. The following antibodies were used for Western Blotting: mouse anti-Hsp90 (Stressgen/Enzo Life Sciences), rabbit anti-Raf-1 (SantaCruz), rabbit anti-Her2 (Invitrogen), and rabbit anti-Actin (SantaCruz).

VII. References

1. Pearl, L. H.; Prodromou, C. Structure and mechanism of the Hsp90 molecular chaperone machinery. *Ann. Rev. Biochem.* **2006**, *75*, 271-294.
2. Pearl, L. H.; Prodromou, C.; Workman, P. The Hsp90 molecular chaperone: an open and shut case for treatment. *Biochem. J.* **2008**, *410*, 439-453.
3. Hanahan, D.; Weinberg, R. A. The hallmarks of cancer. *Cell* **2000**, *100*, 57-70.
4. Hanahan, D.; Weinberg, Robert A. Hallmarks of cancer: The next generation. *Cell* **2011**, *144*, 646-674.
5. Bishop, S. C.; Burlison, J. A.; Blagg, B. S. J. Hsp90: a novel target for the disruption of multiple signaling cascades. *Curr. Cancer Drug Tar.* **2007**, *7*, 369-388.
6. McDonald, E.; Workman, P.; Jones, K. Inhibitors of the Hsp90 molecular chaperone: attacking the master regulator in cancer. *Curr. Top. Med. Chem.* **2006**, *6*, 1091-1107.
7. Roe, S. M.; Prodromou, C.; O'Brien, R.; Ladbury, J. E.; Piper, P. W.; Pearl, L. H. Structural basis for inhibition of the Hsp90 molecular chaperone by the antitumor antibiotics radicicol and geldanamycin. *J. Med. Chem.* **1999**, *42*, 260-266.
8. Stebbins, C. E.; Russo, A. A.; Schneider, C.; Rosen, N.; Hartl, F. U.; Pavletich, N. P. Crystal structure of an Hsp90-geldanamycin complex: targeting of a protein chaperone by an antitumor agent. *Cell* **1997**, *89*, 239-250.
9. Biamonte, M. A.; Van de Water, R.; Arndt, J. W.; Scannevin, R. H.; Perret, D.; Lee, W. Heat shock protein 90: inhibitors in clinical trials. *J. Med. Chem.* **2010**, *53*, 3-17.
10. Kim, Y. S.; Alarcon, S. V.; Lee, S.; Lee, M. J.; Giaccone, G.; Neckers, L.; Trepel, J. B. Update on Hsp90 inhibitors in clinical trial. *Curr. Top. Med. Chem.* **2009**, *9*, 1479-1492.
11. Marcu, M. G.; Chadli, A.; Bouhouche, I.; Catelli, M. G.; Neckers, L. The heat shock protein 90 antagonist novobiocin interacts with a previously unrecognized ATP-binding domain in the carboxyl terminus of the chaperone. *J. Biol. Chem.* **2000**, *2000*, 37181-37186.
12. Marcu, M. G.; Schulte, T. W.; Neckers, L. Novobiocin and related coumarins and depletion of heat shock protein 90-dependent signalling proteins. *J. Natl. Cancer Inst.* **2000**, *92*, 242-248.
13. Allan, R. K.; Mok, D.; Ward, B. K.; Ratajczak, T. Modulation of chaperone function and cochaperone interaction by novobiocin in the C-terminal domain of Hsp90: evidence that coumarin antibiotics disrupt Hsp90 dimerization. *J. Biol. Chem.* **2006**, *281*, 7161-7171.
14. Yun, B.-G.; Huang, W.; Leach, N.; Hartson, S. D.; Matts, R. L. Novobiocin induces a distinct conformation of Hsp90 and alters Hsp90-cochaperone-client interactions. *Biochemistry* **2004**, *43*, 8217-8229.

15. Galam, L.; Hadden, M. K.; Ma, Z.; Ye, Q.-Z.; Yun, B.-G.; Blagg, B. S. J.; Matts, R. L. High-throughput assay for the identification of Hsp90 inhibitors based on Hsp90-dependent refolding of firefly luciferase. *Bioorg. Med. Chem.* **2007**, *15*, 1939-1946.
16. Nemoto, T.; Ohara-Nemoto, Y.; Ota, M.; Takagi, T.; Yokoyama, K. Mechanism of dimer formation of the 90-kDa heat-shock protein. *Eur. J. Biochem.* **1995**, *233*, 1-8.
17. Harris, S. F.; Shiau, A. K.; Agard, D. A. The crystal structure of the carboxy-terminal dimerization domain of htpG, the Escherichia coli Hsp90, reveals a potential substrate binding site. *Structure* **2004**, *12*, 1087-1097.
18. Richter, K.; Muschler, P.; Hainzl, O.; Buchner, J. Coordinated ATP Hydrolysis by the Hsp90 Dimer. *J. Biol. Chem.* **2001**, *276*, 33689-33696.
19. Ali, M. M.; Roe, S. M.; Vaughan, C. K.; Meyer, P.; Panaretou, B.; Piper, P. W.; Prodromou, C.; Pearl, L. H. Crystal structure of an Hsp90-nucleotide-p23/Sba1 closed chaperone complex. *Nature* **2006**, *440*, 1013-1017.
20. Dollins, D. E.; Warren, J. J.; Immormino, R. M.; Gewirth, D. T. Structures of GRP94-nucleotide complexes reveal mechanistic differences between the hsp90 chaperones. *Mol. Cell* **2007**, *28*, 41-56.
21. Krukenberg, K. A.; Bottcher, U. M.; Southworth, D. R.; Agard, D. A. Grp94, the endoplasmic reticulum Hsp90, has a similar solution conformation to cytosolic Hsp90 in the absence of nucleotide. *Protein Sci.* **2009**, *18*, 1815-1827.
22. Bron, P.; Giudice, E.; Rolland, J. P.; Buey, R. M.; Barbier, P.; Diaz, J. F.; Peyrot, V.; Thomas, D.; Garnier, C. Apo-Hsp90 coexists in two open conformational states in solution. *Biol. Cell* **2008**, *100*, 413-425.
23. Krukenberg, K. A.; Forster, F.; Rice, L. M.; Sali, A.; Agard, D. A. Multiple conformations of E. coli Hsp90 in solution: insights into the conformational dynamics of Hsp90. *Structure* **2008**, *16*, 755-765.
24. Southworth, D. R.; Agard, D. A. Species-dependent ensembles of conserved conformational states define the Hsp90 chaperone ATPase cycle. *Mol. Cell* **2008**, *32*, 631-640.
25. Ratzke, C.; Mickler, M.; Hellenkamp, B.; Buchner, J.; Hugel, T. Dynamics of heat shock protein 90 C-terminal dimerization is an important part of its conformational cycle. *P. Natl. Acad. Sci.* **2010**, *107*, 16101-16106.
26. Retzlaff, M.; Stahl, M.; Eberl, H. C.; Lagleder, S.; Beck, J.; Kessler, H.; Buchner, J. Hsp90 is regulated by a switch point in the C-terminal domain. *EMBO Rep.* **2009**, *10*, 1147-1153.
27. Louvion, J.-F.; Warth, R.; Picard, D. Two eukaryote-specific regions of Hsp82 are dispensable for its viability and signal transduction functions in yeast. *P. Natl. Acad. Sci.* **1996**, *93*, 13937-13942.
28. Owen, B. A. L.; Sullivan, W. P.; Felts, S. J.; Toft, D. O. Regulation of Heat Shock Protein 90 ATPase Activity by Sequences in the Carboxyl Terminus. *J. Biol. Chem.* **2002**, *277*, 7086-7091.
29. Chen, S.; Sullivan, W. P.; Toft, D. O.; Smith, D. F. Differential interactions of p23 and the TRP-containing proteins Hop, Cyp40, FKBP52 and FKBP51 with Hsp90 mutants. *Cell Stress Chaperon.* **1998**, *3*, 118-129.
30. Wegele, H.; Muschler, P.; Bunck, M.; Reinstein, J.; Buchner, J. Dissection of the Contribution of Individual Domains to the ATPase Mechanism of Hsp90. *J. Biol. Chem.* **2003**, *278*, 39303-39310.
31. Young, J. C.; Schneider, C.; Hartl, F. U. In vitro evidence that Hsp90 contains two independent chaperone sites. *FEBS Lett.* **1997**, *418*, 139-143.
32. Scheibel, T.; Weikl, T.; Buchner, J. Two Chaperone Sites in Hsp90 Differing in Substrate Specificity and ATP Dependence. *P. Natl. Acad. Sci.* **1998**, *95*, 1495-1499.
33. Soti, C.; Racz, A.; Csermely, P. A nucleotide-dependent molecular switch controls ATP binding at the C-terminal domain of Hsp90. *J. Biol. Chem.* **2002**, *277*, 7066-7075.

34. Garnier, C.; Lafitte, D.; Tsvetkov, P. O.; Barbier, P.; Leclerc-Devin, J.; Millot, J. M.; Briand, C.; Makarov, A. A.; Catelli, M. G.; Peyrot, V. Binding of ATP to heat shock protein 90: evidence for an ATP-binding site in the C-terminal domain. *J. Biol. Chem.* **2002**, *277*, 12208-12214.
35. Soti, C.; Vermes, A.; Haystead, T. A. J.; Csermely, P. Comparative analysis of the ATP-binding sites of Hsp90 by nucleotide affinity cleavage: a distinct nucleotide specificity of the C-terminal ATP-binding site. *Eur. J. Biochem.* **2003**, *270*, 2421-2428.
36. Tsai, F. T. F.; Singh, O. M. P.; Skarzynski, T.; Wonacott, A. J.; Weston, S.; Tucker, A.; Pauptit, R. A.; Breeze, A. L.; Poyser, J. P.; O'Brien, R.; Ladbury, J. E.; Wigley, D. B. The high-resolution crystal structure of a 24-kDa gyrase B fragment from *E. coli* complexed with one of the most potent coumarin inhibitors, clorobiocin. *Proteins* **1997**, *28*, 41-52.
37. Hartson, S. D.; Thulasiraman, V.; Huang, W.; Whitesell, L.; Matts, R. L. Molybdate Inhibits Hsp90, Induces Structural Changes in Its C-Terminal Domain, and Alters Its Interactions with Substrates†. *Biochemistry* **1999**, *38*, 3837-3849.
38. Burlison, J. A.; Avila, C.; Vielhauer, G.; Lubbers, D. J.; Holzbeierlein, J.; Blagg, B. S. J. Development of novobiocin analogues that manifest anti-proliferative activity against several cancer cell lines. *J. Org. Chem.* **2008**, *73*, 2130-2137.
39. Burlison, J. A.; Blagg, B. S. J. Synthesis and Evaluation of Coumermycin A1 Analogues that Inhibit the Hsp90 Protein Folding Machinery. *Org. Lett.* **2006**, *8*, 4855-4858.
40. Burlison, J. A.; Neckers, L.; Smith, A. B.; Maxwell, A.; Blagg, B. S. J. Novobiocin: Redesigning a DNA Gyrase Inhibitor for Selective Inhibition of Hsp90. *J. Am. Chem. Soc.* **2006**, *128*, 15529-15536.
41. Donnelly, A.; Blagg, B. S. J. Novobiocin and additional inhibitors of the Hsp90 C-terminal nucleotide binding pocket. *Curr. Med. Chem.* **2008**, *15*, 2702-2717.
42. Donnelly, A.; Mays, J. R.; Burlison, J. A.; Nelson, J. T.; Vielhauer, G.; Holzbeierlein, J.; Blagg, B. S. J. The design, synthesis, and evaluation of coumarin ring derivatives of the novobiocin scaffold that exhibit antiproliferative activity. *J. Org. Chem.* **2008**, *73*, 8901-8920.
43. Donnelly, A. C.; Zhao, H.; Reddy, K. B.; Blagg, B. S. J. Cytotoxic sugar analogues of an optimized novobiocin scaffold. *Med. Chem. Comm.* **2010**, *1*, 165-170.
44. Kusuma, B. R.; Peterson, L. B.; Zhao, H.; Vielhauer, G.; Holzbeierlein, J.; Blagg, B. S. J. Targeting the heat shock protein 90 dimer with dimeric inhibitors. *J. Med. Chem.* **2011**, *54*, 6234-6253.
45. Matthews, S. B.; Vielhauer, G. A.; Manthe, C. A.; Chaguturu, V. K.; Szabla, K.; Matts, R. L.; Donnelly, A. C.; Blagg, B. S.; Holzbeierlein, J. M. Characterization of a novel novobiocin analogue as a putative C-terminal inhibitor of heat shock protein 90 in prostate cancer cells. *Prostate* **2010**, *70*, 27-36.
46. Shelton, S. N.; Shawgo, M. E.; Matthews, S. B.; Lu, Y.; Donnelly, A. C.; Szabla, K.; Tanol, M.; Vielhauer, G. A.; Rajewski, R. A.; Matts, R. L.; Blagg, B. S.; Robertson, J. D. KU135, a novel novobiocin-derived C-terminal inhibitor of the 90-kDa heat shock protein, exerts potent antiproliferative effects in human leukemic cells. *Mol. Pharmacol.* **2009**, *76*, 1314-1322.
47. Shen, G.; Wang, M.; Welch, T. R.; Blagg, B. S. J. Design, Synthesis, and Structure Activity Relationships for Chimeric Inhibitors of Hsp90. *J. Org. Chem.* **2006**, *71*, 7618-7631.
48. Yu, X. M.; Shen, G.; Neckers, L.; Blake, H.; Holzbeierlein, J.; Cronk, B.; Blagg, B. S. Hsp90 inhibitors identified from a library of novobiocin analogues. *J. Am. Chem. Soc.* **2005**, *127*, 12778-12779.
49. Zhao, H.; B., R. K.; Blagg, B. S. J. Synthesis and Evaluation of Noviose Replacements on Novobiocin That Manifest Antiproliferative Activity. *ACS Med. Chem. Lett* **2010**, *1*, 311-315.
50. Zhao, H.; Donnelly, A. C.; Kusuma, B. R.; Brandt, G. E. L.; Brown, D.; Rajewski, R. A.; Vielhauer, G.; Holzbeierlein, J.; Cohen, M. S.; Blagg, B. S. J. Engineering an Antibiotic to Fight Cancer: Optimization of the Novobiocin Scaffold to Produce Anti-proliferative Agents. *J. Med. Chem.* **2011**, *54*, 3839-3853.

51. Huang, X. Y.; Shan, Z. J.; Zhai, H. L.; Li, L. N.; Zhang, X. Y. Molecular Design of Anticancer Drug Leads Based on Three-Dimensional Quantitative Structure–Activity Relationship. *J. Chem. Inf. Model.* **2011**, *51*, 1999-2006.
52. Bellon, S.; Parsons, J. D.; Wei, Y.; Hayakawa, K.; Swenson, L. L.; Charifson, P. S.; Lippke, J. A.; Aldape, R.; Gross, C. H. Crystal structures of Escherichia coli topoisomerase IV ParE subunit (24 and 43 kilodaltons): a single residue dictates differences in novobiocin potency against topoisomerase IV and DNA gyrase. *Antimicrob. Agents Ch.* **2004**, *48*, 1856-1864.
53. Holdgate, G. A.; Tunnicliffe, A.; Ward, W. H.; Weston, S. A.; Rosenbrock, G.; Barth, P. T.; Taylor, I. W.; Pauptit, R. A.; Timms, D. The entropic penalty of ordered water accounts for weaker binding of the antibiotic novobiocin to a resistant mutant of DNA gyrase: a thermodynamic and crystallographic study. *Biochemistry* **1997**, *36*, 9663-9673.
54. Matts, R. L.; Dixit, A.; Peterson, L. B.; Sun, L.; Voruganti, S.; Kalyanaraman, P.; Hartson, S. D.; Verkhivker, G. M.; Blagg, B. S. J. Elucidation of the Hsp90 C-Terminal Inhibitor Binding Site. *ACS Chem. Biol.* **2011**, *6*, 800-807.
55. Shen, G.; Yu, X. m.; Blagg, B. S. J. Syntheses of photolabile novobiocin analogues. *Bioorg. Med. Chem. Lett.* **2004**, *14*, 5903-5906.
56. Sali, A.; Blundell, T. L. Comparative protein modelling by satisfaction of spatial restraints. *J. Mol. Biol.* **1993**, *234*, 779-815.
57. Sgobba, M.; Degliesposti, G.; Ferrari, A. M.; Rastelli, G. Structural models and binding site prediction of the C-terminal domain of human Hsp90: a new target for anticancer drugs. *Chem. Biol. Drug Des.* **2008**, *71*, 420-433.
58. Sgobba, M.; Forestiero, R.; Degliesposti, G.; Rastelli, G. Exploring the Binding Site of C-Terminal Hsp90 Inhibitors. *J. Chem. Inf. Comp. Sci.* **2010**, *50*, 1522-1528.
59. Richter, K.; Soroka, J.; Skalniak, L.; Leskovar, A.; Hessling, M.; Reinstein, J.; Buchner, J. Conserved Conformational Changes in the ATPase Cycle of Human Hsp90. *J. Biol. Chem.* **2008**, *283*, 17757-17765.
60. Duerfeldt, A. S.; Blagg, B. S. J. Hydrating for Resistance to Radicicol. *ACS Chem. Biol.* **2009**, *4*, 245-247.
61. Peterson, L. B.; Blagg, B. S. J. Click chemistry to probe Hsp90: Synthesis and evaluation of a series of triazole-containing novobiocin analogues. *Bioorg. Med. Chem. Lett.* **2010**, *20*, 3957-3960.
62. Kolb, H. C.; Sharpless, K. B. The growing impact of click chemistry on drug discovery. *Drug Discov. Today* **2003**, *8*, 1128-1137.
63. Tron, G. C.; Pirali, T.; Billington, R. A.; Canonico, P. L.; Sorba, G.; Genazzani, A. A. Click chemistry reactions in medicinal chemistry: Applications of the 1,3-dipolar cycloaddition between azides and alkynes. *Med. Res. Rev.* **2008**, *28*, 278-308.
64. Sivakumar, K.; Xie, F.; Cash, B. M.; Long, S.; Barnhill, H. N.; Wang, Q. A fluorogenic 1,3-dipolar cycloaddition reaction of 3-azidocoumarins and acetylenes. *Org. Lett.* **2004**, *6*, 4603-4606.
65. Ikehata, K.; Duzhak, T. G.; Galeva, N. A.; Ji, T.; Koen, Y. M.; Hanzlik, R. P. Protein Targets of Reactive Metabolites of Thiobenzamide in Rat Liver in Vivo. *Chem. Res. Toxicol.* **2008**, *21*, 1432-1442.
66. Altschul, S. F.; Gish, W.; Miller, W.; Myers, E. W.; Lipman, D. J. Basic local alignment search tool. *J. Mol. Biol.* **1990**, *215*, 403-410.
67. Larkin, M. A.; Blackshields, G.; Brown, N. P.; Chenna, R.; McGettigan, P. A.; McWilliam, H.; Valentin, F.; Wallace, I. M.; Wilm, A.; Lopez, R.; Thompson, J. D.; Gibson, T. J.; Higgins, D. G. Clustal W and Clustal X version 2.0. *Bioinformatics* **2007**, *23*, 2947-2948.
68. Tripos International, SYBYL, 1699 South Hanley Rd., St. Louis, Missouri, 63144, USA.
69. Yu, X. M.; Shen, G.; Blagg, B. S. J. Synthesis of (–)-Noviose from 2,3-O-Isopropylidene-D-erythrulactol. *J. Org. Chem.* **2004**, *69*, 7375-7378.

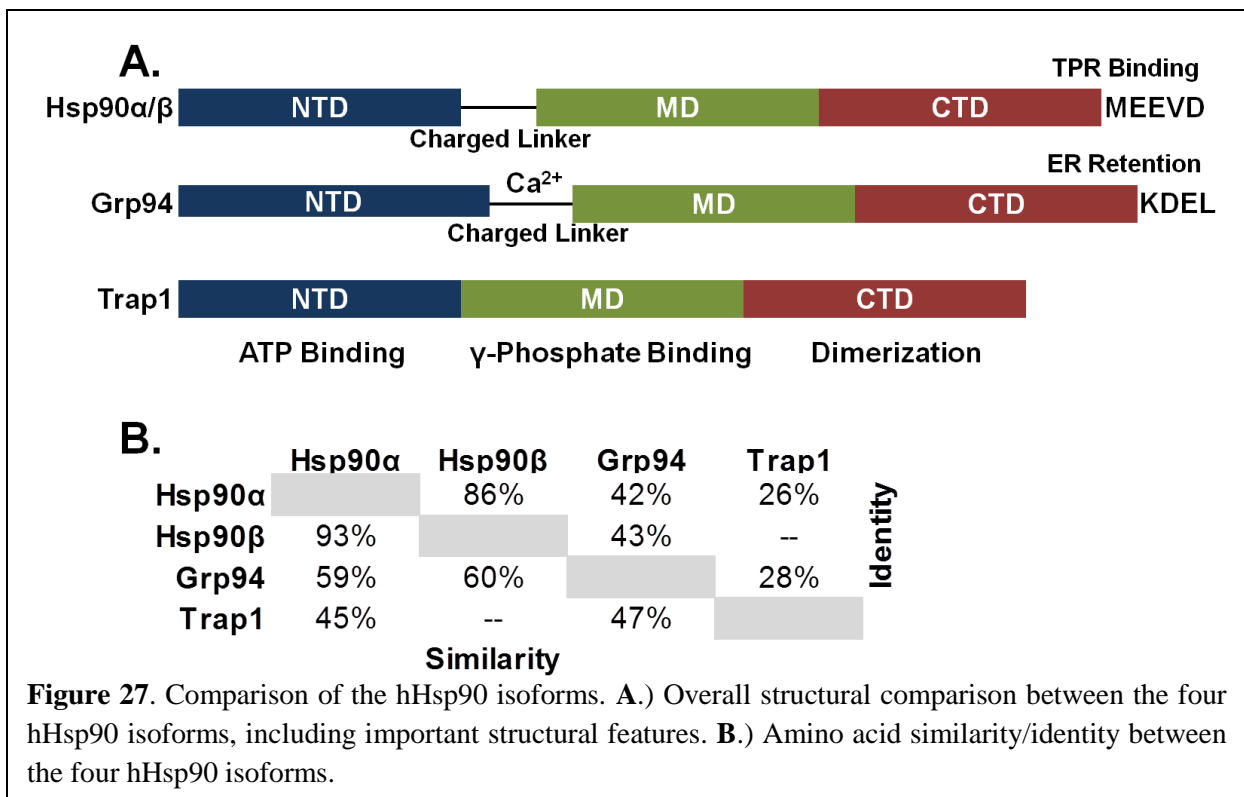
70. Albert, B. J.; Sivaramakrishnan, A.; Naka, T.; Czaicki, N. L.; Koide, K. Total syntheses, fragmentation studies, and antitumor/antiproliferative activities of FR901464 and its low picomolar analogue. *J. Am. Chem. Soc.* **2007**, *129*, 2648-2659.
71. Miwa, K.; Aoyama, T.; Shioiri, T. A new synthesis of aldehydes from ketones utilizing trimethylsilyldiazomethane. *Synlett* **1994**, *2*, 109.
72. Perez-Serrano, L.; Casarrubios, L.; Dominguez, G.; Gonzalez-Perez, P.; Perez-Castells, J. Synthesis of enyndoindoles via vinyl and ethynyl indoles. *Synthesis* **2002**, *13*, 1810-1812.
73. Hadden, K. M.; Hill, S. A.; Davenport, J.; Matts, R. L.; Blagg, B. S. J. Synthesis and evaluation of Hsp90 inhibitors that contain the 1,4-naphthoquinone scaffold. *Bioorg. Med. Chem* **2009**, *17*, 634-640.
74. Mueller, S.; Liepold, B.; Roth, G. J.; Bestmann, H. J. An improved one-pot procedure for the synthesis of alkynes from aldehydes. *Synlett* **1996**, *6*, 521-522.
75. Mothes, C.; Lavielle, S.; Karoyan, P. Amino-Zinc-Ene-Enolate cyclization: a short access to *cis*-3-substituted proline-homotryptophane derivatives. *J. Org. Chem.* **2008**, *73*, 6707-6710.

Chapter III

Biological Evaluation of Isoform Selective Hsp90 Inhibitors and Characterization of Isoform Dependent Client Proteins

I. Introduction

In humans, there are four Hsp90 isoforms: Hsp90 α and Hsp90 β reside primarily in the cytoplasm and are stress-inducible and constitutively expressed, respectively.¹ Glucose regulated protein 94 (Grp94) is localized to the endoplasmic reticulum, while tumor necrosis factor receptor associated protein1 (Trap1) is the mitochondrial-resident chaperone (**Figure 27**).



Distinguishing the role played by each Hsp90 isoform has been a significant challenge, especially those manifested by the two cytosolic isoforms, which are structurally very similar.¹⁻² The responsibility of each cytosolic isoform appears to overlap with some client proteins. However, recent evidence has emerged that suggests co-chaperones and client proteins interact with each isoform in a unique manner.² Delineating the roles and responsibilities of each isoform

has become a major goal for this field, as such information will provide insight into some of the clinically observed toxicities and detriments manifested by Hsp90 inhibitors that exhibit *pan*-inhibition. In addition, isoform selective inhibitors may help elucidate the role of each isoform as well as understand the clinical implications of inhibiting a single isoform. This chapter describes the evaluation of the human ether a-go-go (hERG) channel as an Hsp90 α isoform-dependent client, the progress towards elucidating other isoform-dependent clients and the development of an assay to identify Grp94 inhibitors.

A. Hsp90 α/β

The cytosolic Hsp90 isoforms, Hsp90 α and Hsp90 β , have been the most widely studied chaperones. Many of the client proteins for Hsp90 α/β have been identified and much is known about the structure and function of these isoforms. Several crystal structures and co-crystal structures of the N-terminal domain (NTD) exist, which have provided valuable insights into the mechanism for ATP binding and hydrolysis. Hsp90 α and Hsp90 β , encoded by the HSP90AA1 and HSP90AB1 genes respectively, are 86% identical and 93% similar in amino acid sequence, while the highly conserved NTD is 95% identical between the two isoforms. The vast array of over 200 client proteins that depend upon Hsp90 α/β include numerous protein kinases, transcription factors, mutated signaling proteins and cell cycle regulators. An up-to-date list of these client proteins is maintained by Didier Picard at the University of Geneva.³⁻⁴ It has been difficult to biochemically distinguish the roles manifested by each Hsp90 isoform due to the high structural similarity, significant antibody cross reactivity, and the presence of Hsp90 α/β heterodimers.

Only a few Hsp90 isoform-dependent client proteins have been identified this far. Prior studies have demonstrated that the cellular inhibitor of apoptosis protein 1 (c-IAP1) depends

upon Hsp90 β ,⁵ while some intermediates in the major histocompatibility complex (MHC) class I, but not MHC class II, pathway depend solely upon Hsp90 α .⁶⁻⁷ Phenotypic screens have also been used to identify the unique roles played by each cytosolic Hsp90 isoform. For example, Hsp90 β appears to be critical for embryonic development, as an Hsp90 β null mutation results in embryonic lethality.⁸ Meanwhile, Hsp90 α is overexpressed in many cancer cells and has been linked to cancer cell invasiveness, which is directly related to matrix metalloproteinase 2 activity.⁹ Chadli et al. provided rationale to support Hsp90 isoform dependence of co-chaperones.¹⁰ In their studies, they found the general cell UNC45 (GCUNC45) binds preferentially to Hsp90 β and was capable of stalling the chaperone machinery during the progression/activation of the progesterone receptor. In this example, the specific co-chaperone required for client protein activation/folding determines the isoform dependence. In a yeast model system in which the endogenous Hsp90 was replaced with either hHsp90 α or hHsp90 β as the sole Hsp90, differences in activation of client proteins and sensitivity to Hsp90 inhibitors were observed.¹¹⁻¹² Using RNA interference (RNAi) and other genetic manipulation strategies, it has become possible to investigate the roles manifested by each cytosolic isoform. It is expected that the list of isoform dependent client proteins and co-chaperones will grow exponentially over the coming years.

B. Grp94

Glucose-regulated protein 94 (Grp94), also called gp96 and endoplasmin, resides in the lumen of the endoplasmic reticulum (ER), is encoded by the HSP90B1 gene in humans and is not present in most unicellular organisms, including yeast, most fungi, and most bacteria.^{1,13} The expression of Grp94 is controlled by different mechanisms and transcription factors as compared to Hsp90 α/β . Grp94 is not overexpressed following heat shock, but following ER stress, such as

redox stress, calcium imbalance, and hypoxia, Grp94 is upregulated as part of the unfolded protein response (UPR).¹³ Grp94 is 42-43% identical and 59-60% similar in primary sequence to the two cytosolic isoforms, Hsp90 α/β (**Figure 27B**). The overall structure of Grp94 resembles that of Hsp90 α/β , as Grp94 contains the same four domains: NTD, charged linker, MD, and CTD (**Figure 27**).¹ Grp94 contains a Bergerat fold in the NTD that binds ATP and other compounds known to bind Hsp90 α/β , such as geldanamycin and radicicol, and is 55% identical and over 70% similar to the Hsp90 α/β NTD.¹⁴⁻¹⁷ However, the NTD of Grp94 is longer than the NTD of Hsp90 α/β because of a 21-residue sequence in the NTD that targets Grp94 to the ER, which is subsequently cleaved to produce the mature form of Grp94. In addition, a 5-amino acid insertion proximal to the ATP binding site provides a unique hydrophobic cleft that allows binding of the adenosine analogue, N-ethylcarboxamidoadenosine (NECA), which does not bind to Hsp90 α/β .¹⁸ This unique pocket was proposed to allow for the development of isoform-selective Hsp90 inhibitors, as described below.

The charged linker of Grp94 is comprised of an E/D-rich sequence that is capable of binding Ca²⁺ ions, followed by a positively charged poly-K stretch.¹⁹⁻²⁰ The analogous region in Hsp90 α/β does not bind Ca²⁺ ions, as the positively and negatively charged residues are interspersed and prevent formation of the negatively charged cleft that is capable of binding the positively charged divalent metal. The middle domain (MD) of Grp94 is highly homologous to the MD contained within Hsp90 α/β and provides similar functionalities, namely client and co-chaperone binding and cooperation with the NTD for nucleotide binding and hydrolysis.

The C-terminal domain (CTD) of Grp94 contains the required dimerization domain, similar to Hsp90 α/β . In contrast to the MEEVD motif in Hsp90 α/β which is recognized by TPR-containing proteins, Grp94 contains the ER-retention sequence, KDEL, which is recognized by

KDEL receptors. In general, Grp94 is similar in overall structure to Hsp90 α/β but contains a few unique structural elements specific to its function in the ER.

Grp94 functions as a molecular chaperone in the ER and plays a role in the maturation and degradation of a specific subset of client proteins. Grp94 also participates in the translocation of defective, misfolded proteins from the ER to the cytosol for degradation. Generally, client proteins that depend upon Grp94 for maturation are secreted, membrane-localized, glycosylated proteins that contain disulfide bonds. Grp94-dependent client proteins include: Toll-like receptors, integrins, IFG-I, IGF-II, IFN- γ , and IRS-1, many of which are important in intercellular communication.^{13,21} In addition, Grp94 is an essential gene and appears to be crucial for embryonic development, stem cell maintenance, host defense and cell adhesion.²²⁻²⁵ Unlike Grp94, little is known about the function and clientele of the mitochondria-resident chaperone, Trap-1.

C. Trap-1

Tumor necrosis factor receptor-associated protein-1 (Trap1) resides in the mitochondria and is the least structurally conserved of the four human isoforms sharing only 26% identity and 45% similarity with Hsp90 α .²⁶⁻²⁹ The overall domain structure of Trap1 is similar to the other isoforms, with a few notable exceptions. Trap1 does not have a charged linker domain nor the MEEVD motif. However, Trap1 does contain a 60-residue N-terminal mitochondrial-targeting sequence that is cleaved after translocation to the mitochondria.²⁵ Trap1 displays weak ATPase activity and is inhibited by that natural products, geldanamycin and radicicol.³⁰ Functionally, less is known about the responsibilities of Trap1. However, Trap1 plays a role in cytoprotection, specifically from mitochondrial apoptosis and aids in the maintenance of mitochondrial maintenance.³¹⁻³³ It has been suggested that Trap1 is overexpressed in human cancers owing to

its cytoprotective nature.³⁴ Trap1 appears to inhibit mitochondrial apoptosis, suppress reactive oxygen species formation, and aid in the acquisition of resistance mechanisms to chemotherapies.^{25,34}

Delineating the roles played by and clientele dependent upon each Hsp90 isoform has become a significant goal in the Hsp90 field. Advances in biochemical methods have allowed the study of individual isoforms. However, small molecule isoform-selective inhibitors would further progress this deconvolution process, as all known Hsp90 inhibitors demonstrate *pan*-inhibition, which does not provide a means to study individual isoforms.

II. The hERG Channel is Dependent upon the Hsp90 α Isoform for Maturation and Trafficking

All currently described Hsp90 inhibitors manifest pan-inhibition and since cardiotoxicity represents a major hurdle for Hsp90 inhibitor development, we investigated whether the hERG channel was an isoform-dependent Hsp90 client protein. The α -subunit of the voltage gated potassium channel, the human ether-a-gogo-related gene product, hERG, constitutes a major component of the ion channel responsible for repolarization of cardiac action potential.³⁵⁻³⁶ Ficker *et al.* demonstrated previously that hERG depends upon Hsp90 for its functional maturation and that pharmacological inhibition of Hsp90 had deleterious effects on the hERG-related membrane potential.³⁷⁻³⁸ Defects in the hERG channel or off-target pharmacological inhibition of the hERG channel can cause long-QT syndrome, resulting in ventricular arrhythmias and even death.^{36,39} There are three primary classes of compounds that disrupt hERG function; 1) compounds that bind directly to and inhibit the hERG channel (hERG blockers), 2) compounds that inhibit the functional trafficking of hERG, or 3) compounds that exhibit both hERG blocking and hERG trafficking inhibitory abilities.⁴⁰⁻⁴¹ Hsp90 inhibitors have been shown

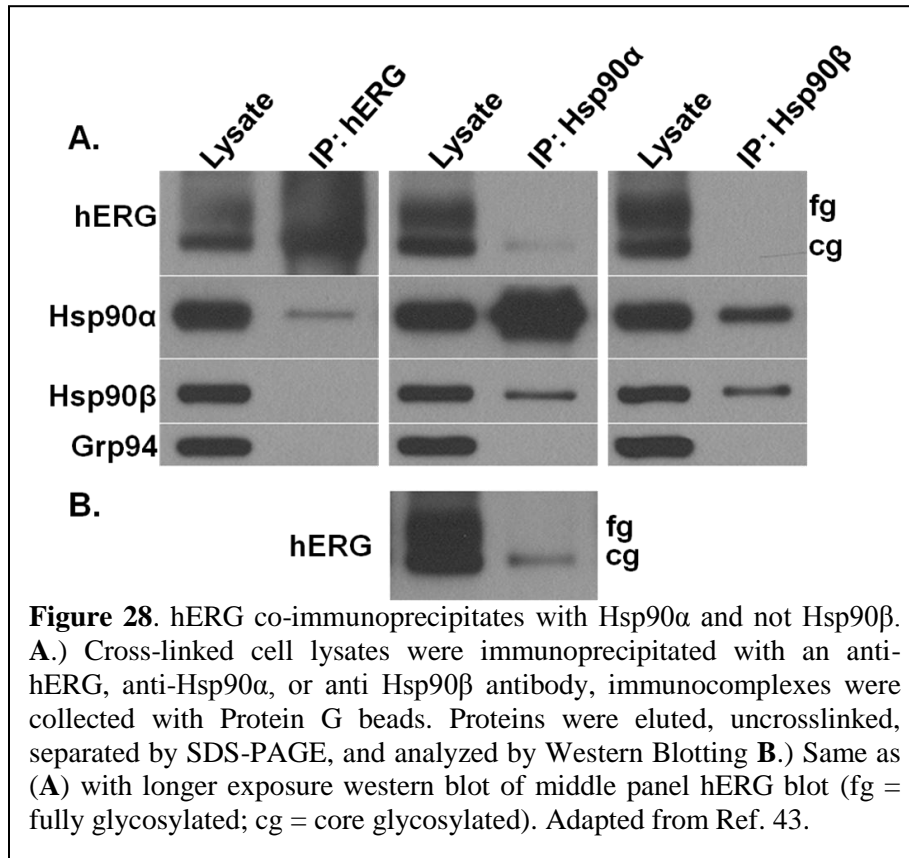
to disrupt hERG function and cause a reduction in hERG-related membrane currents in *in vitro* studies. It has previously been demonstrated that the Hsp90 inhibitor, geldanamycin, inhibits hERG trafficking, presumably through an Hsp90-dependent mechanism.³⁷ Given the intense pharmaceutical interest in the development of Hsp90 inhibitors as therapies for cancer and other diseases, the importance of identifying the isoform dependency of this client protein is clear, as pan-inhibition may result in undesired effects.

A. hERG Interacts Solely with Hsp90 α

The K⁺ channel encoded by hERG gene plays a major role in the repolarization of cardiac myocytes following normal action potential.³⁵ Although pharmacological inhibition of hERG itself is a therapeutic target for the treatment of some cardiac arrhythmias, more often undesired inhibition of hERG is an off-target effect that results in cardiotoxicity and leads to the ultimate failure of pre-clinical or clinical candidates.³⁶ hERG has been previously identified as an Hsp90/Hsp70-dependent client protein, and studies have shown that inhibition of Hsp90 with geldanamycin resulted in proteasome-mediated degradation of hERG which prevented maturation of a fully functional hERG channel.³⁷⁻³⁸ In addition, the Hsp90 co-chaperones Hsp-organizing protein (Hop), Hdj-2, and BCL-associated athanogene 2 (Bag-2), as well as the 38-kDa FK506 binding protein (FKBP38) and calnexin were found to interact with hERG, presumably to aid in hERG maturation.⁴² Based on these observations, we sought to determine whether hERG was dependent upon a sole Hsp90 isoform, which would provide rationale to support the development of Hsp90 isoform-selective inhibitors that avoid such detriments.

Using the method of Ficker et al.³⁷ co-immunoprecipitation studies were performed to evaluate the interaction of hERG with each of the Hsp90 isoforms. hERG expressing HEK

(HEK-hERG) cell lysates were chemically crosslinked and immunoprecipitated utilizing antibodies that recognize Hsp90 α , Hsp90 β , or hERG (**Figure 28**).⁴³



hERG channels exist as either a functional, fully glycosylated mature form (fg) or an immature core-glycosylated protein (cg), and both species can be detected by Western Blot analysis.⁴⁴⁻⁴⁶ As previously determined, Hsp90 only interacts

with the core glycosylated hERG (**Figure 28**).³⁷ In addition, as evidenced in **Figure 28**, hERG only interacts with a single Hsp90 isoform, namely Hsp90 α . The hERG-Hsp90 α interaction can be captured by co-immunoprecipitation with either an anti-hERG or anti-Hsp90 α antibody (**Figure 28A/B**). Due to the harsh conditions of the chemical crosslinking and the existence of Hsp90 α / β heterodimers, some cross-reactivity in terms of the co-immunoprecipitation antibodies of Hsp90 α and Hsp90 β was observed.

In order to identify other proteins involved in this interaction, we performed co-immunoprecipitations with anti-hERG antibody, separated the complexes on SDS-PAGE, excised protein bands and subjected the proteins to tryptic digest and mass spectrometry. Using

this approach we identified Hsp90 α in the hERG-associated complex. Since Hsp90 α and Hsp90 β are overall 86% identical, it is important to note that we observed overlapping peptides derived from both isoforms, however the only unique peptides identified were from Hsp90 α . In addition to the chaperones and co-chaperones previously identified to interact in the hERG complex,⁴² additional proteins were found (**Table 8**). The Hsp/c70 co-chaperone, Hsc70-interacting protein (Hip), was found in this complex and typically directs Hsc70 to the Hsp90 complex with the help of the Hsp organizing protein (Hop). Two additional peptidyl-prolyl cis-trans isomerases were also identified, FK506 binding protein 51 (FKBP51) and Cyclophilin A (CypA). FKBP51 has previously been identified in Hsp90 complexes, specifically those that contain the steroid hormone receptors.⁴⁷ Hsp90 associated immunophilins typically bind to the C-terminus of Hsp90 and mediate interactions between Hsp90 and other co-chaperones.

Table 8. hERG interacting proteins (N=3).⁴³

Protein ¹	Accession Number (NCBI)	No. Unique Peptides	Sequence Coverage (%)
hERG	Q12809.1	9	11
Hsp90 α	P07900	6	22
Hsc70*	P11142	13	29
Hsp70	P08107	21	40
Calnexin*	P27824	3	7
FKBP51	Q02790	3	12
Hip	P50502	2	7
Hop*	P31948	6	16
Cyclophilin A	P62937	7	47
14-3-3	P62258	9	44

¹Confidence level of 95% or greater

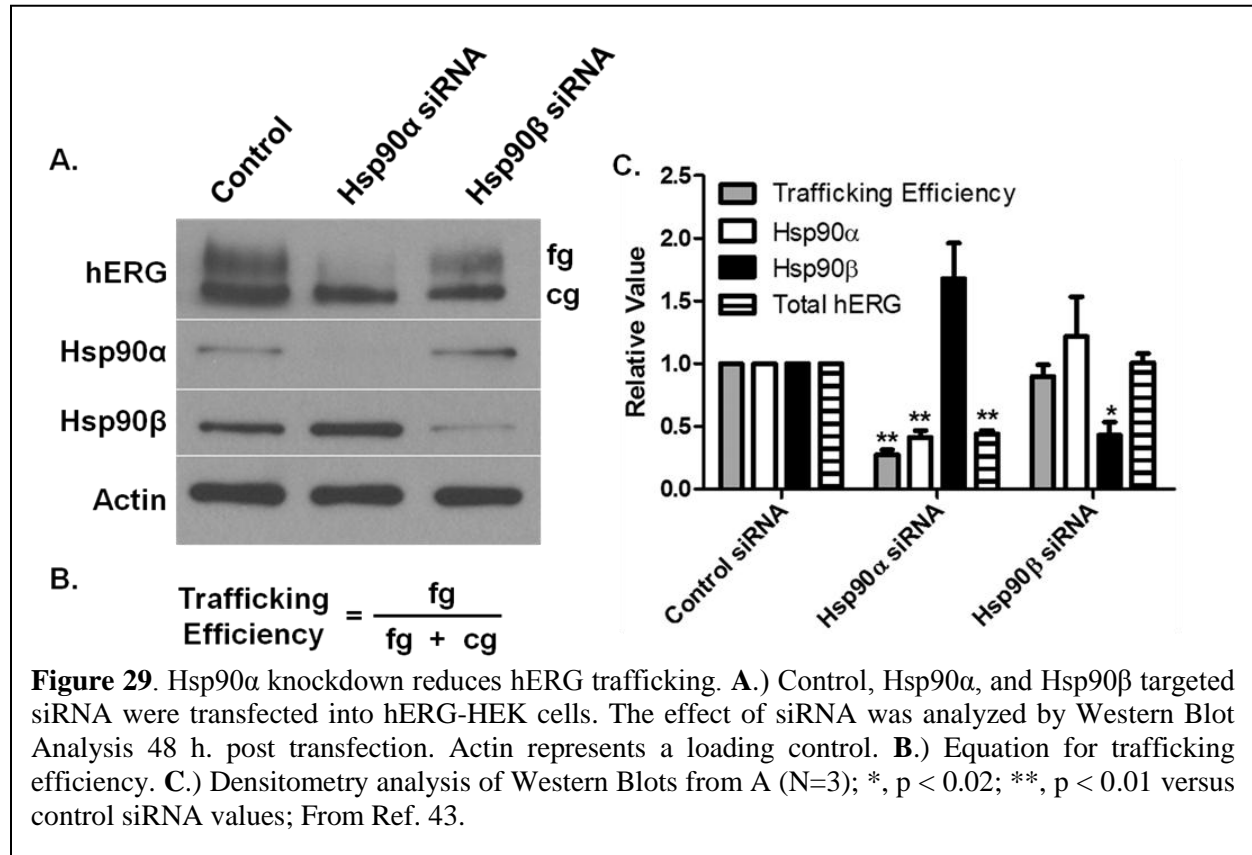
*Also identified in Ref. 42

CypA and Hsp90 have been shown to be necessary for cell membrane translocation of toxins from both *Bacillus anthracis* and *Clostridium difficile*, however, the involvement of CypA in Hsp90-mediated client protein maturation has not been reported.⁴⁸⁻⁴⁹ Another tetratricopeptide

repeat-containing protein, 14-3-3 protein epsilon (14-3-3) was also identified. Its role in client protein maturation is undocumented, however TPR-domain containing proteins typically mediate protein-protein interactions.

B. Hsp90 α and Hsp90 β Knockdown have Differential Effects on hERG Trafficking

To investigate the relationship between each of the cytosolic Hsp90 isoforms and hERG maturation, we analyzed the effects of either Hsp90 α or Hsp90 β knockdown using RNA interference with siRNAs targeted to each isoform. Under control conditions (scrambled siRNA), both the fully glycosylated and core glycosylated hERG proteins were observed (**Figure 29**). Previously, it was shown that Hsp90 inhibitors, such as geldanamycin and radicicol, cause both a



dose-dependent reduction in the hERG-associated current amplitudes in patch clamp experiments and in the trafficking efficiency of hERG, or the ratio of fg hERG over total hERG (fg+cg)

(**Figure 29B**).³⁷ Knockdown of Hsp90 α (60% reduction) caused approximately a 70% reduction in the trafficking efficiency of hERG and a 55% reduction in the total amount of hERG (**Figure 29C**). Conversely, the hERG trafficking efficiency and total amount of hERG remained unchanged after Hsp90 β knockdown (60% reduction).

For further confirmation, we sought to demonstrate a direct relationship between the amount of functional Hsp90 α and the trafficking efficiency of hERG. Using a tetracycline-induced promoter linked to the expression of either an Hsp90 α or Hsp90 β targeted shRNA, this relationship was investigated (**Figure 30**). **Figure 30** demonstrates the direct relationship between the amount of Hsp90 α and the trafficking efficiency of the hERG channel. Decreasing amounts of Hsp90 α in these cells causes a “dose-dependent” decrease in the amount of fully glycosylated, functional hERG after both 24 and 48 hours (**Figure 30A/C/E** and **30B/D/F**). In addition, we observed a reduction in the total amount of hERG (fg+cg) in these cells following shRNA-mediated Hsp90 α reduction (**Figure 30A/C/E/G**). Conversely, reduction in the amount of Hsp90 β had no effect on the glycosylation state, i.e. functional activity, or total hERG (**Figure 30E/F/H**). These data further demonstrate the isoform-dependent nature of the hERG channel for Hsp90 α .

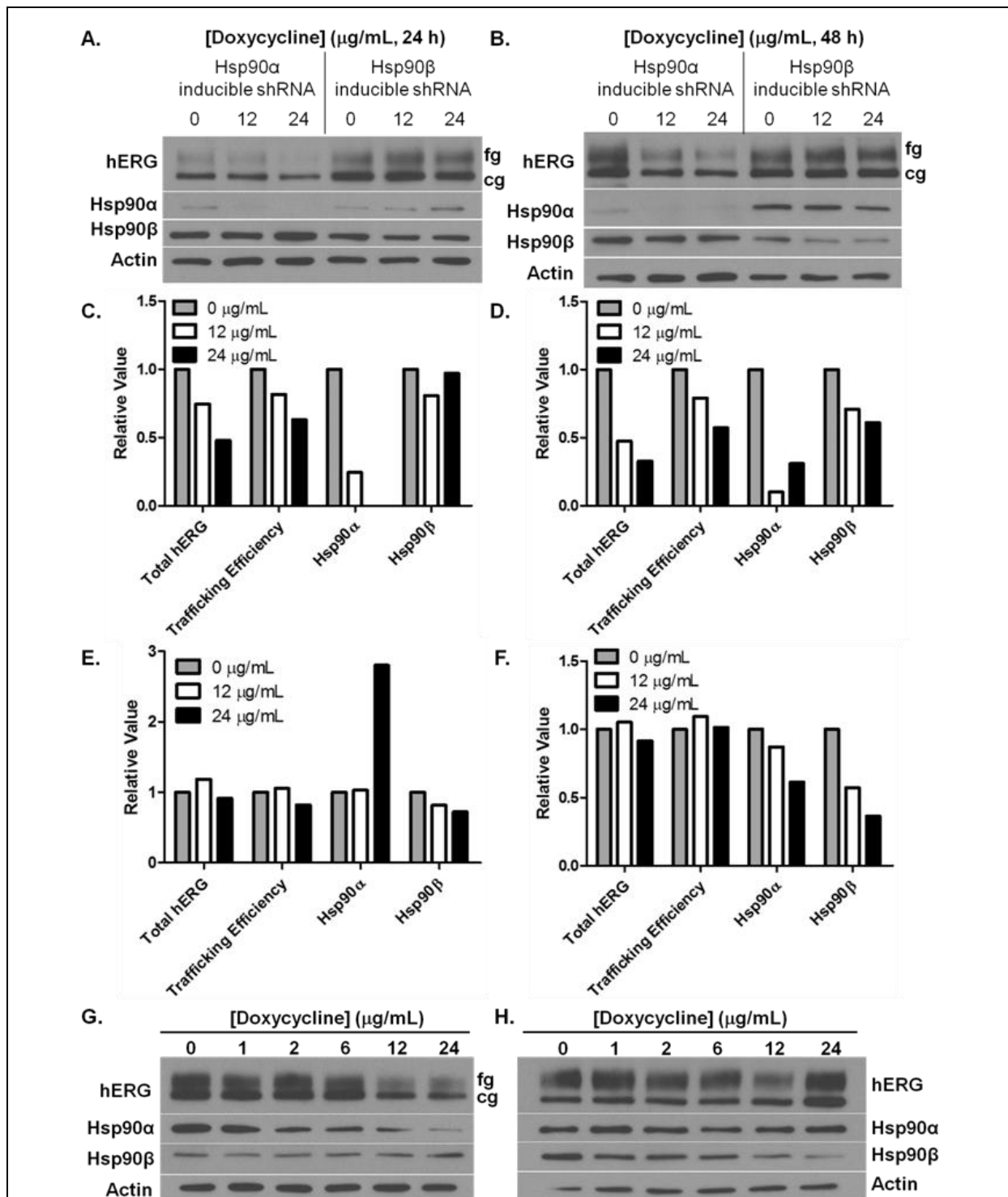


Figure 30. Hsp90 α levels directly affect hERG trafficking efficiency. Western blot analysis of cell lysates from HEK-hERG cells that either express Hsp90 α or Hsp90 β targeted shRNA after doxycycline treatment for (A) 24 h. or (B) 48 h. treatment. (C.) and (D.) Densitometry analysis of Western blots from A and B (Hsp90 α knockdown) respectively. (E.) and (F.) Densitometry analysis of Western blots from A and B (Hsp90 β knockdown) respectively. Western blot analysis of cell lysates from HEK-hERG cells expressing (G) Hsp90 α targeted shRNA or (H.) Hsp90 β targeted shRNA after 48 h. doxycycline treatment; From Ref. 43.

C. Implications for Hsp90 Inhibitor Development

As pharmacological inhibition of hERG can lead to the ultimate failure of pre-clinical drug candidates, it is important to understand the different mechanisms by which hERG function can be affected.³⁶ Drug-like molecules can bind directly to and inhibit hERG. However, it has also been demonstrated that Hsp90 inhibitors halt the functional maturation of hERG and can therefore inhibit hERG function by preventing trafficking to the membrane.⁴⁰⁻⁴¹ Hsp90 inhibitors appear to prevent the glycosylation of hERG and halt translocation from the ER to the cell surface, which results in non-functional hERG accumulation in the cytosol.³⁷ Since small molecule Hsp90 inhibitors are of great interest to the pharmaceutical industry, it is important to outline the liabilities associated with Hsp90 inhibition. These results clearly demonstrate that the cardiotoxic liability associated with pan-Hsp90 inhibition may be avoidable by the development of Hsp90 inhibitors that avoid Hsp90 α .

In addition, these results suggest that deconvolution of the Hsp90-isoform proteome is needed in order to more thoroughly understand the consequences of Hsp90 inhibition. It has been difficult to biochemically distinguish the roles manifested by each Hsp90 isoform due to the high structural similarity, significant antibody cross reactivity, and the presence of Hsp90 α/β heterodimers. Furthermore, only a few Hsp90 isoform-dependent client proteins have been identified. In conclusion, we have shown herein that the hERG channel depends solely on Hsp90 α , providing rationale for the design of isoform selective Hsp90 inhibitors. Furthermore, understanding the responsibilities manifested by each Hsp90 isoform will be crucial to the development of Hsp90 inhibitors and will allow for the development of Hsp90 inhibitors that produce fewer adverse effects.

III. Development of Grp94 Selective Inhibitors and Assays to Evaluate Grp94-inhibitory Activity

Hsp90 contains an atypical nucleotide N-terminal binding pocket, which allows for the development of selective inhibitors.⁵⁰ Several of these Hsp90 N-terminal inhibitors, e.g., 17-AAG (Phase I-III), SNX-5422 (Phase I), CNF2024 (Phase II) and NVP-AUY922 (Phase I/II) have been evaluated clinical trials for various indications, including but not limited to melanoma,

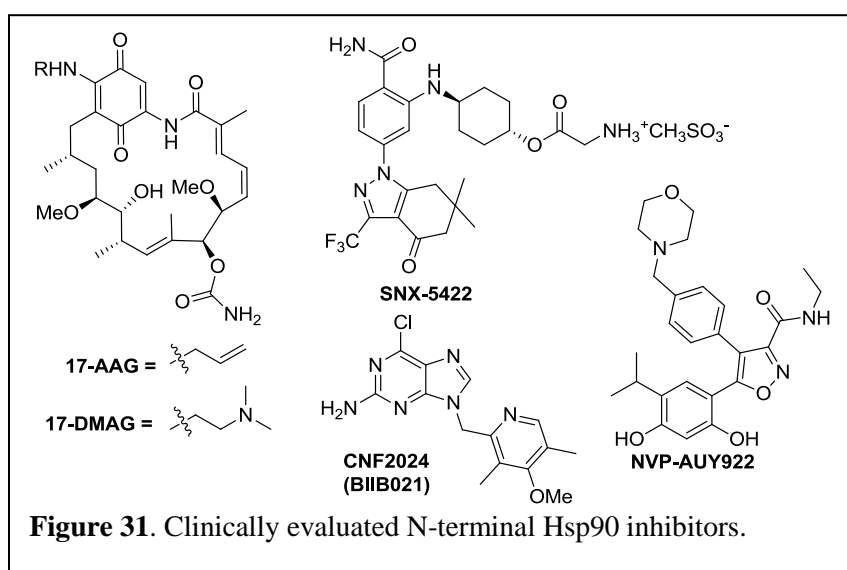


Figure 31. Clinically evaluated N-terminal Hsp90 inhibitors.

multiple myeloma, refractory solid tumors, and breast cancer (**Figure 31**).⁵¹

Unfortunately, cardiovascular, ocular, and/or hepatotoxicities have been observed.⁵¹⁻⁵³ Pan-Hsp90 inhibition may be the cause for these effects, as

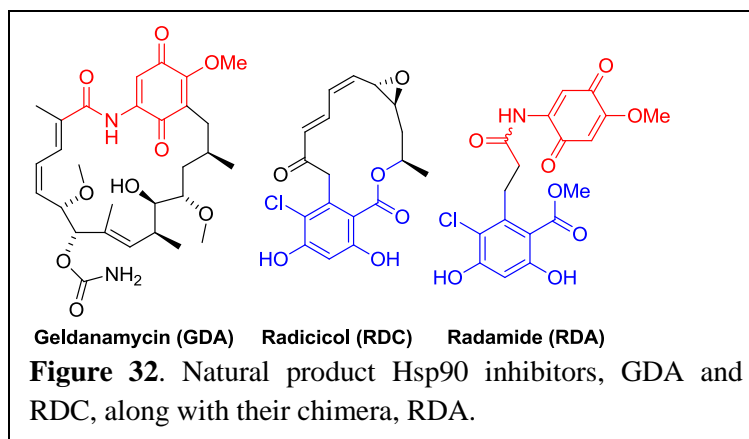
clinical inhibitors are known to target all four human isoforms; Hsp90 α , Hsp90 β , Trap1 and Grp94. Little is known about the client protein selectivity manifested by each of the four isoforms, and this gap in understanding may underlie the toxicity concerns that have arisen in clinical trials. Despite the clinical significance of Hsp90 inhibition, little investigation towards the development of isoform-selective inhibitors has been pursued to delineate isoform-dependent substrates, or as an opportunity to reduce the potential side effects that result from pan-inhibition.

Grp94 co-crystal structures have recently been determined, and demonstrate this isoform to exhibit a unique secondary binding pocket that may provide an opportunity to develop

isoform-selective inhibitors.^{14-18,54-55} Unlike TRAP-1, several substrates dependent upon Grp94 have been identified and include Toll-like receptors (TLR1, TLR2, TLR4 and TLR9), integrins (CD11a, CD18, CD49d, α 4, β 7, α L and β 2), IGF-I and -II and immunoglobulins.^{13,21,23-24,56-62} Since these clients play key roles in cell-to-cell communication and adhesion, Grp94-selective inhibitors may disrupt malignant progression by preventing metastasis, migration, immunoevasion and/or cell adhesion.^{24,56,60,62-66} Interestingly, many of these Grp94-dependent clients have also been identified as key contributors to inflammatory disorders such as rheumatoid arthritis, diabetes and asthma.^{21,24,59,67} Therefore, the ability to develop a Grp94-selective inhibitor may not only provide a new paradigm for Hsp90 inhibition, but may also provide new opportunities for the treatment of diseases other than cancer.

The biological roles manifested by Grp94 have been primarily elucidated through the use of RNAi induced Grp94 knockdown, immunoprecipitation experiments, or through pan-inhibition of all four Hsp90 isoforms. A selective small molecule inhibitor of Grp94 would provide an alternative and potentially powerful method for further elucidation of the roles manifested by Grp94, as well as the identity of other Grp94-dependent processes/substrates.

Recently, the co-crystal structures of the chimeric inhibitor, radamide (RDA), bound to the N-terminal domain of both the yeast ortholog of cytosolic Hsp90 (yHsp82N, PDB: 2FXS) and the canine ortholog of Grp94 (cGrp94N Δ 41,



PDB: 2GFD) were described.¹⁷ Utilizing a structure-based approach that relied upon these co-crystal structures, a new class of inhibitors that target Grp94 has been developed.⁶⁸

A. Design of a Grp94 Inhibitor

The design and synthesis of Grp94-selective inhibitors was carried out by Adam Duerfeldt, a former graduate student in the Blagg Laboratory, and is fully described in his doctoral dissertation.⁶⁹ Briefly, Grp94-selective inhibitors were designed using a structure-based approach with the co-crystal structures of radamide (RDA, **Figure 32**), an N-terminal chimeric

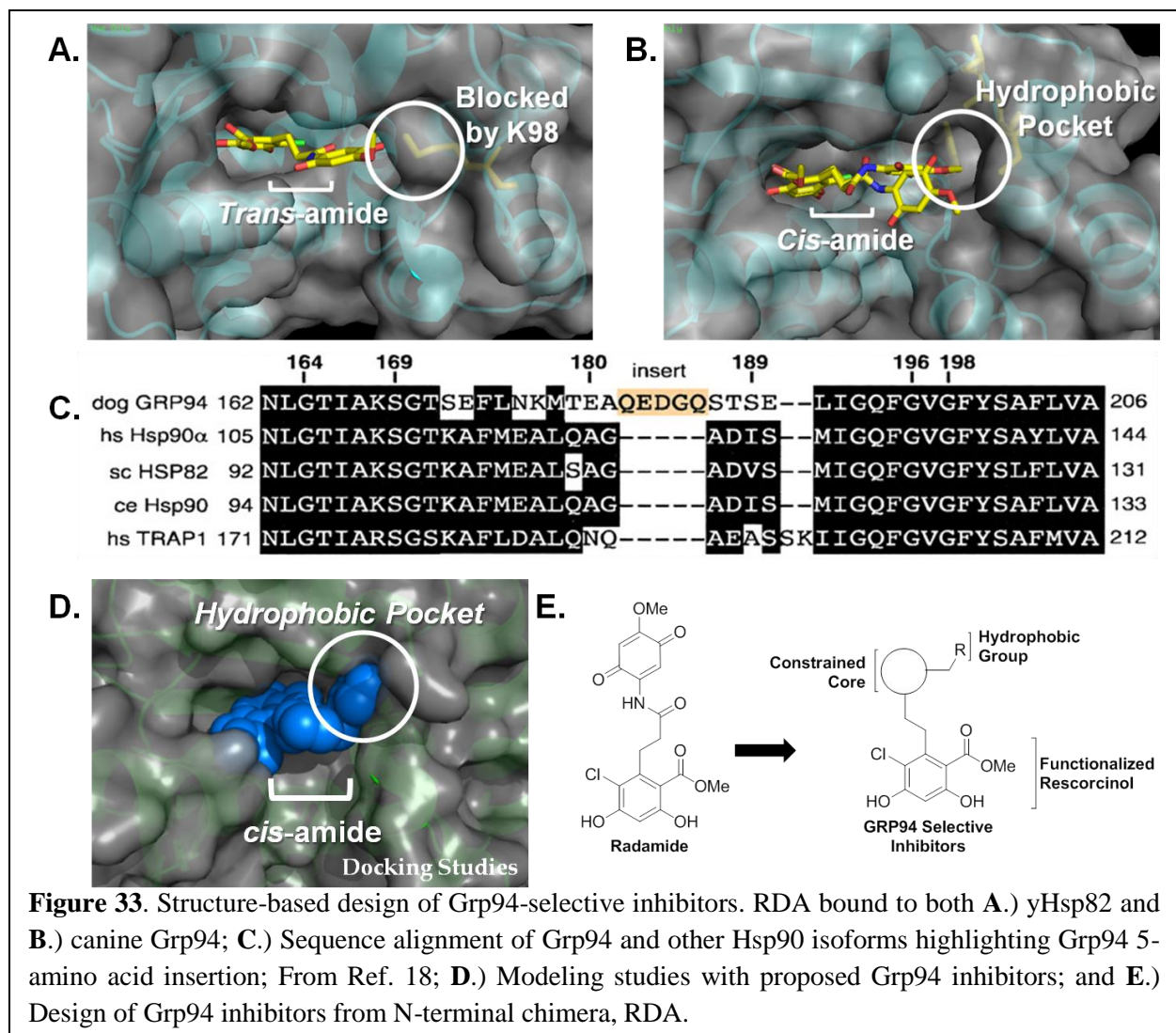
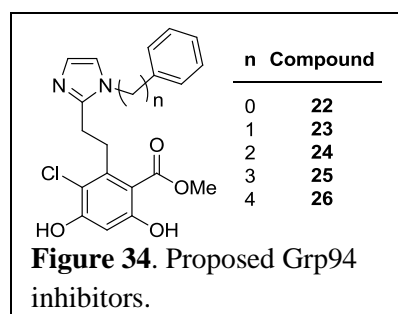


Figure 33. Structure-based design of Grp94-selective inhibitors. RDA bound to both **A.**) yHsp82 and **B.**) canine Grp94; **C.**) Sequence alignment of Grp94 and other Hsp90 isoforms highlighting Grp94 5-amino acid insertion; From Ref. 18; **D.**) Modeling studies with proposed Grp94 inhibitors; and **E.**) Design of Grp94 inhibitors from N-terminal chimera, RDA.

compound, bound to both cytosolic Hsp90 from yeast (yHsp82) and Grp94 from canine (cGrp94NΔ41).^{17,70-71} Analyses of the two co-crystal structures (**Figure 33A/B**) revealed the resorcinol ring to bind similarly in both isoforms, making a direct hydrogen bond with the conserved aspartic acid residue (Asp79 in yHsp82 and Asp149 in cGrp94NΔ41) involved in ATP binding. However, the quinone moiety was found to bind yHsp82N in a linear, trans-amide conformation, which was distinct from one conformation observed in the cGrp94NΔ41 co-crystal structure. Upon binding cGrp94NΔ41, two opposing conformations of RDA were observed (50% occupancy each): One conformation exhibited a cis-amide orientation and projected the quinone moiety into a hydrophobic pocket that exists solely in Grp94 due to a five amino acid insertion into the primary sequence (**Figure 33C**). The second conformation of RDA observed in the RDA·cGrp94NΔ41 co-crystal structure presented the amide in a trans-configuration and projected the quinone toward the outside of the binding pocket, similar to that observed for RDA in the yHsp82N co-crystal structure.²¹ Interestingly, RDA was found to exhibit an approximately 2-fold higher binding affinity for full-length Grp94 than yHsp82.

Further analyses of the RDA·yHsp82N co-crystal structure revealed the quinone to mediate an intricate hydrogen-bonding network, whereas its interaction with cGrp94NΔ41 was limited. For example, in the RDA·yHsp82N structure, direct hydrogen bonds between the RDA quinone and Lys98 and Lys44 were observed. In contrast, no direct hydrogen bonds were observed between cGrp94NΔ41 and the cis-amide quinone, suggesting that functionalities on the quinone ring may be dispensable for Grp94 binding, but obligatory for cytosolic Hsp90 binding. In addition, this Grp94 hydrophobic pocket contains aromatic amino acids (Phe199, Tyr200 and Trp223) that are likely to facilitate π -stacking interactions, and could be utilized for the design of inhibitors that exhibit increased selectivity and affinity for Grp94 over cytosolic Hsp90.

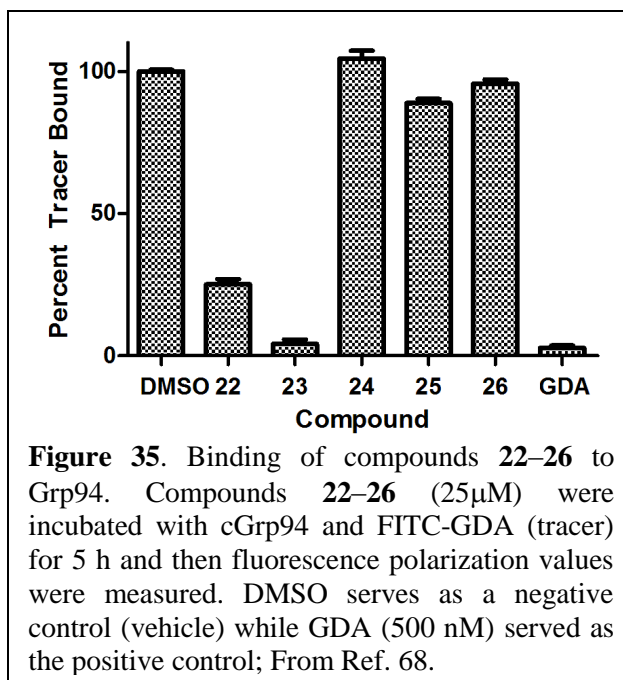
Although the primary sequences and ATP-binding pockets are highly homologous (>70% similar, 55% identical), this minor disparity was exploited for the rational design of Grp94 inhibitors.⁷² Based on these observations, inhibitors containing a more hydrophobic and aromatic surrogate of the quinone linked to the resorcinol through a cis-amide bioisostere were hypothesized to inhibit Grp94 selectively (**Figure 33D/E**). The first generation analogues



included an imidazole ring as the cis-amide isostere linked to both the resorcinol from RDA and an aryl ring, proposed to fill the aromatic-rich hydrophobic pocket, with varying linker lengths between the imidazole and benzene (**Figure 34**). Once the design and synthesis of a Grp94-selective inhibitor was achieved, an assay capable of determining Grp94 inhibitory activity was needed.

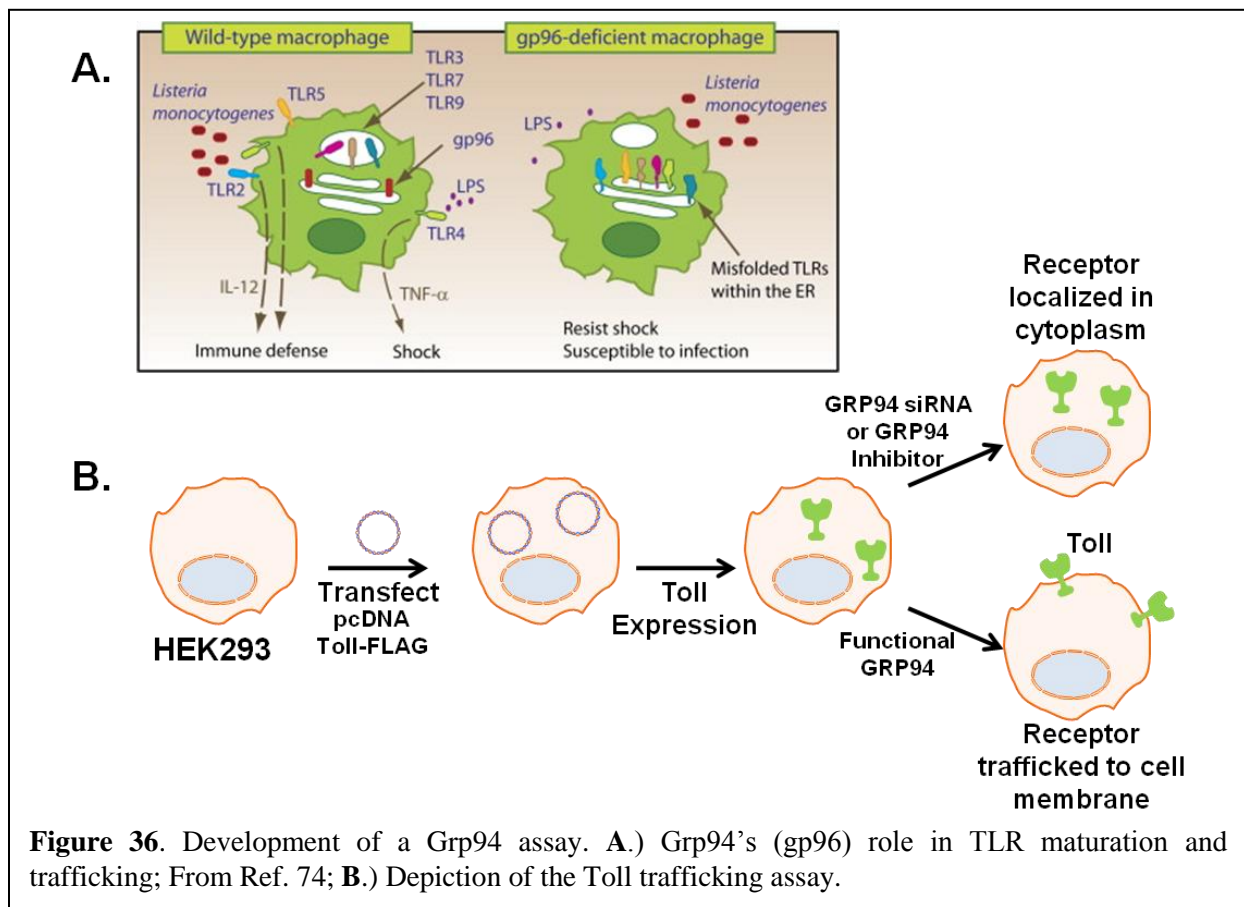
B. Development of a Grp94 Inhibitor Assay

Upon preparation of compounds 22–26, we sought to determine the ability of these compounds to bind to Grp94. Using fluorescence polarization competition assays with recombinant cGrp94 and FITC-GDA, the ability of each compound to bind Grp94 and displace FITC-GDA was determined (**Figure 35**).⁷³ As evidenced in **Figure 35**, compounds 22 and 23 were the only analogues capable of binding Grp94 and displacing FITC-GDA.

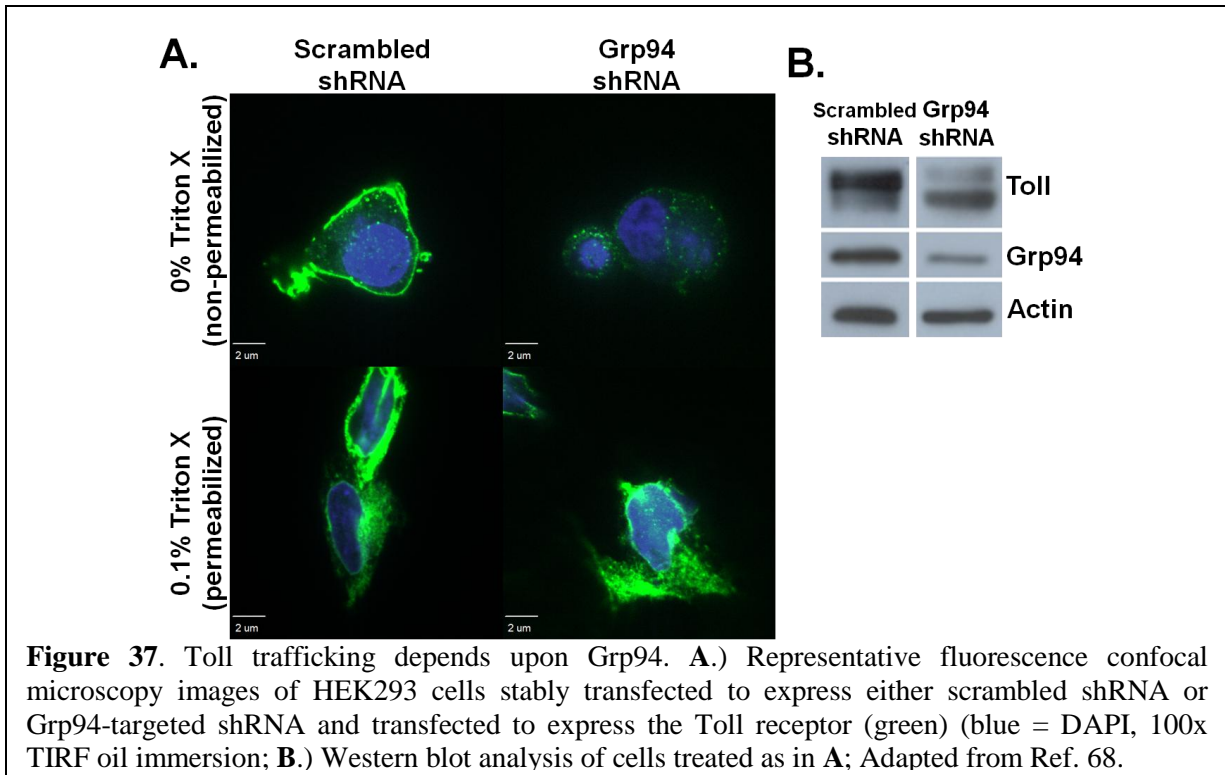


Although FP can be used to determine the ability of these compounds to bind Grp94, it has

previously been demonstrated that Hsp90 inhibitors bind preferentially to the Hsp90 heteroprotein complex.⁷⁴ Therefore, we decided to investigate these compounds further in a cell-based system.

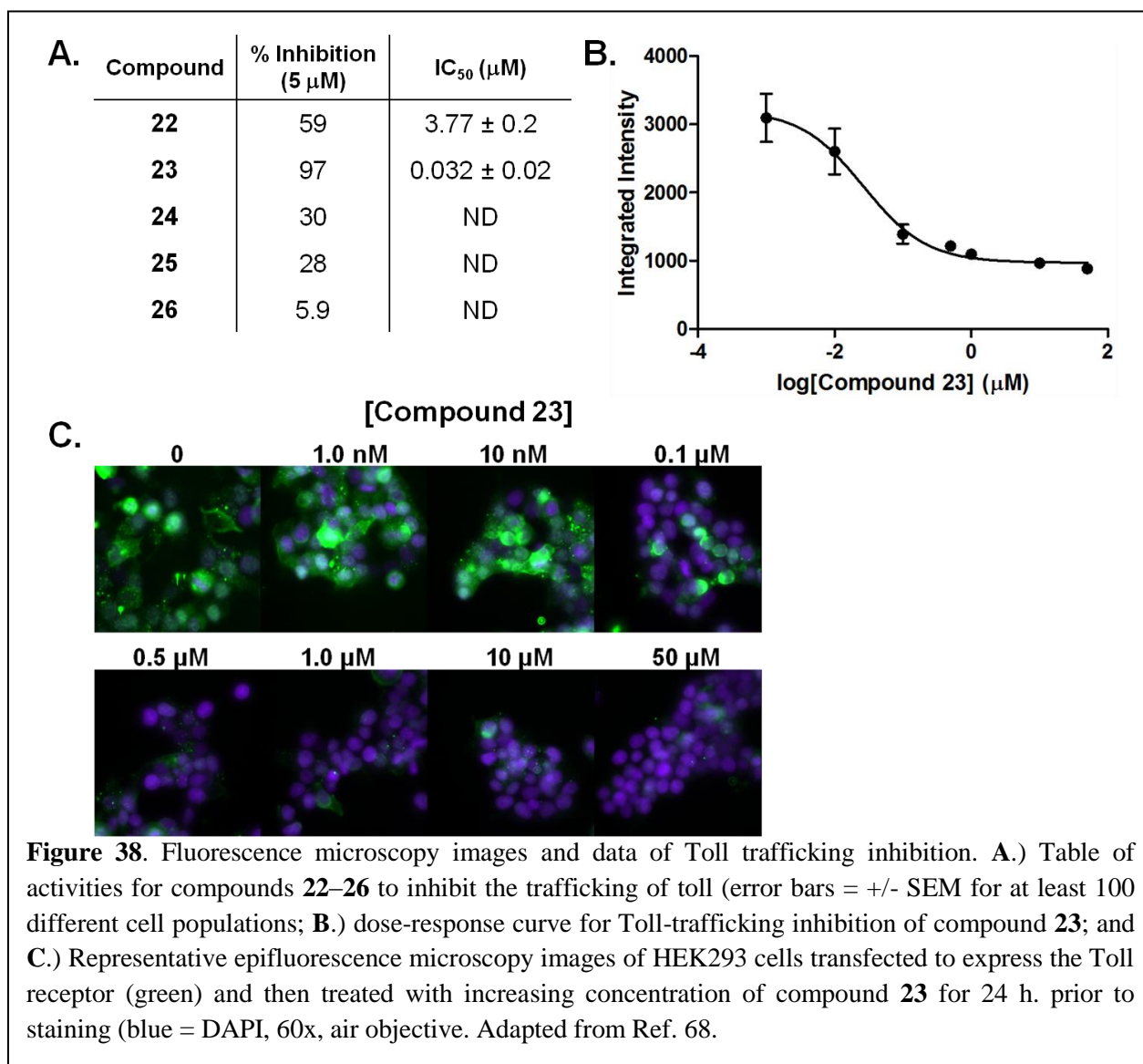


Once it was established that these compounds bind recombinant Grp94, biological studies commenced to validate our hypothesis that imidazoles containing a phenyl moiety provide Grp94 inhibition. Unlike cytosolic Hsp90 inhibitors that exhibit anti-proliferative effects, RNAi experiments have shown that in culture, cell viability is unhampered by knockdown of Grp94.²⁴ Thus, a functional assay was necessary to determine Grp94 inhibition. Grp94 is required for the functional maturation and trafficking of select TLRs.^{24,57} Non-functional Grp94 causes TLR retention in the ER. Furthermore, mice deficient in Grp94 had deficient TLR signaling and did not produce proinflammatory cytokines after treatment with TLR agonists and also could not



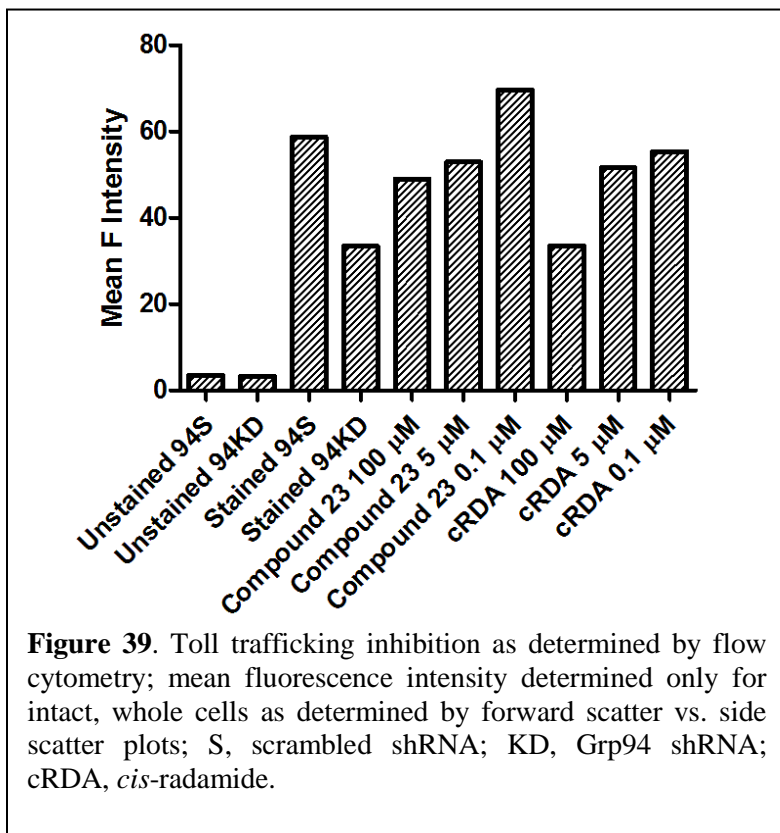
mount an immune response against *Listeria monocytogenes* infection.^{57,75} We reasoned that TLR trafficking could be used as a measure of Grp94 inhibition in *in vitro* assays and could be monitored with either fluorescence microscopy or flow cytometry following immunostaining of the extracellular TLR (**Figure 36**). HEK293 cells were stably transfected to express Grp94 directed or scrambled shRNA. Both cell lines were then transfected with a plasmid encoding expression of the Toll protein, the *Drosophila* homologue of the interleukin 1 receptor and the founding member of the TLR family. Grp94 knockdown prevented presentation of the Toll receptor at the cell surface (**Figure 37**) as indicated by immunostaining and fluorescence microscopy. In order to investigate this inhibition of trafficking, cells were permeabilized with Triton X to effect intracellular staining for Toll. Results clearly indicated that the Toll receptor was expressed in the absence of Grp94, but unable to be trafficked to the cell membrane. Western blot analyses of lysates from Grp94 knockdown cells indicated a difference in the glycosylation pattern of the Toll protein, consistent with ER-retention and providing evidence for

impaired trafficking to the cell membrane (**Figure 37**).⁷⁶⁻⁷⁹ This may indicate that Grp94 interacts with a chaperone or partner protein that is involved in the glycosylation of its clients.



Once functional knockdown of Grp94 was established, and a reduced cell surface expression of Toll observed, this assay served as readout for Grp94 inhibition. HEK293 cells were transfected with the same Toll-expressing plasmid, and subsequently exposed to compound for 24 h. prior to surface staining. The extent of surface expression was then quantified by measuring fluorescence intensity at the cell surface with Cell Profiler.⁸⁰ A dose-response curve

for each of the compounds that inhibited at least 50% of Toll trafficking at 5 μ M was generated to obtain IC₅₀ values (**Figure 38**). Representative fluorescent microscopic images and a dose-response curve are shown for the most active compound, **23**, in **Figure 38**. In parallel with fluorescence microscopy studies, flow cytometry was also used to quantify Toll surface expression. In a similar manner to fluorescence microscopy studies, HEK293 cells were transfected with the plasmid encoding Toll expression and were subsequently treated with compound for 24 h. Cells were fixed and stained for Toll surface expression using an anti-Toll antibody in conjunction with a fluorescently tagged secondary antibody (**Figure 39**). Due to a very limited dynamic range in fluorescence signal between the Grp94 deficient (94KD) and Grp94 expressing cells (94S), only 35 to 60 fluorescence units, flow cytometry was not further



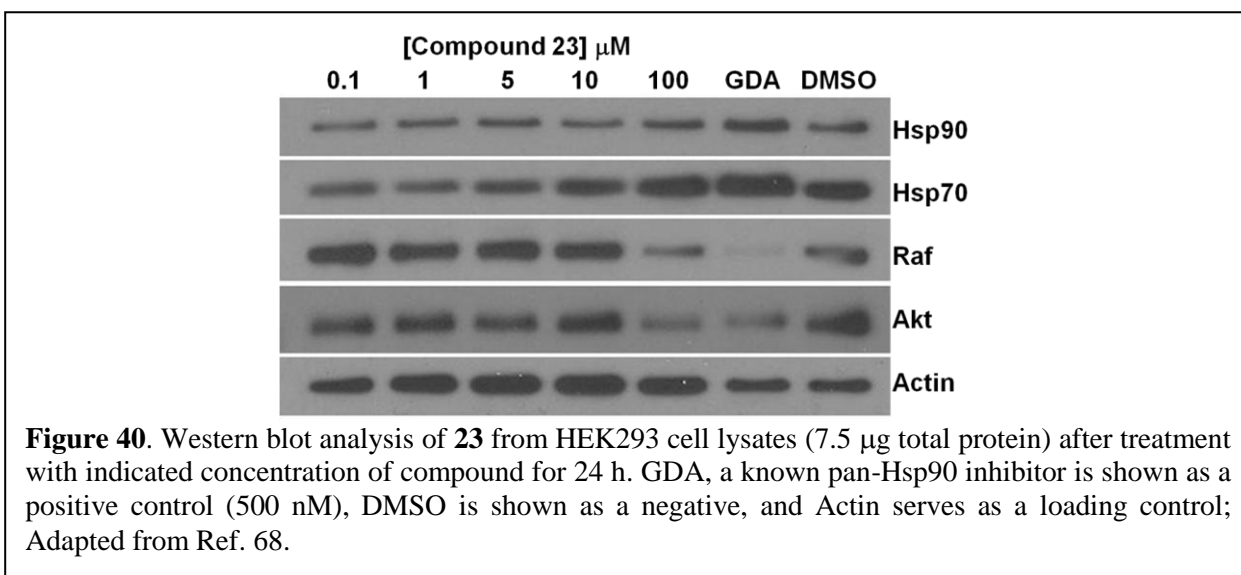
pursued as a method to quantify Toll trafficking inhibition.

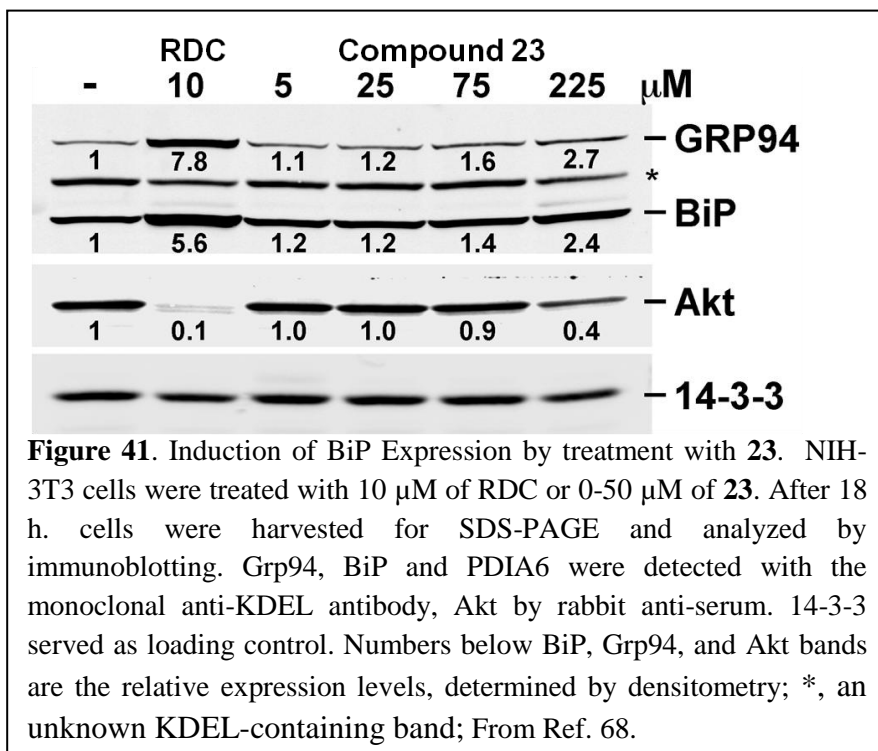
Once we established an assay to monitor Grp94 inhibition, we sought to ensure that compound **23** demonstrates selectivity for Grp94 versus cytosolic Hsp90 (Hsp90 α and Hsp90 β). The effect of compound **23** on both cell proliferation and the stability of Hsp90-obligate clients,

two well-established methods for the evaluation of Hsp90 α/β inhibitors was pursued, in addition to other Grp94-dependent processes.

C. Subsequent Biological Evaluation of a Grp94 Inhibitor

As previously mentioned, it has been shown that Grp94 is not essential for tissue culture cell viability.²³⁻²⁴ In contrast, loss of functional Hsp90 α or Hsp90 β results in cell death. Therefore, we investigated the anti-proliferative effects of compounds **22–26** against two breast cancer cells, MCF7 (ER+) and SKBR3 (Her2 overexpressing, ER-), and against the non-transformed HEK293 cells. None of the compounds evaluated manifested anti-proliferative activity at 100 μ M, indicating these compounds do not target Hsp90 α or Hsp90 β . To support these findings, western blot analyses of Hsp90 α/β client proteins were performed from HEK293 cell lysates. Prototypical pan-Hsp90 inhibitors induce proteasome-mediated degradation of Hsp90 α/β client substrates.⁸¹ As shown in **Figure 40**, compound **23** does not induce the degradation of Raf or Akt, two well-documented Hsp90 α/β -dependent client proteins until 100 μ M concentration.⁸²⁻⁸⁴ Compound **23** inhibits the presentation of the Grp94-dependent Toll

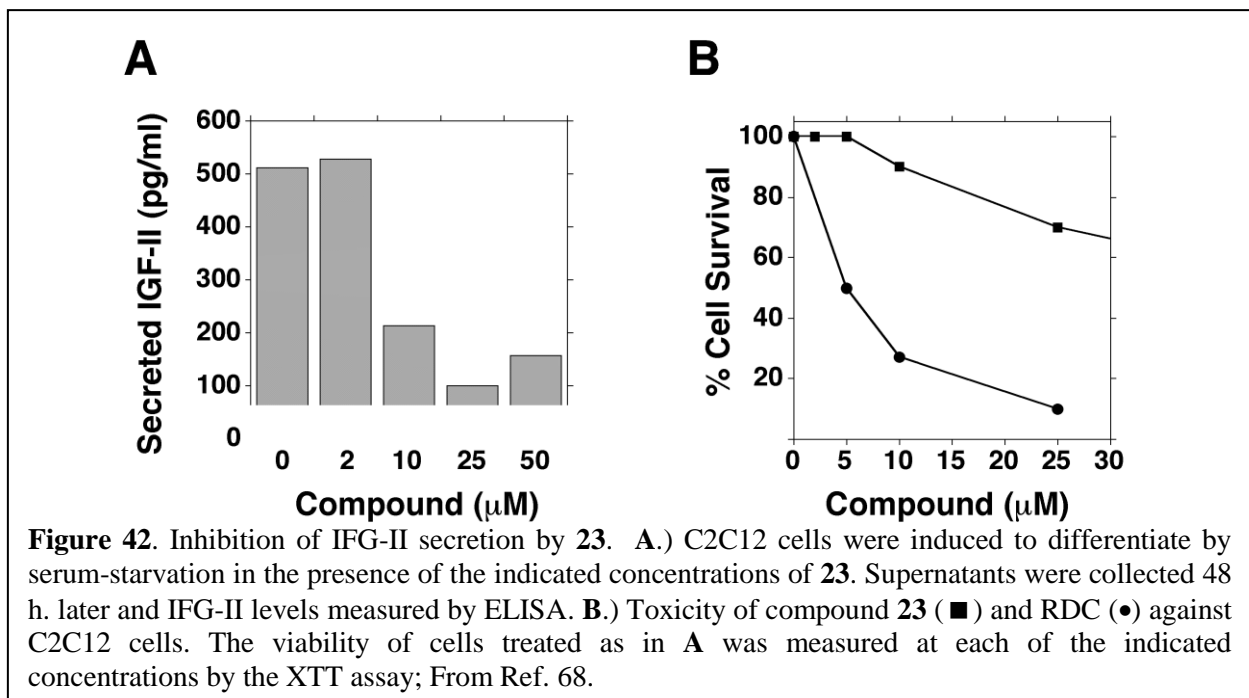




receptor at approximately 30 nM and does not affect cytoplasmic proteins until 100 μM in HEK293 cells, providing evidence for Grp94 selective inhibition. To further understand the implications of Grp94-selective inhibition, compound **23** was

analyzed in other Grp94-dependent processes.

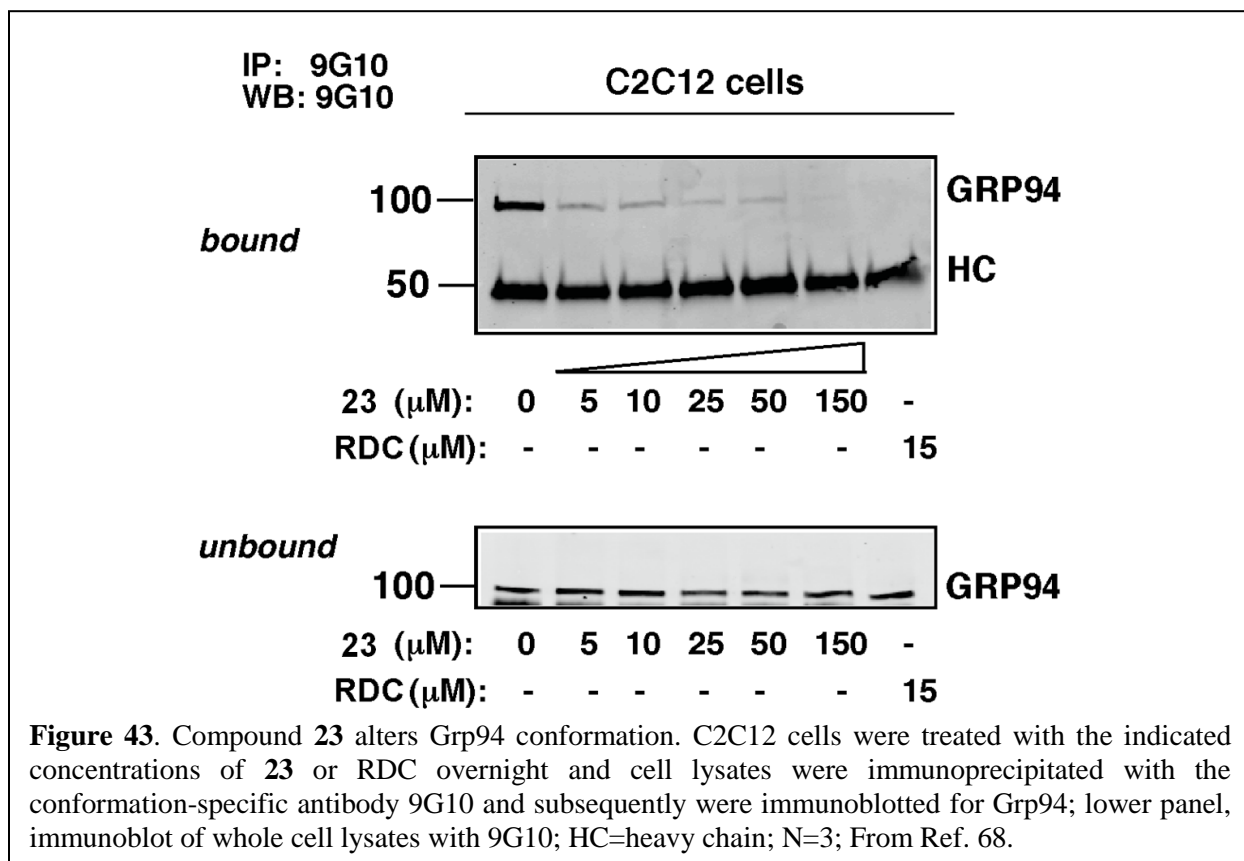
Inhibition of Hsp90 is also known to induce expression of Hsp70 and this response is useful as a diagnostic tool.⁸⁵⁻⁸⁶ A parallel response exists when Grp94 expression is ablated by RNAi, or when its activity is inhibited by Radicicol (RDC) or 17-AAG: a transcriptional response is initiated that leads to upregulation of expression of BiP, the ER member of the Hsp70 family. In collaboration with the Yair Argon Laboratory, we assessed the ability of **23** to cause BiP up-regulation, in comparison to pan-Hsp90 inhibitors. As shown in **Figure 41**, treatment of C2C12 cells with 0-75 μM of compound **23** did not lead to up-regulation of BiP, while treatments with 10μM RDC did cause BiP up-regulation. Only at concentrations above 200 μM did compound **23** resemble RDC and induce BiP expression. However, at these concentrations, the compound also destabilized Akt, a hallmark of inhibition of cytosolic Hsp90 (**Figure 41**). The inability of **23** to upregulate BiP at the 0-75 μM concentration range was surprising, because



this transcriptional response has previously been shown to be a property of Grp94 ablation and not Hsp90.

IGF-II is a second well-defined Grp94-dependent client protein and active Grp94 is required for the secretion of IGF-II.⁶¹ It has been previously demonstrated that pan-Hsp90 inhibitors, such as 17-AAG, prevent the secretion of IGF-II in serum-starved C2C12 myoblast cells.^{23,61-62} Also performed by the Argon Laboratory, serum-starved C2C12 cells were treated with increasing concentrations of compound **23** and the secretion of IGF-II was measured by ELISA (**Figure 42A**). Approximately 60% reduction of IGF-II was observed at 10 μM of **23**, while little effect on cell viability was observed (**Figure 42B**). The effect on IGF-II secretion is consistent with previous observations using pan-Hsp90 inhibitors, while the lack of effect on cell viability by **23** indicates that this compound is working through a Grp94-dependent mechanism and does not exhibit pan-inhibition.

Prior studies have shown that occupation of the Grp94 N-terminal ATP binding pocket by inhibitors results in an altered conformation of this domain.⁸⁷⁻⁸⁸ Anti-Grp94 (9G10) is an



antibody that recognizes the acidic region (residues 290–350) in the second domain of Grp94.⁸⁹ Occupation of the ATP binding site causes a conformational switch in this region and prevents the 9G10 antibody from recognizing Grp94.⁸⁸ Therefore, lysates of C2C12 cells treated with increasing concentrations of compound **23** were immunoprecipitated to assess whether it induces a conformational switch in Grp94. As observed in **Figure 43**, compound **23** induces a conformational switch in Grp94, as the 9G10 antibody is unable to recognize and immunoprecipitate the Grp94 in cells treated with **23**. This result parallels the IGF-II secretion data shown in **Figure 42**, suggesting that an alteration in Grp94 conformation is incompatible with IGF-II secretion. Interestingly, this activity of Grp94 inhibitors appears to be cell-specific,

as analogous experiments performed in CHO cells failed to show an effect on the conformation of Grp94 (data not shown).

Previous studies have demonstrated that Gp93, the *Drosophila* ortholog of Grp94 is an essential gene.⁵⁸ In the *Drosophila* model, maternal Gp93 is sufficient to support embryogenesis in Gp93 homozygous null embryos. In the absence of zygotic expression of Gp93, however, larvae display a pronounced growth defect, commensurate with disrupted gut epithelial morphology, decreased gut nutrient uptake, and marked aberrations in copper cell structure and function. As a consequence, loss of Gp93 expression is larval lethal in *Drosophila*. In collaboration with the Chris Nicchitta Laboratory, the effects of compound **23** on *Drosophila* larval growth were determined. First instar wild type (w1118) larvae were placed onto fly food supplemented with either no supplement (A), 0.1% (B), 0.3% (C), or 0.5% (D) DMSO (vehicle



Figure 44. Effect of compound **23** on *Drosophila* larval growth; From Ref. 68.

controls) or fly food supplemented with 250 $\mu\text{g/ml}$ (E), 500 $\mu\text{g/ml}$ (F), 750 $\mu\text{g/ml}$ (G) or 1 mg/ml (H) compound **23**. As is evident from the micrographs of representative larvae, dietary uptake of **23** was associated with a dramatic growth phenotype (**Figure 44**). In parallel experiments, larval gut tissue was obtained from each of the feeding conditions and gut epithelial morphology evaluated by fluorescence microscopy. No grossly discernible effects on copper cell structure were observed, indicating that under these feeding conditions, the inhibition of Grp93 function was incomplete (data not shown). Pharmacokinetic studies of compound absorption and metabolism may provide additional insights into this partial phenotypic behavior.

D. Summary of and Implications for Grp94 Inhibition

Hsp90 inhibitors have been the subject of intense pharmaceutical research, not only for cancer, but also neurodegeneration.⁹⁰⁻⁹⁸ All Hsp90 inhibitors that have reached clinical trials bind to the Hsp90 N-terminal ATP-binding pocket and demonstrate pan-Hsp90 inhibition, i.e. they inhibit all human Hsp90 isoforms simultaneously.^{51-52,99} Toxicities and off-target effects resulting from Hsp90 inhibition may be a consequence of pan-inhibition. Therefore, the design of Hsp90 isoform-selective inhibitors may provide a valuable pharmacological tool to dissect the roles of each isoform and may lead to more clinically useful inhibitors.

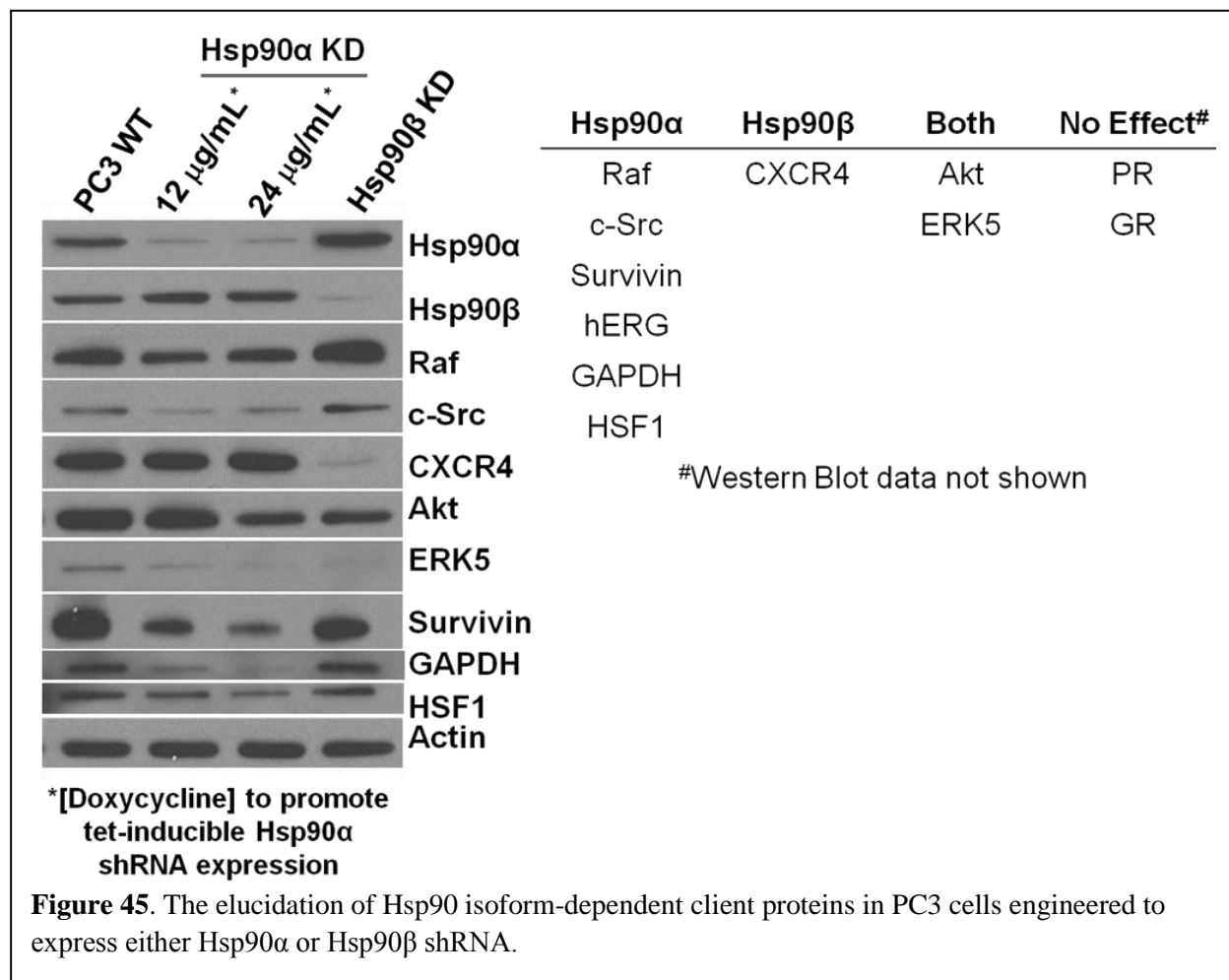
Comparing the crystal structures of several known Hsp90 inhibitors bound to either cytosolic Hsp90 or to the ER-resident Grp94 provided a rational design platform for the development of Grp94 inhibitors. Using structure-based drug design, five compounds were identified as potential leads that contain a phenyl ring appended to an imidazole ring, which serves as a *cis*-amide bioisostere. The predisposed orientation of the phenyl ring was postulated to allow interactions with the unique Grp94 π -rich pocket. Since Grp94 has previously been shown to be responsible for the trafficking of TLRs to the cell membrane,⁵⁷ this activity was

used as a functional assay for Grp94 inhibition. Of the five compounds evaluated, compound **23** manifested the best activity in this assay (35 nM). In subsequent, direct readout assays, including an in-cell conformational assay, compound **23** affected Grp94 itself at the same concentration as that needed to inhibit chaperone activity.

Once the Grp94 inhibitory activity of compound **23** was established by these parameters, we evaluated the isoform selectivity of the compound. Inhibitors of cytosolic Hsp90 (Hsp90 α/β) manifest antiproliferative activity in cell culture. At concentrations wherein the assays observed activity for compound **23**, there were no cytotoxic effects against any cell line tested. In addition, compound **23** exhibited no effect on the prototypical Hsp90 α/β client kinases, Akt or Raf, until concentrations 100x greater than the IC₅₀ for Grp94 inhibition. Therefore, compound **23** appears to manifest considerable selectivity for Grp94 versus Hsp90 α/β , perhaps explaining its low toxicity. Lastly, compound **23** stunted the growth of *Drosophila* larvae in a dose-dependent manner, suggesting that it may be a useful Grp4 inhibitor in vivo. Future studies with **23** will help dissect the roles played by Grp94 and will shed light into the validity of Grp94 as a therapeutic target.

IV. Conclusions and Future Work

Delineating the roles manifested by each Hsp90 isoform and the identification of isoform-selective Hsp90 inhibitors have become major themes of research for the Blagg Laboratory. Throughout the work described above, we have been able to elucidate the Hsp90 isoform-dependency of the hERG subunit of the K⁺ channel. Namely, hERG relies on Hsp90 α , and not Hsp90 β or Grp94, for its maturation and functional trafficking. This finding provides rationale for the development of Hsp90 inhibitors that do not target Hsp90 α . In addition, it is one of the first examples demonstrating the single isoform dependency of an Hsp90 client protein. In



addition, we have been able to identify a rationally designed Grp94 inhibitor, namely compound **23**. This compound not only will aid in the elucidation of Grp94-dependent processes, but it will also provide an avenue to explore Grp94 as a therapeutic target. Overall, these contributions highlight the necessity to fully understand the individual roles of each Hsp90 isoform.

The identification of subsequent isoform-dependent client proteins is underway. The prostate cancer cell line, PC3, has been engineered to express either Hsp90α or Hsp90β shRNA. Using these cell lines, it is possible to determine the isoform dependency of other Hsp90 client proteins (**Figure 45**). It is evident that several proteins are degraded in the absence of Hsp90α, i.e. Raf, c-Src, Survivin, hERG, GAPDH, and HSF1. However, CXCR4 appears to depend upon Hsp90β, as it is degraded upon Hsp90β depletion. The same dependencies of both ERK5 and c-

Srv (v-Src) were observed in a yeast-based system in which the endogenous yeast Hsp90s had been replaced with either hHsp90 α or hHsp90 β as the sole Hsp90 present.¹² Subsequent studies are underway to expand the list of known isoform-dependent client proteins. 2-Dimensional difference gel electrophoresis (2D-DIGE) is underway in the George Vielhauer Laboratory at The University of Kansas Medical Center using this same PC3-based system. In addition, stable isotope labeling by amino acids in cell culture (SILAC) is currently in progress wherein the wild type, Hsp90 α - and Hsp90 β -deficient cell lines were differentially labeled with stable isotope combinations of lysine and arginine.¹⁰⁰ Effects over the entire Hsp90-ome will subsequently be identified using mass spectrometry and bioinformatic techniques. Together, these powerful experimental methods will provide a comprehensive list of Hsp90 isoform-dependent clients, providing insights into the clinical relevance of inhibiting each Hsp90 isoform as well as delineating the toxicities observed with *pan*-Hsp90 inhibition.

V. Materials and Methods

A. The hERG Channel is Dependent upon the Hsp90 α Isoform for Maturation and Trafficking

Antibodies. The following antibodies were used for Western Blotting and/or co-immunoprecipitation: rabbit anti-Hsp90 α (Neomarkers), goat anti-Hsp90 β (SantaCruz), goat anti-hERG (SantaCruz), rabbit anti-Grp94 (SantaCruz) and rabbit anti-Actin (SantaCruz).

Cell Lines. The HEK-hERG¹⁰¹ (HEK 293 stably transfected with human hERG WT) cell line was a kind gift from Eckhard Ficker (MetroHealth Medical Center/Case Western Reserve University). The HEK-hERG cell line was maintained in DMEM supplemented with 10% FBS, streptomycin, penicillin, and geneticin at 37°C, 5% CO₂. Inducible knockdown of Hsp90 α or Hsp90 β in the HEK-hERG cell line was accomplished using a tetracycline inducible shRNA

construct containing a hairpin sequence specific for either the Hsp90 α or Hsp90 β isoform. These constructs were made by subcloning the isoform specific hairpin sequences from pGIPZ vectors (Open Biosystems, Lafayette, CO) into pTRIPZ vectors using MluI and XhoI restriction sites. The mature shRNA sequences were 5'-AGGAAGAATTTGGTCAAAA-3' and 5'-ACTAAGAAGATCAAAGAGA-3' for Hsp90 α and Hsp90 β , respectively. Resulting clones were sequenced verified using pTRIPZ sequencing primers 5'-GGAAAGAATCAAGGAGG-3'. The resulting pTRIPZ plasmids containing Hsp90 isoform specific shRNA were packaged into third generation lentivirus particles. Cells were cultured as above but with the addition of 2.5 μ g/mL puromycin to select for stable, transduced cells. Induction of shRNA expression with tetracycline dose was monitored by the increase in TurboRFP fluorescence which is driven by the tetracycline response element (TRE). shRNA expression was induced with the addition of 1-24 μ g/mL doxycycline.

siRNA and Transfection. Cells were plated in 24-well plates at 9.0×10^5 cells/mL (0.5 mL/well) in antibiotic free DMEM supplemented with 10% FBS. After 24 h., media was replaced with 0.2 mL OptiMEM (Invitrogen) and transfected with 43 μ L of transfection mix containing 50 pmol siRNA and 2 μ L oligofectamine (Invitrogen). Proteins were harvested 48 h. post transfection. Hsp90 α siRNA was purchased from Ambion while Hsp90 β siRNA was from SantaCruz Biotechnology.

Western Blot Analysis. The various HEK cells were harvested in cold PBS and lysed in mammalian protein extraction reagent (MPER, Pierce) lysis buffer containing protease inhibitors (Roche) on ice for 1 h. Lysates were clarified at 14,000g for 10 min at 4 $^{\circ}$ C. Protein concentrations were determined using the Pierce BCA protein assay kit per the manufacturer's instructions. Equal amounts of protein (2.5-10 μ g) were electrophoresed under reducing

conditions (6.5% acrylamide gel), transferred to a polyvinylidene fluoride membrane (PVDF), and immunoblotted with the corresponding specific antibodies. Membranes were incubated with an appropriate horseradish peroxidase-labeled secondary antibody, developed with a chemiluminescent substrate, and visualized.

Immunoprecipitation. Using a method analogous to Ficker *et al.*³⁷ and Nanduri *et al.*³⁸, cells were plated in 10 cm cell culture dishes and allowed to grow to 80% confluency. Cells were then washed once with phosphate-buffered saline (PBS) and then crosslinked by incubation with 1.5 mM dithiobis(succinimidyl propionate, DSP, Pierce) in PBS for 15 min at room temperature. DSP was quenched by the addition of pH 7.5 Tris (final concentration 10 mM). Cells in PBS/DSP/Tris were scraped into conical tubes, pelleted, and washed with PBS. Cells were harvested in lysis buffer containing 0.1% NP40, 50 mM Tris (pH 7.5), 150 mM NaCl, 20 mM MoO₄, and protease inhibitors (Roche). Lysates were clarified and protein concentration was determined using BCA assay. For co-immunoprecipitation, 300 µg total protein was diluted to 500 µL total volume in lysis buffer and incubated with 2µg of either anti-hERG, anti-Hsp90α or anti-Hsp90β antibody overnight at 4°C with rocking. Immunocomplexes were captured with 35 µL of DynaBeads Protein G (Invitrogen) for 2 h. with rocking at 4°C. Protein G Bead-complexes were washed three times with lysis buffer and eluted with sample buffer. Samples were then boiled and subjected to SDS-PAGE and Western Blot analysis.

Tryptic Digest and Mass Spectrometry. Lysates were co-immunoprecipitated as above except with 1 mg total protein, 6 µg anti-hERG antibody, and 100 µL DynaBeads Protein G in 1.5 mL total volume. After wash steps, samples were boiled and subjected to SDS-PAGE. Acrylamide gels were stained, bands excised, destained and washed using the Silver Stain Kit for Mass Spectrometry (Pierce). Excised bands were further washed (0.2 M NH₄HCO₃, 50% acetonitrile)

and then dried. Gel pieces were suspended in 0.2 M NH_4HCO_3 and 10 mM DTT (final concentration) was added and heated at 60°C for 15 mins. 20 mM iodoacetamide (final concentration) was then added and gel bands incubated for 30 mins at 25°C in the dark. Gel bands were then washed (0.2 M NH_4HCO_3 , 50% acetonitrile), shrunk in 100% acetonitrile, and dried. Gel bands were re-swelled in 0.2 M NH_4HCO_3 containing 0.5 μg trypsin and 0.2 M NH_4HCO_3 with 10% acetonitrile was added to keep gel pieces submerged. Digest was terminated after 16 h. of incubation at 37°C by the addition of 0.1% trifluoroacetic acid (final concentration). Supernatants were then subjected to LC-MS/MS at the University of Kansas Analytical Proteomics Lab. Results were analyzed using Scaffold software which integrates results from Mascot, Sequest and X!Tandem search engines.

Densitometry and Statistical Analysis. Western Blot films were digitally captured using a standard flatbed scanner (HP). The digital blots were then converted to 16-bit black and white images using ImageJ software. Densitometric measurements were then performed in ImageJ using the “Gels” tool. Peak areas were used as a measure of protein levels. Statistical analysis was performed using GraphPad Prism5, statistical significance was determined using a paired, two-tailed t-test.

B. Development of Grp94 Selective Inhibitors and Assays to Evaluate Grp94-inhibitory Activity

Cell Culture. HEK293 cells were maintained in DMEM supplemented with non-essential amino acids, L-glutamine (2 mM), streptomycin (500 $\mu\text{g}/\text{mL}$), penicillin (100 units/mL), and 10% FBS. Cells were grown to confluence in a humidified atmosphere (37 °C, 5% CO_2). Stable Grp94-siRNA knockdown cell lines were generated as follows: the shRNA sequence 5'-GGCUCAAGGACAGAUGAUGtt-3' was cloned into the A pSilencer 2.0-U6 vector (Ambion)

and positive clones confirmed by sequencing. The pSilencer 2.0-U6-GRP94 siRNA vector and a control, non-targeting pSilencer 2.0-U6 siRNA vector (scrambled, control) were transfected into HEK293 cells using Lipofectamine 2000 and the manufacturers protocol. Cell cultures were selected thirty six hours post-transfection by addition of 1 $\mu\text{g}/\text{mL}$ puromycin to the media. Puromycin resistant clones (both Grp94 siRNA and non-targeting siRNA) were subsequently expanded and screened for knockdown efficiency by immunoblotting, using Grp94 antibody DU120. Clones displaying greater than 90% knockdown were selected. Puromycin-resistant clones from the non-targeting siRNA were obtained in parallel and screened for normal Grp94 expression, also by immunoblotting with DU120.

Fluorescence Polarization. Assay buffer (25 μL , 20 mM HEPES pH 7.3, 50 mM KCl, 5 mM MgCl_2 , 1 mM DTT, 20 mM Na_2MoO_4 , 0.01% NP-40, and 0.5 mg/mL BSA) containing compounds **22–26** or GDA were plated in 96-well plates (black well, black bottom) to provide final concentrations of 25 μM or 500 nM, re-spectively (1% final DMSO concentration).⁷³ Recombinant cGrp94 and FITC-GDA were then added (50 μL and 25 μL) to give final concentrations of 60 nM and 5 nM, respectively. Plates were incubated with rocking for 5 h at 4 $^\circ\text{C}$. Fluorescence polarization values were then read using excitation and emission filters of 485 nm and 528 nm, respectively. Percent FITC-GDA bound was determined by using the DMSO millipolarization unit (mP) as the 100% bound value and the mP value of free FITC-GDA as the 0% bound value.

Toll-Trafficking Assay – Fluorescence Microscopy. HEK293 cells were plated in 6-well cell culture treated plates in Dulbecco's Modified Eagle Medium (1x DMEM) supplemented with 10% fetal bovine serum containing no antibiotics and were maintained at 37 $^\circ\text{C}$, 5% CO_2 , and 95% relative humidity. After 24 h, the cells (95% confluence) were transfected with pcDNA6B-

Toll-Flag using Lipofectamine2000 according the manufacturer's instructions. Cells were transfected for 16 h, then were trypsinized and plated in 96-well microscopy-quality, black walled plates that had been pre-treated with attachment factor. After 3 h. incubation at 37 °C to allow the cells to attach, compound at varying concentrations in DMSO (1% DMSO final concentration) was added and cells were returned to incubator for 24 h. After 24 h, the media was removed and cells were fixed in freshly made 4% paraformaldehyde in Dulbecco's Phosphate Buffered Saline (DPBS) for 10 min at 25 °C. Cells were washed twice with DPBS then stained with Wheat Germ Agglutinin-Texas Red (5 µg/mL in DPBS, 60 min, 25°C). Cells were washed twice with DPBS, blocked in 5% bovine serum albumin (BSA, 10 min, 25 °C) followed by staining for 16 h with an anti-Toll antibody (1:200 in 5%BSA/DPBS, 4°C, Santa Cruz, sc-33741). Cells were washed twice with DPBS and stained with an anti-rabbit-AlexaFluor488 antibody (1:300 in DPBS, 25 °C, Invitrogen, A-11008) for 3 h at 25 °C. Cells were then washed twice with DPBS after which DAPI was added (1 µM in DPBS). Cells were imaged using an inverted Olympus IX-81 microscope with a 60X long working distance air objective using appropriate filter sets for the various tags (AlexaFluor488, Texas Red, DAPI). Images were processed using SlideBook5.0 and analyzed using CellProfiler and CellProfiler Analyst.

Flow Cytometry. HEK293 cells were plated in 6-well plates and transfected as described above in Toll-Trafficking Assay. For drug treated cells, 18 h post transfection, fresh media was added (5 mL) and cells were dosed in the 6-well plate with compound in DMSO (1% DMSO final concentration). Cells were incubated with compound for 24 h at 37 °C. To collect the cells, media was aspirated and cells were scraped into 1 mL of cold PBS. Wells were washed with an additional 1 mL cold PBS and combined with corresponding cells. Cells were centrifuged at

1000 rpm for 5 min. at 4°C and PBS was removed. All washing and staining steps performed at 4 °C, while all centrifugation steps performed at 1000 rpm for 5 min at 4 °C. Cells were fixed with 4% paraformaldehyde in PBS at 4 °C for 30 min. Cells were then washed twice with wash buffer (WB 0.5% BSA in PBS) followed by three washes with blocking buffer (BB, 1% FBS and 0.5% BSA in PBS) for 5 min at 4 °C each. Cells were then stained with an anti-Toll antibody (100 µL of 5.0 µg/mL in BB) for 40 min at 25 °C. Cells were washed twice with BB and were stained with an AlexaFluor488-conjugated secondary antibody (100 µL of 5.0 µg/mL in BB) for 40 min at 25 °C in the dark. Cells were washed twice with WB, suspended in 1 mL of WB, passed through a mesh strainer to obtain a homogenous cell solution and analyzed by flow cytometry.

Western Blotting. HEK293 cells were plated in 6-well plates and treated with various concentrations of drug, GDA in DMSO (1% DMSO final concentration), or vehicle (DMSO) for 24 h. Cells were harvested in cold PBS and lysed in mammalian protein extraction reagent (MPER, Pierce) and protease inhibitors (Roche) on ice for 1 h. Lysates were clarified at 14,000 g for 10 min at 4 °C. Protein concentrations were determined with the Pierce BCA assay kit per the manufacturer's instructions. Equal amounts of protein were electrophoresed under reducing conditions, transferred to a PVDF membrane, and immunoblotted with the corresponding specific antibodies. Membranes were incubated with an appropriate horseradish peroxidase-labeled secondary anti-body, developed with chemiluminescent substrate, and visualized.

Grp94 Immunoprecipitation. Detergent lysates of the indicated cells were immunoprecipitated with 9G10 monoclonal anti-Grp94 (StressGen, Vancouver, BC) followed by protein G-Sepharose (Sigma Chemicals or Pierce) as described in Ref. 102.

VI. References

1. Chen, B.; Piel, W. H.; Gui, L.; Bruford, E.; Monteiro, A. The HSP90 family of genes in the human genome: Insights into their divergence and evolution. *Genomics* **2005**, *86*, 627-637.
2. Johnson, J. L. Evolution and function of diverse Hsp90 homologs and cochaperone proteins. *BBA - Mol. Cell Res.* **2012**, *1823*, 607-613.
3. Picard, D. <http://www.picard.ch/downloads/Hsp90interactors.pdf>.
4. Picard, D. <http://www.picard.ch/downloads/Hsp90facts.pdf>.
5. Didelot, C.; Lanneau, D.; Brunet, M.; Bouchot, A.; Cartier, J.; Jacquelin, A.; Ducoroy, P.; Cathelin, S.; Decolonne, N.; Chiosis, G.; Dubrez-Daloz, L.; Solary, E.; Garrido, C. Interaction of heat-shock protein 90 β isoform (HSP90 β) with cellular inhibitor of apoptosis 1 (c-IAP1) is required for cell differentiation. *Cell Death. Differ.* **2008**, *15*, 859-866.
6. Houlihan, J. L.; Metzler, J. J.; Blum, J. S. HSP90 α and HSP90 β Isoforms Selectively Modulate MHC Class II Antigen Presentation in B Cells. *J. Immunol.* **2009**, *182*, 7451-7458.
7. Kunisawa, J.; Shastri, N. Hsp90 α Chaperones Large C-Terminally Extended Proteolytic Intermediates in the MHC Class I Antigen Processing Pathway. *Immunity* **2006**, *24*, 523-534.
8. Voss, A. K.; Thomas, T.; Gruss, P. Mice lacking HSP90 β fail to develop a placental labyrinth. *Development* **2000**, *127*, 1-11.
9. Eustace, B. K.; Sakurai, T.; Stewart, J. K.; Yimlamai, D.; Unger, C.; Zehetmeier, C.; Lain, B.; Torella, C.; Henning, S. W.; Beste, G.; Scroggins, B. T.; Neckers, L.; Ilag, L. L.; Jay, D. G. Functional proteomic screens reveal an essential extracellular role for hsp90 α in cancer cell invasiveness. *Nat. Cell Biol.* **2004**, *6*, 507-514.
10. Chadli, A.; Felts, S. J.; Toft, D. O. GCUNC45 is the first Hsp90 co-chaperone to show α/β isoform specificity *J. Biol. Chem.* **2008**, *283*, 9509-9512.
11. Millson, S. H.; Prodromou, C.; Piper, P. W. A simple yeast-based system for analyzing inhibitor resistance in the human cancer drug targets Hsp90 α/β . *Biochem. Pharmacol.* **2010**, *79*, 1581-1588.
12. Millson, S. H.; Truman, A. W.; Rácz, A.; Hu, B.; Panaretou, B.; Nuttall, J.; Mollapour, M.; Söti, C.; Piper, P. W. Expressed as the sole Hsp90 of yeast, the α and β isoforms of human Hsp90 differ with regard to their capacities for activation of certain client proteins, whereas only Hsp90 β generates sensitivity to the Hsp90 inhibitor radicicol. *FEBS J.* **2007**, *274*, 4453-4463.
13. Marzec, M.; Eletto, D.; Argon, Y. GRP94: An HSP90-like protein specialized for protein folding and quality control in the endoplasmic reticulum. *BBA - Mol. Cell Res.* **2012**, *1823*, 774-787.
14. Dollins, D. E.; Immormino, R. M.; Gewirth, D. T. Structure of unliganded GRP94, the ER Hsp90: Basis for nucleotide-induced conformational change. *J. Biol. Chem.* **2005**, *280*, 30438-30447.
15. Dollins, D. E.; Warren, J. J.; Immormino, R. M.; Gewirth, D. T. Structures of GRP94-nucleotide complexes reveal mechanistic differences between the hsp90 chaperones. *Mol. Cell* **2007**, *28*, 41-56.
16. Immormino, R. M.; Dollins, D. E.; Shaffer, P. L.; Soldano, K. L.; Walker, M. A.; Gewirth, D. T. Ligand-induced conformational shift in the N-terminal domain of GRP94, an Hsp90 chaperone. *J. Biol. Chem.* **2004**, *279*, 46162-46171.
17. Immormino, R. M.; Metzger Iv, L. E.; Reardon, P. N.; Dollins, D. E.; Blagg, B. S. J.; Gewirth, D. T. Different Poses for Ligand and Chaperone in Inhibitor-Bound Hsp90 and GRP94: Implications for Paralog-Specific Drug Design. *J. Mol. Biol.* **2009**, *388*, 1033-1042.
18. Soldano, K. L.; Jivan, A.; Nicchitta, C. V.; Gewirth, D. T. Structure of the N-terminal domain of GRP94. Basis for ligand specificity and regulation. *J. Biol. Chem.* **2003**, *278*, 48330-48338.
19. van der Vlies, D.; Makkinje, M.; Jansens, A.; Braakman, I.; Verkleij, A. J.; Wirtz, K. W.; Post, J. A. Oxidation of ER resident proteins upon oxidative stress: effects of altering cellular redox/antioxidant status and implications for protein maturation. *Antioxid. Redox. Signal.* **2003**, *5*, 381-387.
20. Van, P. N.; Peter, F.; Söling, H. D. Four intracisternal calcium-binding glycoproteins from rat liver microsomes with high affinity for calcium. No indication for calsequestrin-like proteins in

- inositol 1,4,5-trisphosphate-sensitive calcium sequestering rat liver vesicles. *J. Biol. Chem.* **1989**, *264*, 17494-17501.
21. McLaughlin, M.; Vandenbroeck, K. The endoplasmic reticulum protein folding factory and its chaperones: new targets for drug discovery? *Brit. J. Pharmacol.* **2011**, *162*, 328-345.
 22. Luo, B.; Lam, B. S.; Lee, S. H.; Wey, S.; Zhou, H.; Wang, M.; Chen, S.-Y.; Adams, G. B.; Lee, A. S. The Endoplasmic reticulum chaperone protein GRP94 is required for maintaining hematopoietic stem cell interactions with the adult bone marrow niche. *PLoS ONE* **2011**, *6*, e20364.
 23. Wanderling, S.; Simen, B. B.; Ostrovsky, O.; Ahmed, N. T.; Vogen, S. M.; Gidalevitz, T.; Argon, Y. GRP94 Is Essential for Mesoderm Induction and Muscle Development Because It Regulates Insulin-like Growth Factor Secretion. *Mol. Biol. Cell* **2007**, *18*, 3764-3775.
 24. Randow, F.; Seed, B. Endoplasmic reticulum chaperone gp96 is required for innate immunity but not cell viability. *Nat. Cell Biol.* **2001**, *3*, 891-896.
 25. Altieri, D. C.; Stein, G. S.; Lian, J. B.; Languino, L. R. TRAP-1, the mitochondrial Hsp90. *BBA - Mol. Cell Res.* **2012**, *1823*, 767-773.
 26. Chen, B.; Zhong, D.; Monteiro, A. Comparative genomics and evolution of the HSP90 family of genes across all kingdoms of organisms. *BMC Genomics* **2006**, *7*, 156.
 27. Song, H. Y.; Dunbar, J. D.; Zhang, Y. X.; Guo, D.; Donner, D. B. Identification of a protein with homology to hsp90 that binds the Type 1 Tumor Necrosis Factor Receptor. *J. Biol. Chem.* **1995**, *270*, 3574-3581.
 28. Felts, S. J.; Owen, B. A. L.; Nguyen, P.; Trepel, J.; Donner, D. B.; Toft, D. O. The hsp90-related protein TRAP1 is a mitochondrial protein with distinct functional properties. *J. Biol. Chem.* **2000**, *275*, 3305-3312.
 29. Cechetto, J. D.; Gupta, R. S. Immunoelectron microscopy provides evidence that tumor necrosis factor receptor-associated protein 1 (Trap-1) is a mitochondrial protein which also localizes at specific extramitochondrial sites. *Exp. Cell Res.* **2000**, *260*, 30-39.
 30. Leskovar, A.; Wegele, H.; Werbeck, N. D.; Buchner, J.; Reinstein, J. The ATPase cycle of the mitochondrial Hsp90 analog Trap1. *J. Biol. Chem.* **2008**, *283*, 11677-11688.
 31. Masuda, Y.; Shima, G.; Aiuchi, T.; Horie, M.; Hori, K.; Nakajo, S.; Kajimoto, S.; Shibayama-Imazu, T.; Nakaya, K. Involvement of tumor necrosis factor receptor-associated protein 1 (TRAP1) in apoptosis induced by β -Hydroxyisovalerylshikonin. *J. Biol. Chem.* **2004**, *279*, 42503-42515.
 32. Costantino, E.; Maddalena, F.; Calise, S.; Piscazzi, A.; Tirino, V.; Fersini, A.; Ambrosi, A.; Neri, V.; Esposito, F.; Landriscina, M. TRAP1, a novel mitochondrial chaperone responsible for multi-drug resistance and protection from apoptosis in human colorectal carcinoma cells. *Cancer Lett.* **2009**, *279*, 39-46.
 33. Gesualdi, N. M.; Chirico, G.; Pirozzi, G.; Costantino, E.; Landriscina, M.; Esposito, F. Tumor necrosis factor-associated protein 1 (TRAP-1) protects cells from oxidative stress and apoptosis. *Stress* **2007**, *10*, 342-350.
 34. Kang, B. H.; Plescia, J.; Dohi, T.; Rosa, J.; Doxsey, S. J.; Altieri, D. C. Regulation of tumor cell mitochondrial homeostasis by an organelle-specific Hsp90 chaperone network. *Cell* **2007**, *131*, 257-270.
 35. Perrin, M. J.; Subbiah, R. N.; Vandenberg, J. I.; Hill, A. P. Human ether-a-go-go related gene (hERG) K⁺ channels: Function and dysfunction. *Prog. Biophys. Mol. Bio.* **2008**, *98*, 137-148.
 36. Vandenberg, J. I.; Walker, B. D.; Campbell, T. J. HERG K⁺ channels: friend and foe. *Trends Pharmacol. Sci.* **2001**, *22*, 240-246.
 37. Ficker, E.; Dennis, A. T.; Wang, L.; Brown, A. M. Role of the cytosolic chaperones Hsp70 and Hsp90 in maturation of the cardiac potassium channel hERG. *Circ. Res.* **2003**, *92*, e87-e100.
 38. Nanduri, J.; Bergson, P.; Wang, N.; Ficker, E.; Prabhakar, N. R. Hypoxia inhibits maturation and trafficking of hERG K⁺ channel protein: Role of Hsp90 and ROS. *Biochem. Biophys. Res. Commun.* **2009**, *388*, 212-216.

39. Fermini, B.; Fossa, A. A. The impact of drug-induced QT interval prolongation on drug discovery and development. *Nat. Rev. Drug Discov.* **2003**, *2*, 439-447.
40. Brown, A. M. hERG Assay, QT Liability, and Sudden Cardiac Death. *Cardiac Safety of Noncardiac Drugs*; Humana Press, 2005, 67-81.
41. Wible, B. A.; Hawryluk, P.; Ficker, E.; Kuryshv, Y. A.; Kirsch, G.; Brown, A. M. HERG-Lite: A novel comprehensive high-throughput screen for drug-induced hERG risk. *J. Pharmacol. Toxicol.* **2005**, *52*, 136-145.
42. Walker, V. E.; Atanasiu, R.; Lam, H.; Shrier, A. Co-chaperone FKBP38 promotes HERG trafficking. *J. Biol. Chem.* **2007**, *282*, 23509-23516.
43. Peterson, L. B.; Eskew, J. D.; Vielhauer, G. A.; Blagg, B. S. J. The hERG channel is dependent upon the Hsp90 α isoform for maturation and trafficking. *Mol. Pharmaceutics* **2012**, *Accepted*.
44. Ficker, E.; Dennis, A. T.; Kuryshv, Y. A.; Wible, B. A.; Brown, A. M. hERG channel trafficking. *Novart. Fdn. Symp.* **2005**, *266*, 57-74.
45. Gong, Q.; Anderson, C. L.; January, C. T.; Zhou, Z. Role of glycosylation in cell surface expression and stability of HERG potassium channels. *Am. J. Physiol. Heart Circ. Physiol.* **2002**, *283*, H77-H84.
46. Petrecca, K.; Atanasiu, R.; Akhavan, A.; Shrier, A. N-linked glycosylation sites determine HERG channel surface membrane expression. *J. Physiol.* **1999**, *515*, 41-48.
47. Riggs, D. L.; Cox, M. B.; Cheung-Flynn, J.; Prapapanich, V.; Carrigan, P. E.; Smith, D. F. Functional specificity of co-chaperone interactions with Hsp90 client proteins. *Crit. Rev. Biochem. Mol. Biol.* **2004**, *39*, 279-295.
48. Dmochewitz, L.; Lillich, M.; Kaiser, E.; Jennings, L. D.; Lang, A. E.; Buchner, J.; Fischer, G.; Aktories, K.; Collier, R. J.; Barth, H. Role of CypA and Hsp90 in membrane translocation mediated by anthrax protective antigen. *Cell. Microbiol.* **2011**, *13*, 359-373.
49. Kaiser, E.; Kroll, C.; Ernst, K.; Schwan, C.; Popoff, M.; Fischer, G.; Buchner, J.; Aktories, K.; Barth, H. Membrane Translocation of Binary Actin-ADP-Ribosylating Toxins from *Clostridium difficile* and *Clostridium perfringens* Is Facilitated by Cyclophilin A and Hsp90. *Infect. Immun.* **2011**, *79*, 3913-3921.
50. Dutta, R.; Inouye, M. GHKL, An emergent ATPase/kinase superfamily. *Trends Biochem. Sci.* **2000**, *25*, 24-28.
51. Kim, Y. S.; Alarcon, S. V.; Lee, S.; Lee, M. J.; Giaccone, G.; Neckers, L.; Trepel, J. B. Update on Hsp90 inhibitors in clinical trial. *Curr. Top. Med. Chem.* **2009**, *9*, 1479-1492.
52. Biamonte, M. A.; Van de Water, R.; Arndt, J. W.; Scannevin, R. H.; Perret, D.; Lee, W. Heat shock protein 90: inhibitors in clinical trials. *J. Med. Chem.* **2010**, *53*, 3-17.
53. Holzbeierlein, J.; Windsperger, A.; Vielhauer, G. Hsp90: A Drug Target? *Curr. Oncol. Rep.* **2010**, *12*, 95-101.
54. Krukenberg, K. A.; Bottcher, U. M.; Southworth, D. R.; Agard, D. A. Grp94, the endoplasmic reticulum Hsp90, has a similar solution conformation to cytosolic Hsp90 in the absence of nucleotide. *Protein Sci.* **2009**, *18*, 1815-1827.
55. Krukenberg, K. A.; Southworth, D. R.; Street, T. O.; Agard, D. A. pH-dependent conformational changes in bacterial Hsp90 reveal a Grp94-like conformation at pH 6 that is highly active in suppression of citrate synthase aggregation. *J. Mol. Biol.* **2009**, *390*, 278-291.
56. Saitoh, T.; Yanagita, T.; Shiraishi, S.; Yokoo, H.; Kobayashi, H.; Minami, S.-i.; Onitsuka, T.; Wada, A. Down-Regulation of Cell Surface Insulin Receptor and Insulin Receptor Substrate-1 Phosphorylation by Inhibitor of 90-kDa Heat-Shock Protein Family: Endoplasmic Reticulum Retention of Monomeric Insulin Receptor Precursor with Calnexin in Adrenal Chromaffin Cells. *Mol. Pharmacol.* **2002**, *62*, 847-855.
57. Yang, Y.; Liu, B.; Dai, J.; Srivastava, P. K.; Zammit, D. J.; Lefrancois, L.; Li, Z. Heat shock protein gp96 is a master chaperone for toll-like receptors and is important in the innate function of macrophages. *Immunity* **2007**, *26*, 215-226.

58. Maynard, J. C.; Pham, T.; Zheng, T.; Jockheck-Clark, A.; Rankin, H. B.; Newgard, C. B.; Spana, E. P.; Nicchitta, C. V. Gp93, the Drosophila GRP94 ortholog, is required for gut epithelial homeostasis and nutrient assimilation-coupled growth control. *Dev. Biol.* **2010**, *339*, 295-306.
59. MvLaughlin, M.; Alloza, I.; Vandebroek, K. Different chaperone usage by IL-12 and IL-23 during their assembly reveals novel targets for intervention with cytokine secretion in neuroinflammation. *Neuroimmunol.* **2008**, *203*, 268.
60. Olson, D. L.; Burkly, L. C.; Leone, D. R.; Dolinski, B. M.; Lobb, R. R. Anti- α 4 integrin monoclonal antibody inhibits multiple myeloma growth in a murine model. *Mol. Cancer Ther.* **2005**, *4*, 91-99.
61. Ostrovsky, O.; Ahmed, N. T.; Argon, Y. The Chaperone Activity of GRP94 Toward Insulin-like Growth Factor II Is Necessary for the Stress Response to Serum Deprivation. *Mol. Biol. Cell* **2009**, *20*, 1855-1864.
62. Ostrovsky, O.; Eletto, D.; Makarewich, C.; Barton, E. R.; Argon, Y. Glucose regulated protein 94 is required for muscle differentiation through its control of the autocrine production of insulin-like growth factors. *BBA - Mol. Cell Res.* **2010**, *1803*, 333-341.
63. Belfiore, A.; Pandini, G.; Vella, V.; Squatrito, S.; Vigneri, R. Insulin/IGF-I hybrid receptors play a major role in IGF-I signaling in thyroid cancer. *Biochimie* **1999**, *81*, 403-407.
64. Chavany, C.; Mimnaugh, E.; Miller, P.; Bitton, R.; Nguyen, P.; Trepel, J.; Whitesell, L.; Schnur, R.; Moyer, J. D.; Neckers, L. p185 Binds to GRP94 in Vivo. *J. Biol. Chem.* **1996**, *271*, 4974-4977.
65. Moorehead, R. A.; Sanchez, O. H.; Baldwin, R. M.; Khokha, R. Transgenic overexpression of IGF-II induces spontaneous lung tumors: a model for human lung adenocarcinoma. *Oncogene* **2003**, *22*, 853-857.
66. Supino-Rosin, L.; Yoshimura, A.; Yarden, Y.; Elazar, Z.; Neumann, D. Intracellular Retention and Degradation of the Epidermal Growth Factor Receptor, Two Distinct Processes Mediated by Benzoquinone Ansamycins. *J. Biol. Chem.* **2000**, *275*, 21850-21855.
67. Zuany-Amorim, C.; Hastewell, J.; Walker, C. Toll-like receptors as potential therapeutic targets for multiple diseases. *Nat. Rev. Drug Discov.* **2002**, *1*, 797-807.
68. Duerfeldt, A. S.; Peterson, L. B.; Maynard, J.; Ng, C.; Eletto, D.; Ostrovsky, O.; Shinogle, H.; Moore, D.; Argon, Y.; Nicchitta, C. V.; Blagg, B. S. J. Development of a Grp94 inhibitor. *J. Am. Chem. Soc.* **2012**, *Accepted*.
69. Duerfeldt, A. S. A New Generation of Hsp90 Inhibitors: Addressing Isoform Selectivity and Heat Shock Induction, (Doctoral Dissertation) The University of Kansas, ProQuest/UMI. **2011**.
70. Clevenger, R. C.; Blagg, B. S. J. Design, Synthesis, and Evaluation of a Radicol and Geldanamycin Chimera, Radamide. *Org. Lett.* **2004**, *6*, 4459-4462.
71. Hadden, M. K.; Blagg, B. S. J. Synthesis and Evaluation of Radamide Analogues, A Chimera of Radicol and Geldanamycin. *J. Org. Chem.* **2009**, *74*, 4697-4704.
72. Sreedhar, A. S.; Kalmar, E.; Csermely, P. Hsp90 isoforms: functions, expression and clinical importance. *FEBS Lett.* **2004**, *562*, 11-15.
73. Kim, J.; Felts, S.; Llauger, L.; He, H.; Huezo, H.; Rosen, N.; Chiosis, G. Development of a fluorescence polarization assay for the molecular chaperone Hsp90. *J. Biomol. Screen.* **2004**, *9*, 375-381.
74. Kamal, A.; Thao, L.; Sensintaffar, J.; Zhang, L.; Boehm, M. F.; Fritz, L. C.; Burrows, F. J. A high-affinity conformation of Hsp90 confers tumour selectivity on Hsp90 inhibitors. *Nature* **2003**, *425*, 407-410.
75. Harding, C. V. gp96 Leads the Way for Toll-like Receptors. *Immunity* **2007**, *26*, 141-143.
76. Istomin, A.; Godzik, A. Understanding diversity of human innate immunity receptors: analysis of surface features of leucine-rich repeat domains in NLRs and TLRs. *BMC Immunology* **2009**, *10*, 48.

77. Qiu, L.; Song, L.; Xu, W.; Ni, D.; Yu, Y. Molecular cloning and expression of a Toll receptor gene homologue from Zhikong Scallop, *Chlamys farreri*. *Fish Shellfish Immun.* **2007**, *22*, 451-466.
78. Sun, J.; Duffy, K. E.; Ranjith-Kumar, C. T.; Xiong, J.; Lamb, R. J.; Santos, J.; Masarapu, H.; Cunningham, M.; Holzenburg, A.; Sarisky, R. T.; Mbow, M. L.; Kao, C. Structural and Functional Analyses of the Human Toll-like Receptor 3. *J. Biol. Chem.* **2006**, *281*, 11144-11151.
79. Weber, A. N. R.; Morse, M. A.; Gay, N. J. Four N-linked Glycosylation Sites in Human Toll-like Receptor 2 Cooperate to Direct Efficient Biosynthesis and Secretion. *J. Biol. Chem.* **2004**, *279*, 34589-34594.
80. Carpenter, A.; Jones, T.; Lamprecht, M.; Clarke, C.; Kang, I.; Friman, O.; Guertin, D.; Chang, J.; Lindquist, R.; Moffat, J.; Golland, P.; Sabatini, D. CellProfiler: image analysis software for identifying and quantifying cell phenotypes. *Genome Biol.* **2006**, *7*, R100.
81. Blagg, B. S. J.; Kerr, T. D. Hsp90 inhibitors: small molecules that transform the Hsp90 protein folding machinery into a catalyst for protein degradation. *Med. Res. Rev.* **2006**, *26*, 310-338.
82. Basso, A. D.; Solit, D. B.; Chiosis, G.; Giri, B.; Tschlis, P.; Rosen, N. Akt Forms an Intracellular Complex with Heat Shock Protein 90 (Hsp90) and Cdc37 and Is Destabilized by Inhibitors of Hsp90 Function. *J. Biol. Chem.* **2002**, *277*, 39858-39866.
83. Grbovic, O. M.; Basso, A. D.; Sawai, A.; Ye, Q.; Friedlander, P.; Solit, D.; Rosen, N. V600E B-Raf requires the Hsp90 chaperone for stability and is degraded in response to Hsp90 inhibitors. *P. Natl. Acad. Sci.* **2006**, *103*, 57-62.
84. da Rocha Dias, S.; Friedlos, F.; Light, Y.; Springer, C.; Workman, P.; Marais, R. Activated B-RAF Is an Hsp90 Client Protein That Is Targeted by the Anticancer Drug 17-Allylamino-17-Demethoxygeldanamycin. *Cancer Res.* **2005**, *65*, 10686-10691.
85. Conde, R.; Belak, Z. R.; Nair, M.; O'Carroll, R. F.; Ovsenek, N. Modulation of Hsf1 activity by novobiocin and geldanamycin. *Biochem. Cell Biol.* **2009**, *87*, 845-851.
86. McCollum, A. K.; TenEyck, C. J.; Stensgard, B.; Morlan, B. W.; Ballman, K. V.; Jenkins, R. B.; Toft, D. O.; Erlichman, C. P-Glycoprotein-mediated resistance to Hsp90-directed therapy is eclipsed by the heat shock response. *Cancer Res.* **2008**, *68*, 7419-7427.
87. Loo, M. A.; Jensen, T. J.; Cui, L.; Hou, Y.-x.; Chang, X.-B.; Riordan, J. R. Perturbation of Hsp90 interaction with nascent CFTR prevents its maturation and accelerates its degradation by the proteasome. *EMBO J.* **1998**, *17*, 6879-6887.
88. Vogen, S.; Gidalevitz, T.; Biswas, C.; Simen, B. B.; Stein, E.; Gulmen, F.; Argon, Y. Radicicol-sensitive Peptide Binding to the N-terminal Portion of GRP94. *J. Biol. Chem.* **2002**, *277*, 40742-40750.
89. Edwards, D. P.; Weigel, N. L.; Schrader, W. T.; O'Malley, B. W.; McGuire, W. L. Structural analysis of chicken oviduct progesterone receptor using monoclonal antibodies to the subunit B protein. *Biochemistry* **1984**, *23*, 4427-4435.
90. Banerji, U. Heat shock protein 90 as a drug target: some like it hot. *Clin. Cancer Res.* **2009**, *15*, 9-14.
91. Benson, J. D.; Chen, Y.-N. P.; Cornell-Kennon, S. A.; Dorsch, M.; Kim, S.; Leszczyniecka, M.; Sellers, W. R.; Lengauer, C. Validating cancer drug targets. *Nature* **2006**, *441*, 451-456.
92. Isaacs, J. S.; Xu, W. S.; Neckers, L. Heat shock protein as a molecular target for cancer therapeutics. *Cancer Cell* **2003**, *3*, 213-217.
93. Li, Y.; Schwartz, S. J.; Sun, D. New developments in Hsp90 inhibitors as anti-cancer therapeutics: mechanisms, clinical perspective and more potential. *Drug Resist. Update* **2009**, *12*, 17-27.
94. Neckers, L. Hsp90 inhibitors as novel cancer chemotherapeutic agents. *Trends Mol. Med.* **2002**, *8*, S55-S61.
95. Peterson, L. B.; Blagg, B. S. J. To fold or not to fold: modulation and consequences of Hsp90 inhibition. *Future Med. Chem.* **2009**, *1*.

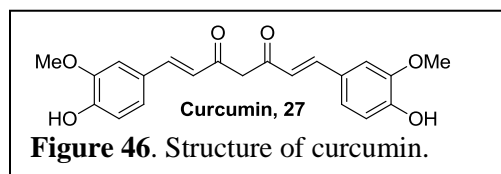
96. Workman, P. Combinatorial attack on multistep oncogenesis by inhibiting the Hsp90 molecular chaperone. *Cancer Lett.* **2004**, *206*, 149-157.
97. Workman, P.; Billy, E. d. Putting the heat on cancer. *Nat. Med.* **2007**, *13*, 1415-1417.
98. Workman, P.; Burrows, F.; Neckers, L.; Rosen, N. Drugging the cancer chaperone Hsp90: Combinatorial therapeutic exploitation of oncogene addiction and tumor stress. *Ann. NY Acad. Sci.* **2007**, *1113*, 202-216.
99. Taldone, T.; Gozman, A.; Maharaj, R.; Chiosis, G. Targeting Hsp90: small-molecule inhibitors and their clinical development. *Curr. Opin. Pharmacol.* **2008**, *8*, 370-374.
100. Ong, S.-E.; Blagoev, B.; Kratchmarova, I.; Kristensen, D. B.; Steen, H.; Pandey, A.; Mann, M. Stable Isotope Labeling by Amino Acids in Cell Culture, SILAC, as a Simple and Accurate Approach to Expression Proteomics. *Mol. Cell. Proteomics* **2002**, *1*, 376-386.
101. Zhou, Z.; Gong, Q.; Ye, B.; Fan, Z.; Makielski, J. C.; Robertson, G. A.; January, C. T. Properties of HERG channels stably expressed in HEK 293 cells studied at physiological temperature. *Biophys. J.* **1998**, *74*, 230-241.
102. Melnick, J.; Dul, J. L.; Argon, Y. Sequential interaction of the chaperones BiP and GRP94 with immunoglobulin chains in the endoplasmic reticulum. *Nature* **1994**, *370*, 373-375.

Chapter IV

Exploration of Curcumin as a Novel Hsp90 Inhibitor

I. Introduction

Curcumin (**27**, **Figure 46**) is the biologically active natural product found in turmeric and yellow curry, and has demonstrated activity for the treatment



of inflammatory diseases, Alzheimer's, and cancer.¹ Curcumin was first isolated from the rhizome of *Curcuma longa* L. (*Zingiberaceae*) and has been used as a botanical medicine by inhabitants of both India and China.² Traditionally, curcumin was used for the treatment of wounds, inflammation, and tumors.³ More recently, it was identified as an anti-tumor agent and was shown to exhibit beneficial activity towards the treatment of Alzheimer's disease.⁴ In regards to curcumin's anticancer activity, several studies have demonstrated that curcumin manifests potent anti-proliferative activity against numerous cancer cell lines, but is not toxic to small and large animals at high doses.⁵⁻⁶ As a result of this exceptional selectivity, curcumin has entered several clinical trials for the treatment of cancer.⁷⁻⁸ Previous studies have shown that curcumin can inhibit topoisomerase II at concentrations of 50 $\mu\text{g/mL}$.⁹ More recently it was shown to inhibit NAD(P)H:quinone oxidoreductase 1 (NQO1) and lead to the degradation of p53 at 40 μM .¹⁰ However, there are a large number of other proteins whose activities curcumin has been shown to alter for which no rational explanation has been provided.¹¹

Curcumin's anti-inflammatory activity has been ascribed to result from its ability to decrease prostaglandin E2 synthase (PGE2), thus reducing prostaglandins responsible for inflammation.¹² In addition, curcumin has been shown to inhibit pathways that modulate inflammatory cascades, including the nuclear transcription factor- κB (NF- κB), activator protein-

1 (AP-1) and c-Jun, all of which are important mediators of cellular response to environmental stress, pro-inflammatory kinases, mitogen stimulation, and apoptotic stimuli.¹³ In regards to curcumin's use for the treatment of Alzheimer's disease, curcumin has been shown to decrease amyloid pathology, decrease aggregated Amyloid β (A β), and protect neuronal cells from A β induced toxicity.^{4,14} Furthermore, curcumin has been shown to increase levels of the 70 kDa heat shock protein (Hsp70), which has been implicated for the refolding and solubilization of these protein aggregates.¹⁵⁻¹⁶ The antioxidant activity afforded by curcumin has been described to result from decreased nitric oxide synthase (NOS) activity.¹⁷ Data obtained from previous studies support the use of curcumin for the treatment of these diseases, several of which are currently in preclinical development.

Curcumin promotes apoptosis in colon, liver, breast, prostate, and leukemia cancer cell lines.¹⁸ Curcumin has been shown to suppress the expression of cyclin D, endothelial growth factor receptor (EGFR), and cause degradation of the p53 tumor suppressor. In addition, curcumin disrupts cell signaling pathways involving phosphokinase B (Akt), nuclear factor κ B (NF- κ B), c-myc, and phospho-Akt (pAkt).¹⁷ Angiogenic growth factor production, tumor necrosis factor 1- β (TNF-1 β), and interleukin 1 (IL-1) have also been shown to be decreased at low micromolar concentrations of curcumin.

Additional proteins affected by administration of curcumin include the aryl hydrocarbon receptor (AHR), survivin, glutathione S-transferase (GST), telomerase (hTERT and hTR assembly), estrogen receptor (ER), androgen receptor (AR), bcr-Abl kinase, calmodulin, cyclin-dependent kinase 4 (CDK4), STAT3, Bcl-2, and others (**Table 9**). Although it is plausible that curcumin could individually disrupt all of these processes, it can be reasoned that curcumin was

more likely inhibiting a single target that was responsible for mediating cascades in which the above proteins were involved.

Table 9. Client proteins of Hsp90 also affected by curcumin.

Protein	Curcumin Reference	Hsp90 Reference
PGE ² synthase	12	19
NF-κB	20	21
AP-1	22	23
c-Jun	24	25
iNOS	17	26
Hsp70	15	27
Cyclin D	28	29
EGFR	30	31
p53	10	32
Akt	33	34
p-Akt	35	36
c-Myc	37	38
TNF-1α	39	40
IL-1	41	40
AHR	42	43
Survivin	35	44
ER	45	46
AR	47	48
Telomerase	49	50
Bcr-Abl	51	52
CDK-4	28	53
Bcl-2	54	55
Calmodulin	56	57
GST	58	59
STAT3	60	61

The Hsp90-family of gene products function as molecular chaperones, which are ubiquitously expressed and required for the viability of all eukaryotic cells. While Hsp90

functions to facilitate the refolding of denatured proteins, Hsp90 is more widely appreciated for its obligatory role in facilitating the post-translational maturation of numerous proteins that regulate a plethora of signal transduction pathways.⁶² More than 100 Hsp90-dependent client proteins have been identified, including those that are involved in inflammatory response such as STAT3, NF- κ B, PGE2, AP-1, and c-Jun.⁶³ Among these Hsp90 clients, many are proteins directly related to oncogenesis,⁶⁴ and numerous Hsp90 clients are represented in all six hallmarks of cancer.⁶⁵⁻⁶⁶ Recent studies by Dou and coworkers provided evidence that increased levels of Hsp90 and/or Hsp70 can refold phosphorylated Tau aggregates and protect neuronal cells from A β induced toxicity.¹⁶ Hsp90 and Hsp70 are induced upon cellular exposure to stress stimuli or Hsp90 inhibitors, which dissociate Hsp90 from Hsp90/HSF1 (heat shock factor 1) complexes, allowing the assembly of HSF1 trimers. HSF1 trimers serve as transcriptional activators by binding to the heat shock response elements and leads to the induction of Hsp's.²⁷ Results from previous studies demonstrated that exposure of neuronal cells to Hsp90 inhibitors led to increased expression of Hsps and the rapid clearance of phosphorylated Tau and protection from A β induced toxicity in a manner dependent upon the concentration of the previously identified Hsp90 inhibitor, geldanamycin.¹⁶

The notable similarities between the pharmacological properties and physiological effects of curcumin and geldanamycin led to a search of the literature to determine whether additional relationships existed. As a result, it became clear that Hsp90 had previously been shown to mediate the activities of cyclin D, EGFR, p53, AKT, NF- κ B, Bcl-2, c-myc, TNF- α , AHR, survivin, GST, telomerase, ER, AR, bcr-Abl kinase, CDK4, calmodulin, Bcl-2, TNF- α , STAT3, and interleukin-1, which have all been shown to be affected by curcumin (**Table 9**). Prior to joining the Blagg Laboratory, the hypothesis that curcumin's inhibitory activity resulted from

Hsp90 inhibition was evaluated. In addition, several other research groups simultaneously recognized the similarities between curcumin's biological activity and those manifested by Hsp90 inhibition.⁶⁷⁻⁶⁸

II. Evaluation of Curcumin as an Hsp90 Inhibitor

The mechanism for conformational maturation of Hsp90's diverse set of client proteins is complex, and involves the interaction of Hsp90 with a number of co-chaperones and partner proteins and the binding/hydrolysis of ATP.⁶² To test the hypothesis that many of the physiological effects of curcumin are manifested through its ability to inhibit Hsp90, the effects of curcumin on Hsp90 activity was investigated previously in the Blagg Laboratory. Subsequently, it was determined that curcumin bound recombinant Hsp90, inhibited its chaperone function, induced a concentration-dependent depletion of Hsp90-dependent client proteins in malignant cells, and induced Hsp90 levels in cells, all which correlated directly with its ability to inhibit cell growth.

A. Curcumin Binds Purified Recombinant Hsp90.

Addition of purified, recombinant Hsp90 to a buffered aqueous solution of curcumin resulted in a three-fold increase in curcumin fluorescence at 523 nm when excited by light at 422 nm, indicating a direct binding interaction between curcumin and Hsp90. Titration of Hsp90 with

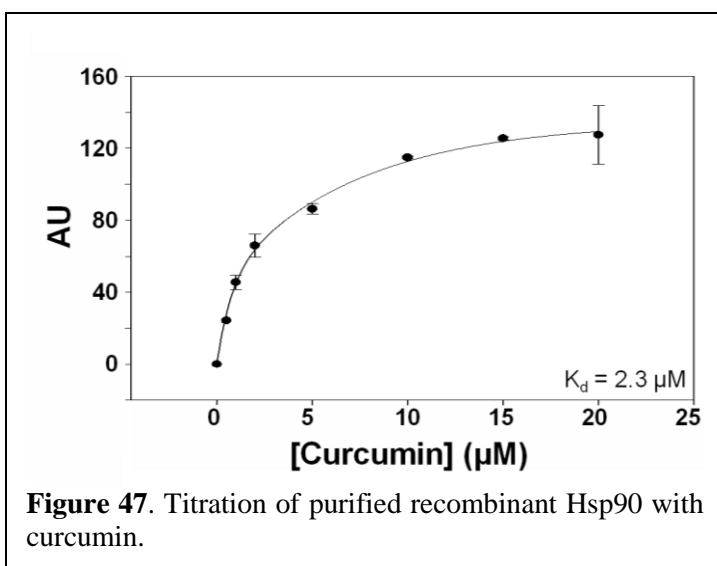


Figure 47. Titration of purified recombinant Hsp90 with curcumin.

curcumin (**Figure 47**) showed saturable binding with an apparent K_d of 2.3 μM .

B. Curcumin Inhibits Hsp90-dependent Refolding of Heat Denatured Luciferase.

Heat denatured firefly luciferase has been utilized as a model substrate for measuring the protein folding activity of the Hsp90 multiprotein complex,⁶⁹ because measurement of the luminescence produced by restoration of its enzymatic activity provides a highly sensitive and reproducible assay for the Hsp90's chaperone activity.

Rabbit reticulocyte lysate provides a

quasi-physiological model system in which to study the activity of Hsp90, as it contains Hsp90 and all the requisite co-chaperones and partner proteins necessary for the refolding denatured luciferase.⁷⁰ Because different sources of rabbit reticulocyte lysate can contain varying levels of the individual components of Hsp90 protein folding machinery,⁷⁰ two lysates were analyzed in this study. When increasing concentrations of curcumin were added to these assays, a 50% decrease in the amount of refolded luciferase was observed at 10 μM and 38 μM (i.e. EC_{50} , **Figure 48**), similar to data obtained from the Hsp90 binding studies. Control experiments indicated that curcumin had no effect on the activity of native luciferase. Thus, the results indicate that curcumin has the capacity to inhibit the refolding of an Hsp90-dependent client protein.

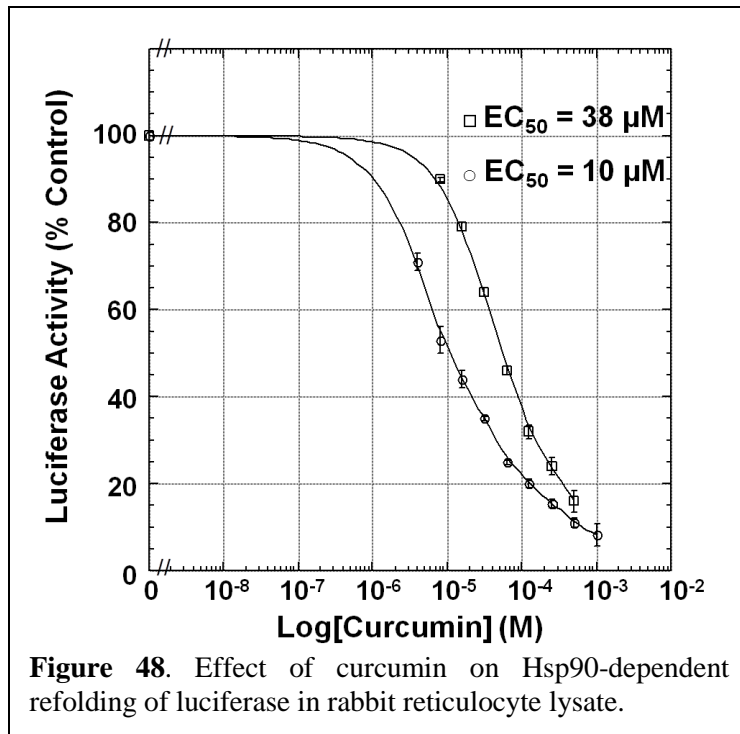
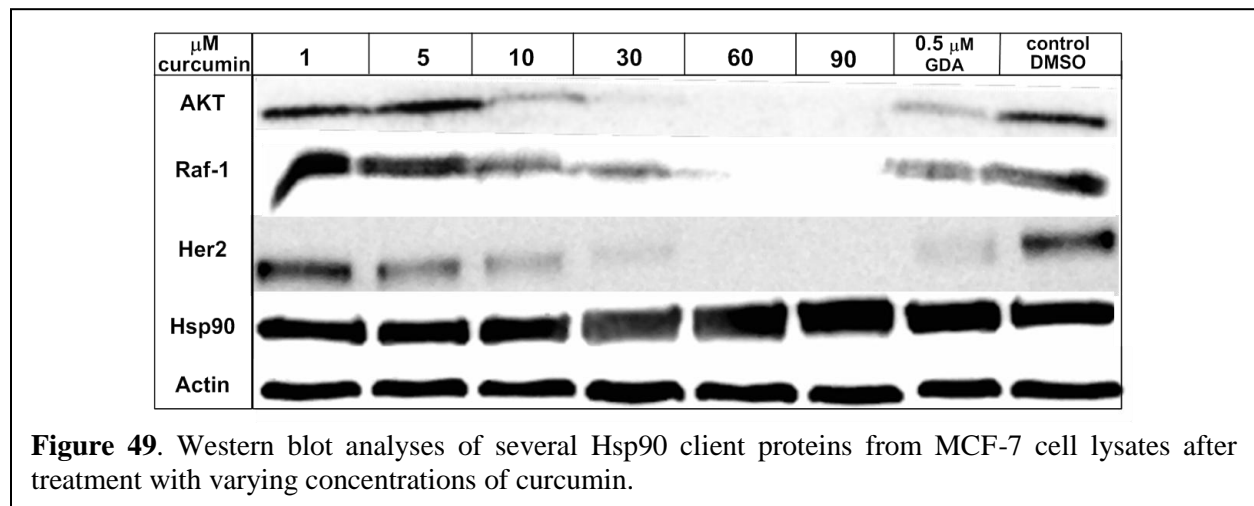


Figure 48. Effect of curcumin on Hsp90-dependent refolding of luciferase in rabbit reticulocyte lysate.

C. Curcumin Inhibits the Maturation of Hsp90-dependent Proteins in MCF-7 Breast Cancer Cells.

Hsp90 inhibitors, such as geldanamycin, exert their activity by competitive inhibition of Hsp90's ATP-driven reaction cycle,⁷¹ as the ability to bind and hydrolyze ATP is required for Hsp90 to facilitate the maturation of its client. In the presence of Hsp90 inhibitors, the multiprotein complex formed between Hsp90, its co-chaperones and clients becomes destabilized, and, the heteroprotein complex is unable to proceed through the normal protein folding process. Consequently, these unproductive complexes become substrates for ubiquitin ligase, which leads to ubiquitination of the client and hydrolysis of the substrate via the



proteasome.⁷²

To determine whether curcumin similarly caused the degradation of well-documented Hsp90 client proteins in transformed cells, increasing concentrations of curcumin were incubated with MCF-7 breast cancer cells for 24 h and equal concentrations of protein from these lysates were probed for the disappearance of Hsp90 client proteins, Akt, Raf-1, and Her2 (erbB2). Since actin is not an Hsp90 dependent protein, its level remains unaffected by Hsp90 inhibitors and ensures no decrease in overall protein levels is observed.⁷³ Western blot analyses of these

proteins indicated that all three client proteins were rapidly degraded between at 5 and 30 μM of curcumin, without affecting actin levels (**Figure 49**). Furthermore, Hsp90 levels were increased. Similar studies have previously shown that curcumin also causes the induction of Hsp70.¹⁵ Both of these results are likely due to curcumin-induced disassembly of the Hsp90/HSF1 complex, as geldanamycin similarly causes the induction of Hsp synthesis by disrupting the interaction of Hsp90 with HSF1.⁷⁴⁻⁷⁵ Therefore, these results indicate that curcumin, like other Hsp90 inhibitors, stimulates the turnover of Hsp90-dependent clients in transformed cells.

D. Curcumin Inhibits Proliferation at a Concentration that Mirrors its Ability to Prevent Folding of Hsp90-dependent Substrates.

MCF-7 cells were incubated with varying concentrations of curcumin and the anti-proliferative activity was determined. Curcumin exhibited anti-proliferative activity with an IC_{50} of 6 μM , approximately the same concentration needed to bind purified recombinant Hsp90 ATPase, inhibit the renaturation of heat denatured luciferase, cause the degradation of Hsp90 client proteins Akt, Raf-1, and Her2 in MCF-7 cells, and induce the expression of Hsp90. These results strongly support the hypothesis that the anti-proliferative effect of curcumin on MCF-7 breast cancer cells is due to curcumin-induced disappearance of Hsp90-dependent client proteins.

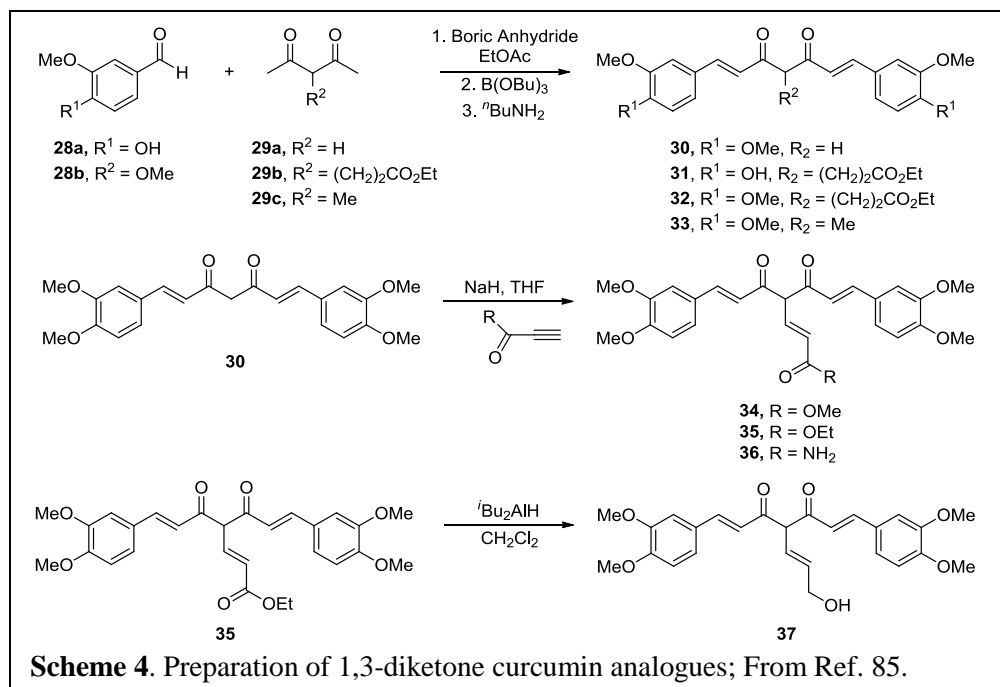
III. Design, Synthesis and Evaluation of Electron Rich Curcumin Analogues

In total, there are over 100 previously reported “biological targets” for curcumin, ranging from transcription factors to various enzymes and receptors.⁷⁶ Although initial studies indicate that curcumin manifests these properties through Hsp90 inhibition, it is not known whether these activities are due to covalent modification of Hsp90 and other targets through its Michael acceptor properties or general promiscuity resulting from the moderately simple scaffold. It has been postulated that conversion of the α , β -unsaturated 1,3-diketone moiety into an electron rich

ring system would lessen the potential for nucleophilic addition.⁷⁷ Therefore, it was proposed that modification of the 1,3-diketone into a comparatively electron rich isoxazole moiety that contains two adjacent hydrogen bond acceptors in similar proximity to the original ketones would accomplish this objective. Furthermore, since the 1,3-diketone can tautomerize into the corresponding enol,⁷⁸ it was proposed that a pyrazole aromatic nucleus would represent an electron rich mimetic of this hydrogen-bonding network and also serve to suppress nucleophilic addition to the adjacent, conjugated olefins. Identification of previously reported curcumin analogues that exhibit increased anti-proliferative,⁷⁹⁻⁸⁰ anti-malarial,⁸¹ antioxidant, and anti-inflammatory activity⁸² as well as improved anti-neurodegenerative properties provided the basis for the heteroaromatic species reported herein.⁸³⁻⁸⁴

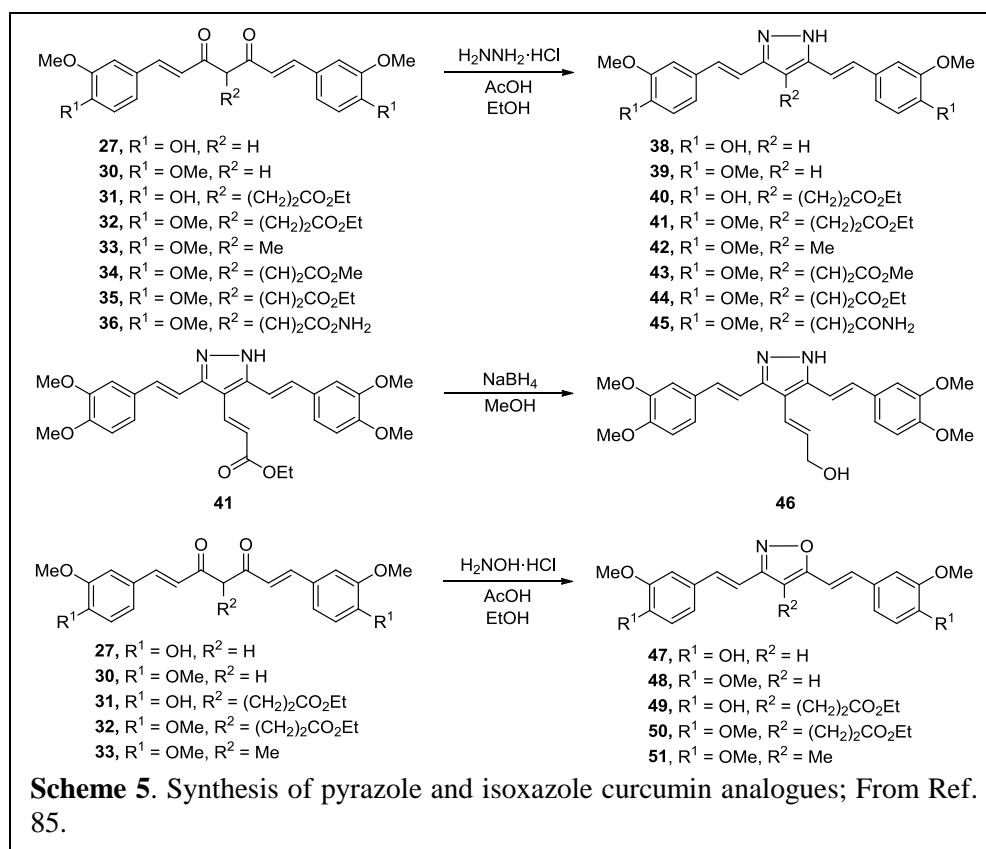
A. Synthesis of 1,3-Diketone Analogues

Chemistry developed by Lin et al. was utilized and expanded upon to prepare 1,3-diketone analogues for the purpose of determining structure–activity relationships (**Scheme 4**).⁷⁹⁻
⁸⁰ A complex was formed between boric anhydride and 2,4-pentanedione, facilitating a 1,5-bis-aldol condensation with 3,4-dimethoxybenzaldehyde to afford dimethylcurcumin, **30**. Similar methodology was used to derive compounds **31**, **32**, and **33** from their respective 3,4-disubstituted benzaldehydes and 3-substituted pentanediones. Compounds **34**, **35**, and **36** were obtained from dimethylcurcumin (**30**) via Michael addition with methyl propiolate, ethyl propiolate, and propiolamide, respectively. Reduction of the α,β -unsaturated ethyl ester **35** with di-isobutyl aluminum hydride at $-78\text{ }^{\circ}\text{C}$ produced the allylic alcohol **37**, in good yield.⁸⁵



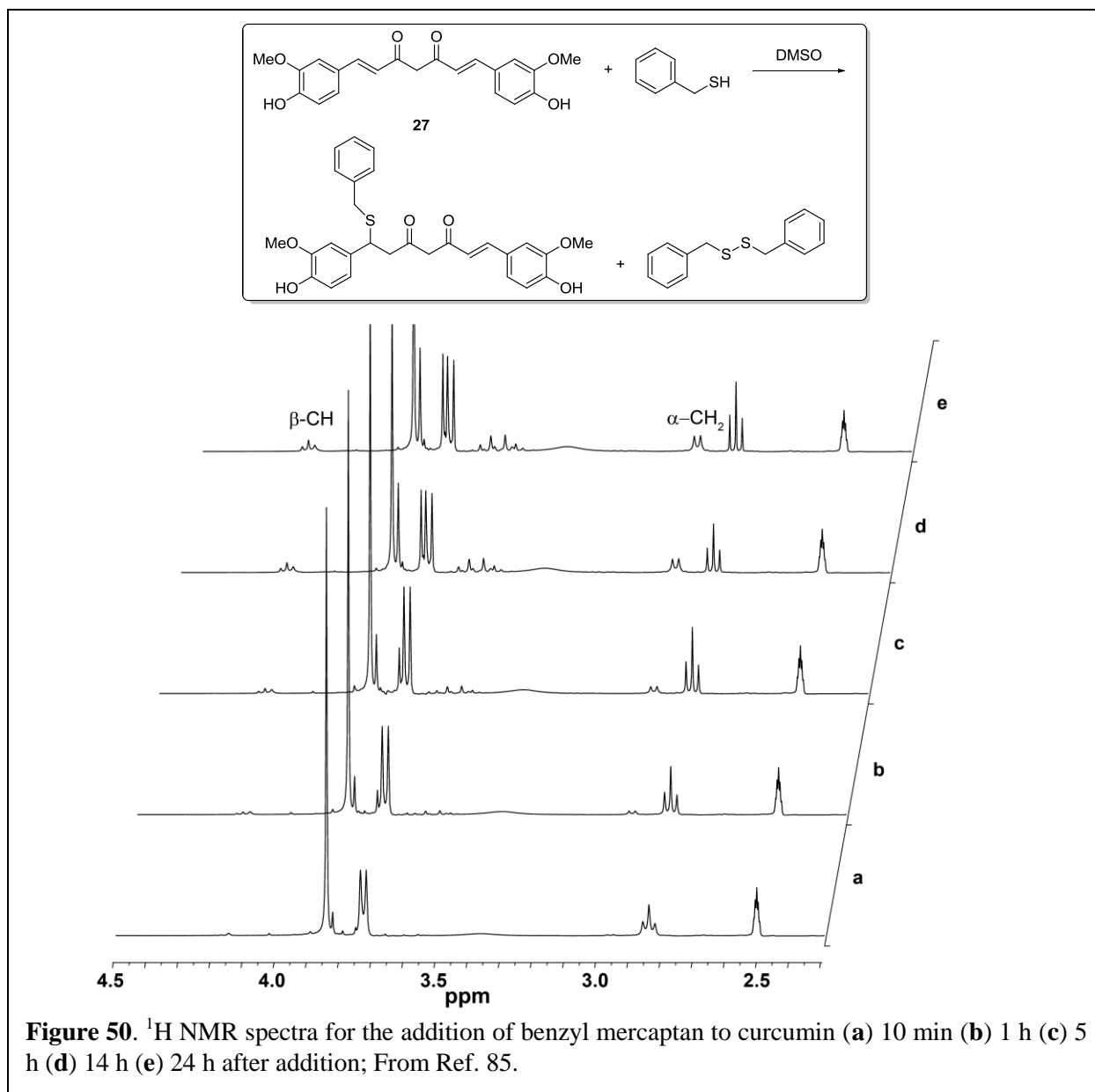
B. Synthesis of Pyrazole and Isoxazole Analogues

The completed diketone species were used to prepare pyrazole analogues through an acid-catalyzed condensation with hydrazine hydrochloride, while stirring at reflux for forty hours. The isoxazole analogues were prepared in similar fashion enlisting hydroxylamine hydrochloride (**Scheme 5**). After discovering the instability of allylic alcohol **37** to these cyclization conditions, an alternative pathway was utilized in which the α,β -unsaturated ethyl ester analogue (**35**) was first cyclized, and subsequently reduced with sodium borohydride to give the cyclized allylic alcohol, **46**.⁸⁵



C. Electrophilicity of Curcumin and Analogues

To compare the electrophilicity of curcumin to the electron rich pyrazole and isoxazole analogues, 1,4 conjugate addition of benzyl mercaptan to the benzylic olefins was monitored over time by ¹H NMR. After incubating an equimolar mixture of curcumin and benzyl mercaptan for 1 hour, new aliphatic protons began to appear at δ2.96 and δ4.17 (**Figure 50**), indicative of conjugate addition. Additionally, the appearance of a multiplet at δ3.57 was attributed to the α-methylene group adjacent to sulfur in the conjugated product. Furthermore, two singlets appeared at δ3.76 and δ3.83 corresponding to the disulfide product of benzyl mercaptan and the desymmetrization of the curcumin scaffold, respectively.



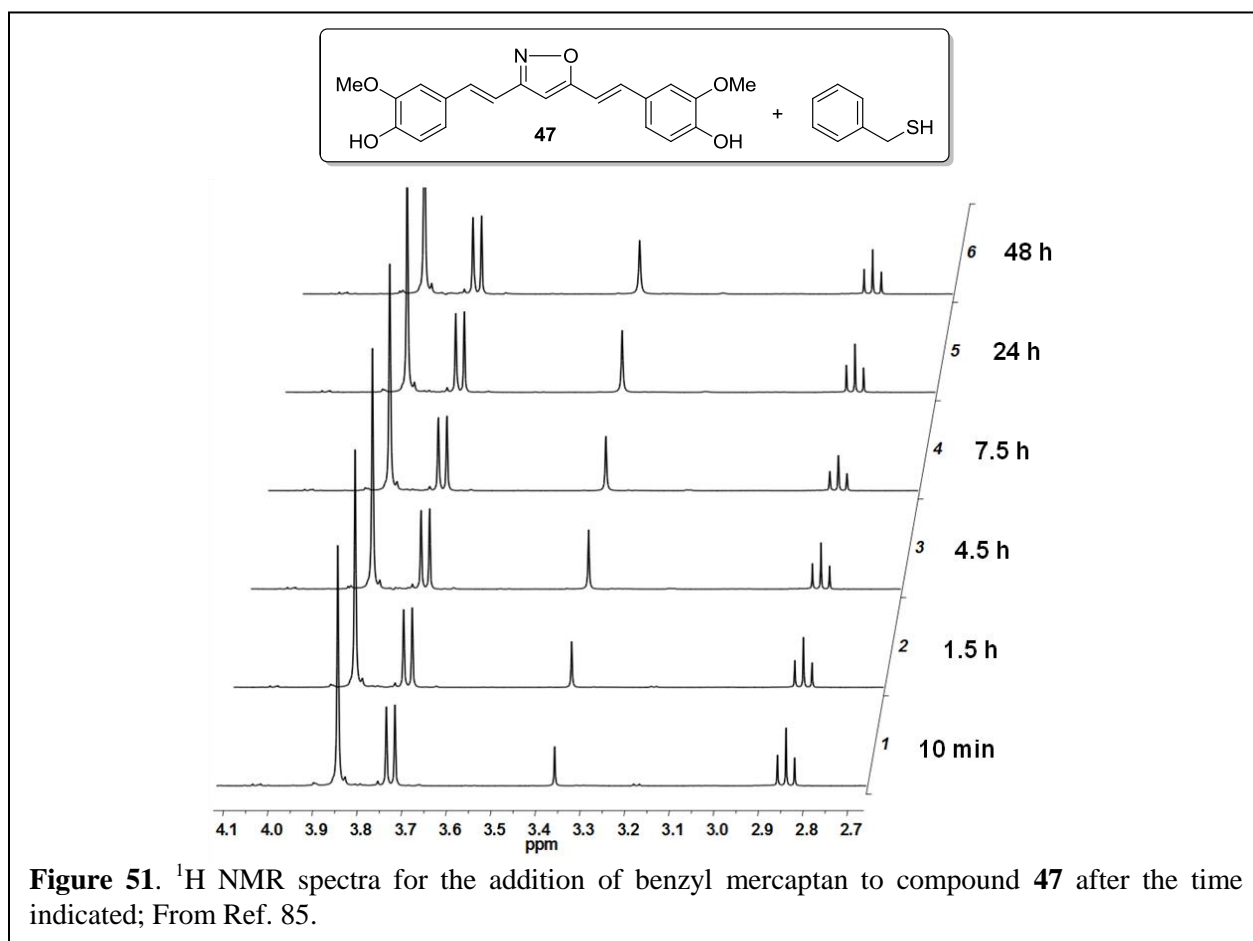
Quantitative addition to the olefin was not observed due to competing disulfide formation, however, integration of the emerging aliphatic protons with respect to the aromatic methoxy protons (**Table 10**) indicated 53% addition after 24 hours. Additionally, mass spectrometry data provided evidence that addition of benzyl mercaptan to curcumin resulted in both mono- and di-conjugate-addition products, as masses were observed for both products.

Table 10. Relative integration^a of protons resulting from 1,4-conjugate addition to curcumin; From Ref 85.

Elapsed Time	δ 2.96 (d, $J = 7.7$, α -CH ₂)	δ 4.16 (t, $J = 7.8$, β -CH)
10 min	0.08	0.03
1 h	0.22	0.12
5 h	0.37	0.21
14 h	0.91	0.56
24 h	1.06	0.62

^aIntegration relative to aromatic OCH₃ substituents (6H)

In contrast, when the related isoxazole (**47**) and pyrazole analogues were incubated with benzyl mercaptan for 48 hours, no change in the ¹H NMR was observed (**Figure 51** and Materials and Methods), indicating that these species were not reactive to nucleophilic attack by



benzyl mercaptan as curcumin itself. This observation can be explained by the electron rich and heteraromatic nature of the pyrazole and isoxazole rings as compared to the diketone species.⁸⁶ The benzylic olefin is less susceptible to Michael addition due to decreased electrophilicity and because the mechanism by which such a transformation occurs involves a non-aromatic intermediate. The electron-rich and heteroaromatic properties of the pyrazole and isoxazole rings appear to make these compounds less electrophilic and thus, less promiscuous than curcumin as a “general” alkylating agent within the cell.

D. Biological Evaluation of Curcumin and Analogues

The data shown in **Table 11** represents the growth inhibitory activity of curcumin and its analogues against MCF-7(ER+) and SKBr-3(ER-, HER2 over-expressing) breast cancer cell lines. The results indicate that compounds **30**, **33**, **34**, **35** and **37** represent the most potent analogues, manifesting submicromolar to low micromolar IC₅₀ values against both cell lines. Upon analysis of the anti-proliferation data for these analogues, it is evident that in most cases, IC₅₀ values for the parent dione are better than the pyrazole and isoxazole analogues. This can be attributed to the promiscuity of the α,β -unsaturated ketone, as well as conformational differences between the 6-membered hydrogen bonding network created by the enol form of the diketone species and the rigid, more conformationally constrained 5-membered ring derivatives. Additionally, the pyrazole analogues exhibited lower IC₅₀ values than the corresponding isoxazole analogues, highlighting the potential significance of a hydrogen bond donor on the pyrazole ring and its related nature to the corresponding enol form of the diketone species. Another interesting observation is the IC₅₀ values between analogues with 3,4-dimethoxy substitution on each of the aromatic rings and the analogues with the 3-methoxy-4-hydroxy substitution, which is similar to the natural product. The diketone species with a 3,4-dimethoxy

substitution generally manifested lower IC₅₀ values than the analogues that contain phenols. In contrast, the pyrazole and isoxazole derivatives possessed the opposite trend, as the phenolic analogues exhibited lower IC₅₀ values than the analogues with dimethoxy substitution. This can be attributed to the electronic effect induced by the pyrazole and isoxazole rings, which impacts the hydrogen bond capability and pKa of the phenols as compared to the diketo species.⁸⁷

Table 11. Anti-proliferative activities of curcumin and analogues;^a From Ref. 85.

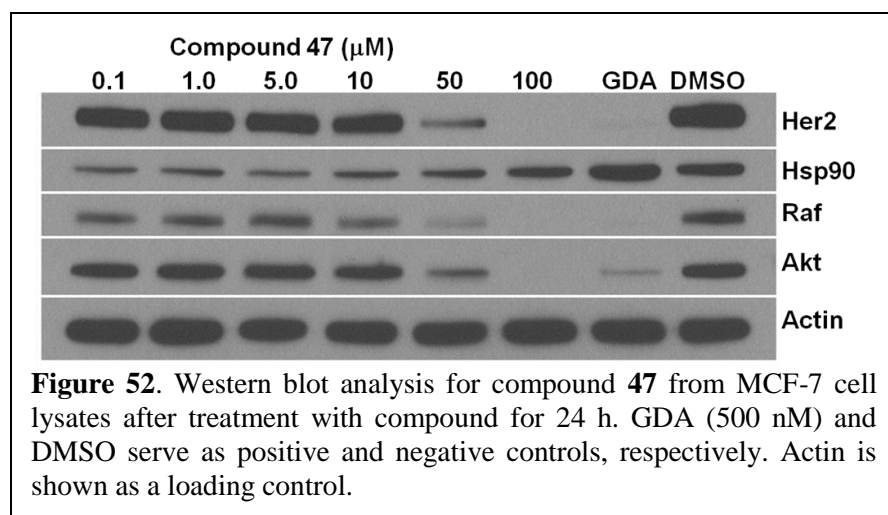
Compound	MCF-7 (IC ₅₀ , μM) ^b	SKBR3 (IC ₅₀ , μM)
27	5.58 ± 0.97	2.11 ± 0.09
30	1.07 ± 0.05	0.955 ± 0.145
31	1.96 ± 0.35	4.38 ± 1.18
32	>100	>100
33	1.09 ± 0.03	1.02 ± 0.05
34	0.512 ± 0.004	0.564 ± 0.020
35	1.28 ± 0.14	1.96 ± 0.65
36	5.35 ± 0.28	9.83 ± 1.12
37	0.796 ± 0.067	1.24 ± 0.58
38	4.19 ± 1.59	0.258 ± 0.034
39	12.7 ± 0.3	1.58 ± 0.46
40	6.01 ± 0.39	5.60 ± 1.24
41	10.1 ± 0.7	11.7 ± 0.5
42	8.16 ± 3.73	>100
43	49.5 ± 2.9	>100
44	11.4 ± 0.5	5.99 ± 0.61
45	39.9 ± 2.6	52.6 ± 7.8
46	>100	>100
47	1.76 ± 0.39	4.00 ± 0.13
48	59.5 ± 6.5	>100
49	13.2 ± 1.6	13.9 ± 1.9
50	>100	>100
51	55.7 ± 5.7	42.5 ± 12.2

^aValues represent mean ± standard error for at least two separate experiments performed in triplicate

^bIC₅₀ is defined as the concentration of compound necessary to inhibit cellular growth by 50%

Finally, the difference in IC₅₀ values between the diketo species with substitutions at the α position indicates that an unsaturated and oxygen-containing moiety generally lowers the IC₅₀ value, as observed with compounds **34** and **37**. Compound **32**, containing 3,4-dimethoxy substitution and a saturated R² substituent (**Scheme 5**) displayed no anti-proliferative activity at the concentrations tested. Further SAR is required to elucidate the origin of this effect as no other compounds in this library shared this group of functionalities. It should be noted that similar compounds bearing the unsaturated amide substituent also manifested decreased activity, indicating that nitrogen-bearing substituents may be detrimental to their anti-proliferative activity. In summary, it was observed that the most active analogues were those that contained a 3,4-dimethoxy aromatic substitution and unsaturated, oxygen-containing substituents flanking the α position, which exhibited low to sub micromolar IC₅₀ values.

Once the anti-proliferative activity of each analogue was determined, we sought to investigate if the analogues with attenuated electrophilicity still manifested Hsp90 inhibitory activity, as monitored by client protein degradation. MCF-7 cells were treated with varying concentrations of compound **47** for 24 h. and Western blot analyses were performed for Raf, Akt,



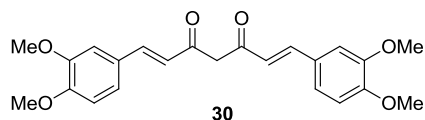
and Her2, three known Hsp90 client proteins (**Figure 52**). As evident in **Figure 52**, compound **47** induces the degradation of Her2, Raf, and Akt, which is indicative of Hsp90-

inhibitory activity, consistent with observations made for curcumin (**Figure 49**).

IV. Conclusions and Future Work

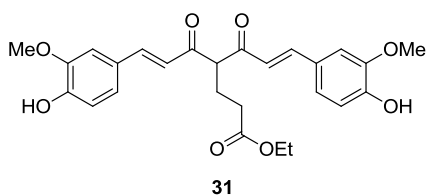
A library of curcumin analogues has been synthesized in an effort to elucidate structure–activity relationships, as well as to determine the relevance of curcumin’s Michael acceptor properties and its ability to act as an anti-cancer agent. Anti-proliferative data from two breast cancer cell lines were obtained, which led to identification of several compounds that exhibit increased growth inhibitory activity versus the natural product. Furthermore, it was determined that the Michael acceptor properties were not critical to retention of inhibitory activity for curcumin and analogues. In fact, both the isoxazole and pyrazole analogues displayed only slightly lower activities than the related diketone species, with the pyrazole species manifesting slightly better activity than the related isoxazole. These studies highlighted the importance of the hydrogen-bonding network demonstrated by curcumin in its enol form, which corresponds favorably to pyrazoles H-bond donor/acceptor moieties. Diminished electrophilicity, while maintaining anti-proliferative activity, makes these non-toxic curcumin analogues potentially a viable target for future drug development. It will be crucial to follow-up these studies by investigating the effects of non-electrophilic curcumin analogues on various Hsp90 functions.

V. Materials and Methods



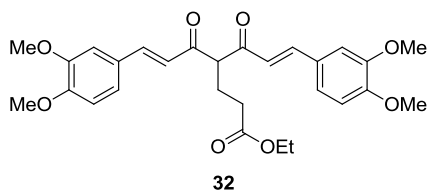
(1E,16E)-1,7-Bis(3,4-dimethoxyphenyl)hepta-1,6-diene-3,5-dione (30). 2,4-Pentanedione (0.32 mL, 3.0 mmol) and boric anhydride (0.15 g, 2.1 mmol) were dissolved in EtOAc (3.0 mL). The solution was stirred for 30 min at 40 °C before 3,4-Dimethoxybenzaldehyde (1.0 g, 6.0 mmol) and tributyl borate (1.64 mL, 6.0 mmol) were added and stirred for 30 min at 40 °C. *n*-

Butylamine (0.45 mL, 4.5 mmol) was dissolved in EtOAc (3.0 mL), and added dropwise over 15 min. The reaction mixture stirred for 24 h at 40 °C, at which point it was quenched by the addition of 4N HCl (10 mL). The mixture was stirred at 60 °C for 30 min, and then the aqueous layer extracted with EtOAc (3 x 50 mL). The combined organic layers were washed with saturated aqueous NaHCO₃ and saturated aqueous NaCl, dried (Na₂SO₄), filtered, and concentrated. The residue was purified by flash chromatography (SiO₂, 2:3 EtOAc in hexanes, then 3:2 EtOAc in hexanes) to afford **30** (438.1 mg, 37%) as a yellow amorphous solid: ¹H NMR (CDCl₃, 500 MHz) δ 3.86 (d, *J* = 6.20 Hz, 12H), 5.76 (s, 1H), 6.43 (d, *J* = 15.8 Hz, 2H), 6.81 (d, *J* = 8.35 Hz, 2H), 7.01 (d, *J* = 1.85 Hz, 2H), 7.08 (dd, *J* = 1.90 Hz, 8.30 Hz, 2H), 7.54 (d, *J* = 15.8 Hz, 2H); ¹³C NMR (CDCl₃, 125 MHz) δ 55.9 (2C), 56.0 (2C), 77.3, 101.4 (2C), 109.6 (2C), 111.1 (2C), 122.0, 122.7, 128.0 (2C), 140.4 (2C), 149.2 (2C), 151.0 (2C), 183.3 (2C); IR (film) *v*_{max} 3001, 2959, 2934, 2912, 2837, 1624, 1582, 1556, 1512, 1462, 1454, 1441, 1421, 1339, 1300, 1263, 1232, 1198, 1159, 1136, 1022, 966 cm⁻¹; HRMS (ES⁺) *m/z*: [M + H] calcd for C₂₃H₂₄O₆ 397.1651; found 397.1640.



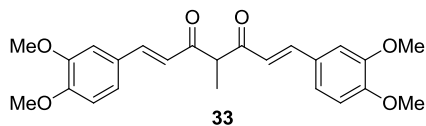
(E)-Ethyl 7-(4-hydroxy-3-methoxyphenyl)-4-((E)-3-(4-hydroxy-3-methoxyphenyl)acryloyl)-5-oxohept-6-enoate (31). Compound **31** was prepared following the same procedure used in the preparation of compound **30**. The residue was purified by flash chromatography (SiO₂, 5:3:2 Hexanes:EtOAc:CH₂Cl₂) to afford **31** (490.0 mg, 32%) as an orange amorphous solid: ¹H NMR (CDCl₃, 500 MHz) δ 1.18 (t, *J* = 9.5 Hz, 3H), 2.48 (t, *J* = 8 Hz, 2H), 2.87 (t, *J* = 9.5 Hz, 2H), 3.90 (s, 6H), 4.06 (q, *J* = 7.15Hz, 2H), 5.82 (s, 2H), 6.87 (s, 1H), 6.88-6.89 (m, 2H), 6.92 (s, 1H),

7.02 (d, $J = 2$ Hz, 2H), 7.10 (d, $J = 8.25$ Hz, 2H), 7.64 (d, $J = 15.3$ Hz, 2H); ^{13}C NMR (CDCl_3 , 125 MHz) δ 14.2, 21.7, 36.6, 56.0 (2C), 60.7, 109.5, 110.1 (2C), 114.9 (2C), 117.8 (2C), 122.9 (2C), 128.0 (2C), 142.2 (2C), 146.8 (2C), 147.9 (2C), 173.0, 182.9 (2C); IR(film) ν_{max} 3400, 3074, 2961, 2926, 2852, 2400, 1722, 1663, 1618, 1587, 1514, 1454, 1429, 1393, 1377, 1275, 1207, 1186, 1161, 1124, 1101, 1032, 976, 945 cm^{-1} ; HRMS (ES^+) m/z : $[\text{M} + \text{Na}]$ calcd for $\text{C}_{26}\text{H}_{28}\text{O}_8$ 491.1682; found 491.1677.

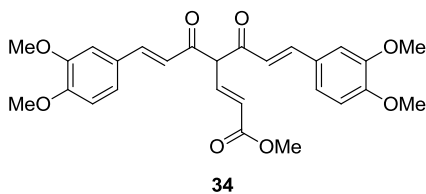


(E)-Ethyl-7-(3,4-dimethoxyphenyl)-4-((E)-3-(3,4-dimethoxyphenyl)acryloyl)-5-oxohept-6-enoate (32). Compound **32** was prepared following the same procedure used in the preparation of compound **30**. The residue was purified by flash chromatography (SiO_2 , 5:3:2 Hexanes:EtOAc: CH_2Cl_2) to afford **32** (351.1 mg, 23%) as a yellow amorphous solid: ^1H NMR (CDCl_3 , 500 MHz) As a mixture of tautomers: δ 1.26 (t, $J = 7.2$ Hz, 3H), 1.26 (t, $J = 7.2$ Hz, 3H), 2.36 (t, $J = 6.9\text{Hz}$, 2H), 2.40 (t, $J = 6.9$, 2H), 2.57 (t, $J = 7.4\text{Hz}$, 2H), 2.97 (t, $J = 7.3\text{Hz}$, 2H), 3.93 (12H), 3.97 (12H), 4.15 (q, $J = 7.1\text{Hz}$, 2H), 4.15 (q, $J = 7.1\text{Hz}$, 2H), 4.26 (t, $J = 7.1\text{Hz}$, 1H), 6.73 (d, $J = 15.9\text{Hz}$, 2H), 6.87 (d, $J = 8.3\text{Hz}$, 2H), 6.90 (d, $J = 8.3\text{Hz}$, 2H), 7.01 (d, $J = 15.3\text{Hz}$, 2H), 7.07 (d, $J = 1.8\text{Hz}$, 2H), 7.14 (d, $J = 1.7\text{Hz}$, 2H), 7.16 (dd, $J_1 = 8.4\text{Hz}$, $J_2 = 1.8\text{Hz}$, 2H), 7.20 (dd, $J_1 = 8.4\text{Hz}$, $J_2 = 1.6\text{Hz}$, 2H), 7.67 (d, $J = 15.9\text{Hz}$, 2H), 7.74 (d, $J = 15.3\text{Hz}$, 2H); ^{13}C NMR (CDCl_3 , 125 MHz) As a mixture of tautomers δ 14.1, 14.2, 23.3, 29.7, 31.6, 36.6, 56.0 (4C), 60.6 (2C), 63.5, 108.9, 109.6, 109.9, 110.2, 110.4, 111.0 (2C), 111.1 (2C), 118.0, 121.7 (2C), 122.7 (2C), 123.9, 126.9 (2C), 127.1 (3C), 128.4 (2C), 142.1, 145.0, 149.2 (4C), 151.1 (2C), 151.8 (2C), 172.9 (2C), 182.9, 190.9, 194.9 (2C); IR (film) ν_{max} 3061, 2959, 2930, 2853, 2617, 2357,

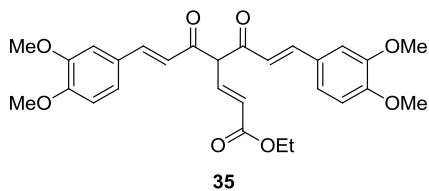
2029, 1732, 1681, 1666, 1639, 1593, 1574, 1556, 1514, 1504, 1454, 1444, 1421, 1377, 1339, 1308, 1263, 1231, 1186, 1161, 1138, 1109, 1022, 984, 945 cm^{-1} ; HRMS (ES^+) m/z : $[\text{M} + \text{Na}]$ calcd for $\text{C}_{28}\text{H}_{32}\text{O}_8$ 519.1995; found 519.1944.



(1E,6E)-1,7-Bis(3,4-dimethoxyphenyl)-4-methylhepta-1,6-diene-3,5-dione (33). Compound **33** was prepared following the same procedure used in the preparation of compound **30**. The residue was purified by flash chromatography (SiO_2 , 1:1Hexanes:EtOAc) to afford **33** (573.7 mg, 44%) as a dark yellow amorphous solid: ^1H NMR (CDCl_3 , 400 MHz) As a mixture of tautomers: δ 1.51(d, $J = 6.9\text{Hz}$, 3H), 2.19(s, 3H), 3.92-3.96(24H), 6.72(d, $J = 15.9\text{Hz}$, 2H), 6.89(d, $J = 8.4\text{Hz}$, 2H), 6.99(d, $J = 15.3\text{Hz}$, 2H), 7.06(d, $J = 1.68$, 2H), 7.10(s, 2H), 7.16(dd, $J_1 = 8.5$, $J_2 = 1.9$, 2H), 7.19(d, $J = 8.2$, 2H), 7.43(s, 1H), 7.48(dd, $J_1 = 8.1$, $J_2 = 2.2$, 1H), 7.65(d, $J = 16.0\text{Hz}$, 2H), 7.70(d, $J = 15.4$, 2H); ^{13}C NMR (CDCl_3 , 125 MHz) As a mixture of tautomers δ 12.1 29.7, 55.9 (4C), 56.0 (4C), 59.0, 105.7, 109.9, 110.0, 110.1, 110.4, 111.0, 111.0, 111.1, 111.2, 116.6, 118.7 (2C), 121.4 (2C), 122.5, 123.7, 124.4, 127.1 (2C), 128.5, 141.3, 144.7, 146.2 (2C), 149.2 (2C), 149.2 (2C), 151.0 (2C), 151.7, 152.0, 182.5, 191.0, 196.1, 196.8; IR(Film) ν_{max} 3412, 3059, 2999, 2959, 2928, 2853, 2839, 2613, 2598, 2536, 2359, 2035, 1713, 1668, 1591, 1514, 1464, 1454, 1443, 1421, 1377, 1340, 1308, 1265, 1238, 1198, 1161, 1140, 1107, 1045, 1024, 982, 947, 924 cm^{-1} ; HRMS (ES^+) m/z : $[\text{M} + \text{H}]$ calcd for $\text{C}_{24}\text{H}_{26}\text{O}_6$ 411.1808; found 411.1800.

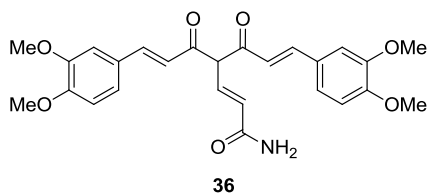


(2E,6E)-Methyl-7-(3,4-dimethoxyphenyl)-4-((E)-(3,4-dimethoxyphenyl)acryloyl)-5-oxohepta-2,6-dienoate (34). Compound **30** (500.0 mg, 1.26 mmol) was dissolved in THF (6.0 mL) and stirred at rt before NaH (45.4 mg, 60% wt in mineral oil, 1.17 mmol) was added. The solution was stirred for 30 min at rt. In a separate flask, methyl propiolate (0.17 mL, 1.95 mmol) was dissolved in THF (9.0 mL) and stirred at room temperature. Contents from the first flask were slowly added via cannula to the methyl propiolate solution over 10 min, and subsequently stirred at rt for 24 h. The reaction was quenched by addition of 5% sulfuric acid (25 mL) and the aqueous layer extracted with EtOAc (3 x 50 mL). The combined organic layers were washed with saturated aqueous NaHCO₃ and saturated aqueous NaCl, dried (Na₂SO₄), filtered, and concentrated. The residue was purified by flash chromatography (SiO₂, 2:3 EtOAc in hexanes, then 3:2 EtOAc in hexanes) to afford **34** (291.0 mg, 53%) as an orange amorphous solid: ¹H NMR (CDCl₃, 500 MHz) δ 3.85 (s, 3H), 3.96 (d, *J* = 1.65, 12H), 6.00 (d, *J* = 11.7 Hz, 1H), 6.92 (d, *J* = 11.7 Hz, 2H), 7.00 (d, *J* = 11.6 Hz, 2H), 7.09 (s, 2H), 7.22 (d, *J* = 6.15 Hz, 2H), 7.79 (d, *J* = 11.6 Hz, 2H), 7.93 (d, *J* = 11.7 Hz, 1H); ¹³C NMR (CDCl₃, 125 MHz) δ 51.8, 56.02 (2C), 56.04 (2C), 109.9, 110.0 (2C), 110.5 (2C), 111.2 (2C), 118.8, 121.9, 123.0, 128.0 (2C), 139.3 (2C), 143.0, 149.3 (2C), 151.5 (2C), 167.3, 183.8 (2C); IR (film) ν_{max} 2999, 2949, 2935, 2910, 2837, 2604, 2359, 1715, 1614, 1597, 1580, 1508, 1437, 1420, 1342, 1308, 1261, 1225, 1190, 1161, 1138, 1022, 1001, 982, 964, 932 cm⁻¹; HRMS (ES⁺) *m/z*: [M + Na] calcd for C₂₇H₂₈O₈ 503.1682; found 503.1667.



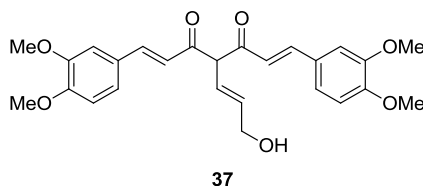
(2E,6E)-Ethyl-7-(3,4-dimethoxyphenyl)-4-((E)-3-(3,4-dimethoxyphenyl)acryloyl)-5-

oxohepta-2,6-dienoate (35). Compound **35** was prepared following the same procedure used in the preparation of compound **34**. The residue was purified by flash chromatography (SiO₂, 1:199 MeOH in CH₂Cl₂, then 1:66 MeOH in CH₂Cl₂) to afford **35** (636.0 mg, 94.4%) as a red amorphous solid: ¹H NMR (CDCl₃, 500 MHz) δ 1.35 (t, *J* = 7.16 Hz, 3H), 3.95 (s, 12H), 4.30 (q, *J* = 7.12 Hz, 2H), 5.98 (d, *J* = 15.64 Hz, 1H), 6.91 (d, *J* = 8.34 Hz, 2H), 7.00 (d, *J* = 15.42 Hz, 2H), 7.09 (d, *J* = 1.84 Hz, 2H), 7.21 (dd, *J* = 1.84, 8.34 Hz, 2H), 7.78 (d, *J* = 15.42 Hz, 2H), 7.91 (d, *J* = 15.64 Hz, 1H); ¹³C NMR (CDCl₃, 125 MHz) δ 14.6, 56.17 (2C), 56.24 (2C), 60.8, 110.2 (3C), 110.5 (2C), 111.4 (2C), 119.2, 122.7, 123.3, 128.3 (2C), 139.2 (2C), 143.1, 149.5 (2C), 151.6 (2C), 167.1, 183.9 (2C); IR (film) *v*_{max} 3061, 2978, 2961, 2935, 2907, 2872, 2837, 2598, 2033, 1715, 1614, 1595, 1580, 1512, 1464, 1443, 1421, 1367, 1308, 1265, 1161, 1140, 1097, 1024, 976cm⁻¹; HRMS (ES⁺) *m/z*: [M + Na] calcd for C₂₈H₃₀O₈ 517.1838; found 517.1826.



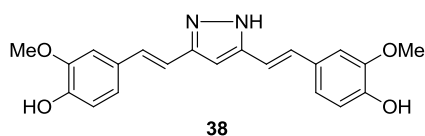
(2E,6E)-7-(3,4-Dimethoxyphenyl)-4-((E)-3-(3,4-dimethoxyphenyl)acryloyl)-5-oxohepta-2,6-dienamide (36). Concentrated aqueous ammonia (6.5 mL) was cooled in a dry ice-isopropyl alcohol bath. Methyl propiolate (2.0 mL, 22.4 mmol) was added dropwise, and after 10 min, the organic layer was extracted with EtOAc (3 x 5 mL), dried over Na₂SO₄, and concentrated, affording crystalline propiolamide (quantitative). Compound **30** (600.0 mg, 1.52 mmol) was dissolved in THF (10.0 mL) and stirred at rt before NaH (54.52 mg, 60% wt in mineral oil, 1.36 mmol) was added. The solution was stirred for 30 min at rt. In a separate flask, propiolamide (209.3 mg, 3.03 mmol) was dissolved in THF (6.0 mL) and stirred at rt. Contents from the first

flask were slowly added via cannula to the propiolamide solution over 10 min, and subsequently stirred at rt for 24 h. The reaction was quenched by addition of 5% sulfuric acid (25 mL) and the aqueous layer extracted with EtOAc (3 x 50 mL). The combined organic layers were washed with saturated aqueous NaHCO₃ and saturated aqueous NaCl, dried (Na₂SO₄), filtered, and concentrated. The residue was recrystallized from EtOAc/hexanes to afford **36** (557.7 mg, 88%) as an orange amorphous solid: ¹H NMR (CDCl₃, 500 MHz) δ 3.94 (d, *J* = 1.9 Hz, 12H), 5.45 (s, -NH₂), 5.95 (d, *J* = 15.2 Hz, 1H), 6.90 (d, *J* = 8.4 Hz, 2H), 6.98 (d, *J* = 15.4 Hz, 2H), 7.07 (d, *J* = 1.9 Hz, 2H), 7.21 (dd, *J* = 1.9, 8.4 Hz, 2H), 7.76 (d, *J* = 15.4 Hz, 2H), 7.90 (d, *J* = 15.2 Hz, 1H); ¹³C NMR (CDCl₃, 125 MHz) δ 55.9 (2C), 56.0 (2C), 110.1 (3C), 110.3 (2C), 111.1 (2C), 118.8, 122.9, 124.1, 128.0 (2C), 137.2 (2C), 142.6, 149.2 (2C), 151.3 (2C), 166.9, 183.4 (2C); IR (film) ν_{max} 3412, 3323, 3292, 3215, 2999, 2943, 2837, 1663, 1614, 1597, 1582, 1510, 1466, 1441, 1421, 1385, 1342, 1308, 1263, 1225, 1161, 1140, 1111, 1020, 1001, 978, 966cm⁻¹; HRMS (ES⁻) *m/z*: [M – H] calcd for C₂₆H₂₇NO₇ 464.1709; found 464.1731.



(1E,6E)-1,7-Bis(3,4-dimethoxyphenyl)-4-((E)-3-hydroxyprop-1-enyl)hepta-1,6-diene-3,5-dione (37). Compound **35** (500.0 mg, 1.0 mmol) was dissolved in CH₂Cl₂ (10.0 mL) and cooled to -78 °C before ^tBu₂AlH (3.0 mL, 1M in CH₂Cl₂, 3.0 mmol) was added drop wise. After 30 min, the solution was warmed to rt and stirred for an additional 1.5 h. The solution was quenched using saturated aqueous sodium potassium tartrate (Rochelle's salt) and the aqueous layer extracted with CH₂Cl₂ (3 x 50 mL). The combined organic layers were washed with saturated aqueous NaCl, dried (Na₂SO₄), and concentrated. The residue was purified by flash

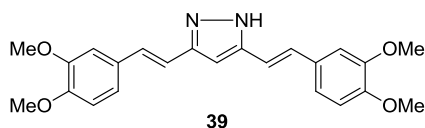
chromatography (SiO₂, 1:5:9:10 MeOH:CH₂Cl₂:EtOAc:hexanes) to afford **37** (301.3 mg, 66%) as a red amorphous solid: ¹H NMR (CDCl₃, 500 MHz) δ 3.92 (d, *J* = 3.9 Hz, 12H), 4.40 (d, *J* = 4.6 Hz, 2H), 5.88 (dt, *J* = 5.7, 15.6 Hz, 1H), 6.58 (dt, *J* = 1.4, 15.6 Hz, 1H), 6.87 (d, *J* = 8.3 Hz, 2H), 6.97 (d, *J* = 15.6 Hz, 2H), 7.05 (d, *J* = 1.8 Hz, 2H), 7.16 (dd, *J* = 1.8, 8.4 Hz, 2H), 7.67 (d, *J* = 15.6 Hz, 2H); ¹³C NMR (CDCl₃, 125 MHz) δ 55.94, 55.98, 56.0 (2C), 63.6, 110.4, 111.0 (2C), 111.1 (2C), 111.5 (2C), 119.7, 122.5, 124.2, 128.4 (2C), 136.5 (2C), 141.2, 149.2 (2C), 151.0 (2C), 182.5 (2C); IR (film) *v*_{max} 3458, 3443, 2997, 2926, 2874, 2853, 2835, 1620, 1595, 1580, 1556, 1510, 1464, 1454, 1435, 1421, 1337, 1306, 1261, 1192, 1159, 1138, 1094, 1022, 959, 930cm⁻¹; HRMS (ES⁻) *m/z*: [M – H] calcd for C₂₆H₂₈O₇ 451.1757; found 451.1766.



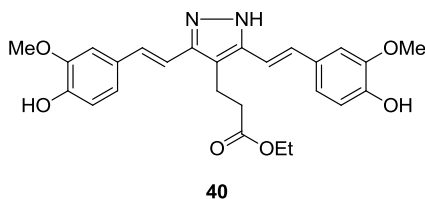
4,4'-(1E,1'E)-2,2'-(1-H-Pyrazole-3,5-diyl)bis(ethene-2,1-diyl)bis(2-methoxyphenol) (38).

Compound **27** (300.0 mg, 0.81 mmol) was dissolved in absolute EtOH (5.0 mL). Hydrazine hydrochloride (66.9 mg, 0.984 mmol) was added followed by a catalytic amount of glacial acetic acid (1.0 mL). The solution stirred at reflux for 40 h. The crude reaction mixture was concentrated in vacuo and re-dissolved in EtOAc (200 mL). The organic layer was washed with saturated aqueous NaHCO₃ and saturated NaCl, dried (Na₂SO₄), filtered, and concentrated in vacuo. The residue was purified by column chromatography (SiO₂, 5:3:2 hexanes:EtOAc:CH₂Cl₂) to afford compound **38** (262.0 mg, 87%) as a dark orange amorphous solid: ¹H NMR (CDCl₃ w/MeOD, 500 MHz) δ 3.79 (s, 6H), 6.43 (s, 1H), 6.72 (s, 2H), 6.73 (s, 1H), 6.75 (s, 1H), 6.85 (dd, *J*₁ = 8.2Hz, *J*₂ = 1.8Hz, 2H), 6.90(d, *J* = 8.3 Hz, 2H), 6.92(d, *J* = 6.4Hz, 2H); ¹³C NMR (CDCl₃ w/MeOD, 125 MHz) δ 55.4 (2C), 98.8, 108.6 (2C), 114.8 (2C), 115.3 (2C), 120.1 (2C), 127.6 (2C), 128.8 (2C), 130.5 (2C), 146.1 (2C), 147.3 (2C); IR (film)

ν_{max} 3383, 2359, 2341, 2332, 1593, 1558, 1512, 1456, 1429, 1277, 1259, 1231, 1211, 1155, 1122 cm^{-1} ; HRMS(ES^+) m/z : $[\text{M}+\text{H}]$ calcd for $\text{C}_{21}\text{H}_{20}\text{N}_2\text{O}_4$ 365.1505; found 365.1484.

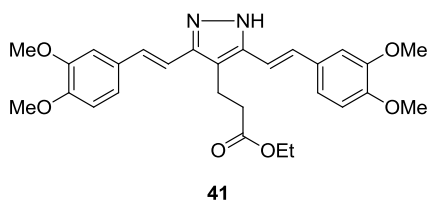


3,5-Bis(3,4-dimethoxystyryl)-1-*H*-pyrazole (39). Compound **39** was prepared following the same procedure used in the preparation of compound **38**. The residue was purified by flash chromatography (SiO_2 , 2:3:5 (CH_2Cl_2 , EtOAc, hexanes)) to afford **39** (54.0 mg, 90%) as a yellow-orange amorphous solid: ^1H NMR (CDCl_3 , 500 MHz) δ 3.85 (d, $J = 15.5$ Hz, 12H), 6.62 (s, 1H), 6.74 (d, $J = 8.10$ Hz, 2H), 6.95 (m, 6H), 7.05 (d, $J = 16.5$ Hz, 2H); ^{13}C NMR (CDCl_3 , 125 MHz) δ 55.6 (2C), 55.8 (2C), 99.4, 99.9 (2C), 108.5 (2C), 111.0 (2C), 115.8 (2C), 119.9 (2C), 129.6 (2C), 130.6 (2C), 149.0 (2C), 149.1 (2C); IR (film) ν_{max} 3331, 3177, 3126, 3078, 3065, 2999, 2959, 2934, 2910, 2835, 1599, 1583, 1558, 1514, 1464, 1441, 1420, 1331, 1311, 1265, 1196, 1157, 1138, 1103, 1024, 960cm^{-1} ; HRMS (ES^+) m/z : $[\text{M} + \text{H}]$ calcd for $\text{C}_{23}\text{H}_{24}\text{N}_2\text{O}_4$ 393.1814; found 393.1801.

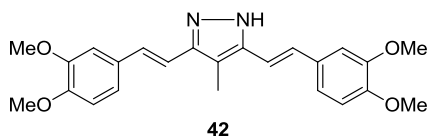


Ethyl 3-(3,5-bis(4-hydroxy-3-methoxystyryl)-1-*H*-pyrazol-4-yl)propanoate (40). Compound **40** was prepared following the same procedure used in the preparation of compound **38**. The residue was purified by flash chromatography (SiO_2 , 5:3:2 Hexanes:EtOAc: CH_2Cl_2) to afford **40** (63.5 mg, 81%) as a yellow-orange amorphous solid: ^1H NMR (CDCl_3 , 500 MHz) δ 1.23 (t, $J = 7.1$ Hz, 3H), 2.57 (t, $J = 7.8$ Hz, 2H), 3.01 (t, $J = 7.8$ Hz, 2H), 3.83 (s, 6H), 4.12 (q, $J = 7.2$ Hz, 2H), 6.82 (d, $J = 16.6$ Hz, 2H), 6.85 (d, $J = 8.3$ Hz, 2H), 6.89 (d, $J = 1.5$ Hz, 2H), 6.93 (dd, $J_1 =$

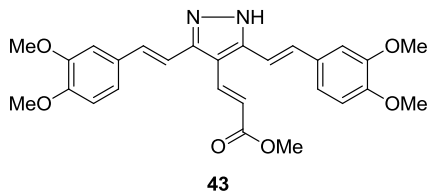
8.2 Hz, $J_2 = 1.6$ Hz, 2H), 7.06 (d, $J = 16.5$ Hz, 2H); ^{13}C NMR (CDCl_3 , 125 MHz) δ 14.2, 18.8, 35.5, 55.8 (2C), 60.6, 108.4 (2C), 113.9, 114.6 (2C), 115.3 (2C), 120.5 (2C), 129.4 (2C), 130.1 (2C), 144.0 (2C), 145.9 (2C), 146.8 (2C), 173.0; IR(Film) ν_{max} 3323, 3041, 3034, 2957, 2924, 2851, 2320, 1724, 1661, 1593, 1556, 1514, 1464, 1429, 1375, 1277, 1238, 1205, 1159, 1124, 1099, 1068, 1034, 962 cm^{-1} ; HRMS (ES^+) m/z : $[\text{M} + \text{H}]$ calcd for $\text{C}_{26}\text{H}_{28}\text{N}_2\text{O}_6$ 465.2026; found 465.2005.



Ethyl 3-(3,5-bis(3,4-dimethoxystyryl)-1-*H*-pyrazol-4-yl)propanoate (41). Compound **41** was prepared following the same procedure used in the preparation of compound **38**. The residue was purified by flash chromatography (SiO_2 , 5:3:2 Hexanes:EtOAc: CH_2Cl_2) to afford **41** (43.0 mg, 73%) as a yellow-orange amorphous solid: ^1H NMR (CDCl_3 , 500 MHz) δ 1.23 (t, $J = 7.1$ Hz, 3H), 2.58 (t, $J = 7.7$ Hz, 2H), 3.03 (t, $J = 7.8$ Hz, 2H), 3.87 (12H), 4.12 (q, $J = 4.1$ Hz, 2H), 6.77 (m, 2H), 6.85 (m, 2H), 6.93 (d, $J = 8.25$ Hz, 2H), 6.97 (s, 2H), 7.07 (m, 2H); ^{13}C NMR (CDCl_3 , 125 MHz) 14.2, 18.8, 35.6, 55.9 (4C), 60.6, 108.2 (2C), 111.1, 114.3 (2C), 115.4 (2C), 120.1 (2C), 129.3 (2C), 129.7 (2C), 129.9 (2C), 149.1 (2C), 149.1 (2C), 173.0; IR (Film) ν_{max} 3333, 3173, 3078, 3030, 2957, 2924, 2851, 1728, 1666, 1601, 1583, 1556, 1514, 1464, 1443, 1420, 1373, 1335, 1265, 1234, 1159, 1138, 1095, 1068, 1026, 962 cm^{-1} ; HRMS (ES^+) m/z : $[\text{M} + \text{H}]$ calcd for $\text{C}_{28}\text{H}_{32}\text{N}_2\text{O}_6$ 493.2339; found 493.2321.

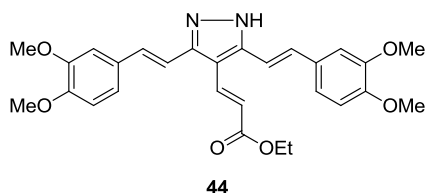


3,5-Bis(3,4-dimethoxystyryl)-4-methyl-1-*H*-pyrazole (42). Compound **42** was prepared following the same procedure used in the preparation of compound **38**. The residue was purified by flash chromatography (SiO₂, 2:3:5 (CH₂Cl₂, EtOAc, hexanes)) to afford **42** (60.8 mg, 58%) as a yellow-orange amorphous solid: ¹H NMR (CDCl₃, 500 MHz) δ 2.22 (s, 3H), 3.82 (s, 6H), 3.82 (s, 6H), 6.73 (d, 2H, *J* = 8.8Hz), 6.81 (d, 2H, *J* = 16.5Hz), 6.92 (m, 4H), 6.97 (d, 2H, *J* = 16.5Hz); ¹³C NMR (CDCl₃, 125 MHz) δ 9.1, 55.8 (2C), 55.9 (2C), 108.6, 108.7 (2C), 111.1 (2C), 112.2 (2C), 115.1 (2C), 119.9 (2C), 129.5 (2C), 130.1 (2C), 149.1 (2C), 149.1 (2C); IR(Film) *v*_{max} 3416, 3240, 3229, 3111, 2999, 2957, 2932, 2835, 2359, 1636, 1601, 1514, 1464, 1420, 1333, 1265, 1238, 1159, 1138, 1024, 960 cm⁻¹; HRMS (ES⁺) *m/z*: [M + H] calcd for C₂₄H₂₆N₂O₄ 407.1971; found 407.1954.

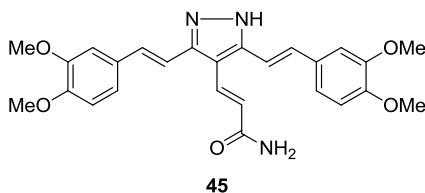


(*E*)-Methyl 3-(3,5-bis(3,4-dimethoxystyryl)-1-*H*-pyrazol-4-yl)acrylate (43). Compound **43** was prepared following the same procedure used in the preparation of compound **38**. The residue was purified by flash chromatography (SiO₂, 1:1 Hexanes:EtOAc) to afford **43** (43.3 mg, 15%) as a yellow-orange amorphous solid: ¹H NMR (CDCl₃, 500 MHz) δ 3.76 (s, 3H), 3.83 (s, 6H), 3.84 (s, 6H), 6.15 (d, *J* = 16.0Hz, 1H), 6.75 (d, *J* = 8.1Hz, 2H), 6.86 (d, *J* = 16.3Hz, 2H), 6.93 (d, *J* = 2.5Hz, 2H), 6.95 (d, *J* = 1.7Hz, 2H), 7.09 (d, *J* = 16.3, 2H), 7.81 (d, *J* = 16.0Hz, 2H); ¹³C NMR (CDCl₃, 125 MHz) δ 51.7, 56.0 (4C), 109.0 (2C), 111.1, 113.0 (2C), 113.5 (2C), 117.8 (2C), 120.6 (2C), 129.3 (2C), 132.6 (2C), 135.2 (2C), 149.2 (2C), 149.7 (2C), 167.9; IR (Film) *v*_{max} 3317, 2923, 2849, 2837, 1701, 1624, 1601, 1582, 1514, 1464, 1437, 1420, 1310, 1265, 1198,

1159, 1138, 1024, 960, 933 cm^{-1} ; HRMS (ES^+) m/z : $[\text{M} + \text{H}]$ calcd for $\text{C}_{27}\text{H}_{28}\text{N}_2\text{O}_6$ 477.2026; found 477.1993.

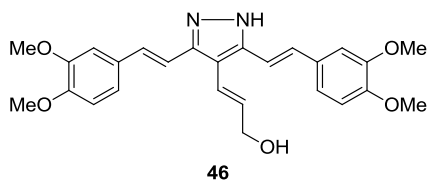


(E)-Ethyl-3-(3,5-bis(3,4-dimethoxystyryl)-1-H-pyrazol-4-yl)acrylate (44). Compound **44** was prepared following the same procedure used in the preparation of compound **38**. The residue was purified by flash chromatography (SiO_2 , 1:7.5:15:26.5 MeOH: CH_2Cl_2 :EtOAc:hexanes) to afford **44** (37.5 mg, 76%) as a yellow-orange amorphous solid: ^1H NMR (CDCl_3 , 500 MHz) δ 1.35 (t, $J = 7.15$ Hz, 3H), 3.93 (d, $J = 8.30$ Hz, 12H), 4.29 (q, $J = 7.15$ Hz, 2H), 6.23 (d, $J = 16.0$ Hz, 1H), 6.86 (d, $J = 8.20$ Hz, 2H), 6.96 (d, $J = 16.3$ Hz, 2H), 7.04 (d, $J = 1.80$ Hz, 2H), 7.06 (dd, $J = 1.80, 8.25$ Hz, 2H), 7.17 (d, $J = 16.3$ Hz, 2H), 7.89 (d, $J = 16.0$ Hz, 2H); ^{13}C NMR (CDCl_3 , 125 MHz) 14.4, 55.90 (2C), 55.92 (2C), 60.5, 108.9 (2C), 111.1 (2C), 113.0, 113.6, 118.3 (2C), 120.5 (2C), 129.2 (2C), 132.4 (2C), 134.9 (2C), 149.06, 149.11 (2C), 149.6 (2C), 167.5; IR (film) ν_{max} 3321, 2995, 2957, 2935, 2835, 1701, 1684, 1624, 1601, 1583, 1558, 1514, 1464, 1443, 1420, 1394, 1367, 1308, 1263, 1240, 1159, 1140, 1094, 1026, 962cm^{-1} ; HRMS (ES^+) m/z : $[\text{M} + \text{H}]$ calcd for $\text{C}_{28}\text{H}_{30}\text{N}_2\text{O}_6$ 491.2182; found 491.2168.



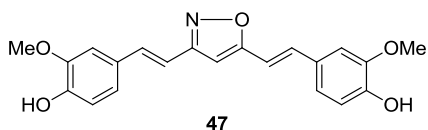
(E)-3-(3,5-bis(3,4-dimethoxystyryl)-1-H-pyrazol-4-yl)acrylamide (45). Compound **45** was prepared following the same procedure used in the preparation of compound **38**. The residue was purified by flash chromatography (SiO_2 , 1:99 MeOH in CH_2Cl_2) to afford **45** (41.7 mg, 84%) as

a yellow-orange amorphous solid: ^1H NMR (CDCl_3 , 500 MHz) δ 3.92 (s, 12H), 5.62 (s, $-\text{NH}_2$), 6.34 (d, $J = 15.6$ Hz, 1H), 6.87 (d, $J = 8.2$ Hz, 2H), 6.92 (d, $J = 16.4$ Hz, 2H), 7.03 (d, $J = 16.4$ Hz, 2H), 7.04 (d, $J = 1.7$ Hz, 2H), 7.10 (dd, $J = 1.7, 8.2$ Hz, 2H), 7.60 (d, $J = 15.6$ Hz, 1H); ^{13}C NMR (CDCl_3 , 125 Hz) δ 55.88 (2C), 55.98 (2C), 105.4 (2C), 109.6 (2C), 111.0 (2C), 111.1(2C), 111.2, 117.1 (2C), 120.1, 122.3 (2C), 127.4 (2C), 142.5 (2C), 149.1 (2C), 150.8, 168.0; IR (film) ν_{max} 3339, 3325, 3198, 3186, 2999, 2957, 2935, 2912, 2835, 1717, 1668, 1634, 1595, 1514, 1464, 1441, 1420, 1394, 1337, 1308, 1265, 1186, 1159, 1140, 1024, 978, 968; HRMS (ES^+) m/z : [M + H] calcd for $\text{C}_{26}\text{H}_{27}\text{N}_3\text{O}_5$ 462.2029; found 462.2010.



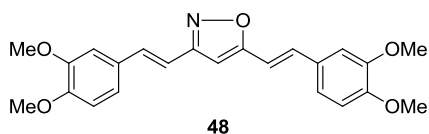
(E)-3-(3,5-Bis(3,4-dimethoxystyryl)-1-*H*-pyrazol-4-yl)prop-2-en-1-ol (46). Compound **44** (80.0 mg, 0.16 mmol) was dissolved in anhydrous MeOH (5.0 mL) and stirred at rt. NaBH_4 (61.7 mg, 1.6 mmol) was added and the solution stirred at reflux. After 1 h, additional NaBH_4 (61.7 mg, 1.6 mmol) was added, and the solution stirred at reflux for 15.5 h. The reaction was quenched by the addition of H_2O , resulting in the formation of a white solid. The precipitate was dissolved by the addition of 10% HCl (10 mL) and the aqueous layer was extracted with CH_2Cl_2 (3 x 20 mL). The combined organic layers were washed with saturated aqueous NaHCO_3 and saturated aqueous NaCl, dried (Na_2SO_4), filtered, and concentrated. The residue was purified by flash chromatography (SiO_2 , 1:7.5:15:26.5 MeOH: CH_2Cl_2 :EtOAc:hexanes) to afford **46** (41.0 mg, 83%) as a yellow-orange amorphous solid: ^1H NMR (CDCl_3 , 500 MHz) δ 3.84 (s, 2H), 3.87 (d, $J = 9.7$ Hz, 12H), 6.21 (d, $J = 16.0$ Hz, 1H), 6.76 (d, $J = 8.45$ Hz, 2H), 6.89 (d, $J = 16.3$ Hz, 2H), 6.92 (m, 4H), 7.16 (d, $J = 16.3$ Hz, 2H), 7.87 (d, $J = 16.0$ Hz, 1H); ^{13}C NMR (CDCl_3 , 125 Hz) δ 51.7, 55.84 (2C), 55.87 (2C), 108.8 (2C), 111.0 (2C), 112.9, 113.3, 117.6 (2C), 120.6 (2C),

129.1 (2C), 132.6 (2C), 135.2 (2C), 149.0, 149.6 (2C), 167.9 (2C); IR (film) ν_{max} 3315, 3153, 3059, 2999, 2949, 2935, 2835, 1713, 1626, 1601, 1583, 1514, 1464, 1441, 1421, 1312, 1265, 1198, 1161, 1140, 1097, 1026, 960, 933 cm^{-1} ; HRMS (ES⁺) m/z : [M + H] calcd for C₂₆H₂₈N₂O₅ 449.2076; found 449.2096.

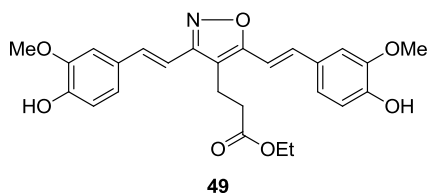


4,4'-(1E,1'E)-2,2'-(isoxazole-3,5-diyl)bis(ethene-2,1-diyl)bis(2-methoxyphenol) (47).

Compound 27 (250 mg, 0.69 mmol) was dissolved in absolute EtOH (5.0 mL). Hydroxylamine hydrochloride (56.6 mg, 0.83 mmol) was added followed by a catalytic amount of glacial acetic acid (750 μL). The solution stirred at reflux for 40 h. The crude reaction mixture was concentrated in vacuo and re-dissolved in EtOAc (200 mL). The organic layer was washed with saturated aqueous NaHCO₃ and saturated NaCl, dried (Na₂SO₄), filtered, and concentrated in vacuo. The residue was purified by column chromatography (SiO₂, 5:3:2 hexanes:EtOAc:CH₂Cl₂) to afford **47** (218.0 mg, 89%) as a dark orange amorphous solid: ¹H NMR (d-DMSO, 500 MHz) δ 3.89 (s, 6H), 6.85 (d, $J = 8.1\text{Hz}$, 1H), 6.87 (d, $J = 8.1\text{Hz}$, 1H), 6.92 (s, 1H), 7.10 (dd, $J_1 = 8.3\text{Hz}$, $J_2 = 1.9\text{Hz}$, 1H), 7.13 (d, $J = 12.4\text{Hz}$, 1H), 7.13 (dd, $J_1 = 8.3\text{Hz}$, $J_2 = 1.8\text{Hz}$, 1H), 7.16 (d, $J = 12.3\text{Hz}$, 1H), 7.33-7.37 (m, 4H), 9.45 (s, 1H), 9.51 (s, 1H); ¹³C NMR (CDCl₃, 125 MHz) δ 55.6, 55.6, 97.8, 109.9, 110.2, 110.3, 112.6, 115.5, 115.5, 121.3, 121.7, 126.9, 127.3, 134.7, 136.4, 147.8, 147.9, 147.9, 148.1, 162.2, 168.3; IR (film) ν_{max} 3402, 2961, 2924, 2851, 2359, 2341, 2332, 1645, 1605, 1593, 1562, 1514, 1464, 1433, 1375, 1279, 1231, 1207, 1188, 1159, 1122, 1032, 960 cm^{-1} ; HRMS (ES⁺) m/z : [M + H] calcd for C₂₁H₁₉NO₅ 366.1342; found 366.1348.

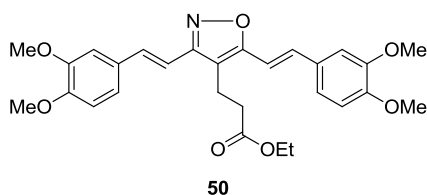


3,5-Bis(3,4-dimethoxystyryl)isoxazole (48). Compound **48** was prepared following the same procedure used in the preparation of compound **47**. The residue was purified by flash chromatography (SiO₂, 2:3:5 (CH₂Cl₂, EtOAc, hexanes)) to afford **48** (54.0 mg, 90%) as a yellow-orange amorphous solid: ¹H NMR (CDCl₃, 500 MHz) δ 3.85 (d, *J* = 2.55 Hz, 6H), 3.88 (d, *J* = 4.20 Hz, 6H), 6.37 (s, 1H), 6.77 (d, *J* = 16.35, 1H), 6.81 (dd, *J* = 3.75, 8.20 Hz, 2H), 6.94 (d, *J* = 16.4 Hz, 1H), 7.03 (m, 5H), 7.23 (d, *J* = 16.4 Hz, 1H); ¹³C NMR (CDCl₃, 125 Hz) δ 55.89, 55.93, 55.98, 56.0, 97.8, 108.6, 108.9, 111.0, 111.1, 114.2 (2C), 120.9, 121.2, 128.6, 128.9, 134.7, 135.4, 149.2 (2C), 149.9, 150.1, 162.2, 168.5; IR (film) *v*_{max} 2995, 2953, 2932, 2916, 2835, 1643, 1599, 1583, 1512, 1504, 1462, 1427, 1416, 1265, 1225, 1159, 1140, 1024, 964cm⁻¹; HRMS (ES⁺) *m/z*: [M + H] calcd for C₂₃H₂₃NO₅ 394.1655; found 394.1649.

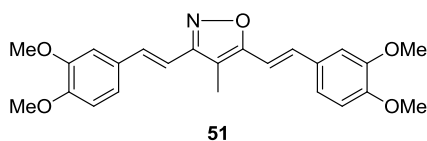


Ethyl 3-(3,5-bis(4-hydroxy-3-methoxystyryl)isoxazol-4-yl)propanoate (49). Compound **49** was prepared following the same procedure used in the preparation of compound **47**. The residue was purified by flash chromatography (SiO₂, 2:3:5 (CH₂Cl₂, EtOAc, hexanes)) to afford **49** (60.7 mg, 76%) as a yellow amorphous solid: ¹H NMR (CDCl₃, 500 MHz) δ 1.23 (t, *J* = 7.2 Hz, 3H), 2.60 (t, *J* = 7.6 Hz, 2H), 2.97 (t, *J* = 7.6 Hz, 2H), 3.96 (s, 6H), 4.13 (q, *J* = 7.2 Hz, 2H), 5.90 (bs, 2H), 6.79 (d, *J* = 16.5 Hz, 1H), 6.80 (d, *J* = 16.3 Hz, 1H), 6.94 (d, *J* = 8.1 Hz, 1H), 6.94 (d, *J* = 8.2 Hz, 1H), 7.05 (d, *J* = 1.8 Hz, 1H), 7.06 (d, *J* = 1.7 Hz, 1H), 7.08 (dd, *J*₁ = 8.3 Hz, *J*₂ = 1.8 Hz, 1H), 7.11 (dd, *J*₁ = 8.3 Hz, *J*₂ = 1.8 Hz, 1H), 7.31 (d, *J* = 16.3 Hz, 1H), 7.37 (d, *J* = 16.5 Hz, 1H)

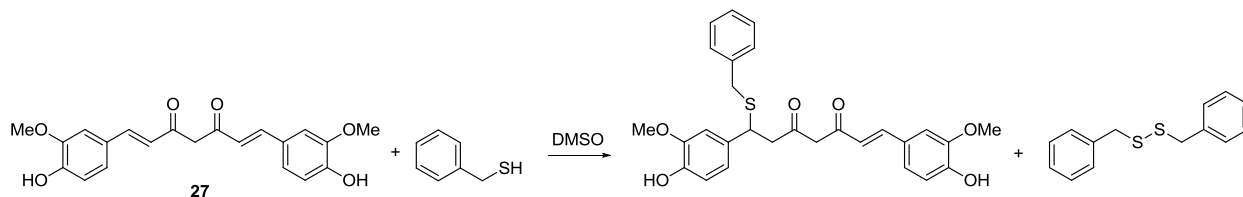
^{13}C NMR (CDCl_3 , 125 MHz) δ 14.2, 17.9, 34.6, 56.0 (2C), 60.9, 108.7, 108.9, 109.4, 112.1, 112.3, 114.7, 114.8 (2C), 121.3, 128.5, 128.8, 133.9, 135.2, 146.7, 146.8, 146.8 (2C), 160.0, 164.7, 172.5; IR(Film) ν_{max} 3499, 3416, 3049, 2962, 2935, 2872, 2853, 2758, 2748, 2644, 2590, 2548, 2311, 2060, 1728, 1634, 1593, 1514, 1450, 1439, 1373, 1275, 1236, 1207, 1184, 1159, 1122, 1095, 1063, 1032, 964, 939 cm^{-1} , HRMS (ES^+) m/z : $[\text{M} + \text{H}]$ calcd for $\text{C}_{26}\text{H}_{27}\text{NO}_7$ 466.1866; found 466.1860.



Ethyl 3-(3,5-bis(3,4-dimethoxystyryl)isoxazol-4-yl)propanoate (50). Compound **50** was prepared following the same procedure used in the preparation of compound **47**. The residue was purified by flash chromatography (SiO_2 , 2:3:5 (CH_2Cl_2 , EtOAc, hexanes)) to afford **50** (64.4 mg, 61%) as a dark yellow amorphous solid: ^1H NMR (CDCl_3 , 500 MHz) δ 1.15 (t, $J = 7.2$ Hz, 3H), 2.52 (t, 7.5 Hz, 2H), 2.91 (t, $J = 7.5$ Hz, 2H), 3.86 (m, 12H), 4.05 (q, $J = 7.15$ Hz, 2H), 6.73 (d, $J = 4.15$ Hz, 1H), 6.75 (d, $J = 4.0$ Hz, 1H), 6.79-6.82 (m, 2H), 7.01-7.06 (m, 4H), 7.21 (d, $J = 19.0$ Hz, 1H), 7.31 (d, $J = 16\text{Hz}$, 1H); ^{13}C NMR (CDCl_3 , 125MHz) δ 14.2, 17.9, 34.6, 56.0, 60.8, 109.0, 109.1, 109.7, 111.1, 111.2, 112.4, 112.5, 120.9, 121.0, 129.0, 133.8, 135.1, 149.2 (2C), 149.9, 150.0, 160.0, 164.7, 172.5; IR (Film) ν_{max} 3541, 3435, 3053, 2959, 2930, 2853, 2839, 2598, 2033, 1728, 1674, 1634, 1591, 1514, 1454, 1443, 1421, 1375, 1339, 1263, 1236, 1159, 1140, 1094, 1063, 1024, 966 cm^{-1} ; HRMS (ES^+) m/z : $[\text{M} + \text{H}]$ calcd for $\text{C}_{28}\text{H}_{31}\text{NO}_7$ 494.2179; found 494.2163.

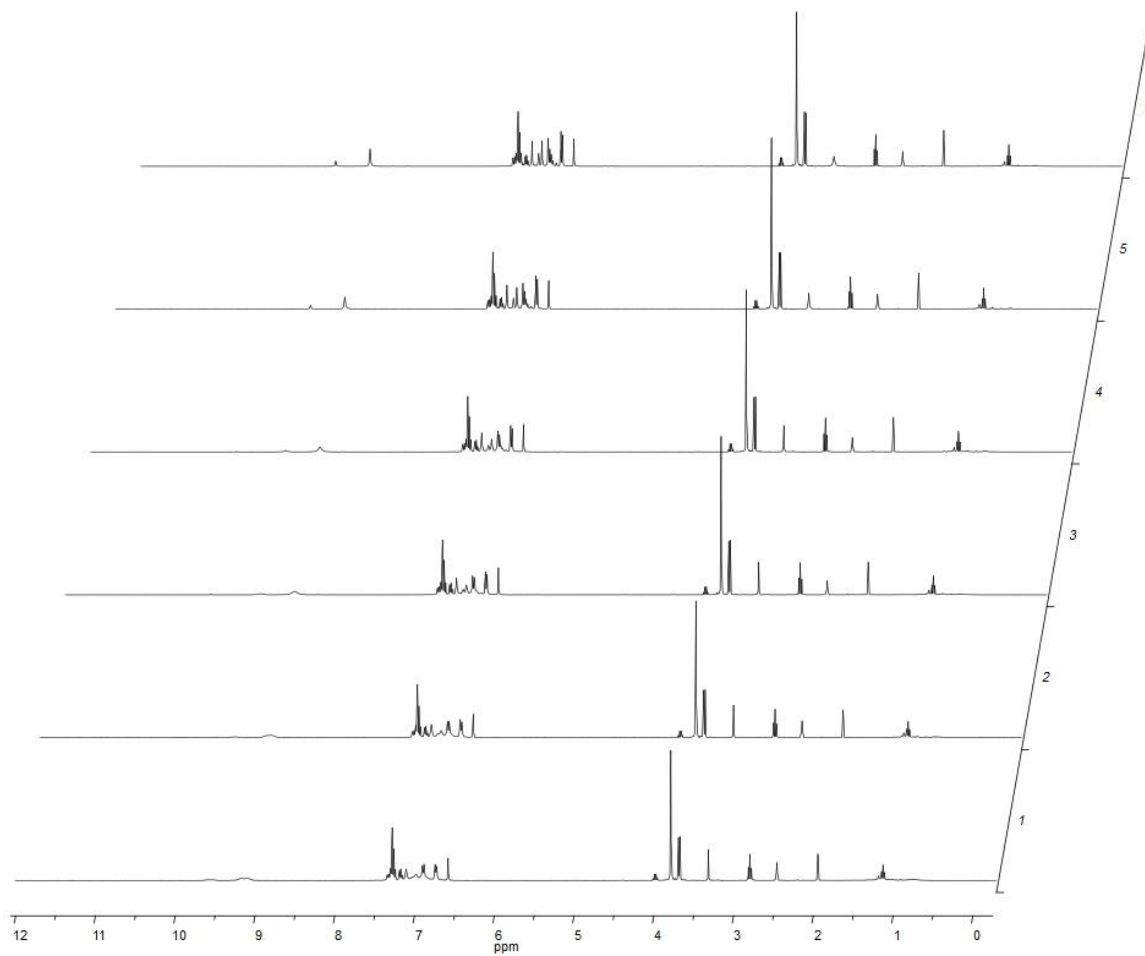
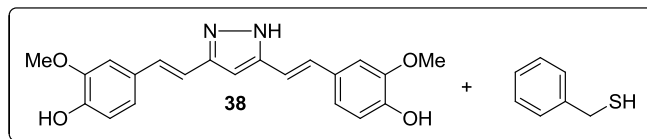


3,5-Bis(3,4-dimethoxystyryl)-4-methylisoxazole (51). Compound **51** was prepared following the same procedure used in the preparation of compound **47**. The residue was purified by flash chromatography (SiO₂, 2:3:5 (CH₂Cl₂, EtOAc, hexanes)) to afford **51** (59.2 mg, 59%) as a yellow-orange amorphous solid: ¹H NMR (CDCl₃, 500 MHz) 2.18 (s, 3H), 3.85 (s, 3H), 3.85 (s, 3H), 3.88 (s, 3H), 3.89 (s, 3H), 6.70 (d, *J* = 16.3Hz, 1H), 6.79-6.83 (3H), 6.99-7.05 (4H), 7.22 (d, *J* = 16.4Hz, 1H), 7.26 (d, *J* = 16.7Hz, 1H); ¹³C NMR (CDCl₃, 125 MHz) δ 29.7, 55.9 (2C), 56.0 (2C), 108.8, 109.0, 109.2, 110.0, 111.1, 111.2, 113.5, 120.8, 129.1, 129.3, 133.2, 134.9, 149.2 (2C), 149.8, 149.9, 160.5, 164.2; IR(Film) *v*_{max} 3541, 3445, 3194, 3051, 2999, 2959, 2930, 2853, 2837, 2600, 2361, 2322, 2280, 2033, 1682, 1645, 1634, 1593, 1514, 1506, 1454, 1441, 1421, 1387, 1339, 1312, 1263, 1236, 1196, 1159, 1138, 1092, 1024, 964 cm⁻¹; HRMS (ES⁺) *m/z*: [M + H] calcd for C₂₄H₂₅NO₅ 408.1811; found 408.1797.

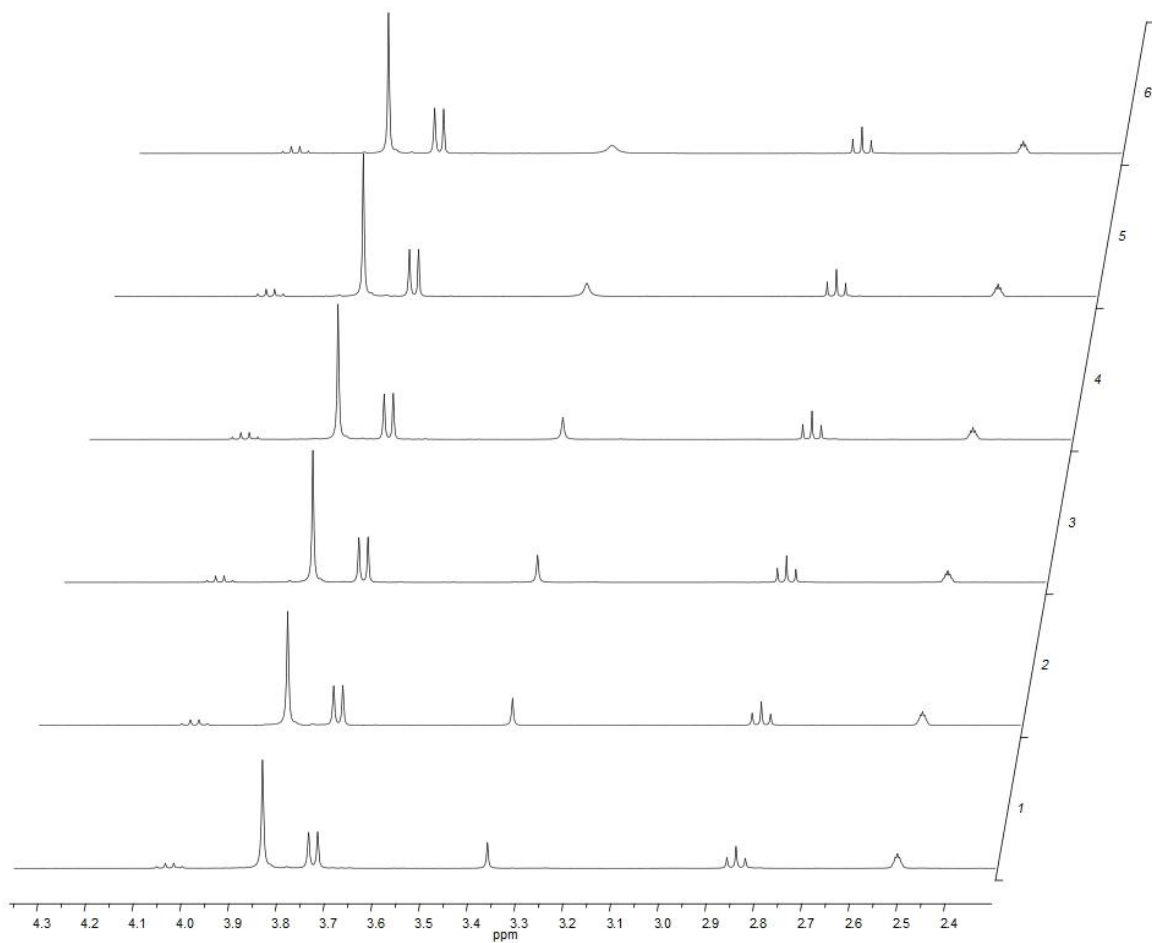


Benzyl Mercaptan Addition Studies. In a 1 dram vial, 15.0 mg curcumin (**27**) (0.041 mmol) was dissolved in 0.60 mL d-DMSO. 4.7 μL of benzyl mercaptan (0.041 mmol) was then added, marking time zero. The contents of the vial were transferred to an NMR tube and ¹H NMR spectra were recorded at set intervals (10 min, 1 h, 5 h, 14 h, and 24 h) to monitor the progress of the reaction. The presence of the benzyl mercaptan-curcumin conjugate was confirmed by HRMS (ES⁺) *m/z*: single addition product: [M + H] calcd for C₂₈H₂₈O₆S 493.1685; found 493.1664; double addition product: [M + Na] 639.1851; found 639.1835. ¹H NMR (d₆-DMSO, 400 MHz) As a mixture of curcumin, benzyl mercaptan and conjugated product: 2.84 (t, *J* = 7.7, 1H), 2.96 (d, *J* = 7.7Hz, 2H), 3.58 (m, 2H), 3.73 (d, *J* = 8Hz, 2H), 3.81 (s, 3H), 3.85 (s, 3H), 3.85

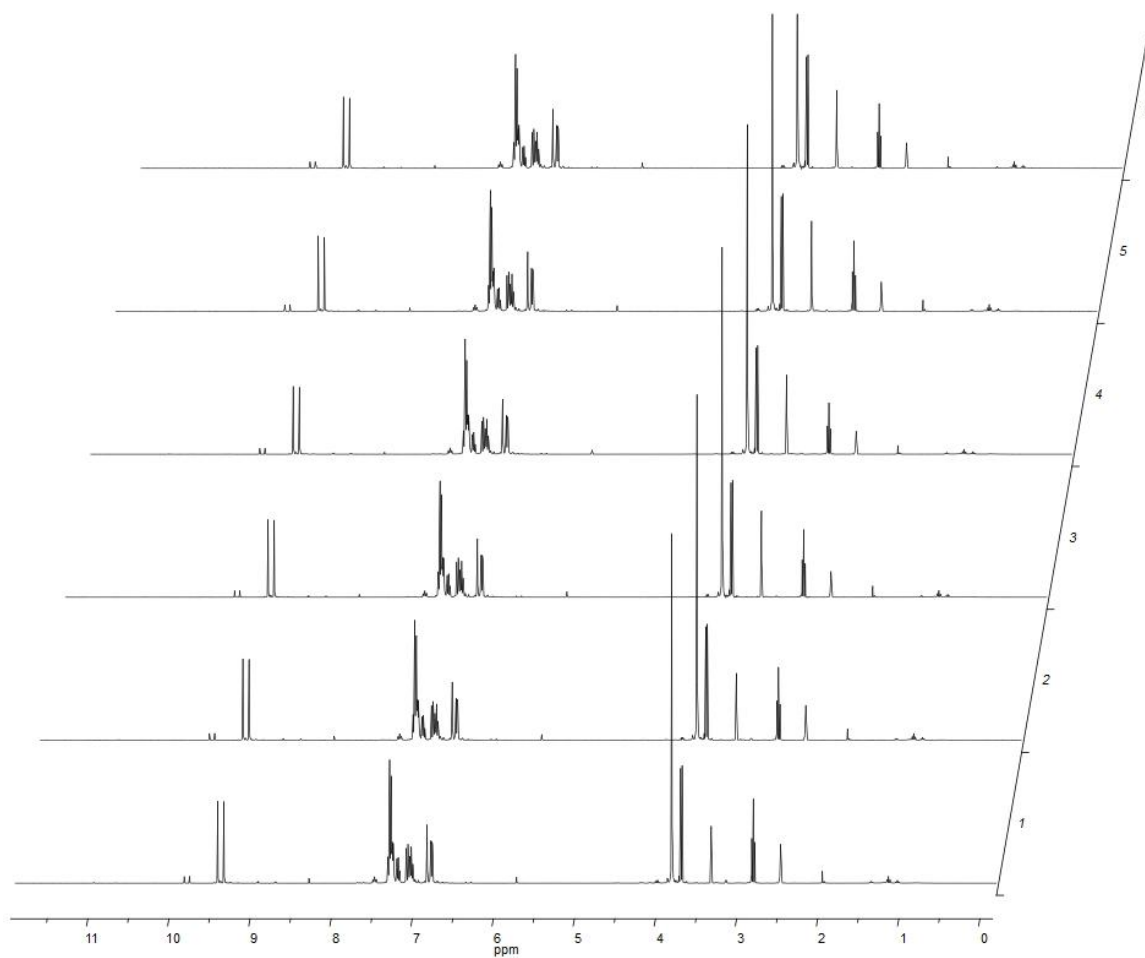
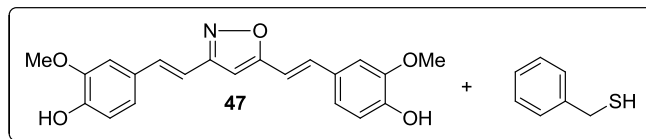
(s, 6H), 4.17 (t, 7.8, 1H), 5.78 (s, 1H), 6.07 (s, 1H), 6.59 (d, $J = 15.9\text{Hz}$, 1H), 6.74 (d, $J = 11.2\text{Hz}$, 2H), 6.77 (d, $J = 15.8\text{Hz}$, 2H), 6.83 (d, $J = 8.2\text{Hz}$, 2H), 7.11 (dd, $J_1 = 1.9$, $J_2 = 8.3$, 2H), 7.16 (dd, $J_1 = 1.9\text{Hz}$, $J_2 = 8.3\text{ Hz}$, 2H), 7.23 (m, 3H), 7.30 (d, $J = 8\text{Hz}$, 2H), 7.32 (m, 5H), 7.46 (d, $J = 15.8\text{Hz}$, 1H), 7.56 (d, $J = 16\text{Hz}$, 2H), 8.97 (s, 1H) 9.68 (s, 2H) 10.07 (s, 1H); ^{13}C NMR (d_6 -DMSO, 500 MHz) δ 34.8, 34.8, 34.8, 43.1, 43.1, 44.0, 48.8, 55.5, 55.6, 79.1, 101.2 101.3, 111.1, 111.5, 111.6, 115.1, 115.6, 119.4, 120.0, 120.1, 120.1, 126.8, 128.3, 128.8, 131.6, 131.7, 131.9, 138.1, 140.5, 145.6, 145.6, 145.7, 147.4, 147.5, 149.3, 156.3, 156.4, 177.5, 190.7, 196.7, 202.1; IR (Film) ν_{max} 3028, 2959, 2930, 2916, 1601, 1574, 1556, 1514, 1494, 1452, 1429, 1367, 1360, 1269, 1236, 1209, 1177, 1153, 1121, 1070, 1032, 916 cm^{-1} . Similar experiments were carried out with the pyrazole and isoxazole derivatives of curcumin, compounds **38** and **47**, respectively:



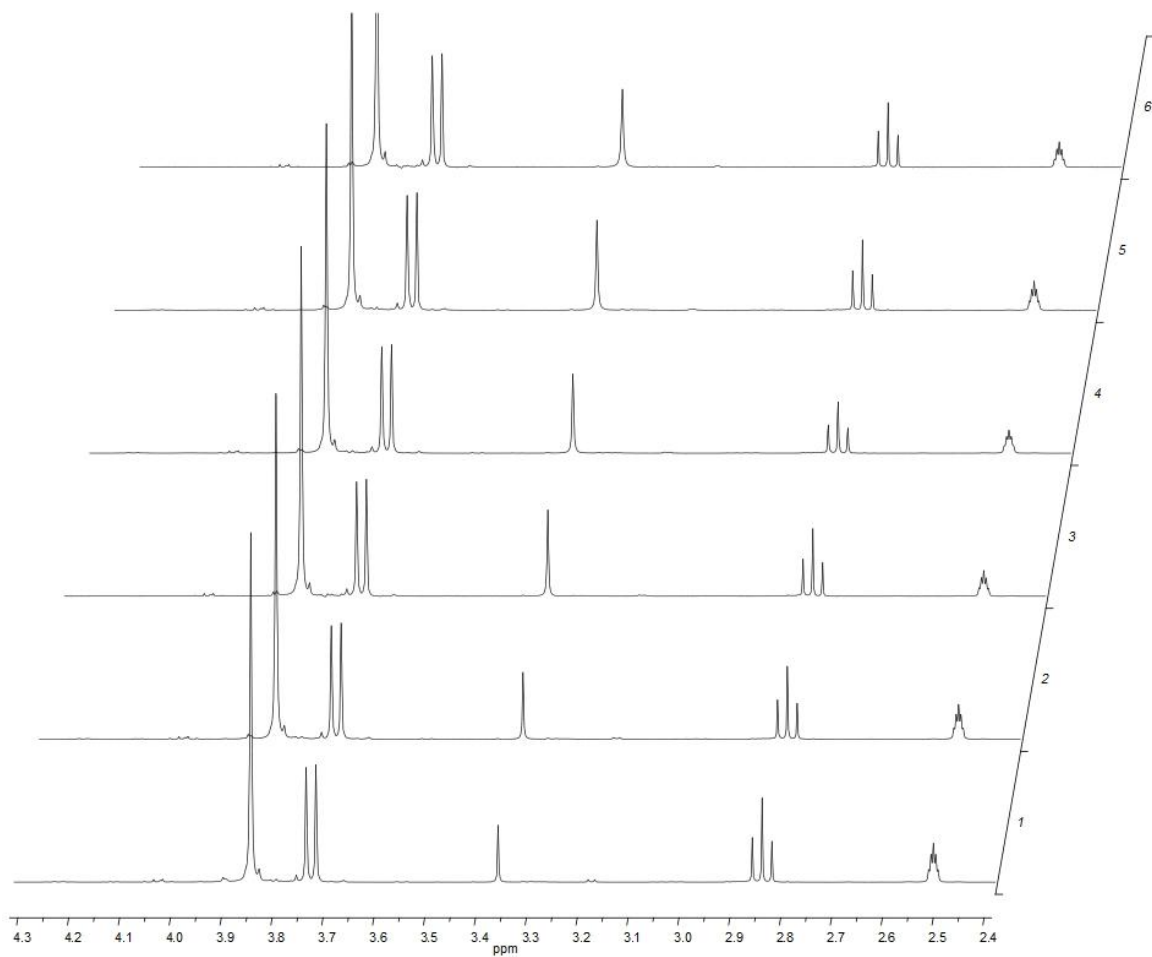
¹H NMR spectra for the addition of benzyl mercaptan to compound **38** after (1) 10 min, (2) 1.5 h, (3) 4.5 h, (4) 7.5 h, (5) 24 h, and (6) 48 h.



^1H NMR spectra for the addition of benzyl mercaptan to compound **38** after (1) 10 min, (2) 1.5 h, (3) 4.5 h, (4) 7.5 h, (5) 24 h, and (6) 48 h.



¹H NMR spectra for the addition of benzyl mercaptan to compound **47** after (1) 10 min, (2) 1.5 h, (3) 4.5 h, (4) 7.5 h, (5) 24 h, and (6) 48 h.



^1H NMR spectra for the addition of benzyl mercaptan to compound **47** after (1) 10 min, (2) 1.5 h, (3) 4.5 h, (4) 7.5 h, (5) 24 h, and (6) 48 h.

Anti-Proliferation Assays. MCF-7 and SKBr3 cells were maintained in a 1:1 mixture of Advanced DMEM/F12 (Gibco) supplemented with non-essential amino acids, L-glutamine (2 mM), streptomycin (500 µg/mL), penicillin (100 units/mL), and 10% FBS. Cells were grown to confluence in a humidified atmosphere (37 °C, 5% CO₂), seeded (2000/well, 100 µL) in 96-well plates, and allowed to attach overnight. Compound or geldanamycin at varying concentrations in DMSO (1% DMSO final concentration) was added, and cells were returned to the incubator for 72 h. At 72 h, the number of viable cells was determined using an MTS/PMS cell proliferation kit (Promega) per the manufacturer's instructions. Cells incubated in 1% DMSO were used as 100% proliferation, and values were adjusted accordingly. IC₅₀ values were calculated from separate experiments performed in triplicate using GraphPad Prism.

Western Blot Analysis. MCF-7 cells were grown to confluence as described above, seeded in 10 cm culture dishes (1x10⁶ cells/dish) and allowed to attach overnight. Compound was added at varying concentrations in DMSO (1% DMSO final concentration) and the cells were incubated with drug for 24 h. Cells were harvested in cold PBS and lysed in mammalian protein extraction reagent (MPER, Pierce) lysis buffer containing protease inhibitors (Roche) on ice for 1 h. Lysates were clarified at 14,000g for 10 min at 4° C. Protein concentrations were determined using the Pierce BCA protein assay kit per the manufacturer's instructions. Equal amounts of protein (2.5-10 µg) were electrophoresed under reducing conditions (10% acrylamide gel), transferred to a polyvinylidene fluoride membrane (PVDF), and immunoblotted with the corresponding specific antibodies. Membranes were incubated with an appropriate horseradish peroxidase-labeled secondary antibody, developed with a chemiluminescent substrate, and visualized.

VI. References

1. Aggarwal, B. B.; Kumar, A.; Bharti, A. C. Anticancer potential of curcumin: Preclinical and clinical studies. *Anticancer Res.* **2003**, *23*, 363-398.
2. Aggarwal, B. B.; Sundaram, C.; Malani, N.; Ichikawa, H. Curcumin: the Indian solid gold. *Adv. Exp. Med. Biol.* **2007**, *595*, 1-75.
3. Sharma, R. A.; Gescher, A. J.; Steward, W. P. Curcumin: The story so far. *Euro. J. Cancer* **2005**, *41*, 1955-1968.
4. Park, S.-Y.; Kim, D. S. H. L. Discovery of natural products from *Curcuma longa* that protect cells from Beta-Amyloid insult: A Drug discovery effort against Alzheimer's Disease. *J. Nat. Prod.* **2002**, *65*, 1227-1231.
5. Ammon, H. P. T.; Wahl, M. A. Pharmacology of *Curcuma longa*. *Planta Med.* **1991**, *57*, 1-7.
6. Wahlstrom, B.; Blennow, G. A study on the fate of curcumin in the rat. *Acta Pharmacol. Toxicol.* **1978**, *43*, 86-92.
7. Cheng, A.-L.; Hsu, C.-H.; Lin, J.-K.; Hsu, M.-M.; Ho, Y.-F.; Shen, T.-S.; Ko, J.-Y.; Lin, J.-T.; Lin, B.-R.; Wu, M.-S.; Yu, H.-S.; Jee, S.-H.; Chen, G.-S.; Chen, T.-M.; Chen, C.-A.; Lai, M.-K.; Pu, Y.-S.; Pan, M.-H.; Wang, Y.-J.; Tsai, C.-C.; Hsieh, C.-Y. Phase I clinical trial of curcumin, a chemopreventive agent, in patients with high-risk or pre-malignant lesions. *Anticancer Res.* **2001**, *21*, 2895-2900.
8. Sharma, R. A.; Euden, S. A.; Platton, S. L.; Cooke, D. N.; Shafayat, A.; Hewitt, H. R.; Marczylo, T. H.; Morgan, B.; Hemingway, D.; Plummer, S. M.; Pirmohamed, M.; Gescher, A. J.; Steward, W. P. Phase I Clinical Trial of oral curcumin: Biomarkers of systemic activity and compliance. *Clin. Cancer Res.* **2004**, *10*, 6847-6854.
9. Roth, G. N.; Chandra, A.; Nair, M. G. Novel bioactivities of *Curcuma longa* constituents. *J. Nat. Prod.* **1998**, *61*, 542-545.
10. Tsvetkov, P.; Asher, G.; Reiss, V.; Shaul, Y.; Sachs, L.; Lotem, J. Inhibition of NAD(P)H:Quinone oxidoreductase 1 activity and induction of p53 degradation by the natural phenolic compound curcumin. *Proc. Natl. Acad. Sci.* **2005**, *102*, 5535-5540.
11. Lin, J. K.; Lin-Shiau, S. Y. Mechanisms of cancer chemoprevention by curcumin. *Proc. Natl. Sci. Counc. Repub. China B* **2001**, *25*, 59-66.
12. Kao, E.-S.; Wang, C.-J.; Lin, W.-L.; Yin, Y.-F.; Wang, C.-P.; Tseng, T.-H. Anti-inflammatory Potential of Flavonoid Contents from Dried Fruit of *Crataegus pinnatifida* in Vitro and in Vivo. *J. Agric. Food Chem.* **2005**, *53*, 430-436.
13. Joe, B.; Vijaykumar, M.; Lokesh, B. R. Biological properties of curcumin-cellular and molecular mechanisms of action. *Crit. Rev. Food Sci. Nutr.* **2004**, *44*, 97-111.
14. Lim, G. P.; Chu, T.; Yang, F.; Beech, W.; Frautschy, S. A.; Cole, G. M. The curry spice curcumin reduces oxidative damage and amyloid pathology in an Alzheimer transgenic mouse. *J. Neurosci.* **2001**, *21*, 8370-8377.
15. Chen, Y.-C.; Kuo, T.-C.; Lin-Shiau, S.-Y.; Lin, J.-K. Induction of HSP70 gene expression by modulation of Ca²⁺ ion and cellular p53 protein by curcumin in colorectal carcinoma cells. *Mol. Carcinog.* **1996**, *17*, 224-234.
16. Dou, F.; Netzer, W. J.; Tanemura, K.; Li, F.; Hartl, U.; Takashima, A.; Gouras, G. K.; Greengard, P.; Xu, H. Chaperones increase association of Tau protein with microtubules. *P. Natl. Acad. Sci.* **2003**, *100*, 721-726.
17. Chan, M. M.-Y.; Huang, H.-I.; Fenton, M. R.; Fong, D. In vivo inhibition of nitric oxide synthase gene expression by curcumin, a cancer preventive natural product with anti-inflammatory properties. *Biochem. Pharmacol.* **1998**, *55*, 1955-1962.
18. Rashmi, R.; Santhosh, K. T. R.; Karunakaran, D. Human colon cancer cells differ in their sensitivity to curcumin-induced apoptosis and heat shock protects them by inhibiting the release of apoptosis-inducing factor and caspases. *FEBS Lett.* **2003**, *538*, 19-24.
19. Tanioka, T.; Nakatani, Y.; Kobayashi, T.; Tsujimoto, M.; Oh-ishi, S.; Murakami, M.; Kudo, I. Regulation of cytosolic prostaglandin E2 synthase by 90-kDa heat shock protein. *Biochem. Biophys. Res. Commun.* **2003**, *303*, 1018-1023.

20. Plummer, S. M.; Holloway, K. A.; Manson, M. M.; Munks, R. J. L.; Kaptein, A.; Farrow, S.; Howells, L. Inhibition of cyclo-oxygenase 2 expression in colon cells by the chemopreventive agent curcumin involves inhibition of NF- κ B activation via the NIK/IKK signalling complex. *Oncogene* **1999**, *18*, 6013-6020.
21. Lewis, J.; Devin, A.; Miller, A.; Lin, Y.; Rodriguez, Y.; Neckers, L.; Liu, Z.-G. Disruption of Hsp90 function results in degradation of the death domain kinase, receptor-interacting protein (RIP), and blockage of tumor necrosis factor-induced nuclear factor- κ B activation. *J. Biol. Chem.* **2000**, *275*, 10519-10526.
22. Han, S.-S.; Keum, Y.-S.; Seo, H.-J.; Surh, Y.-J. Curcumin suppresses activation of NF- κ B and AP-1 induced by phorbol ester in cultured human promyelocytic leukemia cells. *J. Biochem. Mol. Biol.* **2002**, *35*, 337-342.
23. Murata, M.; Miura, Y.; Hashiramoto, A.; Kitamura, H.; Kawasaki, H.; Shiozawa, K.; Yoshiya, S.; Baba, H.; Chihara, K.; Shiozawa, S. Heat shock protein 90 is required for increased DNA binding activity of activator protein-1, a heterodimer of Fos/JunD, in rheumatoid synovial cells under inflammatory stimuli. *Int. J. Mol. Med.* **2005**, *15*, 649-653.
24. Huang, T. S.; Lee, S. C.; Lin, J. K. Suppression of c-Jun/AP-1 activation by an inhibitor of tumor promotion in mouse fibroblast cells. *Proc. Natl. Acad. Sci.* **1991**, *88*, 5292-5296.
25. Vasilevskaya, I. A.; O'Dwyer, P. J. Effects of geldanamycin on signaling through activator-protein 1 in hypoxic HT29 human colon adenocarcinoma cells. *Cancer Res.* **1999**, *59*, 3935-3940.
26. Yoshida, M.; Xia, Y. Heat shock protein 90 as an endogenous protein enhancer of inducible nitric-oxide synthase. *J. Biol. Chem.* **2003**, *278*, 36953-36958.
27. Pearl, L. H.; Prodromou, C. Structure and in vivo function of Hsp90. *Curr. Opin. Struc. Biol.* **2000**, *10*, 46-51.
28. Mukhopadhyay, A.; Banerjee, S.; Stafford, L. J.; Xia, C.; Liu, M.; Aggarwal, B. B. Curcumin-induced suppression of cell proliferation correlates with down-regulation of cyclin D1 expression and CDK4-mediated retinoblastoma protein phosphorylation. *Oncogene* **2002**, *21*, 8852-8861.
29. Muise-Helmericks, R. C.; Grimes, H. L.; Bellacosa, A.; Malstrom, S. E.; Tschlis, P. N.; Rosen, N. Cyclin D expression is controlled post-transcriptionally via a phosphatidylinositol 3-kinase/Akt-dependent pathway. *J. Biol. Chem.* **1998**, *273*, 29864-29872.
30. Chen, A.; Xu, J. Activation of PPAR γ by curcumin inhibits Moser cell growth and mediates suppression of gene expression of cyclin D1 and EGFR. *Am. J. Physiol.* **2005**, *288*, G447-G456.
31. Shimamura, T.; Lowell, A. M.; Engelman, J. A.; Shapiro, G. I. Epidermal growth factor receptors harboring kinase domain mutations associate with the heat shock protein 90 chaperone and are destabilized following exposure to geldanamycins. *Cancer Res.* **2005**, *65*, 6401-6408.
32. Esser, C.; Scheffner, M.; Hohfeld, J. The chaperone-associated ubiquitin ligase CHIP is able to target p53 for proteasomal degradation. *J. Biol. Chem.* **2005**, *280*, 27443-27448.
33. Chaudhary, L. R.; Hruska, K. A. Inhibition of cell survival signal protein kinase B/Akt by curcumin in human prostate cancer cells. *J. Cell. Biochem.* **2003**, *89*, 1-5.
34. Sato, S.; Fujita, N.; Tsuruo, T. Modulation of Akt kinase activity by binding to Hsp90. *Proc. Natl. Acad. Sci.* **2000**, *97*, 10832-10837.
35. Shishodia, S.; Amin, H. M.; Lai, R.; Aggarwal, B. B. Curcumin (diferuloylmethane) inhibits constitutive NF- κ B activation, induces G1/S arrest, suppresses proliferation, and induces apoptosis in mantle cell lymphoma. *Biochem. Pharmacol.* **2005**, *70*, 700-713.
36. Xu, W.; Yuan, X.; Jung, Y. J.; Yang, Y.; Basso, A.; Rosen, N.; Chung, E. J.; Trepel, J.; Neckers, L. The heat shock protein 90 inhibitor geldanamycin and the ErbB inhibitor ZD1839 promote rapid PP1 phosphatase-dependent inactivation of AKT in ErbB2 overexpressing breast cancer cells. *Cancer Res.* **2003**, *63*, 7777-7784.
37. Han, S.-S.; Chung, S.-T.; Robertson, D. A.; Ranjan, D.; Bondada, S. Curcumin causes the growth arrest and apoptosis of B cell lymphoma by downregulation of egr-1, C-myc, Bcl-XL, NF- κ B, and p53. *Clin. Immunol.* **1999**, *93*, 152-161.

38. Ramana, C. V.; Grammatikakis, N.; Chernov, M.; Nguyen, H.; Goh, K. C.; Williams, B. R. G.; Stark, G. R. Regulation of c-myc expression by IFN- γ through Stat1-dependent and -independent pathways. *EMBO J.* **2000**, *19*, 263-272.
39. Chan, M. M.-Y. Inhibition of tumor necrosis factor by curcumin, a phytochemical. *Biochem. Pharmacol.* **1995**, *49*, 1551-1556.
40. De Nardo, D.; Masendycz, P.; Ho, S.; Cross, M.; Fleetwood, A. J.; Reynolds, E. C.; Hamilton, J. A.; Scholz, G. M. A Central role for the Hsp90-Cdc37 molecular chaperone module in Interleukin-1 receptor-associated-kinase-dependent signaling by Toll-like receptors. *J. Biol. Chem.* **2005**, *280*, 9813-9822.
41. Abe, Y.; Hashimoto, S.; Horie, T. Curcumin inhibition of inflammatory cytokine production by human peripheral blood monocytes and alveolar macrophages. *Pharmacol. Res.* **1999**, *39*, 41-47.
42. Ciolino, H. P.; Daschner, P. J.; Wang, T. T. Y.; Yeh, G. C. Effect of curcumin on the aryl hydrocarbon receptor and cytochrome P450 1A1 in MCF-7 human breast carcinoma cells. *Biochem. Pharmacol.* **1998**, *56*, 197-206.
43. Bell, D. R.; Poland, A. Binding of aryl hydrocarbon receptor (AhR) to AhR-interacting protein. The role of hsp90. *J. Biol. Chem.* **2000**, *275*, 36407-36414.
44. Fortugno, P.; Beltrami, E.; Plescia, J.; Fontana, J.; Pradhan, D.; Marchisio, P. C.; Sessa, W. C.; Altieri, D. C. Regulation of survivin function by Hsp90. *Proc. Natl. Acad. Sci.* **2003**, *100*, 13791-13796.
45. Shao, Z.-M.; Shen, Z.-Z.; Liu, C.-H.; Sartippour, M. R.; Go, V. L.; Heber, D.; Mai, N. Curcumin exerts multiple suppressive effects on human breast carcinoma cells. *Int. J. Cancer* **2002**, *98*, 234-240.
46. Kuduk, S. D.; Zheng, F. F.; Sepp-Lorenzino, L.; Rosen, N.; Danishefsky, S. J. Synthesis and evaluation of geldanamycin-estradiol hybrids. *Bioorg. Med. Chem. Lett.* **1999**, *9*, 1233-1238.
47. Nakamura, K.; Yasunaga, Y.; Segawa, T.; Ko, D.; Moul, J. W.; Srivastava, S.; Rhim, J. S. Curcumin down-regulates AR gene expression and activation in prostate cancer cell lines. *Int. J. Oncol.* **2002**, *21*, 825-830.
48. Kuduk, S. D.; Harris, C. R.; Zheng, F. F.; Sepp-Lorenzino, L.; Ouerfelli, O.; Rosen, N.; Danishefsky, S. J. Synthesis and evaluation of geldanamycin-testosterone hybrids. *Bioorg. Med. Chem. Lett.* **2000**, *10*, 1303-1306.
49. Ramachandran, C.; Fonseca, H. B.; Jhabvala, P.; Escalon, E. A.; Melnick, S. J. Curcumin inhibits telomerase activity through human telomerase reverse transcriptase in MCF-7 breast cancer cell line. *Cancer Lett.* **2002**, *184*, 1-6.
50. Holt, S. E.; Aisner, D. L.; Baur, J.; Tesmer, V. M.; Dy, M.; Ouellette, M.; Trager, J. B.; Morin, G. B.; Toft, D. O.; Shay, J. W.; Wright, W. E.; White, M. A. Functional requirement of p23 and Hsp90 in telomerase complexes. *Genes Dev.* **1999**, *13*, 817-826.
51. Wu, L.-x.; Xu, J.-h.; Wu, G.-h.; Chen, Y.-z. Inhibitory effect of curcumin on proliferation of K562 cells involves down-regulation of p210bcr/abl-initiated ras signal transduction pathway. *Acta Pharmacol. Sin.* **2003**, *24*, 1155-1160.
52. An, W. G.; Schulte, T. W.; Neckers, L. M. The heat shock protein 90 antagonist geldanamycin alters chaperone association with p210bcr-abl and v-src proteins before their degradation by the proteasome. *Cell Growth Differ.* **2000**, *11*, 355-360.
53. Stepanova, L.; Leng, X.; Parker, S. B.; Harper, J. W. Mammalian p50Cdc37 is a protein kinase-targeting subunit of Hsp90 that binds and stabilizes Cdk4. *Genes Dev.* **1996**, *10*, 1491-1502.
54. Woo, J.-H.; Kim, Y.-H.; Choi, Y.-J.; Kim, D.-G.; Lee, K.-S.; Bae, J. H.; Min, D. S.; Chang, J.-S.; Jeong, Y.-J.; Lee, Y. H.; Park, J.-W.; Kwon, T. K. Molecular mechanisms of curcumin-induced cytotoxicity: induction of apoptosis through generation of reactive oxygen species, down-regulation of Bcl-XL and IAP, the release of cytochrome c and inhibition of Akt. *Carcinogenesis* **2003**, *24*, 1199-1208.
55. Cohen-Saidon, C.; Carmi, I.; Keren, A.; Razin, E. Antiapoptotic function of Bcl-2 in mast cells is dependent on its association with heat shock protein 90 β . *Blood* **2006**, *107*, 1413-1420.

56. Shim, J. S.; Lee, J.; Park, H.-J.; Park, S.-J.; Kwon, H. J. A New Curcumin derivative, HBC, interferes with the cell cycle progression of colon cancer cells via antagonization of the Ca²⁺/Calmodulin function. *Chem. Biol.* **2004**, *11*, 1455-1463.
57. Okada, M.; Hatakeyama, T.; Itoh, H.; Tokuta, N.; Tokumitsu, H.; Kobayashi, R. S100A1 Is a novel molecular chaperone and a member of the Hsp70/Hsp90 multichaperone complex. *J. Biol. Chem.* **2004**, *279*, 4221-4233.
58. Duvoix, A.; Morceau, F.; Delhalle, S.; Schmitz, M.; Schnekenburger, M.; Galteau, M.-M.; Dicato, M.; Diederich, M. Induction of apoptosis by curcumin: mediation by glutathione S-transferase P1-1 inhibition. *Biochem. Pharmacol.* **2003**, *66*, 1475-1483.
59. Mayama, J.; Kumano, T.; Hayakari, M.; Yamazaki, T.; Aizawa, S.; Kudo, T.; Tsuchida, S. Polymorphic glutathione S-transferase subunit 3 of rat liver exhibits different susceptibilities to carbon tetrachloride: differences in their interactions with heat-shock protein 90. *Biochem. J.* **2003**, *372*, 611-616.
60. Bharti, A. C.; Donato, N.; Aggarwal, B. B. Curcumin (diferuloylmethane) inhibits constitutive and IL-6-inducible STAT3 phosphorylation in human multiple myeloma cells. *J. Immunol.* **2003**, *171*, 3863-3871.
61. Fumo, G.; Akin, C.; Metcalfe, D. D.; Neckers, L. 17-allylamino-17-demethoxygeldanamycin (17-AAG) is effective in down-regulating mutated, constitutively activated KIT protein in human mast cells. *Blood* **2004**, *103*, 1078-1084.
62. Chiosis, G.; Vilenchik, M.; Kim, J.; Solit, D. Hsp90: the vulnerable chaperone. *Drug Discov. Today* **2004**, *9*, 881-888.
63. Blagg, B. S. J.; Kerr, T. D. Hsp90 inhibitors: small molecules that transform the Hsp90 protein folding machinery into a catalyst for protein degradation. *Med. Res. Rev.* **2006**, *26*, 310-338.
64. Zhang, H.; Burrows, F. Targeting multiple signal transduction pathways through inhibition of Hsp90. *J. Mol. Med.* **2004**, *82*, 488-499.
65. Hanahan, D.; Weinberg, R. A. The hallmarks of cancer. *Cell* **2000**, *100*, 57-70.
66. Kamal, A.; Thao, L.; Sensintaffar, J.; Zhang, L.; Boehm, M. F.; Fritz, L. C.; Burrows, F. J. A high-affinity conformation of Hsp90 confers tumour selectivity on Hsp90 inhibitors. *Nature* **2003**, *425*, 407-410.
67. Lee, J. H.; Chung, I. K. Curcumin inhibits nuclear localization of telomerase by dissociating the Hsp90 co-chaperone p23 from hTERT. *Cancer Lett.* **2010**, *290*, 76-86.
68. Wu, L.-x.; Xu, J.-h.; Huang, X.-w.; Zhang, K.-z.; Wen, C.-x.; Chen, Y.-z. Down-regulation of p210bcr/abl by curcumin involves disrupting molecular chaperone functions of Hsp90. *Acta Pharmacol. Sin.* **2006**, *27*, 694-699.
69. Thulasiraman, V.; Matts, R. L. Effect of geldanamycin on the kinetics of chaperone-mediated renaturation of firefly luciferase in rabbit reticulocyte lysate. *Biochemistry* **1996**, *35*, 13443-13450.
70. Schumacher, R. J.; Hurst, R.; Sullivan, W. P.; McMahon, N. J.; Toft, D. O.; Matts, R. L. ATP-dependent chaperoning activity of reticulocyte lysate. *J. Biol. Chem.* **1994**, *269*, 9493-9499.
71. Roe, S. M.; Prodromou, C.; O'Brien, R.; Ladbury, J. E.; Piper, P. W.; Pearl, L. H. Structural basis for inhibition of the Hsp90 molecular chaperone by the antitumor antibiotics radicicol and geldanamycin. *J. Med. Chem.* **1999**, *42*, 260-266.
72. Sreedhar, A. S.; Soti, C.; Csermely, P. Inhibition of Hsp90: a new strategy for inhibiting protein kinases. *Biochim. Biophys. Acta.* **2004**, *1697*, 233-242.
73. Yu, X. M.; Shen, G.; Neckers, L.; Blake, H.; Holzbeierlein, J.; Cronk, B.; Blagg, B. S. Hsp90 inhibitors identified from a library of novobiocin analogues. *J. Am. Chem. Soc.* **2005**, *127*, 12778-12779.
74. Conde, R.; Belak, Z. R.; Nair, M.; O'Carroll, R. F.; Ovsenek, N. Modulation of Hsf1 activity by novobiocin and geldanamycin. *Biochem. Cell Biol.* **2009**, *87*, 845-851.
75. Kim, H. R.; Kang, H. S.; Kim, H. D. Geldanamycin induces heat shock protein expression through activation of HSF1 in K562 erythroleukemic cells. *IUBMB Life* **1999**, *48*, 429-433.

76. Goel, A.; Kunnumakkara, A. B.; Aggarwal, B. B. Curcumin as "Curecumin": From kitchen to clinic. *Biochem. Pharmacol.* **2008**, *75*, 787-809.
77. Simoni, D.; Rizzi, M.; Rondanin, R.; Baruchello, R.; Marchetti, P.; Invidiata, F. P.; Labbozzetta, M.; Poma, P.; Carina, V.; Notarbartolo, M.; Alaimo, A.; D'Alessandro, N. Antitumor effects of curcumin and structurally β -diketone modified analogs on multidrug resistant cancer cells. *Bioorg. Med. Chem. Lett.* **2008**, *18*, 845-849.
78. Payton, F.; Sandusky, P.; Alworth, W. L. NMR Study of the Solution Structure of Curcumin. *J. Nat. Prod.* **2007**, *70*, 143-146.
79. Lin, L.; Shi, Q.; Nyarko, A. K.; Bastow, K. F.; Wu, C.-C.; Su, C.-Y.; Shih, C. C. Y.; Lee, K.-H. Antitumor Agents. 250. Design and synthesis of new curcumin analogues as potential anti-prostate cancer agents. *J. Med. Chem.* **2006**, *49*, 3963-3972.
80. Lin, L.; Shi, Q.; Su, C.-Y.; Shih, C. C. Y.; Lee, K.-H. Antitumor agents 247. New 4-ethoxycarbonyl ethyl curcumin analogs as potential antiandrogenic agents. *Bioorg. Med. Chem.* **2006**, *14*, 2527-2534.
81. Mishra, S.; Karmodiya, K.; Surolia, N.; Surolia, A. Synthesis and exploration of novel curcumin analogues as anti-malarial agents. *Bioorg. Med. Chem.* **2008**, *16*, 2894-2902.
82. Selvam, C.; Jachak, S. M.; Thilagavathi, R.; Chakraborti, A. K. Design, synthesis, biological evaluation and molecular docking of curcumin analogues as antioxidant, cyclooxygenase inhibitory and anti-inflammatory agents. *Bioorg. Med. Chem. Lett.* **2005**, *15*, 1793-1797.
83. Narlawar, R.; Baumann, K.; Schubanel, R.; Schmidt, B. Curcumin derivatives inhibit or modulate Beta-Amyloid precursor protein metabolism. *Neurodegener. Dis.* **2007**, *4*, 88-93.
84. Narlawar, R.; Pickhardt, M.; Leuchtenberger, S.; Baumann, K.; Krause, S.; Dyrks, T.; Weggen, S.; Mandelkow, E.; Schmidt, B. Curcumin-derived pyrazoles and isoxazoles: swiss army knives or blunt tools for Alzheimer's disease? *ChemMedChem* **2008**, *3*, 165-172.
85. Amolins, M. W.; Peterson, L. B.; Blagg, B. S. J. Synthesis and evaluation of electron-rich curcumin analogues. *Bioorg. Med. Chem.* **2009**, *17*, 360.
86. Bird, C. W. Heteroaromaticity. 5. A unified aromaticity index. *Tetrahedron* **1992**, *48*, 335-340.
87. Ohtsu, H.; Xiao, Z.; Ishida, J.; Nagai, M.; Wang, H.-K.; Itokawa, H.; Su, C.-Y.; Shih, C.; Chiang, T.; Chang, E.; Lee, Y.; Tsai, M.-Y.; Chang, C.; Lee, K.-H. Antitumor Agents. 217. Curcumin analogues as novel androgen receptor antagonists with potential as anti-prostate cancer agents. *J. Med. Chem.* **2002**, *45*, 5037-5042.